A patch-clamp study of ion-channels in membrane vesicles prepared from the parasitic helminths *Ascaris suum* and *Schistosoma mansoni.*

A thesis submitted for the degree of

DOCTOR OF PHILOSOPHY

in the

Faculty of Veterinary Medicine,

UNIVERSITY OF EDINBURGH

by

Alan P Robertson

Department of Preclinical Veterinary Sciences,

Royal (Dick) School of Veterinary Studies,

University of Edinburgh

April, 1997

Declaration: The experimental work described herein was performed under the supervision of Dr R.J. Martin (University of Edinburgh) and Prof. J.R. Kusel (University of Glasgow) during the tenure of a BBSRC studentship in the Department of Preclinical Veterinary Sciences, R.(D.)S.V.S., University of Edinburgh.

I, hereby, declare that the experimental work is entirely my own composition and that it has not previously been submitted in whole, or in part, to this or any other University. The substance of Sections I and II have been accepted for publication. Reprints are included in Appendix III of the thesis.

Alan Patrick Robertson BSc.

Acknowledgements: I would like to thank Dr Richard Martin for the facilities placed at my disposal and for the frequent and helpful discussions. I would also like to thank Professor John Kusel for reading the draft of the manuscript and for valuable advice.

Thanks to Steve Mitchell of the E.M suite for his advice and assistance during the electron microscopy studies. I am particularly grateful to Colin Warwick of the photographic unit for his help and artistic advice in preparing the numerous figures in the manuscript. This work was partly funded by the Biotechnology and Biological Sciences Research Council.

Thanks to Peter Hill for our numerous discussions scientific, or otherwise, during this project. Finally sincere thanks to family and friends who wouldn't let me give up.

CONTENTS

ABBREVIATIONS

4-AP	4-aminopyridine
AF18	5-N-(octadecanoyl)aminofluorescein
con A	concanavalin A
DIDS	4,4'-diiso-thiocyanostilbene-2,2' disulfonate
E_{rev}	reversal potential
HSP70	heat shock protein 70
GABA	γ-aminobutyric acid
GPI	glycosylphosphatidylinositol
mV	millivolts
pA	picoamps
P_{open}	probability of channel opening
pH^o	pH on the outside (extracellular) surface of an isolated inside-out membrane patch
pH^i	pH on the inside (intracellular) surface of an isolated inside-out membrane patch
P_{ion}	permeability of an ion-channel or membrane to an ion species *e.g.*
P_{Na}	is the pereability of sodium ions
pS	picoseimens
PZQ	praziquantel
SITS	4 acetamide-4'-isothiocyanostilbene-2,2' disulfonate
TBPS	tert-butylbicyclophosphothionate

ABSTRACT

Ascaris lumbricoides and *Schistosoma mansoni* are major parasites of man in the developing world. The possible development of drug resistant strains means that continuing and improved treatments require the selection of novel target sites. Membrane ion-channels have proved to be suitable targets for many therapeutic agents. The purpose of this thesis was to further characterise distinct ion-channels present in parasite membranes. The properties of the ion-channels found in membranes of the two parasite species were assessed using standard single-channel recording techniques.

Membrane vesicles prepared from the bag region of the somatic muscle cells of the parasitic nematode *Ascaris suum* (a close relative of *A. lumbricoides*) contain high-conductance, voltage-sensitive, Ca-dependent chloride channels. The effect of altered pH on these channels was investigated using the patch-clamp technique and isolated inside-out membrane patches. Changes in pH had little effect on channel conductances and reversal potentials. Under control conditions (symmetrical pH 7.2) the channel had the highest probability of opening at ~-35mV (the resting membrane potential of the cell). At positive membrane potentials the probability of opening decreased. The Boltzmann equation was used to describe the relationship between membrane potential and probability of channel opening, and to calculate the effective gating charge. Reduction of external pH produced an increase in the probability of channel opening at hyperpolarised membrane potentials. An increase in internal pH caused a voltage independent increase in the probability of channel opening and made the effective gating charge less negative. The effect of reducing internal pH was marked: the channel then opened most frequently at positive membrane potentials and the probability of opening at -35mV was greatly reduced.

The decrease in internal pH changed the polarity of the effective gating charge. A simple model was constructed to describe the effects of pH on channel gating.

Treatment of *S. mansoni* in low pH media results in the formation of vesicles from the tegument. Parasites pre-treated with 5-N-(octadecanoyl)aminofluorescein (AF18) and examined using fluorescence microscopy showed at least some of the vesicles were outer tegument in origin. Scanning electron microscopy studies show the vesicles possess a smooth surface suitable for the application of the patch-clamp technique. Transmission electron microscopy studies indicate that some vesicles posses the unique heptalaminate membranes found in the outer tegument. Patch-clamp studies have shown the presence of a large-conductance, non-selective cation channel. Other channel types with different ionic selectivities and conductances were observed.

The properties of the observed ion-channel types are discussed; comment is made on these ion-channels as possible target sites.

SECTION I: THE EFFECT OF PH ON THE HIGH-CONDUCTANCE CA-DEPENDENT CHLORIDE CHANNEL IN MEMBRANE VESICLES PREPARED FROM THE SOMATIC MUSCLE CELLS OF *ASCARIS SUUM*: A PATCH-CLAMP STUDY.

CHAPTER 1: INTRODUCTION

1 General Introduction

1.1 *Ascaris* and Ascariasis

Ascaris suum is a large nematode parasite found in the small intestine of the pig. *Ascaris suum* is closely related to another nematode parasite, *Ascaris lumbricoides*, which normally infects humans. Infestation with nematodes is thought to be the most common cause of parasitism in man and animals. *Ascaris lumbricoides* has been estimated to infect around 1008 million people world-wide, or in other words approximately 22% of the world population (Crompton, 1988). The knowledge that the worms are able to live in a human host dates back to the era of ancient Rome at least (Lancet, 1989). One of the earliest scientific descriptions of *A. lumbricoides* was given by Tyson (1683) who referred to the parasite as *Lumbricus teres* (a name also dating back to the Roman era). The name probably arose from the similarity of the parasite to dead earthworms, however Tyson demonstrated clear differences between the two species. The modern names of *A. lumbricoides* and *A. suum* are attributed to Linnaeus (1758) and Goeze (1782) respectively (both cited in Crompton, Nesheim and Pawlowski, 1989). *Ascaris suum* and *Ascaris lumbricoides* are so similar that they have previously been described as a single species (Soulsby, 1965). The lack of equivalent parasites in apes and monkeys suggests that man originally acquired *Ascaris* infection from close contact with pigs rather than phylogenetically. However, at present cross transmission of *Ascaris lumbricoides* to pigs and of *Ascaris suum* to humans is rare. *Ascaris suum* is an economically important parasite in the pig industry. Additionally the similarity between *A. suum* and *A. lumbricoides* results in the former being an excellent experimental model for an exceptionally widespread parasite of humans.

Adult female worms produce eggs in the gut which are passed out in the faeces. Transmission is direct by the faeco-oral route with the second stage larva enclosed in the eggshell as the infective form. On swallowing infective larvae (still enclosed in the eggshell) the eggs hatch and burrow through the mucosal wall into the bloodstream. The larvae move to the lungs where they leave the bloodstream and migrate up the trachea. Larvae are then swallowed by the host and mature to the adult form in the gut. For *A. suum* in pigs the prepatent period, the time between initial infection and the first detection of eggs in the host faeces, is between 49 and 56 days (Wood, Pankarich, Berger. 1963). The duration of egg release, the patent period, is approximately 55 weeks (Olsen, Kelley, Sen. 1958). The eggs of *A. lumbricoides* have been reported to retain their infectivity for up to 15 years (Storey and Phillips. 1985) although they are sensitive to desiccation and direct sunlight. The widespread prevalence of ascariasis can be explained by a combination of factors which have been discussed in detail by Crompton *et al* (1989). These include the longevity of the infective stage, poor levels of sanitation and hygiene, and the use of night soil as fertiliser on crops destined for human consumption.

There is limited information on mortality in humans directly due to infection with *A. lumbricoides*, the small amount of data available has been summarised in Crompton *et al* (1989). Estimates of mortality range from a low of 8000 to a high of 100000 people annually from an estimated global population of just over a billion infected individuals. This figure is small compared with mortality estimates for other parasitic infections *e.g.* malaria, however this figure takes no account of the level of morbidity caused by *Ascaris*, information on which is also sparse (Crompton *et al.* 1989).

1.2 Anatomy and morphology of adult worm.

Ascaris, in common with other nematodes, has a fixed number of cells and cell divisions. The adult *Ascaris* can reach up to 40 cm in length, the females are generally longer than the males. Healthy adult worms are turgid and are frequently an orange\pink colour, the colouring arises from the production of two types of haemoglobin by the worm (Smith and Lee, 1963). The body of *Ascaris* is composed of three concentric layers (Figure. 1.1), which are from the outside: the cuticle, the hypodermis, and the somatic muscle layer. The cuticle forms the interface between host and parasite. The main structural component of the cuticle is collagen, with the outer layers being stabilised by disulphide bridges. The hypodermis forms longitudinal troughs which house the major and minor dorsal and ventral nerve cords. The hypodermis also forms the two lateral lines which are believed to have an excretory function. The somatic muscle layer surrounds the central perienteric (or pseudocoelomic) cavity containing the digestive tract and gonads. The somatic muscle layer is composed of 5×10^4 mononucleated muscle cells organised into dorsal and ventral fields separated by the two lateral lines (Stretton, 1976). The contractile spindles of the muscle cells all lie longitudinally, there are no circular muscles. Adult *Ascaris* maintain their position in the host gut using sinusoidal swimming motions. The most common movement is a large amplitude wave that moves anteriorly, starting from around half way along the animal. In all nematodes the somatic musculature is separated into dorsal and ventral halves, each half being innervated by the respective nerve cords (either dorsal or ventral). The arrangement and innervation of the muscle cells restricts the sinusoidal waves of movement to the dorso-ventral plane. It is believed that the main excitatory and inhibitory neurotransmitters are acetylcholine and GABA (γ-amino butyric acid) respectively, although there are probably co-transmitters present in the motor neurones. The co-transmitters are immunologically similar to FMFRamide and a number have been

synthesised (summarised in Maule, A.G., Bowman, J.W., Thompson, D.P., Marks, N.J., Friedman, , A.R., Geary, T.G. 1996). Adult *Ascaris* feed by pumping their food through a powerful pharyngeal muscle. The muscle must be powerful to counteract the relatively large pressures generated by the parasites hydrostatic skeleton. The head region of the worm shows more complex innervation that allows the more complex movements of this region required for feeding.

Figure 1.1

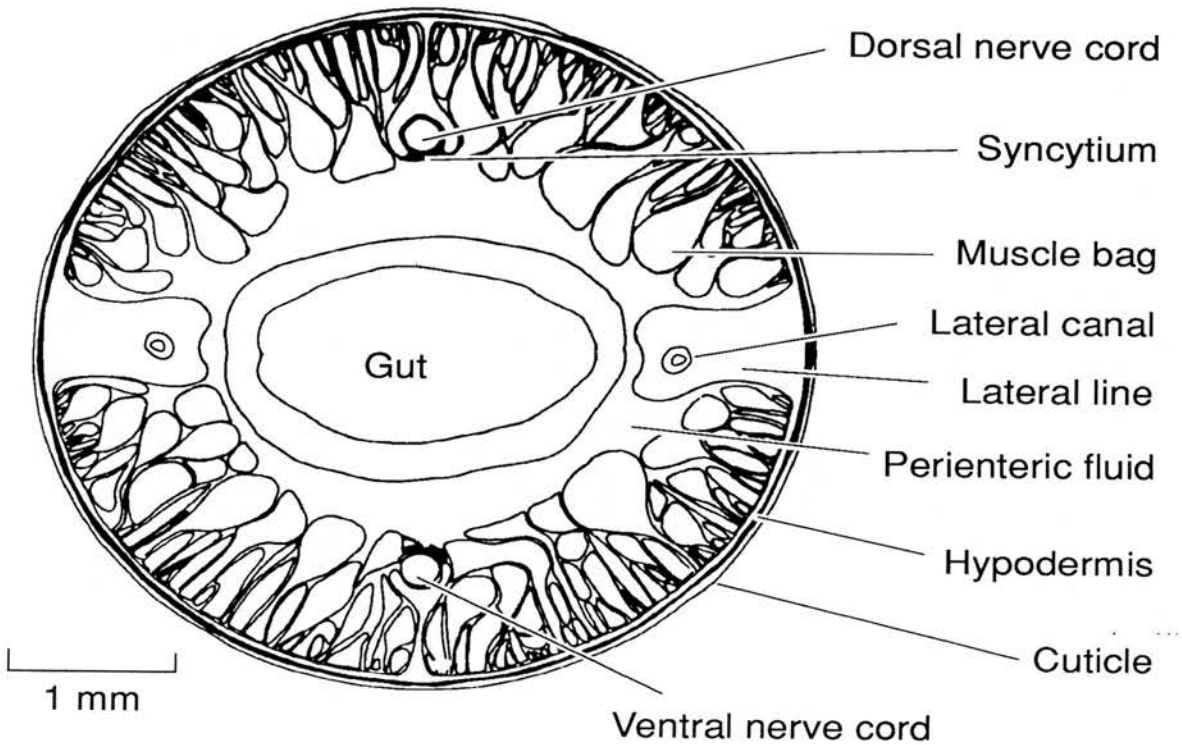

Figure 1.1: Diagram representing a cross section through the body wall of an adult *Ascaris suum* parasite. The worm is bounded by the collagen containing cuticle. Underlying the cuticle is the hypodermis housing the nerve cords and lateral lines. Underlying the hypodermis is the somatic musculature. The somatic muscle layer surrounds the central perienteric (or pseudocoelomic) cavity containing the digestive tract and gonads (from Martin *et al.* 1996).

2 The *Ascaris suum* somatic muscle cell

2.1 Anatomy of the muscle cell

The anatomy of the of the *Ascaris* muscle cell has been reviewed as early as 1911 (Cappe de Baillon quoted by Duittoz 1990). The muscle was divided into three separate anatomical regions by Cappe de Baillon: the arm ("bras"), the belly ("panse") and the spindle ("fuseau"). The belly is commonly referred to as the bag region in the more recent literature. A diagram of the *Ascaris* muscle cell is shown in Figure 1.2.

The belly or bag region

The belly is a large, round, bag-shaped region (*ca* 200-250 μm in diameter) of the muscle cell. The cell nucleus is located in the bag cytoplasm which also contains a large amount of particulate glycogen (Rosenbluth 1963) which may act as an energy store for muscular contraction. Harris and Crofton (1957) have postulated that the muscle bags fulfil the role of an endoskeleton in the parasite. The large size of the muscle bag makes it ideal for electrophysiological study. Treatment of muscle cells with collagenase results in membranous vesicles "budding" from the surface of the bag region. Application of the patch-clamp technique to the vesicles reveals the presence of several functional ion-channel types including a GABA-gated chloride channel, a Ca-dependent chloride channel and a non-junctional nicotinic acetylcholine receptor (Martin *et al.* 1996).

The arm

The arm is a thin process leaving the base of the bag region in the direction of a nerve cord. The majority of muscle cells have multiple arms (mean 2.7). The cells receive innervation from both the major (dorsal and ventral) and the minor nerve cords (Stretton 1976). Upon reaching the nerve cord the arm branches into thin

terminal processes, often called fingers. The muscle arms approach the nerve in bundles separated by wide gaps. Processes from adjacent arms intertwine to form a ribbon-shaped plexus of non-contractile muscle tissue. The muscle cell arms do not fuse together but experimental evidence suggests the cells are electrically coupled (Del Castillo *et al* 1989). Synapses are formed between this so called syncytium (Del Castillo *et al* 1989) and the nerve cord.

The spindle

The spindle (or fibre) is the contractile region of the muscle cell. The spindle branches off the base of the bag region of the cell, is approximately 2 mm in length and is anchored to the hypodermis. The muscle spindles combine to form a long tube lying against the hypodermis. *Ascaris* muscle has been classed as obliquely striated (Rosenbluth 1973), obliquely striated muscle has been found widely in invertebrates but has yet to be described in vertebrates (see Rosenbluth 1973 for review). Obliquely striated muscle has the extensibility of smooth muscle and the velocity of contraction of skeletal muscle (Duittoz 1990).

Figure 1.2

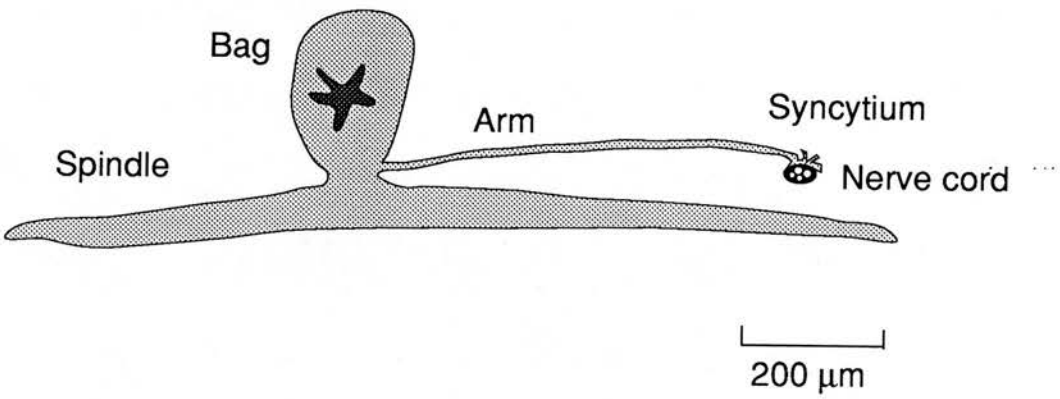

Figure 1.2: Diagram representing a somatic muscle cell of *Ascaris suum*. The cell is composed of three regions. The contractile region or "spindle". The glycogen and nucleus containing "bag" region and the "arm" which forms the neuromuscular junction with the nerve cord (from Martin *et al.* 1996).

2.2 Energy metabolism of the muscle cell

In *Ascaris* the carbohydrate store is glycogen. Glycogen synthesis relies on glucose supplied from the host as adult parasitic helminths have no proven gluconeogenesis ability (Tielens and van der Bergh, 1993). During the first 18 hrs of *in vitro* incubation the adult worms lose up to 27% of their muscle glycogen (Harpur, 1963). Adult *Ascaris* require no oxygen in their energy yielding metabolic pathways and can survive equally well *in vitro* under either aerobic or anaerobic conditions (Saz, 1981). In *Ascaris* carbohydrate is degraded to phosphoenolpyruvate (PEP) by the Embden-Meyerhof pathway: the PEP is carboxylated to form oxaloacetate which in turn is reduced to malate (Tielens and van der Bergh, 1993). The metabolic steps from glucose to malate occur in the cytoplasm, malate then permeates the mitochondrial membranes to become the main mitochondrial substrate (Saz, 1981). Inside the mitochondria, anaerobic fermentation in *Ascaris* results in the production of several compounds: acetone, acetate, propionate, butyrate, 2-methylbutyrate, n-valerate, cis-2-methylcrotonate (tiglate)and 2-methylvalerate (Saz, 1981). The overall pathway for the formation of succinate and volatile fatty acids is shown in Figure 1.3.

Figure 1.3

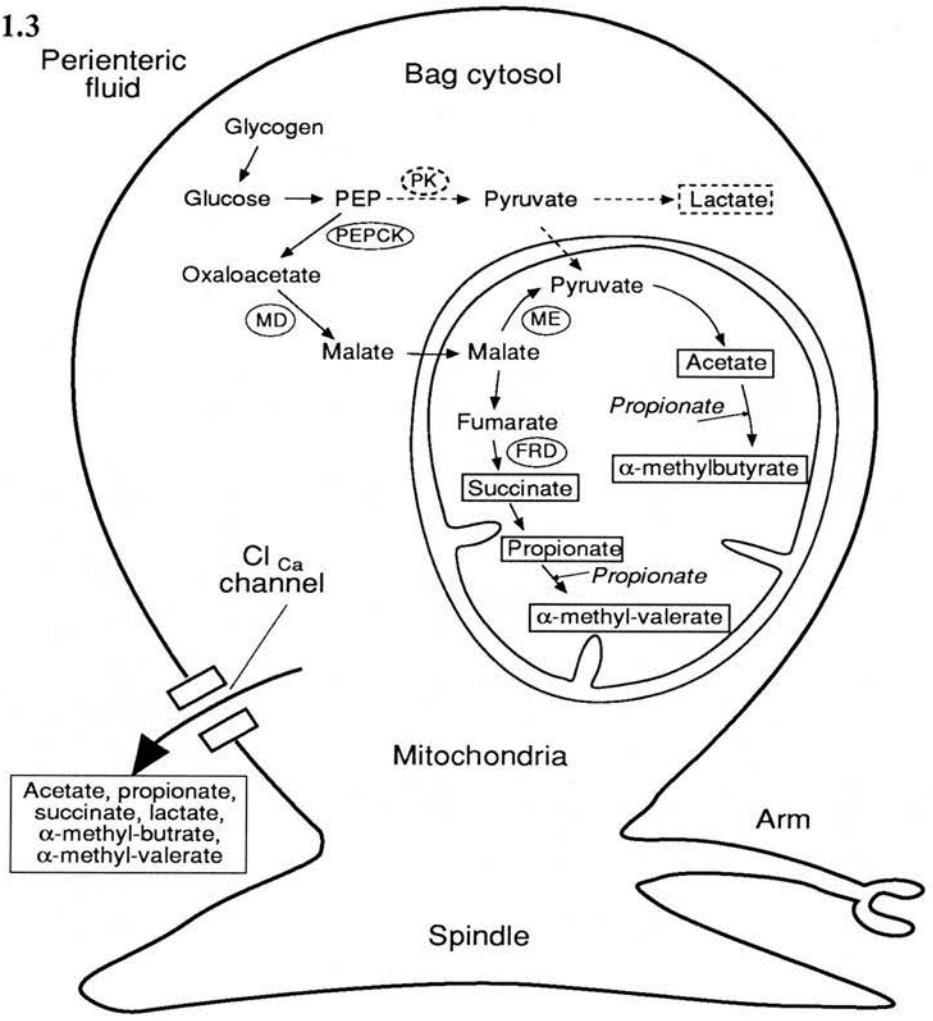

Figure 1.3: Diagram of the breakdown pathway of glycogen in the cytoplasm and mitochondria in *Ascaris*. The end-products like succinate, propionate, acetate, α-methylbutyrate, α-methyl valerate are shown in a rectangular box outside the cell in the perienteric fluid and in a rectangular box at the original site of their production. PEP, phosphoenol pyruvate; PK, pyruvate kinase; PEPCK, phosphoenol pyruvate carboxy kinase; MD, malate dehydrogenase; ME, malic enzyme; FRD, fumarate reductase. The pathway outlined by the dashed arrows is absent or only present at a low level. One possible route for excretion through the muscle membrane is through the Ca^{2+}-dependent Cl^- channel (from Martin *et al.,* 1996).

2.3 Resting membrane potential of the muscle cell

The first description of the resting membrane potential of *A. suum* somatic muscle cells was by Jarman (1959) who obtained a relatively low value of around -30 mV. He also described regular spike-like depolarisations which were superimposed on the basic resting potential. The resting membrane potential of the *Ascaris* muscle cell is relatively insensitive to changes in the concentration of extracellular potassium: a tenfold increase in external potassium concentration gave only a 1.5mV decrease in the resting membrane potential. A similar result was reported for altered sodium concentrations (Brading and Caldwell 1964). The resting membrane potential of the muscle cell was found to be most sensitive to changes in the chloride concentration, but even this change was small (13 mV per tenfold change in chloride concentration). Ion flux experiments have recorded a permeability ratio of 1:4:7 for potassium, sodium and chloride respectively (Caldwell and Ellory, 1968). The relative insensitivity of the resting potential to changes in extracellular ion concentrations led to the hypothesis that there is another major factor contributing to the resting potential of the muscle cell which may be an electrogenic active transport system (Brading and Caldwell, 1971).

In vivo the muscle bags are surrounded by perienteric fluid with the ionic concentration (mM): Na 129; K 24; Ca 6; Mg 5; Cl 53; organic anions 120 (Hobson, Stephenson, Beadle, 1952). It is pointed out that the majority of electrophysiological experiments (Brading and Caldwell, 1964; Caldwell and Ellory, 1968; Martin, 1980;1982) use solutions where the effects of different organic anions were not considered and in most cases they are only replaced by acetate or chloride. The importance of the high organic anion concentrations to the maintenance of the resting potential of the muscle cell has yet to be investigated. The mechanism by which the cell maintains the resting potential has yet to be elucidated although

several possible mechanisms have been suggested, none of which are completely satisfactory, these are described as follows:

(I) Compensatory changes in membrane conductance

The idea that, in *Ascaris*, compensatory changes in membrane permeability counteracted changes in ion concentration was first raised by Brading and Caldwell (1964). Subsequent work using ion flux experiments (Caldwell and Ellory, 1968) have disproved this hypothesis.

(II) The Na shunt conductance.

The muscle cell was found to be insensitive to alterations in the external potassium concentration but responded to changes in external chloride concentrations. From these observations Del Castillo, De Mellow and Morales (1964a) concluded that a chloride battery with a low internal resistance was largely responsible for maintenance of the resting potential. Both the Cl and the K batteries in *Ascaris* were shunted by a high sodium conductance. It is interesting that the membrane potential of vertebrate smooth muscle is also dominated by a Cl battery which is shunted by a high Na conductance.

(III) Operation of an electrogenic pump.

Brading and Caldwell (1971) studied the effect of ion replacement on muscle cells using the Goldman-Hodgkin-Katz equation (Hille 1992) and the assumption that the constant field theory is applicable to *Ascaris* muscle cells. Their findings implied that the contribution of K, Na and Cl ions could not account for the whole resting membrane potential of the muscle cell and another major factor (as yet unidentified)

had to be considered. Brading and Caldwell (1971) suggested a carboxylic acid transport system associated with Na transport. However they also concluded from their experimental results that GABA did not affect P_{Cl} or P_K but inhibited the carboxylic acid transport system. More recent work has demonstrated that GABA does not exert its effect by such a mechanism, instead GABA activates a chloride conductance in the parasite muscle (Martin, 1980). The differences in the findings of Brading and Caldwell (1971) on the effects of GABA make the above hypothesis difficult to accept. However, it seems plausible that organic anions play an important (if undefined) role in the maintenance of the resting membrane potential.

2.4 Ionic currents and ion-channel types observed in the muscle cell

Three types of voltage activated currents have been observed (using the two electrode voltage-clamp technique) in *Ascaris* muscle (Martin, Thorn, Gration and Harrow, 1992). There are two types of potassium current (I_A-like and I_K-like). The I_A-like current is a transient current that inactivates with time constants of 10-50 ms at holding potentials more positive than -40 mV and is blocked by 4-aminopyridine (4-AP). The I_K-like current is not blocked by 4-AP and is not significantly deactivated at potentials more positive than -40 mV. Both the I_A-like and I_K-like currents have been observed in *Ascaris* somatic muscle cells. A calcium current has also been described in *Ascaris* muscle. The properties of the calcium current of *Ascaris* differ from those described in other cell types (*e.g.* Kostyuk *et al.* 1988). The Ca current of *Ascaris* inactivated but required a relatively depolarised potential for activation. The current was not inactivated by a holding potential of -35mV. Martin *et al* (1992) postulate that the Ca current allows the production of depolarising spikes in *Ascaris* muscle; they further postulate that the potassium currents contribute to the "slow

waves" and "modulation waves" observed in *Ascaris* muscle by Weisblat, Byerly and Russell (1976).

Application of acetylcholine to *Ascaris* muscle strips caused depolarisation and contraction (Del Castillo, De Mellow and Sanchez, 1963). Martin (1982) demonstrated that the acetylcholine receptors were not restricted to the muscle syncytium region and were present on the bag region of the muscle cell. These non-junctional receptors were shown to be non-selective cation channels (permeable to calcium ions) and classed as nicotinic. Patch-clamp of the *Ascaris* nicotinic acetylcholine receptor have shown two conductance levels (40-50pS and 25-35pS) both with mean open times around 2 ms (Pennington and Martin, 1990). More recent studies by Martin and Valkanov (1996) have shown that acetylcholine also effects a slow voltage-activated non-selective cation current in the bag region of the *Ascaris* muscle cell. The current was called I_{bcat} and displayed certain similarities to the I_K-like current recorded from whole muscle cells. Application of acetylcholine increased the amplitude of I_{bcat} however, the current was not antagonised by either mecamylamine or tubocurarine demonstrating that the receptors involved were not nicotinic. Atropine had no antagonistic effect on I_{bcat} demonstrating the current was also pharmacologically different from mammalian muscarinic receptors however the authors postulate that the current may have physiological similarities to muscarinic receptors *i.e.* receptor indirectly coupled to ion-channel via a G protein (Martin and Valkanov, 1996)

Bath application of GABA produces muscle relaxation, cell membrane hyperpolarisation (Del Castillo *et al.* 1964b) and an increase in membrane conductance (Martin, 1980; Holden-Dye, Hewitt, Wann, Krogsgarard-Larsen and Walker, 1988). The GABA receptor (in common with the *Ascaris* acetylcholine

receptor) was found not only at the neuromuscular junction but also extrasynaptically on the muscle bag region (Martin, 1980). The GABA receptor was found to be a chloride channel with a linear conductance of 22±1.2 pS and multiple subconductance levels (Martin, 1985; Duittoz and Martin, 1991). The *Ascaris* GABA operated chloride channel differs from those found in vertebrates and other invertebrates in that it is not blocked by picrotoxin or by tert-butylbicyclophosphothionate (TBPS)(Holden-Dye *et al.* 1988) although it does display similar permeability characteristics to all other GABA-operated chloride channels (Parri, Holden-Dye and Walker, 1991). The muscle bags also contain a high-conductance calcium-dependent chloride channel (Thorn and Martin, 1987). The properties and function of the high-conductance calcium-dependent chloride channel are discussed in section three of this chapter.

3 Anion Selective Ion-channels

3.1 Classification of chloride channels

Generally chloride currents can be divided into three main classes with subdivisions within in these classes (Franciolini and Petris, 1990; Kuriyama, Kitamura and Nabata, 1995). The first major class of chloride current are the voltage-dependent type. These can be further subdivided into depolarisation induced chloride currents, hyperpolarisation-induced chloride currents and bell-shaped voltage-dependent currents, many of the channels in these groups display the property of "excision excitation". The second major class of chloride current are the calcium-dependent chloride currents. The third class of chloride channel are the ligand gated chloride channels.

3.2 Properties and examples of each class of chloride channel.

Depolarisation-induced chloride currents

These chloride channels are activated by depolarisation (Franciolini and Petris, 1990). The group can be subdivided on the basis of conductance. Large conductance channels are found in several cell types including molluscan nerve and aortic smooth muscle, conductances are in the range of 150 to 500pS. Intermediate channels with conductances in the range of 20 to 70pS have been observed in keratinocytes and skeletal muscle (Blatz, 1990). Small conductance channels have been observed in aorta, keratinocytes and *Torpedo* with conductances between 1pS and 15pS. In general, channel activity in this group is independent of calcium concentration.

Hyperpolarisation-induced chloride currents

In aplysia neurons, hyperpolaristaion of the membrane from -50mV to -80mV increased the current amplitude in a time-dependent manner (Franciolini and Petris,

1990). The increase in current was due to a chloride channel with a unitary conductance of 10-15pS. A similar channel in rat pyramidal cells reached maximum activity at -90mV and was completely inactivated at -10mV, the channel was active at the cells resting potential of between -55mV and -70mV. The channel was blocked by the classical chloride channel blockers 4-acetamide-4′-isothiocyanostilbene-2,2′ disulfonate (SITS), 4,4′-diiso-thiocyanostilbene-2,2′ disulfonate (DIDS), and also by phorbol esters (Madison *et al.* 1986).

Bell-shaped voltage-dependent chloride currents

Ion-channels in this class have some unusual features. The single-channel conductance is large ("maxi"); between 210pS and 630pS. The channel is most active at 0mV, depolarisation or hyperpolarisation by as little 20mV away from 0mV closes the channel giving the "bell-shaped" voltage dependence. The channel also displays excision activation (Gray *et al.* 1984). To date the channel type has been identified in several cell types, including secretory epithelial cells (Kolb *et al.* 1985), rat skeletal muscle (Blatz and Magelby, 1983), alveoli (Schneider *et al.* 1985), and Schwann cells (Gray *et al.* 1984).

Calcium-dependent chloride currents

Channels in this group generally display less voltage sensitivity than members of the previous three groups. Channel opening is largely dependent on the concentration of calcium *e.g.* chloride channels from rat spinal cord were closed in the presence of 10nM calcium but the probability of channel opening was markedly increased in the presence of 0.5μM calcium. Channels in this class display a wide range of conductances from 380pS in oocytes (Young *et al.* 1984) to 23pS in rat spinal cord (Mayer *et al.* 1990), channel conductances as small as 0.4 to 0.5pS have been reported in mast cells and *Xenopus* oocytes.

Ligand gated chloride channels

There are at least three major agonists that have been demonstrated to activate chloride channels (for review see Franciolini and Petris, 1990): γ-aminobutyric acid (GABA) and glycine both of which are transmitters at inhibitory synapses in the central nervous system; acetylcholine induces the cholinergic response in molluscan neurons. In *Ascaris suum,* a GABA-gated chloride channel has been recorded from somatic muscle derived membrane vesicles (Martin, 1980). More recently a glutamate-gated chloride channel has been isolated from *C. elegans* and expressed in *Xenopus* oocytes; it is believed that this channel is the site of action for the avermectin group of anthelminthics (Cully, Vassilatis, Liu, Paress, Vanderploeg, Schaeffer, 1994). The GABA and glycine gated chloride channels have been studied in detail in cultured mouse spinal neurons (Bormann *et. al.* 1987). In general the channels display multiple conductance levels ranging between 46 pS and 12 pS in 143 mM KCl. There was no apparent voltage sensitivity in the range -90 mV to +50 mV.

3.3 Properties of the high conductance, Ca-dependent chloride channel in *Ascaris suum.*

The single-channel conductance has been reported as 200±7 pS in symmetrical 175mM chloride solution (Thorn and Martin 1987) and 144.3±1.4 pS in symmetrical 140mM chloride solution (Dixon, Valkanov and Martin, 1993). At positive membrane potentials the channel has been observed to rectify in around 50% of experiments and subconductance states are frequently observed (Thorn and Martin, 1987). A halide selectivity sequence of I > Br > Cl > F has been deduced indicating a cationic binding site of low field strength within the channel pore (Dixon *et al*, 1993). Substitution of internal chloride with various carboxylic anions caused large hyperpolarising shifts in the reversal potential (Valkanov *et al*, 1994). The channel has a pore diameter of ≈6.55 Å predicted from plots of organic ion permeability ratios against ionic size (Valkanov *et al,* 1994). The 6.55 Å channel pore is larger than the 5.6 Å and 5.2 Å pores reported for GABA and glycine gated chloride channels (Bormann *et al*, 1987) but smaller than the predicted pore size of 20 Å for the large conductance chloride channel found in Schwann cells (Gray, Bevan and Ritchie, 1984).

The channel has its highest probability of opening close to the observed resting membrane potential of the cell (around -30 to -40 mV) and has a much reduced probability of opening at positive membrane potentials (Thorn, 1987). During single-channel recording experiments it was observed that the channel frequently "ran down" and no channel activity could be observed after a few minutes. The rapidity of channel run down was increased at positive membrane potentials compared to negative potentials (Robertson and Martin, unpublished observations). The last observation may suggest that second messengers, other than calcium, may also be involved in activation of this channel.

3.4 Function of the high conductance, Ca-dependent chloride channel in *Ascaris suum.*

The inward rectification exhibited by the channel (Thorn and Martin, 1987) excludes an effective role for the channel in repolarisation of the cell as opposed to some other chloride channel types. Since the channel is open at the resting membrane potential of the cell (Thorn and Martin 1987) and can conduct volatile fatty acids across the muscle membrane a role in the excretion of waste carboxylic anions (produced during anaerobic respiration of glycogen) has been suggested (Valkanov *et al*, 1994). The channel is more likely to open as the internal calcium concentration is increased (Thorn and Martin, 1987) which also supports the excretory hypothesis: an increased calcium concentration usually accompanies muscular activity which in turn gives an increase in respiratory waste products. The normal intracellular pH of the *Ascaris* muscle cell has been reported to be 7.37 (Del Castillo, Rivera, Solorzano and Serrato, 1989), but changes with muscle activity have not been studied.

The possibility of an excretory function for the Ca-dependent chloride channel was examined in more detail by Valkanov and Martin (1995) who studied the permeability of the channel to various dicarboxylic anions plus lactate and pyruvate. It was found that all the anions tested, except for malate were conducted by the channel. The ability of the channel to conduct oxaloacetate, lactate and pyruvate might be regarded as evidence against an excretory role for the channel as these compounds are important metabolic intermediates and not waste products. Loss of these ions would represent a significant energy drain on the cell. However, although the channel is capable of conducting these ions, the situation *in vivo* due to the activities of various metabolic enzymes means that the pyruvate, lactate and oxaloacetate ions do not have high cytoplasmic concentrations (Saz, 1981; Tielens,

1994). The only metabolic intermediate that does reach a high concentration in the muscle cell cytoplasm is malate which does not pass current through the channel.

CHAPTER 2: MATERIALS AND METHODS: Effect of pH on the high-conductance Ca-dependent Cl^- channel from *Ascaris* muscle vesicles

2.1 *Ascaris* Preparation

Collection and maintenance of Ascaris suum

Adult *Ascaris* (Figure 2.1) were obtained from the local slaughter house on a weekly basis. After removal from the intestines of freshly slaughtered pigs, the worms were placed in a thermos flask containing Locke's solution (Table 2A) at ~35°C. On arrival in the laboratory, worms were transferred to 1.5 litre plastic beakers containing warmed Locke's solution. The beakers were placed in a water bath at 35°C: the 2°C reduction from the *in vivo* temperature was to assist parasite longevity by slowing down the worm's metabolic processes. The water bath was located in a fume hood to protect staff from inhalation of the fatty acyl waste products of the worm and prevent exposure to the potent antigens these worms produce. The Locke's solution was changed daily and, in general, parasites were discarded after 4 days. Parasites <10cm in length were discarded as dissection was difficult and often resulted in damage to the somatic muscle cells. Parasites showing little motility when disturbed were also discarded.

The Ascaris vesicle preparation

Parasites were selected daily and the anterior (3-5cm) section was discarded. The next 2cm section of worm was removed and dissected along one of the lateral lines. The resulting flap preparation was pinned, cuticle side down, onto Sylgard™ (Sylgard184 silicone elastomer kit, Dow Corning Corporation, Midland, M.I. 48640, USA) and the gut removed with a fine pair of forceps. The muscle flap preparation (Figure 2.2a) was washed (x3) with warm (37°C) extracellular solution (Table 2A). The washed flap was then incubated in collagenase solution (Table 2A) for 10

minutes at 37°C. Following collagenase treatment and three washes with warm extracellular solution the preparation was maintained in extracellular solution at 37°C. Approximately 1 hour after collagenase treatment vesicles could be observed "budding off" the membrane of the bag region of the somatic muscle cells (Figure 2.2b and2.2c). Collagenase treatment digested away the extracellular matrix and induced the formation of smooth, clean, vesicles suitable for obtaining seals of giga-ohm resistance. Vesicles were harvested with a Pasteur pipette and used within 4 hours. Longer collagenase treatments tended to produce fragile vesicles which ruptured when brought into contact with the patch pipettes. Vesicles were transferred to the experimental chamber and bathed in recording solution (Table 2A). Experiments were carried out at room temperature (15-22°C). The vesicle preparation has been described previously (Dixon and Martin, 1993).

Figure 2.1:

Figure 2.1: A photograph of a mature *Ascaris suum.* The scale bar is in centimetre divisions. The anterior of the parasite is the more pointed of the two ends, also clearly observable is one of the lateral lines. The distinctive orange\pink colouring is due to the haemoglobin produced by the mature worm.

Figure 2.2:

A: Photograph of *Ascaris* muscle flap preparation. One lateral line and nerve cord are labelled and easily distinguished.

B: An area of the flap preparation at higher magnification. Vesicles can be observed forming from the bag region of the muscle cell.

C: A higher magnification photograph of an individual vesicle.

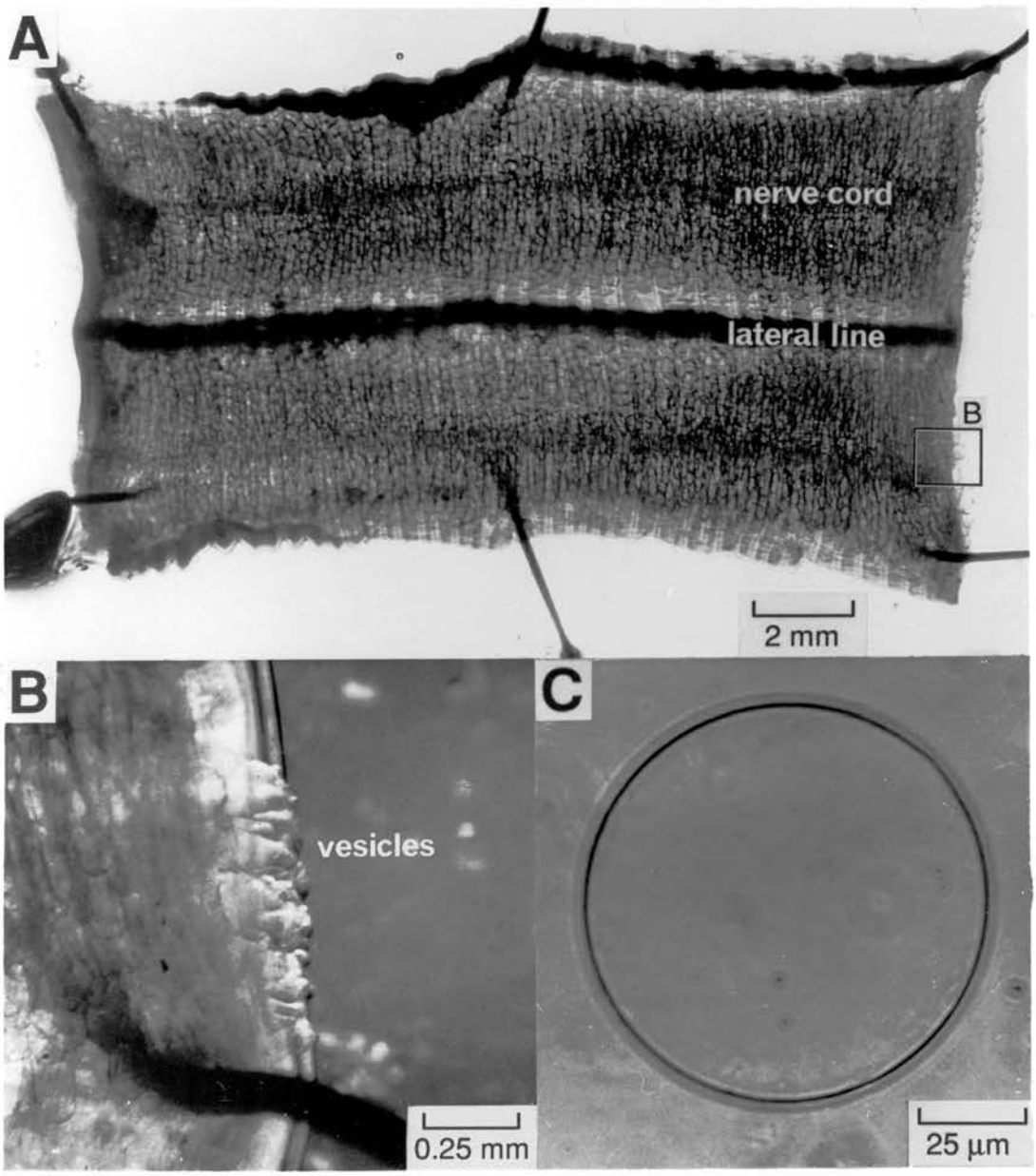
A
nerve cord
lateral line
B
2 mm
B
vesicles
0.25 mm
C
25 µm

Table 2A

Solution	Constituents
Locke's Solution	NaCl, 154; KCl, 5.6; $CaCl_2$, 2; $NaHCO_3$, 1.7; glucose, 5.5.
Extracellular Solution	NaCl, 35; NaAcetate, 105; KCl, 2; $MgCl_2$, 2; HEPES, 10; glucose, 3; ascorbic acid, 2; EGTA, 1; pH adjusted to 7.2 using NaOH.
Collagenase Solution	NaCl, 35; NaAcetate, 105; KCl, 2; $MgCl_2$, 2; HEPES, 10; glucose, 3; ascorbic acid, 2; pH adjusted to 7.2 using NaOH; 0.5mg/ml Collagenase (Type 1A, SIGMA).
Recording Solution	CsCl, 140; $Mg(Acetate)_2$, 2; $Ca(Acetate)_2$, 1; HEPES, 10 adjusted to desired pH with CsOH.

Table 2A: Solutions used in experiments on *A. suum*. Concentrations are in mM.

2.2 The patch-clamp technique

The patch-clamp technique allows the resolution of currents from single ion-channels in an isolated patch of membrane. Briefly, a small glass pipette is brought into contact with a "cleaned" cell membrane and gentle suction applied. This results in the formation of a "giga-ohm seal". The high resistance of the seal reduces background noise when a voltage is clamped across the membrane patch thus allowing the resolution of current changes in the pA range. The patch-clamp technique has been described previously (Hamill *et al.,* 1981) and is outlined below.

Manufacture of patch electrodes

The bath electrode was composed of a silver/silver chloride wire, prepared by fusing silver wire with molten silver chloride. The electrode was inserted into a polythene tube containing 2% agar made up with 150mM KCl solution. This "agar bridge" was used to minimise junction potentials. In experiments where the junction potentials between the bath solution and electrode were not significant the agar bridge was not employed.

Patch electrodes were made from capillary glass (Garner Glass 7052, internal diameter 1.15mm, external diameter 1.55mm) pulled on a two stage vertical puller (David Kopf Instruments, Narishige Instruments). The diameter of the resulting pipettes was observed to be ~0.5μm. Pipette tips were coated with Sylgard™ to within 50μm. Sylgard™ coating produced a hydrophobic surface which reduced pipette/bath capacitance and background noise. Pipettes were then fire polished using a heated platinum wire viewed under the microscope (Vickers, x400). Fire polishing ceased when a visible change in tip geometry could be observed. Polishing smoothed any jagged edges of the pipette tip to facilitate seal formation. The pipette

tip was then filled with recording solution (Table 2A) using suction, the remainder of the pipette was back filled with the same solution.

Recording set-up

The experimental chamber was mounted on the stage of a Nikon (TMS-PH3) inverted microscope and viewed at x200 magnification. The microscope was placed on an Ealing-Bec anti-vibration table to reduce mechanical interference, this was further reduced by placing the table on a large concrete slab. The microscope was located inside an aluminium cage to screen out electrical interference. Patch pipettes were mounted in a suction pipette holder connected to the amplifier headstage by a BNC connector. The headstage was mounted on a Narishige hydraulic micromanipulator which in turn was mounted on a mechanical manipulator (Mitutoyo). Currents were monitored using a LIST EPC-7 current-voltage converter. Currents were filtered at 1kHz (3dB) by an 8-pole Bessel-type filter (Electronic Workshop, R.(D.)S.V.S.) and recorded on a Racal Thermionic Store Four FM tape recorder. Currents were viewed on a dual beam storage oscilloscope (HITACHI VC-6025) and a two channel pen recorder (Lectromed, type MX 216). A digitimer was used to trigger an isolated stimulator (Digitimer, model DS 2) which produced a 1mV voltage pulse at the pipette tip. The voltage pulse allowed the measurement of the pipette and seal resistance using Ohms law. Pipettes with a resistance of 1-5MΩ were used. A schematic diagram of the electrical set-up is shown in Figure 2.3. Each pipette was used only once, if a giga-ohm seal was not obtained, the pipette was discarded.

Figure 2.3: A schematic diagram representing the electrical components of the experimental set-up.

Figure 2.3

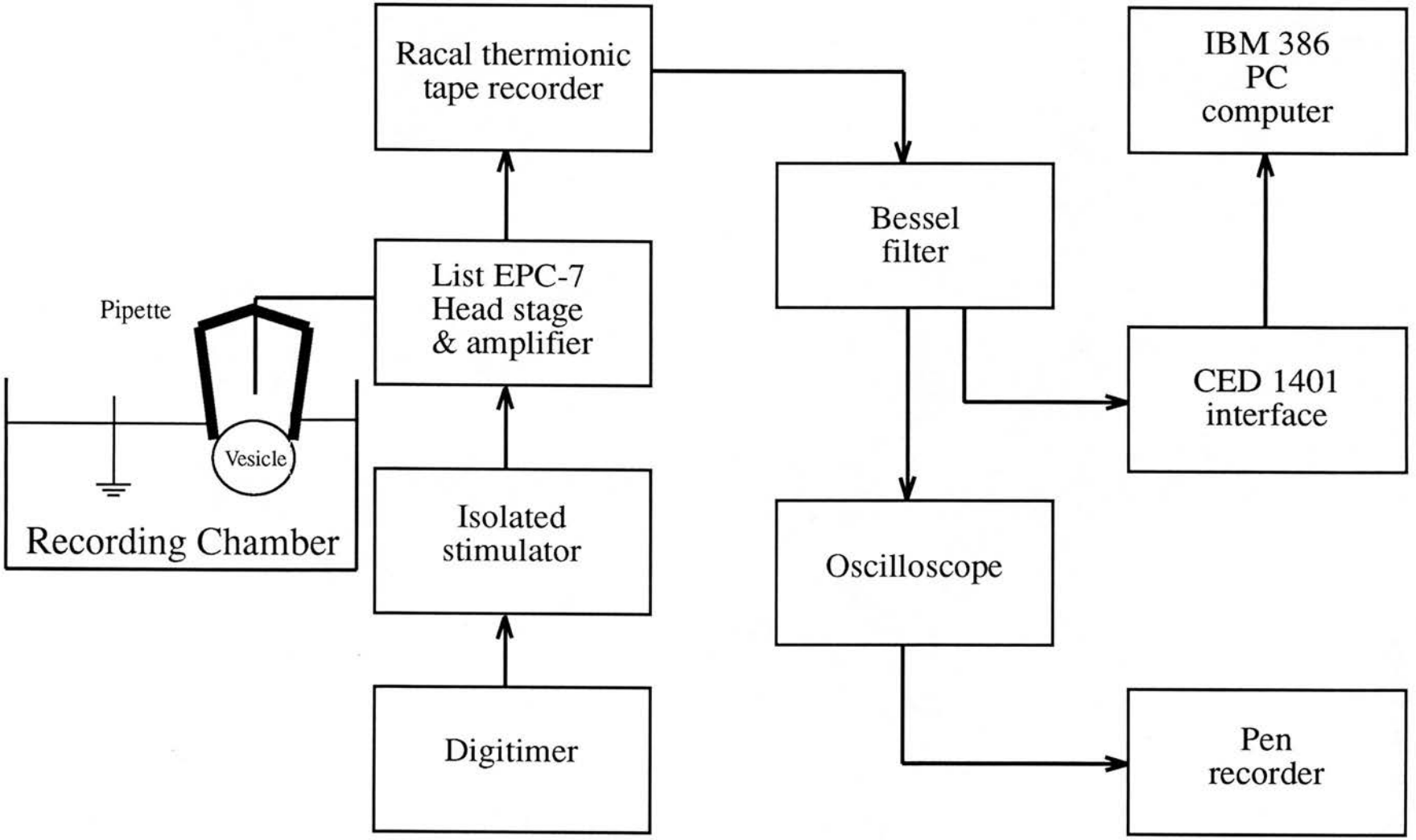
Racal thermionic tape recorder
IBM 386 PC computer
Bessel filter
List EPC-7 Head stage & amplifier
Pipette
Vesicle
Recording Chamber
CED 1401 interface
Isolated stimulator
Oscilloscope
Digitimer
Pen recorder

2.3 Obtaining an isolated inside-out membrane patch

The pipette tip was brought into close proximity of a vesicle using the coarse controls of the micromanipulator. The pipette tip was then carefully manoeuvred, using the fine controls of the micromanipulator, until it was in contact with the vesicle surface. Contact with the vesicle surface resulted in an increase in pipette resistance as a "loose" (low resistance) seal was formed between the pipette glass and the vesicle membrane. Gentle suction was applied via a silicone tube connecting a 1ml plastic syringe to the pipette holder. Suction brought the vesicle membrane and the glass of the pipette tip into closer association and resulted in an increase in the resistance of the seal from several MΩ to at least 1 GΩ. An isolated inside-out membrane patch was obtained by lifting the pipette tip from the surface of the vesicle whilst maintaining gentle suction. On isolation of the membrane patch the suction was released. At this point seal resistance was re-assessed and patches with a seal resistance < 1 GΩ were not studied further.

2.4 Experimental procedure

All experiments were carried out at room temperature (15-20°C). The bath and pipette were both filled with Recording Solution (Table 2A) adjusted to the desired pH with CsOH. Initial experiments involved recording single-channel currents with the pipette pH fixed at 7.2 and a bath pH of 6.0. Records were obtained at various positive and negative membrane potentials. The bath pH was then increased to 7.2 by adding CsOH. Further single-channel recordings were obtained at various membrane potentials. In many experiments the frequency of single-channel events, either openings or closures, decreased rapidly with time regardless of the membrane potential. The phenomenon was described as channel "run-down". Channel run-down occurred frequently and the time required for the above experiments was found to be prohibitively long.

Subsequent experiments involved the bath and pipette pH remaining constant throughout. Experiments were carried out with the pipette pH fixed at 7.2 and the bath pH fixed at either 6.0, 7.2 or 8.4. Additional experiments involved a pipette solution of pH 6.0 and a bath solution of pH 7.2. For each patch, current records were obtained for membrane potentials of -40, -30, -20, -10, 10, 20, 30 and 40mV.

2.5 Determination of channel conductance and current-voltage relationships

During each experiment the membrane potential was fixed at a steady level for periods >20 seconds, generally within the voltage range -40 to +40mV. The potential was fixed using the voltage clamp mode of the current-voltage converter (LIST EPC-7). At hyperpolarised membrane potentials the channel amplitude was calculated as the average value of 60 individual channel openings. This value was similar to the channel amplitude calculated by fitting a Gaussian curve to the amplitude histogram generated by the PAT analysis program version 6.1 (John Dempster, Strathclyde University). Briefly, the Pat analysis program sampled the current values every 0.1 s and plotted the results (as no. of observations versus current) to create the all points amplitude histogram. Peaks on the histogram correspond to the conductance state of the channels present *e.g.* for a patch with only one channel there would be two peaks corresponding to the channel in the closed- and the open-state. Gaussian curves were then fitted to the peaks on the amplitude histogram. The channel amplitude was calculated by subtracting the value of the closed peak from the value of the open peak. At positive membrane potentials, the presence of subconductance states made the determination of channel amplitude more difficult. At these potentials the channel amplitude was calculated as the mean value of the 60 largest single-channel openings. This value corresponded to one of the peaks on the amplitude histogram generated by the PAT program.

Current-voltage plots were compiled from the channel amplitude data for each experiment. A line of best fit to the current-voltage plots was obtained using a least squares regression program for the BBC-B microcomputer. The slope of the line of best fit gave the single-channel conductance. The point at which line of best fit crossed the voltage axis was the reversal potential. Since the solutions on each side of the membrane were identical, the reversal potential predicted by the Nernst equation was 0mV (Hille, 1992).

2.6 Determination of the probability of channel opening

The single-channel amplitude values and the amplitude histograms generated by the PAT program were used to determine the probability of channel opening (P_{open}). Values of P_{open} were obtained at each membrane potential for each individual experiment using the following equation:

$$P_{open} = (T_1 + 2T_2 + 3T_3 + \ldots\ldots\ldots nT_n)(n \times total\ time) \ldots\ldots\ldots\ldots\ldots [1]$$

where P_{open}= probability of channel opening; T_n= time with n (and only n) channels open; n= total number of active channels in the patch; *total time*= duration of patch recording at fixed membrane potential. T_n was calculated from the area under the amplitude histograms constructed from the channel records. n was determined from the all points amplitude histogram at membrane potentials where the channels were observed to be most active, n was calculated as the number of peaks on the amplitude histogram excluding the peak that corresponded to no channels open.

2.7 Determination of "Effective Gating Charge"

The relationship between mean $P_{open} \pm s.e.m.$ and membrane potential was plotted for each of the experimental conditions. The Boltzmann equation [2] was fitted to these plots by non-linear least squares regression using a FORTRAN program containing the NAG E04CCF subroutine:

$$P_{open} = P_{max} / [1 + Exp\ \{(V_{half} - V) / V_{slope}\}] \quad \text{.....[2]}$$

Where P_{max} is the maximum value of P_{open} allowed by the equation; V is the membrane potential in mV; V_{half} is the voltage at which the function is half its maximum value; V_{slope} is the slope factor. The values obtained from the Boltzmann equation were used to calculate the "effective gating charge" of the channel under each of the experimental conditions. The "effective gating charge" was calculated using:

$$Effective\ Gating\ Charge = (kT/ze) / V_{slope} \quad \text{.....[3]}$$

where k is Boltzmann's constant; T is absolute temperature on the Kelvin scale; z is the valence of the permeant ion and e is the elementary charge. The value of kT/ze under all experimental conditions was determined as 24mV (Hille, 1992).

2.8 Hill Coefficients

For experiments with a pipette pH (pH^o) of 7.2 the mean P_{open} ± s.e.m. at each bath pH (pH^i) was plotted for each of the hyperpolarised membrane potentials. Hill coefficients were calculated for each membrane potential using a FORTRAN computer program containing the NAG E04CCF subroutine and equation [4]:

$$P_{open} = \frac{R_{max}}{1 + \left(K_{50} / [H^+] \right)^{nH}} \quad \text{.....[4]}$$

where R_{max} is the maximum value of P_{open} allowed by the equation, K_{50} is the hydrogen ion concentration at which the equation reaches half of R_{max}, $[H^+]$ is the hydrogen ion concentration and nH is the hill coefficient.

2.9 Statistics

Values for P_{open} and reversal potential are given as mean± standard error. Statistical significance was assessed using analysis of variance.

CHAPTER 3: RESULTS: Effect of pH on the high-conductance Ca-dependent Cl^- channel from *Ascaris* muscle vesicles

3.1 Vesicle Preparation

Vesicles were prepared daily and used within 5 hours of enzyme treatment, after which time the preparation deteriorated to an extent where giga-seal formation was unlikely. Giga-seals were obtained from ~33% of attempts with new patch pipettes but channel activity was detected in only ~25% of all giga-seals. Not more than 15% of seals displaying channels retained activity for long enough to allow sufficient recordings to be made.

3.2 Initial Experiments

The initial experimental protocol, which involved recording channel activity, altering the bath pH (by adding CsOH) and making further recordings was found to be prohibitively long. In numerous experiments the occurrence of single-channel events (either openings or closures) declined rapidly with time, regardless of the holding potential, until no channel activity could be observed. The phenomenon was called channel run-down and was observed to occur under each of the experimental conditions. Channel rundown frequently prevented completion of these experiments. However, these experiments did demonstrate that a change in bath pH had a striking effect on single-channel activity. These experiments were not analysed further due to the difficulty of obtaining complete data sets. All other analyses were carried out on experiments obtained using the simplified protocol (pH fixed for duration of experiment) and then only on complete data sets.

3.3 Single-channel conductances

Figure 3.1 shows current-voltage relationships for individual experiments under each of the test conditions. For all experiments (regardless of pH) the current-voltage relationship was linear. The mean conductances ± s.e.m. for each pH condition are shown in Table 3A. Under control conditions the mean single-channel conductance was observed as 149.0 ± 5.8 pS, similar values for the conductance of the Ca-activated chloride channel have been reported previously (Thorn and Martin, 1987; Dixon, Valkanov, Martin, 1993). The changes in pH tested on each side of the membrane had no statistically significant effect on the conductance of the channel (Table 3A).

3.4 Reversal Potentials

Mean reversal potential values ± s.e.m. (for each of the experimental conditions) are shown in Table 3A. For each test condition the mean observed reversal potential values were within 3mV of 0mV; the reversal potential predicted by the Nernst equation (Hille, 1992). Analysis of variance demonstrated a statistically significant ($p<0.05,>0.02$) effect of pH on the reversal potential of the Ca-dependent chloride channel. The differences in reversal potentials between the control and test conditions were small but most evident when the pipette pH was reduced to 6.0

Figure 3.1: Single-channel current-voltage plots from isolated inside-out membrane patches under each of the pH environments tested (A-D). Each current-voltage plot is labelled with the pH conditions, the date the recordings were made, and the number of the experiment. Lines were fitted to the data points using least squares regression.

A: $pH^o=7.2, pH^i=7.2$. **B:** $pH^o=6.0, pH^i=7.2$. **C:** $pH^o=7.2, pH^i=6.0$. **D:** $pH^o=7.2, pH^i=8.4$.

Figure 3.1

(a)

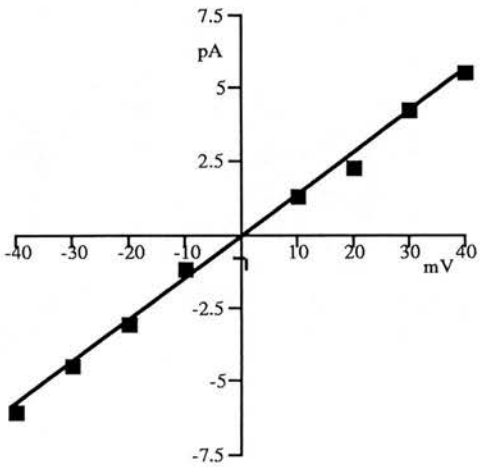

(b)

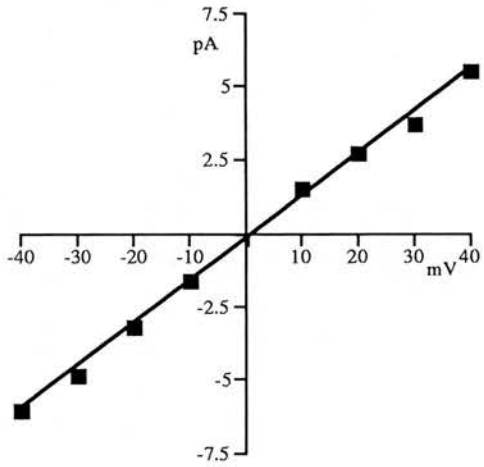

(c)

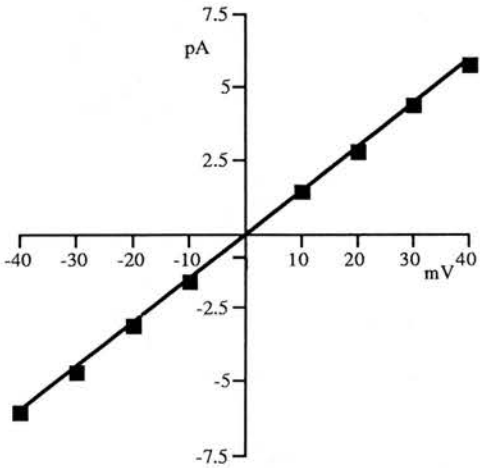

(d)

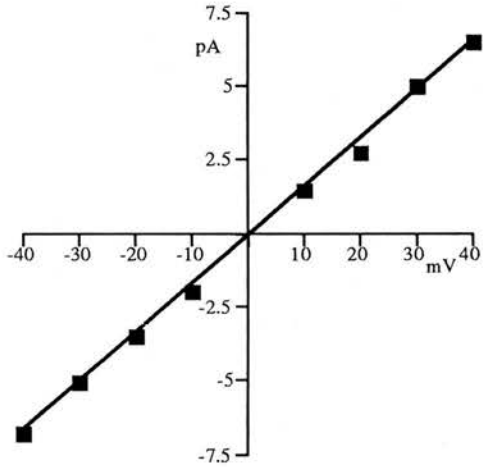

Table 3A

	Bath pH (pH^i)	Pipette pH (pH^o)	N	Mean Conductance ± s.e.m. (pS)	Mean Reversal Potential ± s.e.m. (mV)
Control	7.2	7.2	5	149.0 ± 5.8	+0.9 ± 0.4
Acid Bath	6.0	7.2	4	168.2 ± 4.5	+0.5 ± 0.4
Alkali Bath	8.4	7.2	4	146.0 ± 9.0	+0.7 ± 0.2
Acid Pipette	7.2	6.0	4	139.3 ± 4.0	+2.2 ± 0.3

Table 3A: Table summarising the current-voltage relationships under each of the experimental conditions. Conductance and reversal potential values are given as mean ± standard error. *N* = the number of patch experiment for each of the pH conditions.

3.5 Effect of pH on P_{open}

Figure 3.2 shows representative channel recordings at -40mV and +40mV from patches under each of the experimental conditions examined. The records suggest that the proportion of time the channels are open is greater at hyperpolarised membrane potentials compared to positive membrane potentials, except where there is a reduction in the bath pH to 6.0 where the converse applies. Analysis of variance showed that the effect of pH on the P_{open} - voltage relationship was highly significant ($P<0.0001$).

Effect of Reducing Pipette pH

Figure 3.3 shows the mean P_{open} ± s.e.m. values when the pipette pH (pH^o) was reduced to 6.0 Control values are presented for comparison. The control plot shows that the channel is most likely to be open around the resting membrane potential of the cell, (-30 to -40mV) with the mean P_{open} for -40mV and -30mV being 0.2071 and 0.2903 respectively. In contrast, P_{open} at +40mV is much smaller with a mean value of 0.0064 Previous studies have produced similar results for a symmetrical pH of 7.6 and a chloride concentration of ~175mM (Thorn and Martin, 1987). The reduced pH^o produced a marked increase in P_{open} over the range of hyperpolarised potentials tested: P_{open} -30mV = 0.502 at pH^o=6.0 There was also a small increase in P_{open} at most positive membrane potentials: pH^o7.2, P_{open} +30mV = 0.0269; pH^o6.0, P_{open}+30mV = 0.0577. The slope of the line generated by the best fit to the Boltzmann equation showed that the effective gating charge was negative for both conditions (Table 3B, pp59).

Figure 3.2: Inward (-40mV) and outward (+40mV) currents in isolated inside-out patches under each of the experimental conditions; **A:** Control; Bath pH=7.2, Pipette pH=7.2 (n=5); **B:** Bath pH=7.2, Pipette pH=6.0 (n=4); **C:** Bath pH=6.0, Pipette pH=7.2 (n=4); **D:** Bath pH=8.4, Pipette pH=7.2 (n=4). The pH conditions for each set of records are displayed in the diagrams of patches above each set of single-channel records. The labels c, o_1 and o_2 refer to closed (no channels open), one channel open and two channels open respectively. For each experimental condition n=number of experiments.

Figure 3.2

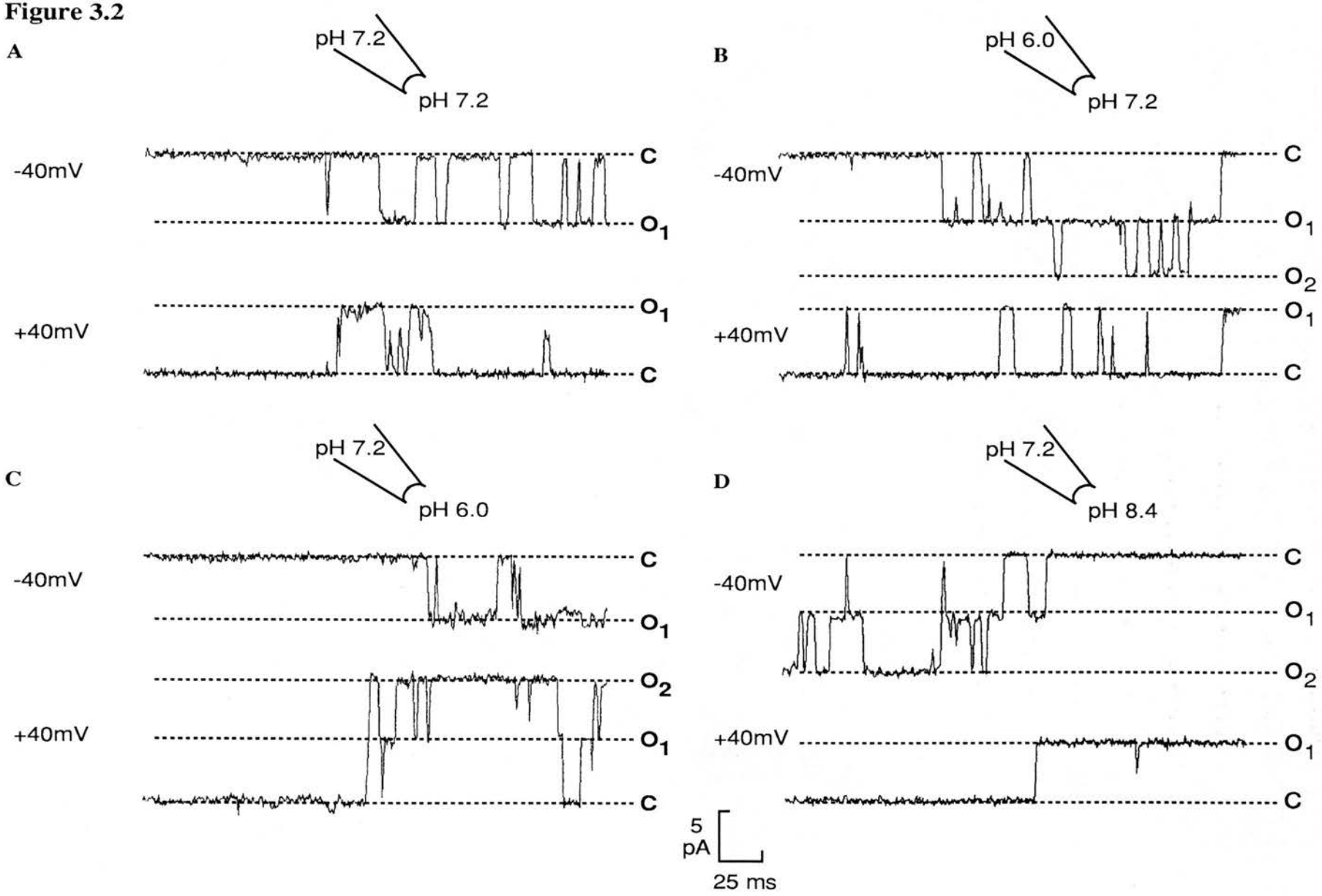
A
pH 7.2
pH 7.2
-40mV
C
O1
+40mV
O1
C
B
pH 6.0
pH 7.2
-40mV
C
O1
O2
+40mV
O1
C
C
pH 7.2
pH 6.0
-40mV
C
O1
O2
+40mV
O1
C
D
pH 7.2
pH 8.4
-40mV
C
O1
O2
+40mV
O1
C
5
pA
25 ms

Figure 3.3: Effect of acid pH^o on the P_{open} / membrane potential relationship. P_{open} values ± s.e.m. Control (■): pH^o 7.2, pH^i 7.2. Test (□): pH^o 6.0, pH^i 7.2.
Lines of best fit to each data set were obtained from the Boltzmann equation (see Materials and Methods, pp45).

Figure 3.3

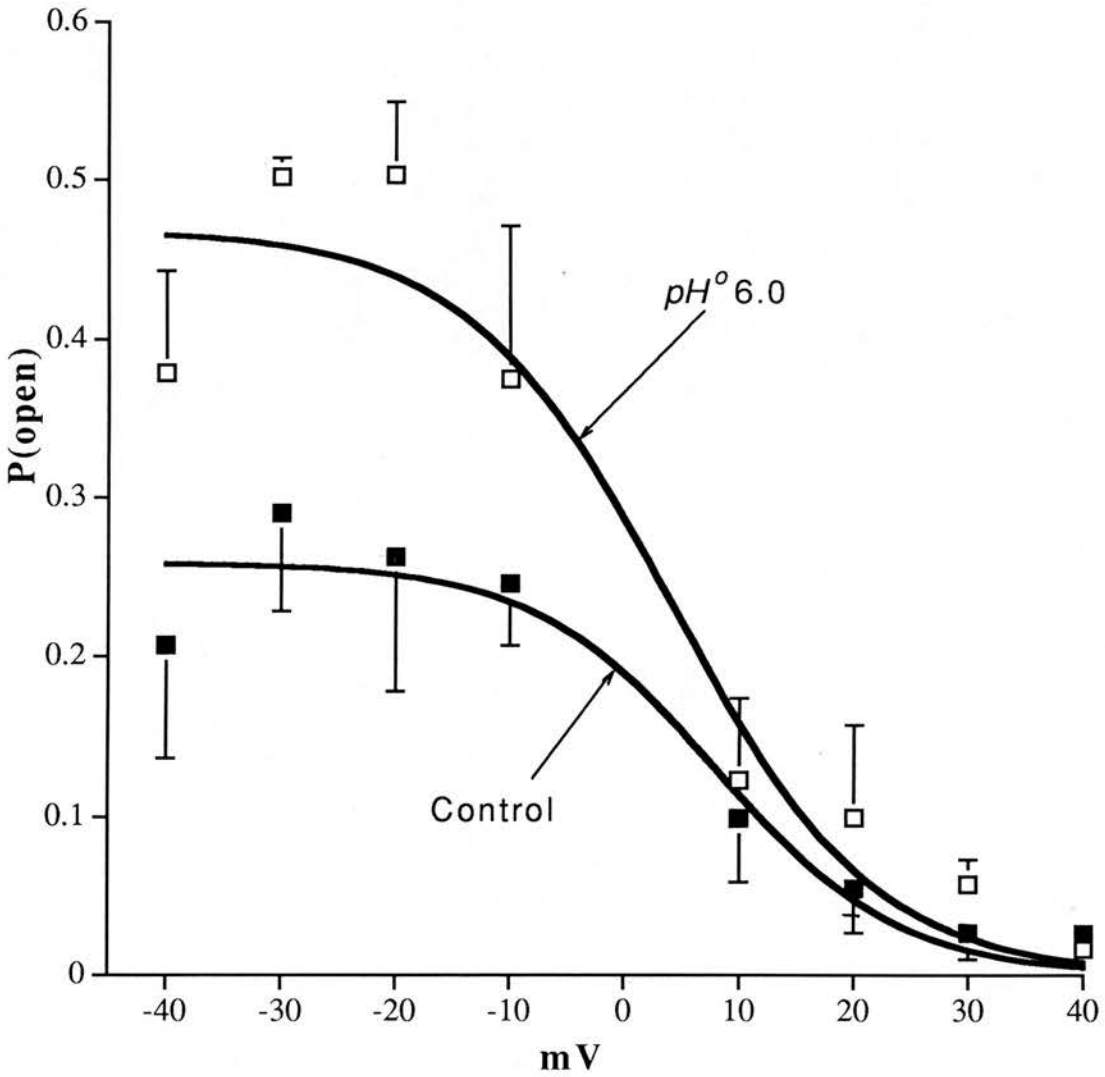

Effect of Increased bath pH

The effects of an increased bath pH (pH^i) are shown in Figure 3.4 with the values for control conditions present for comparison. The slopes of the fits to the Boltzmann equation indicate no change in sign of the "effective gating charge" associated with an increase in pH^i. However, the increase in pH^i produced a vertical shift in the P_{open}-voltage plot with P_{open} values at -30mV and +30mV of 0.2903 and 0.0269 respectively for pH^i=7.2 ; and 0.3544 and 0.0722 for pH^i=8.4. An increase in bath pH had the effect of increasing the probability of channel opening, the observed increase was independent of membrane potential.

Figure 3.4: Effect of alkali pH^i on the P_{open} -voltage relationship. P_{open} values ± s.e.m. Control (■): pH^o 7.2, pH^i 7.2. Test (□): pH^o 7.2, pH^i 8.4.

Lines of best fit to each data set were obtained using the Boltzmann equation (see Materials and Methods, pp45).

Figure 3.4

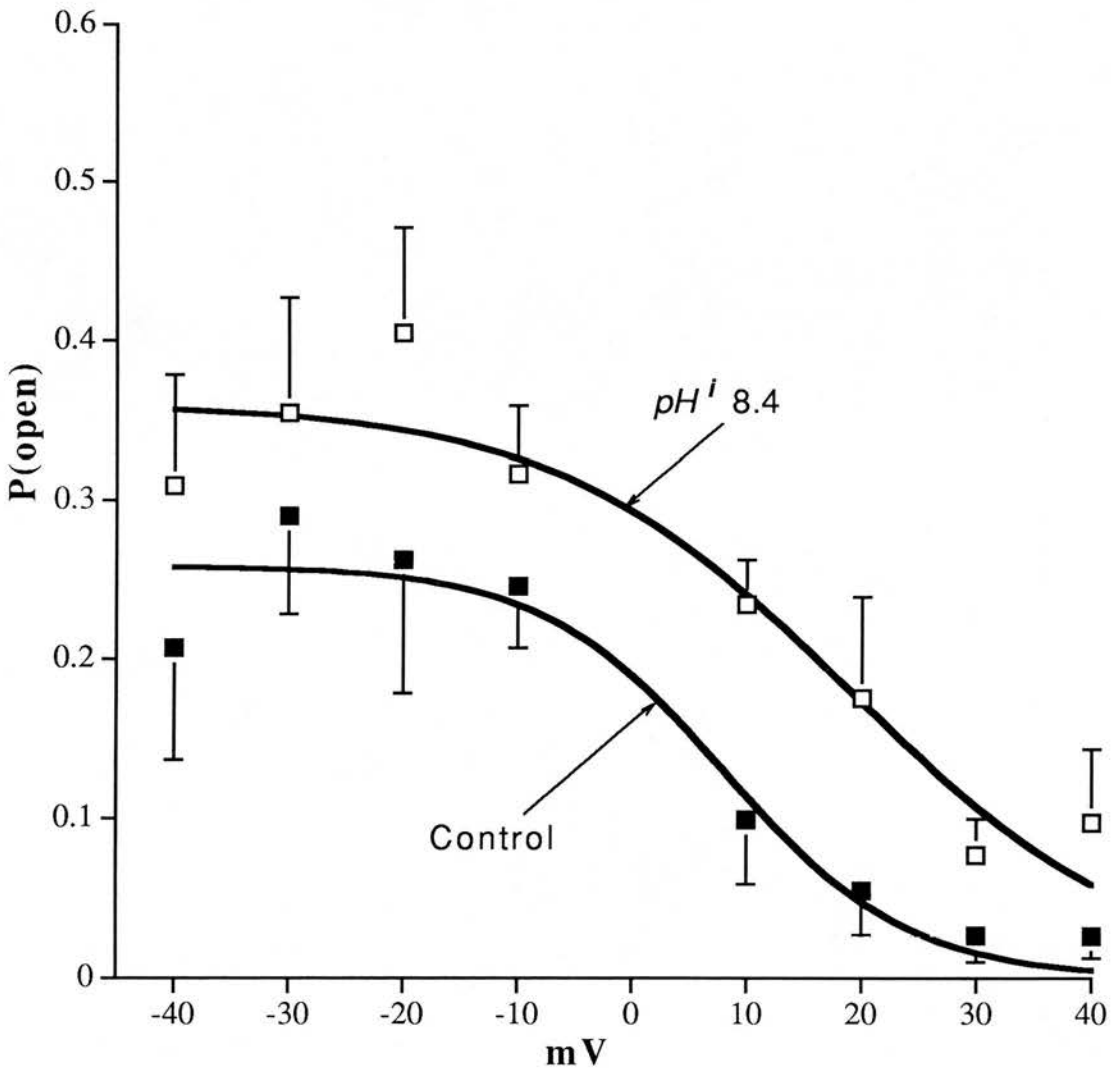

Effect of reduced bath pH

Figure 3.5 shows the effect of reducing bath pH (pH^i): Figure 3.5A shows the values obtained for mean P_{open}±s.e.m. when pH^i was reduced to 6.0; the mean P_{open}±s.e.m. for each of the potentials tested under the control conditions (symmetrical pH 7.2) are shown in Figure 3.5B for comparison. The results show that a fall in pH^i produced a reduction in P_{open} at hyperpolarised potentials (pH^i 7.2 P_{open} -30mV=0.290; pH^i 6.0 P_{open} -30mV=0.027). At positive membrane potentials P_{open} is increased when pH^i is reduced: under control conditions P_{open} +30mV=0.0269 this rises to P_{open} +30mV=0.2732 when pH^i=6.0. The slope of the line obtained from the Boltzmann equation is positive (Table 3B), indicating that the "effective gating charge" had become positive when pH^i was reduced. It is pointed out that the P_{open}-voltage relationship at pH^i=6.0 may be more complicated than described by the simple Boltzmann equation; depolarisation led to an increase in P_{open} followed by a small decrease. However, for comparative purposes and simplicity the relationship was described by a simple Boltzmann.

Hill Coefficients

The results obtained from the modified Hill equation for membrane potentials -10 mV to -40 mV are shown in Table 3C (pp 60). The Hill coefficients (nH) tend to decrease as the membrane potential tends towards 0 mV. At -30 mV and -40mV the nH values are greater than one, indicating that more than one proton is involved. At -20 mV and -10 mV the nH values were less than 1 indicating that only one proton was involved. The apparent variation can be explained if at more negative membrane potentials (-30 mV and -40 mV) a proton was removed from the ion-channel gate. Thus at -30 mV and -40 mV there were two binding sites for protons while at less negative (-20 mV and-10 mV) membrane potentials there was only one proton binding site available. The results for K_{50} tend to increase in value

from -40mV (0.105 μM) to -10mV (0.286 μM). As the membrane potential became more negative the K_{50} values decreased; if the voltage was affecting the local $[H^+]$ concentration the opposite effect would be observed. The Hill equation values were obtained from a curve fitted using three pH values for each membrane potential. The low number of points used to fit the curves and the resultant variation in the values across the potentials examined means that these results will not be discussed further.

Figure 3.5:

A: Relationship between mean P_{open}±s.e.m. and membrane potential with pH^i =6.0.

B: Relationship between mean P_{open}±s.e.m. and membrane potential under symmetrical pH 7.2 conditions.

Lines of best fit were obtained for both data sets from the Boltzmann equation (see Materials and Methods, pp45).

Figure 3.5

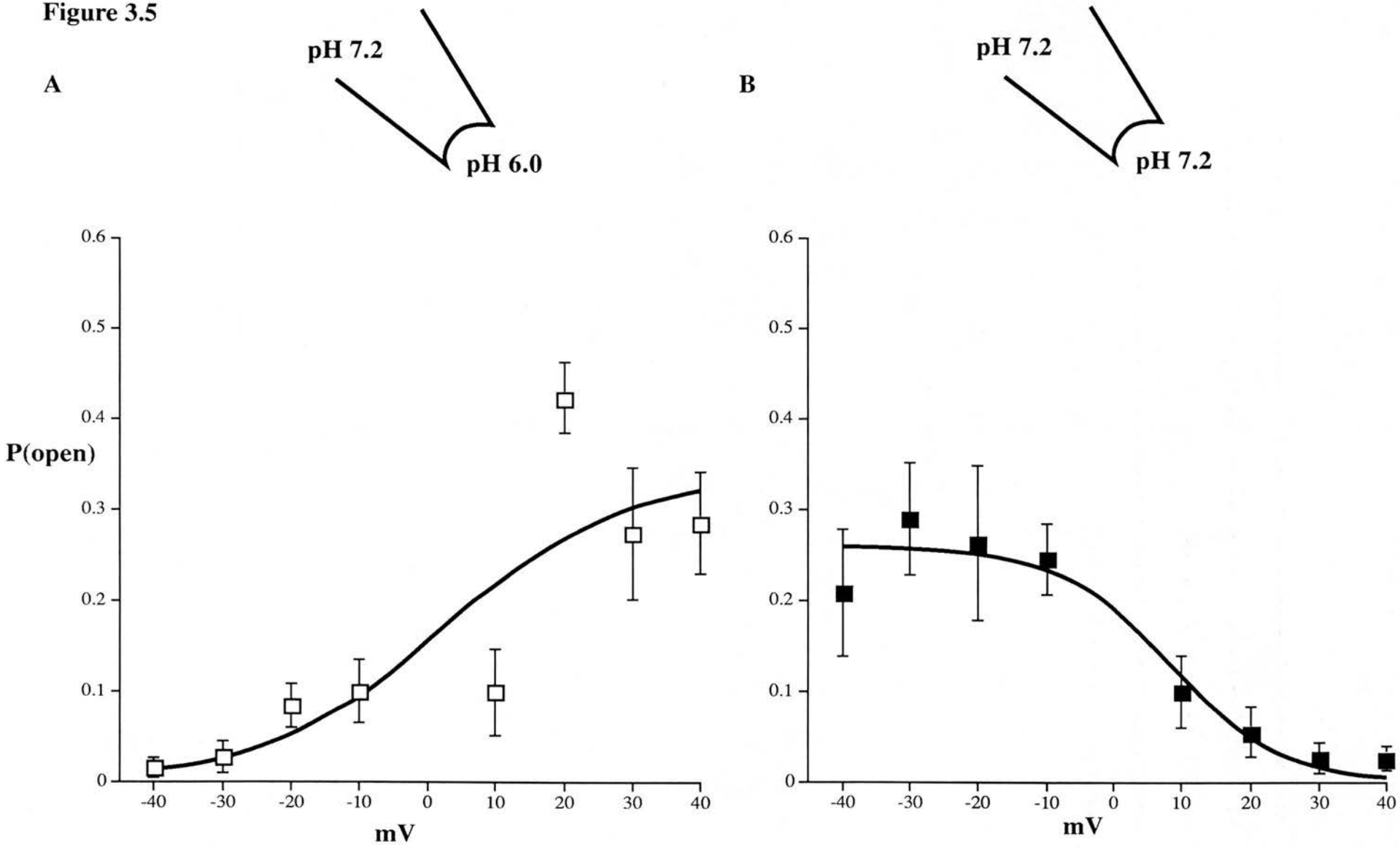
A
pH 7.2
pH 6.0
B
pH 7.2
pH 7.2
P(open)
0.6
0.5
0.4
0.3
0.2
0.1
0
-40
-30
-20
-10
0
10
20
30
40
mV
0.6
0.5
0.4
0.3
0.2
0.1
0
-40
-30
-20
-10
0
10
20
30
40
mV

Table 3B:

	Bath pH (pH^i)	**Pipette pH (pH^o)**	P_{max}	V_{half}	V_{slope}	**Effective Gating Charge**
Control	7.2	7.2	0.26	8.0	-8.0	-3.0
Acid Bath	6.0	7.2	0.34	2.6	13.1	+1.8
Alkali Bath	8.4	7.2	0.36	18.9	-12.9	-1.9
Acid Pipette	7.2	6.0	0.47	4.0	-8.8	-2.7

Table 3B: A summary of the values obtained from the Boltzmann equation for each of the experimental conditions. P_{max} is the maximum value of P_{open} allowed by the Boltzmann equation. V_{half} is the voltage at which the function reaches half P_{max}. V_{slope} is the slope of the line at the V_{half} voltage. The table also contains estimates for the Effective Gating Charge of the channel molecule calculated from the V_{slope} values.

Table 3C

	-40mV.	-30 mV.	-20 mV.	-10 mV.
R_{max}	0.313	0.356	0.452	0.333
K_{50}	0.105	0.176	0.104	0.286
nH	1.330	1.447	0.658	0.682

Table 3C: Table summarising the data from the modified Hill equation. Values are given for each of the negative membrane potentials tested (-40mV to -10mV). Where R_{max} is the maximum value for P_{open} predicted by the equation; K_{50} is the hydrogen ion concentration (μM) at which half the value of R_{max} is reached; and *nH* is the Hill coefficient. The Hill co-efficient values were greater than one for -30mV and -40mV and less than one for -20mV and -10mV.

CHAPTER 4: DISCUSSION: Effect of pH on the high-conductance Ca-dependent Cl^- channel from *Ascaris* muscle vesicles

The results show that changes in pH have no significant effect on single-channel conductances. The relationship between P_{open} and membrane potential, described by a Boltzmann equation, was significantly altered by changes in pH. The mechanisms involved in the pH sensitivity of this channel are considered and the physiological significance of the effects of pH is discussed.

4.1 Effect of pH on Surface Potential

Altered pH can lead to changes in surface charge that result in shifts in voltage dependence: negative shifts occur on increased extracellular pH and positive shifts occur on increased intracellular pH (Hille *et al.,* 1975; Hille, 1992). For example, extracellular acidification to pH 4.5 leads to a +25mV shift in the Na activation curve, whilst an increase in extracellular pH to 10 gives a -8mV shift (Hille, 1968).

The significant positive shift in reversal potential on extracellular acidification in the *Ascaris* chloride channel (Table 3A) implies that protons are altering the surface potential in a similar manner. The changes observed in V_{half} on altered pH^i are also consistent with proton concentration altering surface potential. The shift in V_{half} from the control value on reduced pH^o is not predicted by $[H^+]$ influencing surface potential and implies that protons are interacting directly with the channel molecule.

4.2 Channel Model and pH Sensitivity of Gating

Figure 4.1 shows a simple plausible model that explains the observed effects of pH on our *Ascaris* chloride channel. The selectivity filter (site A) may possess one or two cationic binding sites (Dixon, Valkanov and Martin, 1993); the lack of variation in the single-channel conductances suggests altered $[H^+]$ has no effect on these sites within the pH range tested.

Extracellular acidification produced increases in P_{open} without affecting gating charge, indicating the presence of a site (site B) only approachable from the extracellular solution. Binding of protons to site B causes conformational changes in the channel associated with an increased P_{open}.

Under symmetrical pH 7.2 conditions the voltage sensor (site C) has an overall charge of -3e (Table 3B, pp 59). Interestingly, the gating charge on *Torpedo* chloride channels is smaller, at +1e (Hanke and Miller, 1983) whilst Na, Ca and K channels have larger gating charges of between +4e and +6e (Zagotta and Aldrich, 1990). The dramatic effects that changes in pH^i have on gating charge indicate that the voltage sensor is located intracellularly to the selectivity filter. The Ca-dependent chloride channel is anion selective and will not conduct a significant amount of cations, including protons. The selectivity filter of the ion-channel (bearing positive charge) will not allow protons to pass from one side of the membrane to the other. The effective gating charge was most dramatically affected by changes in pH^i whilst pH^o had little effect. The above observation demonstrates that the voltage sensor (the area of the ion-channel bearing the amino acid residues that contribute to the effective gating charge) is located intracellularly to the selectivity filter.

The charge on the voltage sensor is sensitive to pH^i (in the range 7.2 to 6.0) and becomes positive at pH 6.0. The *pKa* values of amino acids suggest that only histidine has the appropriate properties to achieve the change in gating charge; the *pKa's* of other amino acids lie outside the pH range tested. It is therefore suggested that histidine is one of the constituent amino acids of the voltage sensor. The number of histidines that can be protonated is at least five (to allow for the change in gating charge from -3*e* to +2*e*); but probably more, for two reasons. Firstly, if the voltage sensor only moves part way across the membrane electric field (as the channel opens) the measured gating charge is less than the actual number of charges present on the channel "gate" (Hille, 1992). Secondly, studies on K^+ channels have shown that not all the charges on the voltage sensor contribute equally to the effective gating charge (Papazian et al. 1991; Logothetis et al. 1992).

Site D (Figure 4.1) is required to explain the increase in P_{open} with the increase in pH^i. It is suggested that the site located at D normally contains a positively charged residue that forms an ion pair with one of the negative charges on the voltage sensor, similar to suggestions made for Na channels (Stümer et al. 1989). The positively charged residue would lose its proton at high pH, facilitating the opening of the gate and explaining the observed increase in P_{open} at increased pH^i.

4.3 Limitations of the Model

The above model explains the effects of the pH values tested on the Ca-dependent chloride channel, but there are several obvious limitations. The Boltzmann model employed only allows for a single step between channel opening⇔closing, whereas previous studies have shown several open and closed states (Thorn and Martin, 1987) demonstrating that the gating process is more complex. Our model also shows the "effective gating charge" located on a single "gate" whereas, in K^+ channels, activation is brought about by 4 identical gating charges acting independently (Zagotta and Aldrich. 1980). The gating charges in the Ca-dependent chloride channel may also act independently: the reduction in the effective gating charge on increased pH^i could be caused by one of these charges being held in the open conformation due to decreased $[H^+]$.

Figure 4.1: A simple model of the Ca-activated chloride channel under control conditions.

A: Selectivity filter of the channel.

B: Proton binding site on the extracellular surface of the channel molecule, proton binding increases P_{open}.

C: Voltage sensor or "gate", under control conditions bears a charge of -3e. Decreased pH^i causes binding of protons to imidazolium side chains of histidine molecules which results in a change in the charge on the "gate" to +1.8e.

D: Positively charged site, binds to a negative charge on channel "gate" (site **C**)

Figure 4.1

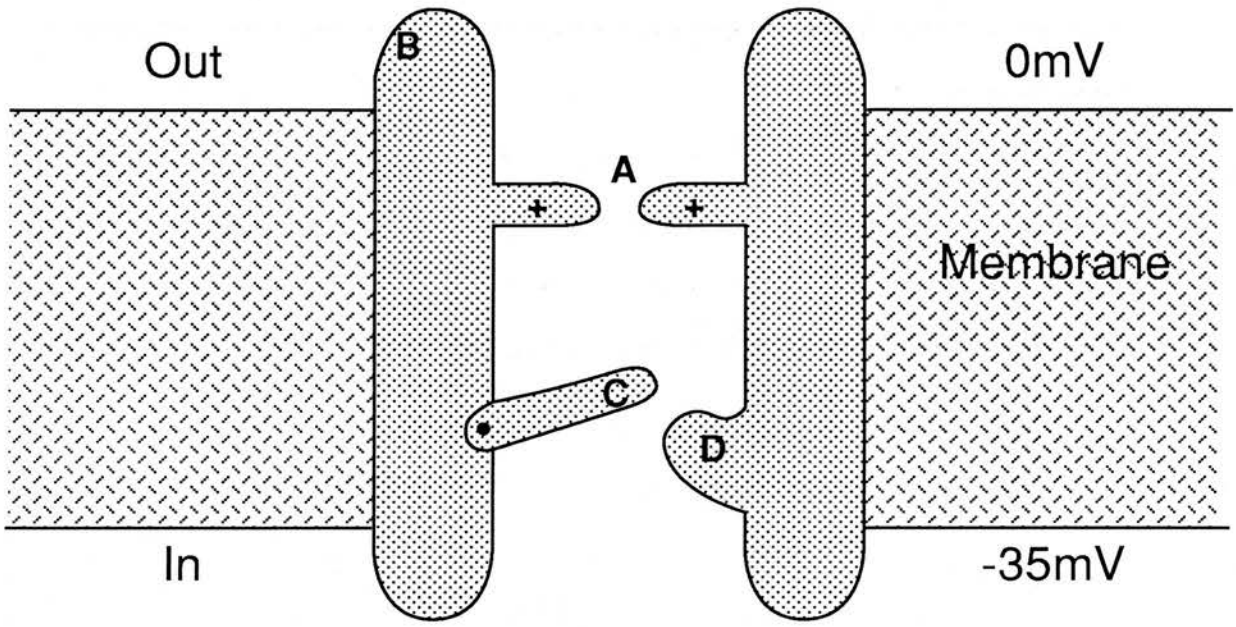

4.4 Physiological Significance

Our results show that the Ca-dependent chloride channel is dramatically affected by changes in pH. At a symmetrical pH of 7.2 the channel has a relatively high P_{open} at the resting membrane potential of the cell; when the pH on the intracellular side of the membrane (pH^i) is reduced to 6.0 channel opening is virtually abolished. We have hypothesised that the protonation state of several histidine residues in the channel molecule play an important part in this pH sensitivity. It is interesting that one of the glycolytic enzymes (phosphofructokinase) in *Ascaris* muscle also displays pH sensitivity (Rao *et al*, 1987), due to the protonation of histidine residues present within the enzyme.

In *Ascaris* the anaerobic respiration of glycogen gives rise to carboxylic acids as waste products (Saz and Weil, 1962). The pH of the muscle cell cytoplasm is reported as 7.37 (Del Castillo *et al,* 1989), while the *pKa* values of the waste carboxylic anions have an upper limit of 4.7. At physiological pHs the waste carboxylic acids are >99.2 % ionised suggesting that passive diffusion of the uncharged acid across the muscle cell membrane is an unlikely method of excretion. Under symmetrical (pH 7.2) conditions the Ca-dependent chloride channel is permeable to the waste carboxylic anions (Valkanov *et al,* 1994) and has its highest P_{open} around the resting membrane potential of the cell. These observations led to the hypothesis that the channel was responsible for the excretion of waste carboxylic anions (Valkanov *et al,* 1994). Anaerobic respiration in *Ascaris* also results in the production of protons which must be removed from the cell. The presence of an active ionic pump mechanism in the muscle cell has been suggested (Brading and Caldwell 1971). If there is an active proton pump in the bag membrane, its action would lead to an increased pH^i and an increase in the ionised:unionised concentration ratio of carboxylic anions. In turn the raised pH^i favours opening of

the Ca-dependent Cl channel. Thus the pH sensitivity of the channel may facilitate the excretion of waste anions.

SECTION II: MEMBRANE VESICLES PREPARED FROM THE TEGUMENT OF ADULT *SCHISTOSOMA MANSONI*: MICROSCOPY AND ELECTROPHYSIOLOGY.

CHAPTER 5: INTRODUCTION

5.1 General introduction and life-cycle of *Schistosoma mansoni*

Schistosomiasis is a debilitating parasitic tropical disease caused by a digenetic trematode worm of the genus schistosoma. The adult parasite lives in the blood vessels of man and the archaeological record shows the parasitic relationship to be at least 3500 years old. At present there are ~200 million people infected with schistosomiasis in >76 countries with an estimated 600 million people at risk of infection world-wide. At present, treatment of the disease relies heavily on praziquantel (PZQ). The effectiveness and lack of sided effects of PZQ are well documented (Andrews *et al*, 1983; Harnet, 1988) however, recent reports suggest that resistant strains may have developed (Fallon *et al,* 1995).

Schistosomiasis in man is mainly due to three species: *Schistosoma japonicum* is responsible for intestinal schistosomiasis in China; *S. haematobium* is responsible for urinary schistosomiasis in Africa and the Middle East; and *S. mansoni* which causes intestinal schistosomiasis in Africa, parts of Latin America and the Caribbean. Only the latter species was studied in this report and it's life cycle is outlined below (see also figure 5.1).

A vertebrate (man) and invertebrate (water snail) host are required for the completion of the *S. mansoni* life cycle. Mature eggs are ejected from the final (vertebrate) host via the faeces. On contact with fresh water the eggs hatch to release the miracidium, the first larval stage. The small ciliated miracidium must then encounter the correct species of invertebrate host to continue the life cycle. On contact with the invertebrate host the miracidium penetrates and transforms into the sporocyst. Within the sporocyst, permanently embryonic cells divide and

differentiate into the second generation of sporocysts. The pattern of cell division and differentiation is repeated but this time to generate cercariae, the next larval stage. The cercaria leaves the snail and is temporarily free living, this is the life cycle stage infective to the vertebrate host. Infection occurs by direct penetration of the host skin by the cercaria. After successful penetration the cercaria sheds it's tail and transforms into a schistosomulum. This life cycle stage follows a migratory path, via the bloodstream, to the lungs and finally the liver. Growth and maturation to the adult form occurs in the liver, adult male and female worms then pair and move into the veins of the mesenteries. The complete life cycle may take five weeks.

5.2 Schistosomiasis

Schistosomiasis is a chronic disease which produces a long term debilitating pathology. The first phase of the disease becomes apparent about two months after the initial cercarial exposure. The majority of infected humans display only minor symptoms or none at all. A few individuals develop an acute febrile illness at this stage due to the heavy new antigen burden produced by egg release. The majority of infected individuals continue in apparent good health during the chronic phase of the disease. Five or more years post infection there develops fibrovascular pathology with portal fibrosis, hypertension and with congestive splenomegaly. These conditions are difficult to resolve completely.

Figure 5.1

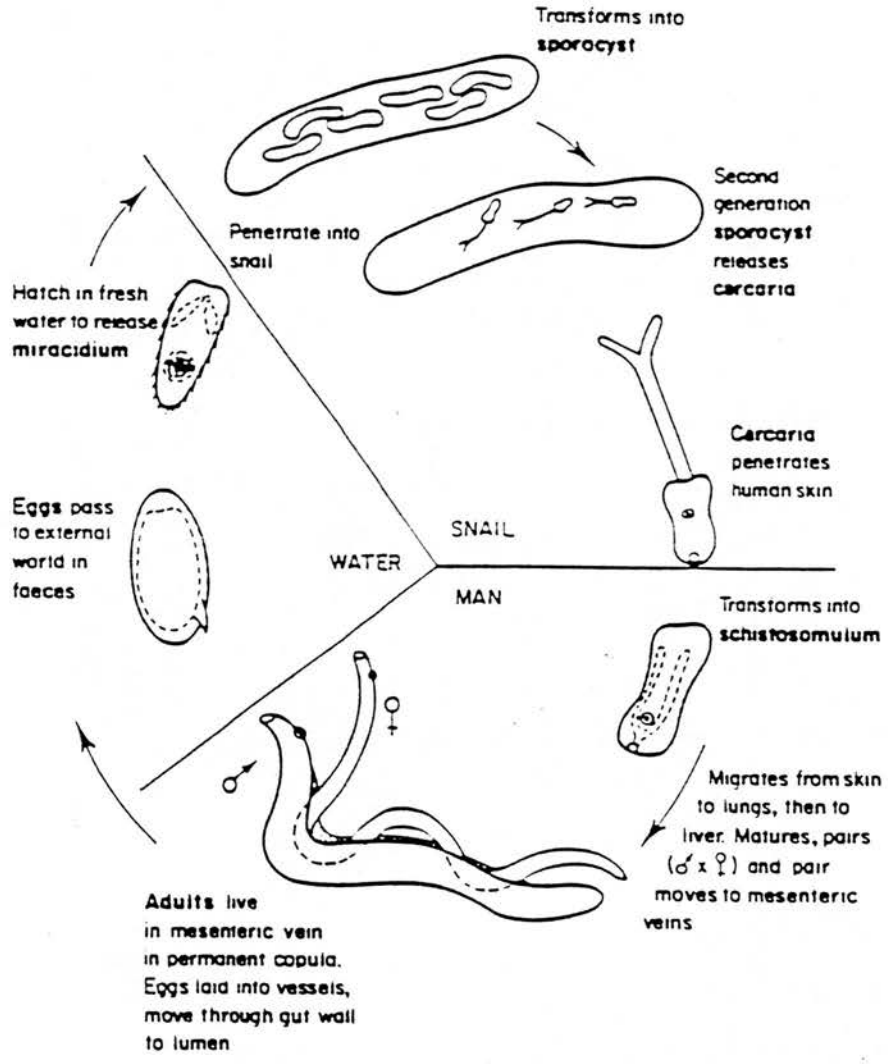

Figure 5.1: The life cycle of *Schistosoma mansoni* (reproduced from Wakelin 1984).

5.3 Anatomy of the schistosome

Schistosomes are almost unique among digeneans in that the sexes are separate and they live in the blood vascular system of the host: almost all other digeneans are hermaphrodite and live in the gut or associated body cavities of their host. *Schistosoma mansoni* was the first of the digeneans to be studied with the transmission electron microscope (Gönnert, 1955).

Both male and female worms are approximately 1cm in length, elongated and slender. The lateral margins of the male worm curve ventrally and overlap to form a gynaecophoric canal. The female worm is cylindrical, longer and more slender than the male; once paired the female lies in the gynaecophoric canal of the male with only its head and tail exposed.

5.4 *Schistosoma mansoni:* Surface Morphology

The dorsal surface of the adult male bears a large number of dome shaped structures known as tubercles. The tubercles bear a large number of pointed spines which are believed to anchor the worm in position by catching the blood vessel walls. The surface between tubercles bears some ciliated sensory organelles and is characteristically pitted in appearance. The ventral surface of the male displays the gynaecophoric canal; formed by the lateral edges of the body folding over each other. The ventral surface of the canal has a ridged appearance and also bears spines (although shorter and blunter in appearance to those on the tubercles). The spines are thought to hold the female parasite in position. Two suckers (oral and ventral) can also be observed on the ventral surface of the parasite. Both suckers bear spines and are pitted in appearance. The surface of the female is much smoother in appearance; the surface is pitted but bears relatively few spines and the dome shaped tubercles are absent. In addition, both sexes display dome-shaped protuberances on the surface

which are thought to have a sensory function (Senft and Gilber, 1977). The complex surface topography of the adult worm (especially the male) renders it unsuitable for patch-clamp studies.

5.5 The tegument of the adult schistosome

The tegument of the adult is ~4.0 μm thick. The pitted surface of the worm greatly increases its overall surface area. The presence of blood plasma in the surface pits (Bruce *et al,* 1971) suggest the tegument may play an important role in absorption. The spines of the schistosome are completely enclosed by the tegumental membranes and appear to be a crystalline lattice structure.

The syncytial cytoplasm of the tegument is Golgi and ribosome free and is a dense granular matrix mainly composed of protein and neutral mucopolysaccharides (Wilson and Barnes, 1974). The small number, simple structure and small size of the mitochondria indicate the tegument has a limited energy requirement. Also present within the tegumental cytoplasm are numerous "discoid bodies"; around 40 nm x 200 nm, comprising a dense granular matrix surrounded by trilaminate membrane and are thought to be a biconcave disc shape. The discoid bodies were believed to break down to form the dense granular substance of the cytoplasm (Wilson and Barnes, 1974), although a role in the formation of the surface spines of the parasite has been suggested on the basis that both stain similarly with phosphotungstic acid (Smith, Reynolds and Lichtenberg, 1969). More recent work suggests that the discoid bodies contribute to the double outer membrane of the tegument. The major glycoprotein in the discoid bodies was also found in the fraction enriched in surface membranes after differential centrifugation (MacGregor, Kusel and Wilson, 1988) Less numerous concentric whirls of membrane (membranous bodies) are also found in the cytoplasm. These are limited by a single bilayer and are ~150 - 200 nm in diameter. The contents of the membranous bodies are rich in phospholipid and appear superficially similar to unit membranes leading to the suggestion that they are involved in the turnover of the outer membrane of the tegument (Wilson and Barnes, 1974).

The nuclei of the tegument are located in subtegumental cells found below the muscle layers (Smith *et al,* 1969). Microtubule lined connections join the subtegumental cells with the syncytial cytoplasm. The subtegumental (sometimes multi nucleate) cells contain ribosomes, a few mitochondria and Golgi bodies. The subtegumental cells are responsible for the generation of membranous and discoid bodies which arise from separate types of Golgi apparatus (Wilson and Barnes, 1974)

The most interesting feature of the tegument is the outer plasma membrane; it encloses the entire outer surface of the worm and, uniquely, appears to consist of two closely opposed phospholipid bilayers which have a unique heptalaminate appearance after the use of uranyl acetate as a tertiary fixative (Hockley and McLaren, 1973). The outer tegumental membrane is heptalaminate in appearance and ~17 nm thick. The two bilayers in the outer membrane have differing lipid compositions, the two bilayers in close opposition have been termed a "double outer membrane" (McLaren and Hockley, 1977). Although the tegumental membrane is almost entirely heptalaminate in appearance it is often possible to observe small regions that are trilaminate or multilaminate in appearance. McLaren and Hockley (1977) have demonstrated the double outer membrane is an adaptation to the vascular habitat of these parasites: related species with differing habitats possess a more conventional outer membrane, usually bearing a glycocalyx. The schistosome tegument contains several integral proteins (reviewed by Abath and Warkhauser, 1996) including Sm 23, a member of a superfamily of integral membrane proteins, which has one or more transmembrane domains. The function of this protein remains unknown.

5.6 Electrophysiology of the adult tegument

Micro-electrode studies, using inorganic bathing media, have distinguished between three compartments in the adult male schistosome: the tegument, with a membrane potential of -45.9±2.5mV and an input resistance of 4.5 MΩ; muscle tissue, with a membrane potential of -22±1.1mV and an input resistance of 9.2 MΩ; and the extracellular spaces with a membrane potential of -4.7±0.3mV and an input resistance of 3.5 MΩ (Thompson *et al.* 1982).

The tegument of the schistosome is an electrical syncytia. Injection of large depolarising currents often invoke active membrane responses; these spikes vary considerably in size (between 4mV and 75mV) and are between 10msec and 40msec in duration. These active membrane responses are propagated along the length of the worm and are hypothesised as forming the basis by which excitation can spread through the body of the schistosome (Thompson *et al.* 1982). It has also been reported that chemical or physical alterations in the environment of the parasite that induce changes in the tegumental resting potential also exert a simultaneous change in the intramuscular potential (Bricker *et al,* 1982).

The tegumental resting potential is primarily dependent on the external potassium concentration (Fetterer *et al,* 1980a). Low temperature, or bath application of ouabain or lithium all cause depolarisation of the tegument; in addition they all reduce sodium efflux and potassium influx (Fetterer *et al,* 1981). Changes in the extracellular Na^+ concentration have little effect on the intrategumental sodium ion activity (which is maintained at a lower concentration than the bathing media). Application of ouabain causes an influx of Na^+ to the tegument which reaches equilibrium with the bathing solution (Pax, Chen and Bennett, 1987). The above effects together with the presence of an active sodium/potassium ATPase (Fetterer *et*

al, 1980b) indicate the importance of Na-K transport to the parasite and suggests the Na/K pump is electrogenic (Fetterer *et al,* 1981). Studies using pH sensitive microelectrodes indicate a sodium-hydrogen exchanger is also present in the adult male tegument (Pax and Bennett, 1990).

Bathing parasites in organic media (RPMI-1640) was found to give a significantly increased tegumental membrane potential (-63±2.9mV) in contrast to parasites in an inorganic bathing media (-26±7.3mV). The tegumental potential was found to be dependent on the presence of L-glutamine and to a lesser extent phosphate, suggesting that L-glutamine is required as a fuel for the enzyme glutaminase (used to buffer protons produced during anaerobic respiration) which requires phosphate to act as a polyanionic activator (Lane *et al,* 1987).

The above electrophysiological data was obtained from adult male parasites only. The smaller size of females making them less amenable to micro-electrode studies. The uneven surface of the male schistosome tegument (described previously) has made the application of the patch-clamp technique impossible to date. However, a recent study using ligand-binding assays suggests the presence of a nicotinic acetylcholine receptor on the dorsal surface of the male tegument (Camacho, Alsford, Jones and Agnew, 1995). The adult female parasite, with its smoother tegument has proved to be more suitable for patch-clamping. Even so, the difficulty in obtaining seals of sufficient resistance means that information on individual ion-channel types present within the tegument of this parasite is extremely limited.

To date, only one ion-channel type has been described in the tegument of the adult schistosome. This is a non-selective cation channel with a conductance of 295pS. At positive membrane potentials (in isolated inside-out patches) the channel was open

between 0 and 50% of the time, this rises to >99% open at negative membrane potentials. The main conductance level of 295pS appears to result from the co-operative opening of several ion-channels with a unitary conductance of 95pS (Day *et al,* 1992b). The physiological relevance of the above ion-channel has yet to be elucidated.

5.7 Electrophysiology of schistosome muscle

Micro-electrode studies demonstrate the presence of a membrane potential (-22±1.1mV) in the muscle of adult schistosomes. The muscle of the schistosome is not an anatomical syncytium but appears to act as a functional electrical syncytium in that it has similar current spreading abilities as the tegument (a true anatomical syncytium)(Thompson *et al,* 1982). Electron microscopy has shown the presence in the muscle layers of structures similar in appearance to gap junctions (Silk and Spence, 1969) that may be pathways of low electrical resistance. Multiple electrode studies demonstrate that electronic signals initiated in the tegument suffer only a 15-25% reduction upon passing into the muscle layer. This suggests the presence of low resistance pathways connecting the tegument with the underlying muscle (Thompson *et al,* 1982). The adult male schistosome possess several groupings of muscle which can be roughly divided into either longitudinal muscle or circularly orientated muscle (Silk and Spence, 1969). It is believed that the longitudinal muscle groups are involved in locomotory behaviour whilst the circular grouping of muscle may be responsible for maintaining the male-female pair. Application of various compounds (including dopamine, serotonin and acetylcholine) suggest that these muscle groups possess distinct pharmacological differences (Pax, Siefker and Bennett, 1984).

A method for obtaining isolated muscle fibres has been developed by Blair *et al* (1991). The isolated muscle fibres have been divided into three distinct morphological types and studied using standard electrophysiological techniques (Day *et al,* 1993):

(a) "frayed" fibres, ≈20μm in length, membrane potential = -22±3mV.

(b)"crescent" fibres, ≈60μm in length, membrane potential = -17±9mV.

(c) "spindle" fibres, ≈25μm in length, membrane potential = 28±11mV.

Voltage-clamp experiments revealed the presence of two types of voltage gated currents. The most prominent being a potassium current of the delayed rectifier type. The other current was also carried by potassium but activated faster and completely deactivated within 100msec, this second current was described as an "A" current as classified by Castle *et al* (1989). Subsequent experiments have lead to the cloning and functional expression of a *Shaker* related, voltage gated, potassium channel gene that, when expressed in *Xenopus laevis* oocytes, shows similar properties to the "A" current (Kim *et al,* 1995). No voltage gated inward currents were observed and alteration of the external calcium concentration had no effect on the amplitude of the outward currents in any of the muscle fibre types (Day *et al,* 1995). Patch-clamp experiments however, have shown the presence of calcium dependent potassium currents in each type of muscle fibre (Blair *et al,* 1991). The "frayed" type of muscle fibre has been shown to contract in response to molluscan FMRFamide and two FMRFamide-related peptides (isolated from the cestode *Moniezia expansa* and the turbellarian *Artioposthia triangulata*) indicating the presence of a FaRP receptor on the schistosome muscle fibres. The FMFRamide induced contractions were shown to be calcium dependent (Day, Maule, Shaw, Halton, Moore, Bennett and Pax, 1994).

5.8 Praziquantel

The pyrazinoisoqoinoline compound praziquantel (for structure see Figure 5.2) was initially screened as a potential tranquilliser but subsequently found to exhibit anthelminthic properties (Thomas *et al,* 1975). Schistosomiasis and a number of other cestode and trematode infections can be treated safely and economically using praziquantel. The specific mode of action of the drug is still uncertain and will be discussed subsequently. Praziquantel is also marketed as a veterinary drug by Bayer under the generic name Droncit, and is effective against several tapeworm species.

Figure 5.2

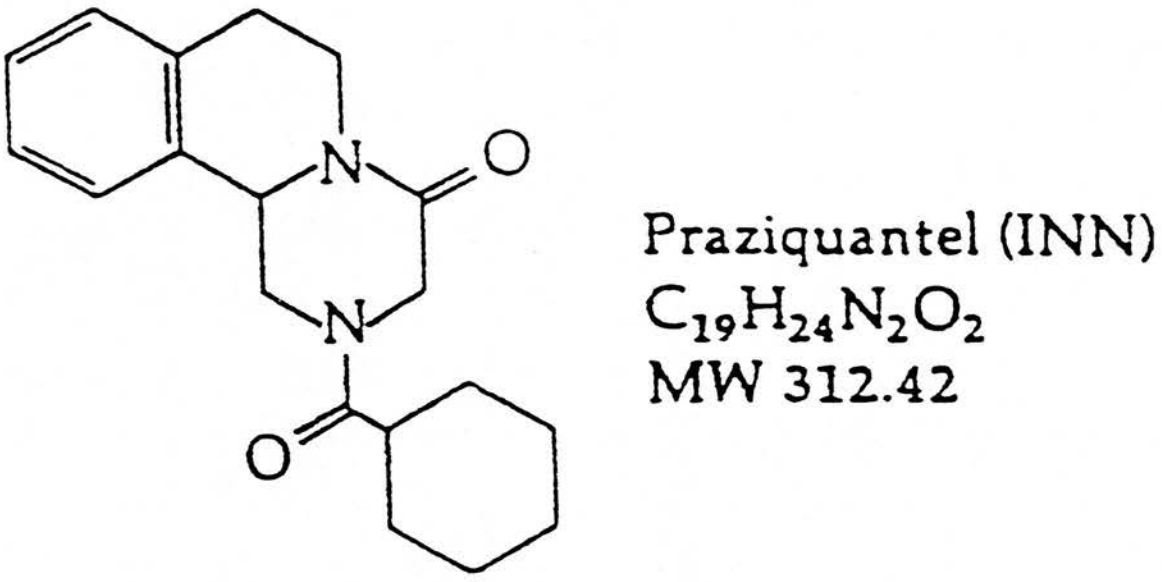

Figure 5.4: Structure of praziquantel (reproduced from Andrews *et al,* 1983)

5.9 Praziquantel sensitive sites and mode of drug action ?

To date the mode of action of praziquantel has yet to be elucidated. The possible mode of action of praziquantel has been reviewed by Andrews *et. al.* (1983), Day *et al* (1992a) and more recently by Redman, Robertson, Fallon, Modha, Kusel, Doenhoff and Martin, (1996) and is briefly discussed below.

Praziquantel sensitive sites

Parasites exposed to praziquantel exhibit an immediate and lasting paralytic increase in muscle tone; this is accompanied by an influx of Ca^{2+} across the tegument. The influx of Ca^{2+} is thought to be vital to the drug action as parasites bathed in Ca^{2+} free media do not contract (Pax *et al,* 1984; Fetterrer *et al,* 1980a; Wolde-Mussie *et al,* 1982; Pax *et al,* 1979). The lack of contraction of parasites bathed in Ca^{2+} free media is not immediate and is preceded by a brief period of unsustained contraction; suggested to result from Ca^{2+} being drained from intracellularly located stores.

When parasites are bathed in media with a high Mg^{2+}:Ca^{2+} ratio praziquantel causes a biphasic contraction. Bathing parasites with the tegument removed in the same media results in only the second (and larger) contraction being observed on exposure to praziquantel; suggesting the presence of praziquantel sensitive sites in the tegument. The electrical coupling between the tegument and muscle cells of the schistosome may result in the increase in intrategumental Ca^{2+} concentration being transmitted to the muscle cells and causing contraction (Thompson *et al,* 1982). Silk and Spence (1969) reported the presence of junctional complexes between muscle cells and the tegument which are possible candidates for the electrical coupling observed between these compartments. Detegumented parasites also contract in the presence of praziquantel suggesting the presence of sensitive sites on the muscle cell as well as on the tegument.

The observed influx of Ca^{2+} across the tegument on addition of praziquantel hints that the praziquantel sensitive sites may be Ca^{2+} permeable ion-channels. The lack of toxic effects on humans indicate that these channels are pharmacalogically distinct from Ca^{2+} channels present in host tissue. Praziquantel induced Ca^{2+} influx can be blocked by Mg^{2+} or La^{3+} but not by Ni^{2+} or Co^{2+}. The Ca channel blocker D-600 has no effect on praziquantel induced Ca^{2+} influx. Figure 5.3 describes several possible sites concerned with calcium homeostasis that praziquantel may interact with.

Figure 5.3 Diagram representing the *Schistosoma* tegument, underlying muscle layers and parenchyma, and showing the three electrical compartments recognised by an advancing micropipette. (1)-(10) are common cellular factors\components responsible for modulating intracellular [Ca^{2+}]: (1) second messenger-gated Ca^{2+} channel; (2) calcium release activated Ca^{2+} channel; (3) agonist-gated Ca^{2+} channel; (4) voltage-gated Ca^{2+} channel. PZQ increasing the P_{open} of (1)-(4) could account for the observed influx of Ca^{2+} across the tegument. (5) Na/Ca^{2+} exchange pump; (6) Ca^{2+} pump, inhibition of either (5) or (6) by PZQ could lead to an increase in intrategumental [Ca^{2+}]; (7) reduction in buffering capacity induced by PZQ would lead to an increase in the free [Ca^{2+}]. PZQ can also induce effects when the parasite is bathed in Ca^{2+} free media, suggesting the drug also interacts with intracellular calcium stores (found in rough endoplasmic reticulum); (8) and (9) are release channels for Ca^{2+} stores, sensitive to inositol trisphosphate and Ca^{2+} respectively. PZQ may cause either of these types of channels to open and release calcium from these stores. (10) SERCA (sarco endoplasmic reticulum calcium) pumps responsible for filling the intracellular calcium stores. Inhibition of SERCA pumps by PZQ is a possibility. Factors (1) to (10) will be present in the muscle cells of the parasite, thus accounting for the action of the drug on detegumented worms. However, there are pathways of low electrical resistance between tegument and muscle cell (11), and from muscle cell to muscle cell (12), which may be conduits for PZQ action. (1)-(6) could also face onto extracellular spaces. Factors (1)-(6) are shown spanning the double membrane of the *Schistosoma* outer tegument as their specific location in this structure has not been determined (Diagram derived from Kostyuk and Verkhratsky, 1994).

Figure 5.3

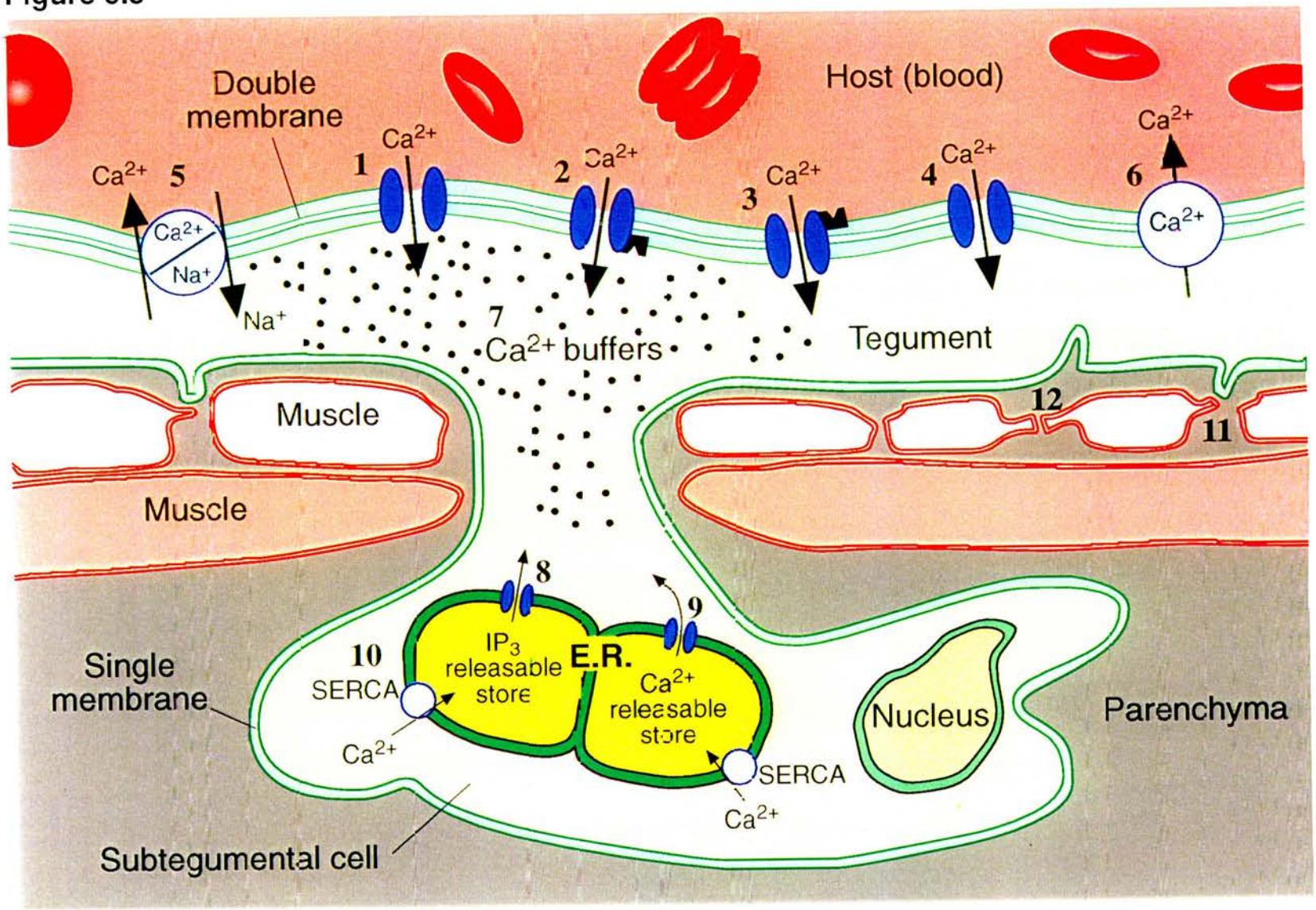
Host (blood)
Double membrane
Ca2+
1
2
3
4
5
6
Ca2+
Na+
Na+
7
Ca2+ buffers
Tegument
Muscle
Muscle
12
11
8
9
10
SERCA
IP3 releasable store
E.R.
Ca2+ releasable store
SERCA
Ca2+
Ca2+
Nucleus
Parenchyma
Single membrane
Subtegumental cell

5.10 Other possible modes of praziquantel action

Antigen exposure.

Praziquantel treatment, at curative doses, results in tegumental disruption with the consequent exposure of several tegumental antigens (Harnett and Kusel, 1986). Using subcurative doses the worms are able to repair the resulting tegumental lesions. The majority of identified antigens exposed on praziquantel treatment are glycoproteins, which is consistent with reports of carbohydrates exposed on the surface of praziquantel treated worms (Doenhoff *et al,* 1988; Lima *et al,* 1994).

The host immune system plays an important role (*in vivo*) in parasite killing during praziquantel treatment (Fallon *et al,* 1992). The synergistic activity of antibody and praziquantel is attributed to antibodies binding to specific epitopes exposed by praziquantel and enhancing worm death immunologically (Fallon *et al*, 1992). It is possible that specific antibodies allow an immunological action to occur against epitopes exposed on praziquantel treatment before the worm can repair the damaged tegument. Praziquantel treatment exposes alkaline phosphatase on the parasite surface. Antibody has been demonstrated to inhibit this enzyme in praziquantel treated worms (Fallon *et al*, 1994) and may inhibit other enzymes essential to the parasite which are exposed to the immune system on praziquantel treatment.

Membrane fluidity and metabolism

Praziquantel has short- and longer-term effects on the properties of the schistosome surface. Within the first few minutes of praziquantel treatment there is a rapid decrease in membrane fluidity observed in photobleaching experiments using 5-N-(octadecanoyl)aminofluorescein (AF18) as a probe. Membrane fluidity was observed to increase after praziquantel treatment when another probe, PKH2 (Sigma)

was used. The observed differences may indicate that the two probes enter different domains of the parasite surface membrane. It is possible that praziquantel inserts into different domains of the parasite surface rather than a general insertion. It has been hypothesised that that praziquantel inserts into domains of the parasite membrane rich in antigens. These antigens are anchored to the membranes by glycosylphosphatidylinositol (GPI) anchors. Praziquantel induced membrane damage then exposes these antigens to host immune attack (Redman *et al,* 1996). It is not known whether the GPI-anchored antigens are released from the parasite *in vivo*.

Several longer-term effects of praziquantel have been observed. Praziquantel stimulates the synthesis of heat shock protein 70 (HSP70) over a 24 h period. HSP70 is likely to be important in membrane repair, also its secretion may stimulate the host immune response and thus play a role in the immune dependence of drug action. Praziquantel may cause the shedding of antigenic carbohydrate moieties from damaged regions of the tegument. The lipid uptake of the parasite is decreased by praziquantel treatment; over a period of days the lack of lipid could inhibit repair of membrane damage induced by praziquantel.

Drug resistance

In schistosomes (and many other parasitic) infections the definition of resistance becomes difficult when there are differences in susceptibility to a compound at different stages in the parasite life cycle and differences between different sexes. One definition of "true resistance" is a genetically transmitted loss of sensitivity in a parasitic population that was previously sensitive to that that drug (Harnett, 1988: Day *et al,* 1992a). Using the above definition a praziquantel resistant strain has been bred in mice (Fallon and Doenhoff, 1994). Isolates of *S. mansoni* obtained from

Senegal are also insensitive to praziquantel, however it remains unclear whether these parasites are "truly resistant" or are a "tolerant" strain of the worm. Tolerance being defined as a parasite population on which the drug has no effect and have had no previous exposure to the drug (for discussion see Fallon *et al.* 1996). More practically, any parasites that are not killed by a drug concentration that is fatal to the host are effectively resistant to that drug. To date there are reports of resistance or tolerance in schistosomes to hycanthone, oxaminiquine, oltipraz and praziquantel but there have been no reports of cross resistance between praziquantel and other schistosomicidal drugs as yet (Cioli *et al,* 1993; Fallon *et al*, 1996). The method by which resistance to praziquantel develops and how to combat it relies on determining the exact mode of action of the drug.

CHAPTER 6: MICROSCOPY TO INVESTIGATE THE NATURE OF TEGUMENT DERIVED VESICLES.

6.1 INTRODUCTION

The aim of the project was to investigate ion-channels in the membranes of parasitic helminths using the patch-clamp technique. The previous section demonstrates the suitability of membrane vesicle preparations for the study of single ion-channels in parasites. Treatment of the adult *Schistosoma mansoni* with low pH media results in the formation of membranous vesicles on the surface of the worm (Robertson, Martin, Kusel, 1996). A brief initial study revealed these vesicles were capable of forming the high resistance (GΩ) seals with glass pipettes required for patch-clamping (Hamill, Marty, Neher, Sackman, Sigworth, 1981). The object of this chapter was to determine the region of the parasite from which the vesicles originated. Initial observations using the light microscope suggested the vesicles were forming from the tegument of the worm. Initial experiments used a fluorescent dye to determine that the vesicles originated from the outer tegument of the parasite. Scanning and transmission electron microscopy were then used to assess several features of the vesicle preparation:

(1) Transmission electron microscopy was used to confirm that vesicles were forming from the outer tegumental membranes of the parasite.

(2) Scanning electron microscopy was used to determine whether the vesicles were of a clean smooth nature suitable for patch-clamping (Hamill *et al.*, 1981).

(3) The transmission electron microscope was used to determine whether the unique heptalaminate structure of the schistosome outer tegument was conserved during vesicle formation.

The chapter presents the results of these studies. The effects of low pH on the parasite tegument are discussed and contrasted with the effects of praziquantel (Simpson and McLaren, 1982) and concanavalin A on the tegument (Staudt, Schmahl, Blaschke, Mehlhorn, 1992); both of which cause vesicles to form from the outer tegument of the worm. The importance of these results are related to the single-channel studies carried out using the patch-clamp technique.

6.2 METHODS

Supply of schistosome infected mice

The life cycle of a Puerto Rican strain of *Schistosoma mansoni* is maintained in the Dept. of Biochemistry, University of Glasgow. BALB/c with mature infections of *S mansoni* were supplied on a regular basis by Prof. J. Kusel (Biochemistry, University of Glasgow) and maintained in the Wellcome Animal House, (R.(D.)S.V.S., University of Edinburgh) until required.

Recovery and maintenance of adult schistosomes (Smithers and Terry 1965)

Infected mice were killed by cervical dislocation. The animals were then dissected to expose the thoracic and abdominal cavities. The portal vein was cut as close to the liver as practicable and 50ml of GMEM medium (37°C)(Table 6A) was injected into the heart. The perfusion of medium through the circulation ejected mature worms from the incised portal vein. Schistosomes were collected on fine gauze and transferred to Petri dishes containing GMEM (37°C). Parasites were washed three times in GMEM and maintained in an incubator at 37°C until required. GMEM was prepared daily. Routinely parasites were used for experiments within 4hrs of harvesting from the mice.

Schistosome vesicle formation protocol

Parasites were transferred from GMEM to a Petri dish containing 5-10ml of Vesicle medium (VMEM, Table 6A) and incubated at 37°C for time periods between 15min and 2hrs. Using an inverted light microscope (Nikon, TMS-PH3), at x200 magnification, vesicles could be observed "budding" from the surface of the parasite within 15-30 minutes of immersion in VMEM. After vesicle formation the parasites followed one of three experimental paths:

(a) Parasites examined immediately using light and fluorescence microscopy to determine the site of origin of the vesicles,

(b) Parasites placed immediately in fixative and processed for electron microscopy to examine the process and origin of vesicle formation,

(c) Parasites pinned onto Sylgard™ in recording chamber and bathed in solutions for electrophysiological experiments.

Vesicle formation was dependent on the pH of VMEM. More vesicles were observed on the surface of worms incubated at pH 3.75 compared with worms incubated at either pH 3.5 or pH 4.0. The process of vesicle formation was not dependent on the continued presence of VMEM. Typically, for patch-clamp experiments, an incubation of ~30min was sufficient to cause vesicle formation, but the process was observed to continue after the worms had been pinned onto Sylgard™ and VMEM replaced with a recording solution.

Table 6A

Inorganic Salt	**mg/L**	**mM (where appropriate)**
$CaCl_2.H_2O$	265.00	2.05
$Fe(NO_3)_3.9H_2O$	0.10	
KCl	400.00	5.37
$MgSO_4.7H_2O$	200.00	0.81
NaCl	6400.00	109.50
$NaHCO_3$	30ml 7.5%/litre	2.68
$NaH_2PO_4.H_2O$	124.00	0.90
Other Components	**mg/L**	**mM (where appropriate)**
L-Arginine	42.00	
L-Cystine	24.00	
L-Glutamine	10ml 200mM/litre	2.00
L-Histidine.HCl.H_2O	21.00	
L-Isoleucine	52.40	
L-Leucine	52.40	
L-Lysine.HCl	73.10	
L-Methionine	15.00	
L-Phenylalanine	33.00	
LThreonine	47.60	
L-Tryptophan	8.00	
L-Tyrosine	36.20	
L-Valine	46.8	
Vitamins	**mg/L**	**mM(where appropriate)**
D-CaPantotherate	2.00	
Choline chloride	2.00	
Folic Acid	2.00	
i-Inositol	3.60	
Nicotinamide	2.00	
Pyroxidal.HCl	2.00	
Riboflavin	0.20	
Thiamine.HCl	2.00	
Other components	**mg/L**	**mM(where appropriate)**
D-Glucose	4500.00	25.00
Phenol Red	124.00	

Table 6B: Final constituents of Glasgow minimal essential medium (GMEM: Gibco BRL BHK21 Cat. No. NI2541-025). VMEM was prepared by adjusting the final pH of GMEM to pH 3.5-4.0 using 5M HCl.

Fluorescence Studies of Vesicle Preparation

8 male schistosomes were removed from mice and maintained in GMEM. The parasites were divided into three groups: A, B and C. Group A (n=2) , the unstained control, was incubated in GMEM for 15 min., washed five times in GMEM, then incubated in VMEM for 2 h, followed by five washes in GMEM and maintained in GMEM for examination. Group B (n=3), the stained control, was incubated in 10μM AF18 for 15 min., washed five times in GMEM and maintained for examination in GMEM. Group C (n=3), the stained vesiculated preparation, was incubated in 10μM AF18 for 15 min., then washed five times in GMEM and placed in VMEM for 2 h followed by five washes in GMEM and maintained in GMEM.

Parasites from each group were mounted in welled slides containing a small volume of GMEM and examined using bright field and then fluorescence microscopy using a Leitz Ortholux II microscope, mercury lamp and FITC filters. Parasites from the unstained control group, A, showed no autofluorescence and were not examined further. Photomicrographs and fluorescence photomicrographs were taken of the stained control and the stained vesiculated groups, B and C, with a Wild MPS51 camera and Fujichrome 100 film.

Additional Light Microscopy Experiments

Parasites in GMEM were snap frozen in liquid nitrogen (90 sec) and thawed at 37°C to remove the tegument before undergoing the vesicle forming protocol. After treatment the parasites were examined under the light microscope (Nikon TMS-PH3) for the presence of vesicles. Additional parasites were incubated in GMEM containing 0.1% colloidal coomassie blue for 20 mins to stain the outer membrane of the tegument. Following five washes with warm media the parasites then underwent the vesicle formation protocol and were examined using light microscopy. No

evidence of vesicle formation was observed in the detegumented parasites. Staining with coomassie blue was uneven and no conclusions could be drawn. These experiments are not discussed further.

Electron Microscopy of Schistosome Vesicle Preparation

Parasites were incubated in VMEM for time periods of either 0 min, 15 min, 30 min or 1 hr. After incubation in the vesicle forming media parasites were immediately placed in fixative and processed for electron microscopy.

Scanning Electron Microscopy (S.E.M.)

13 male schistosomes were divided into four groups and incubated in VMEM for time periods of either 0 min. (n=3), 15 min. (n=4), 30 min. (n=4), or 1 h (n=2). The parasites were fixed for a minimum of 3 hours in 3% glutaraldehyde in 0.1 molar sodium cacodylate buffer (pH 7.4). Fixation was followed by three 20 minute washes in the sodium cacodylate buffer, pH 7.4. A 1% osmium tetroxide solution (in 0.1M sodium cacodylate buffer, pH 7.4) was used in a 1-2 hour post-fixation step. Parasites were then washed for 30 minutes in distilled water. Parasites were dehydrated using increasing concentrations of acetone (50-100%) in 30 minute steps. Specimens were dried using carbon dioxide and a critical point drier (Poleron E3000 SIICPD) and sputter coated with 20nm gold/palladium (60/40) in an Emscope SC500 sputter coater. Parasites were viewed under a Philips 505 scanning electron microscope.

Transmission Electron Microscopy (T.E.M.)

Parasites were processed for transmission electron microscopy using the method of Hockley and McLaren (1973) described below.

31 male schistosomes were divided into four groups and incubated in VMEM for time periods of 0 min. (n=5), 15 min. (n=3), 30 min. (n=6), and 1 h (n=17); and were processed for transmission electron microscopy. The parasites were subjected to three consecutive fixation steps: The parasites were initially placed in two percent (v/v) glutaraldehyde in a cacodylate buffer (Lewis and Shute, 1966) containing 0.05M sodium cacodylate and 0.002M calcium acetate, pH 7.4. The worms remained in the glutaraldehyde fixative for four hours at 4°C and were then washed three times in ice cold Lewis/Shute buffer. For the second fixation step the parasites were placed in one percent (w/v) osmium tetroxide in Lewis/Shute buffer for 2 hrs at 4°C followed by ten washes in ice cold deionised distilled water. Finally the parasites were placed in an 0.5% aqueous solution of uranyl acetate (pH 5) containing 45 mg/ml sucrose for 1.5 hrs at 4°C in total darkness (after de Harven, 1967). The worms were then washed three times in ice cold deionised distilled water.

Specimens were dehydrated in a series of incubations in increasing concentrations of ethanol; 25%, 50% and 75% each for ten minutes. Parasites were then resuspended in 100% ethanol and embedded in Araldite. Sections were cut with a Diatome diamond knife and stained using uranyl acetate and lead citrate. Sections were examined using a Phillips EM 400 electron microscope in the Department of Preclinical Veterinary Sciences, University of Edinburgh.

6.3 RESULTS

Fluorescence microscopy of the vesicle preparation

The unstained schistosome control group, A, showed no autofluorescence so that the level of fluorescence was dramatically less than that present in the stained control group, B, incubated in AF18 without undergoing the vesicle forming protocol. The strong fluorescence of group B demonstrated the efficacy of AF18 for our staining technique

Figure 6.1 shows phase contrast and fluorescence photomicrographs of vesicles produced from the stained vesiculated group, C. The intensity of fluorescence varied from vesicle to vesicle with 41% (7 from a sample of 17) showing clear detectable fluorescence. AF18 was selected for staining the tegument because it inserts into the outer bilayer of the schistosome tegumental membrane but does not enter the inner bilayer (Foley *et al.,* 1986). The presence of the stained fluorescent vesicles demonstrates the presence of the outer bilayer in these vesicles. The vesicles that did not fluoresce may not possess the outer bilayer of the tegument or the level of fluorescence may have been too low to detect.

Figure 6.1

A: Light micrograph of male parasite showing membrane vesicles (v) on the surface of the worm.

B: A fluorescence micrograph of the same parasite, membrane vesicles cannot be observed fluorescing.

C: Vesicles from the same parasite at increased magnification.

D: Fluorescence micrograph of vesicles (v) shown in figure 6.1C

Figure 6.1

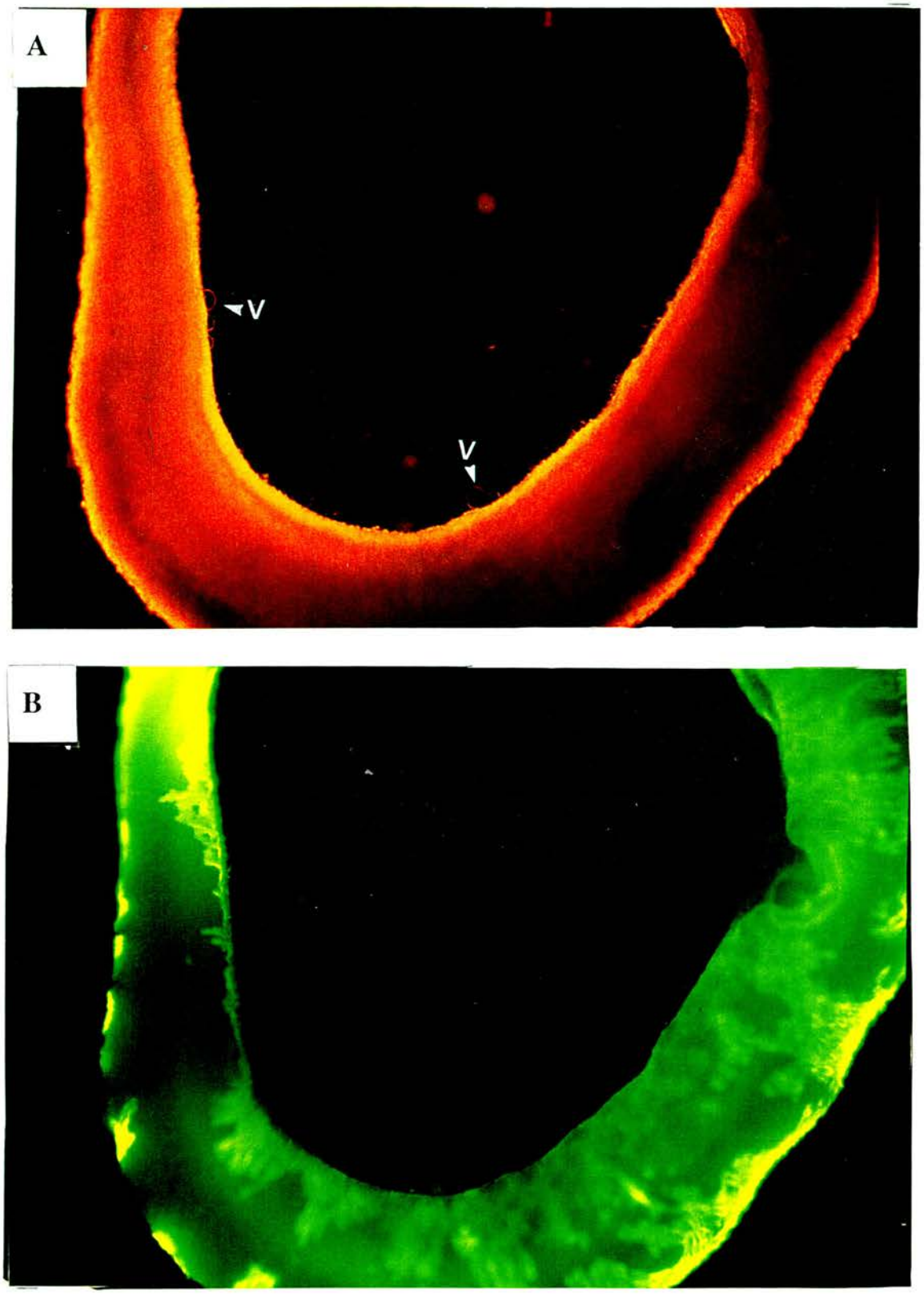

Figure 6.1

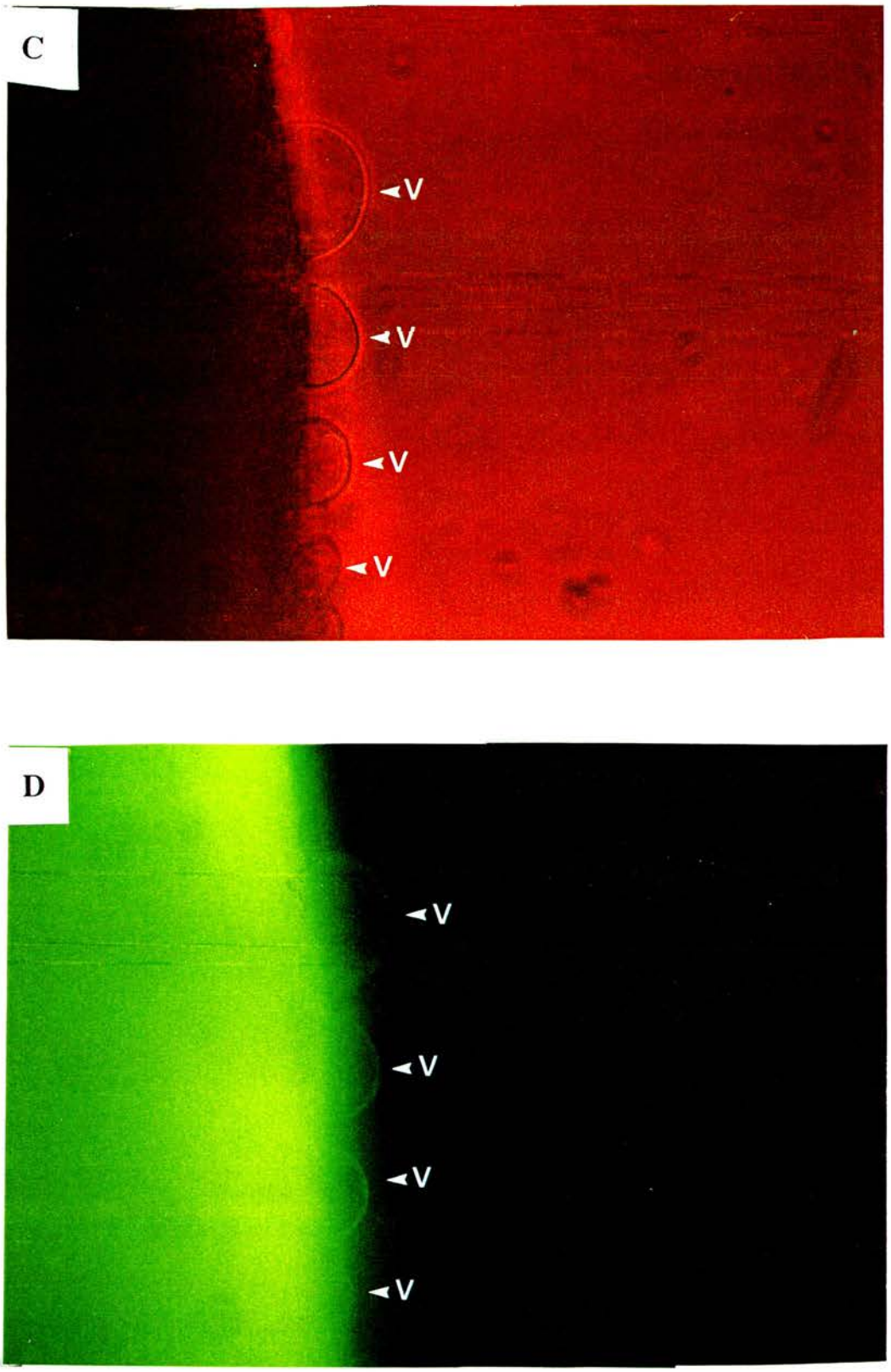

Scanning electron microscopy of the vesicle preparation

Control (untreated) parasites examined using scanning electron microscopy displayed the typical morphological characteristics of the species, including the anterior suckers, reproductive groove and spiny tubercles of the male (Figure 6.2)(reviewed by McLaren, 1980). A fifteen minute incubation in VMEM resulted in small vesicles budding from the surface of the parasite (Figure 6.3). Vesicles are clearly incorporating the outer tegumental membrane. Fifteen minutes of low pH treatment caused no apparent damage or disruption to the tegument, with the exception of the small vesicles forming. A 30 minute enzyme treatment with VMEM resulted in the formation of larger and more numerous vesicles in both sexes of the parasite (Figure 6.4). The vesicles appear to be derived from the outer tegument. A number of vesicles ruptured after 30mins VMEM treatment. I believe this to be a processing artefact because when parasites were examined under the light microscope after 30 mins of VMEM incubation very few burst vesicles could be observed. The longer exposure to low pH resulted in more extensive tegumental damage: the "crater-like" pits in figure 6.4A were probably caused by vesicles breaking from the parasite surface. At 1 hour treatment in low pH media a large number of vesicles formed (Figure 6.5). The parasite tegument was severely disrupted by the prolonged exposure to low pH; cracks were observed and areas of the outer tegument were stripped away. Figure 6.6A shows the smooth appearance of the intact vesicles, suggesting they are suitable candidates for the application of the patch-clamp technique. Figure 6.6B demonstrates the large number of vesicles that are frequently observed on the parasite surface after the vesicle formation protocol. In summary, low pH treatment resulted in vesicle formation from the outer tegument; as the length of the treatment increased the extent of tegumental disruption also increased.

Figure 6.2

A: Scanning micrograph of adult male schistosome showing; ventral sucker(v) and reproductive groove (g). Note the uneven dorsal surface covered in numerous "boss-like" tubercles. Scale bar = 1 mm.

B: Scanning micrograph of the tegument of an untreated adult male. Note the "hill" shaped tubercles topped with spines (s), also the convoluted surface of the tegumental membrane between tubercles. Scale bar = 10 μm.

Figure 6.2

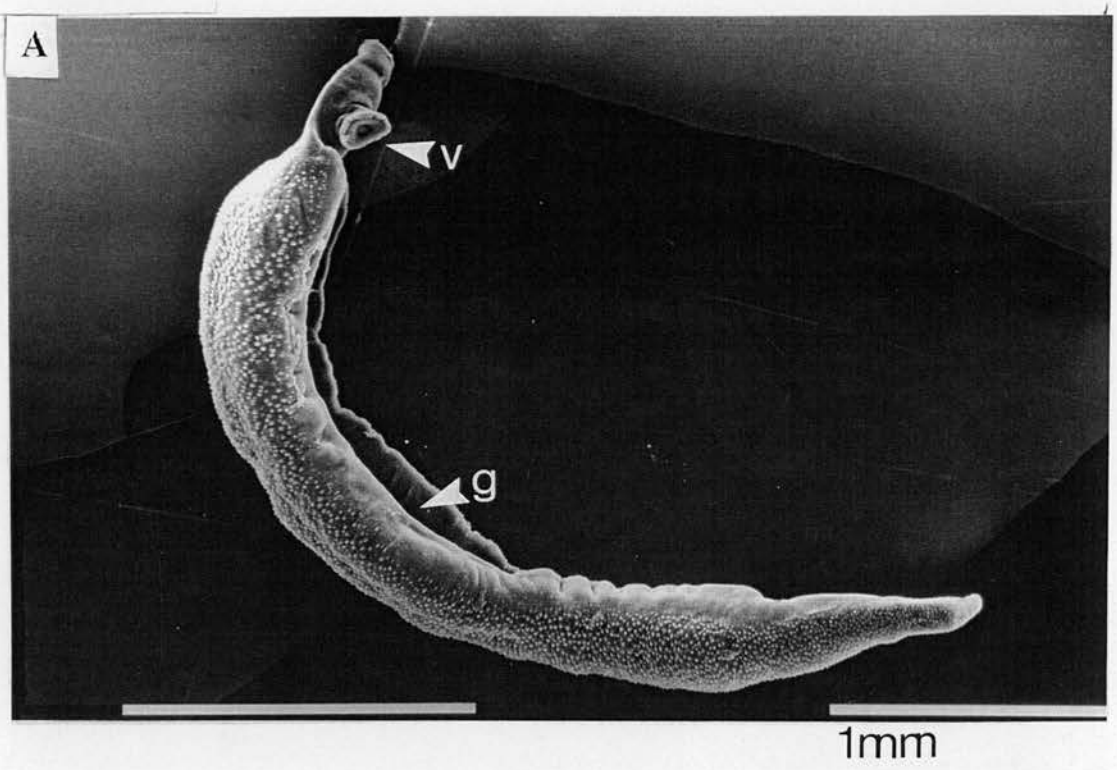

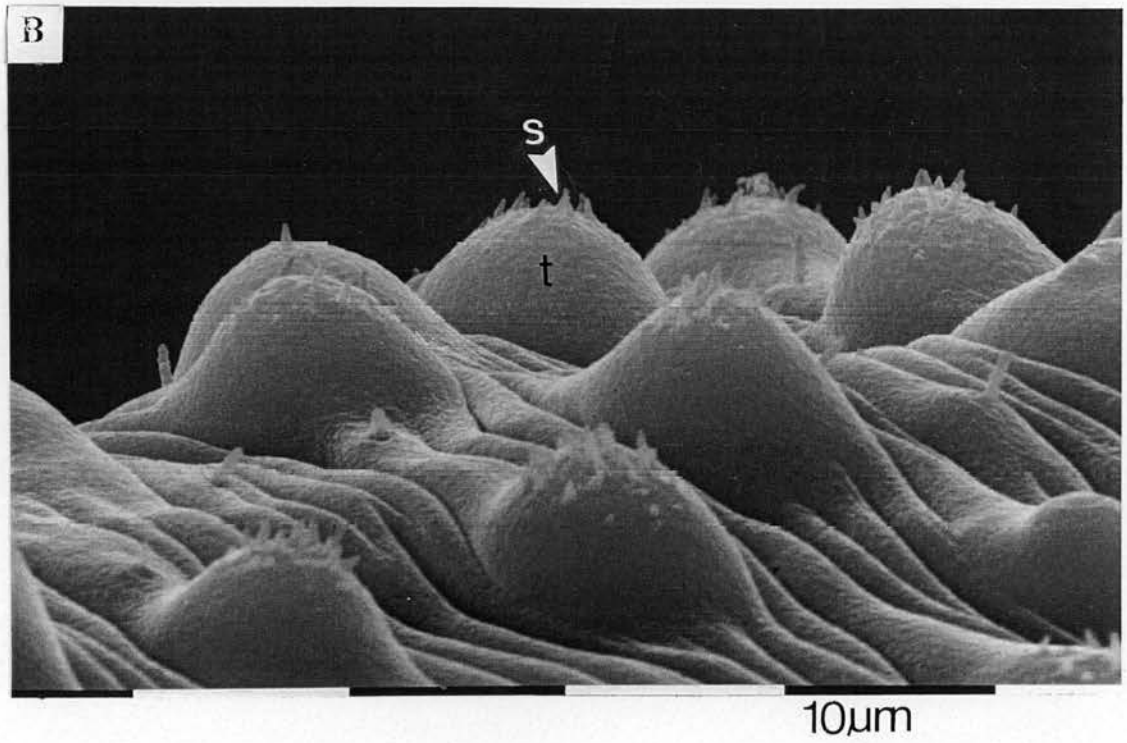

Figure 6.3 Surface of an adult male after a 15 minute treatment in VMEM (vesicle-forming media) at 37°C.

A: Surface of male parasite showing vesicles budding from the tegumental surface (v) and minor tegumental disruption. Scale bar = 10 μm.

B: Surface of male parasite showing a tubercle with spines (s) present and numerous vesicles budding (v). Scale bar = 10 μm.

Figure 6.3

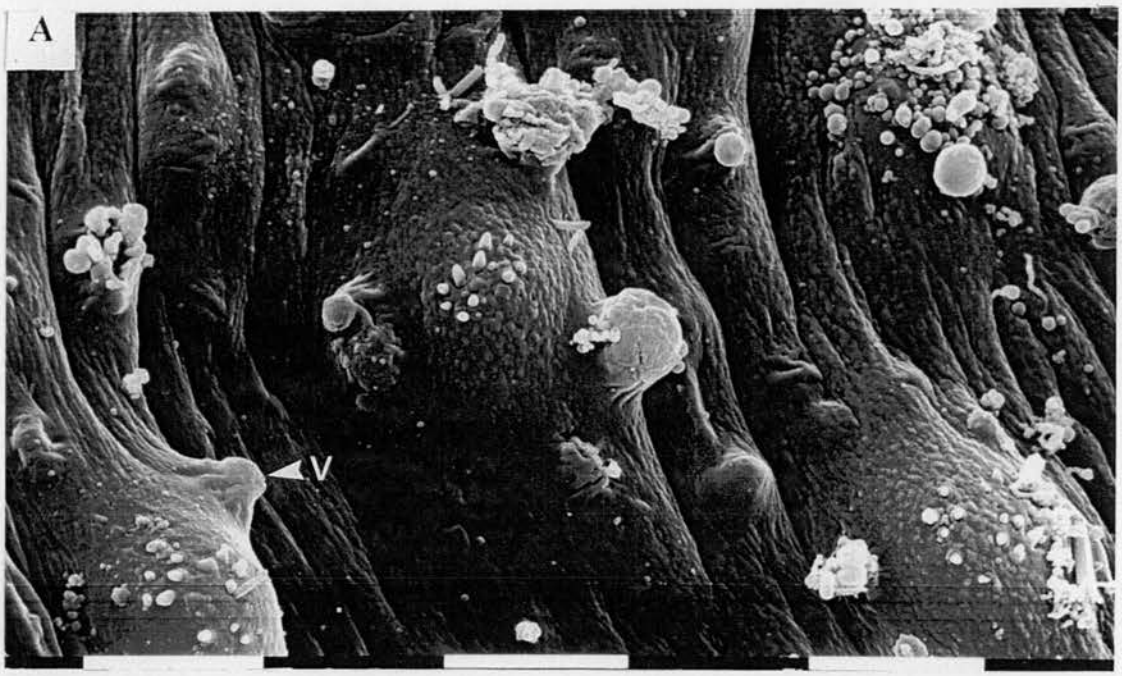

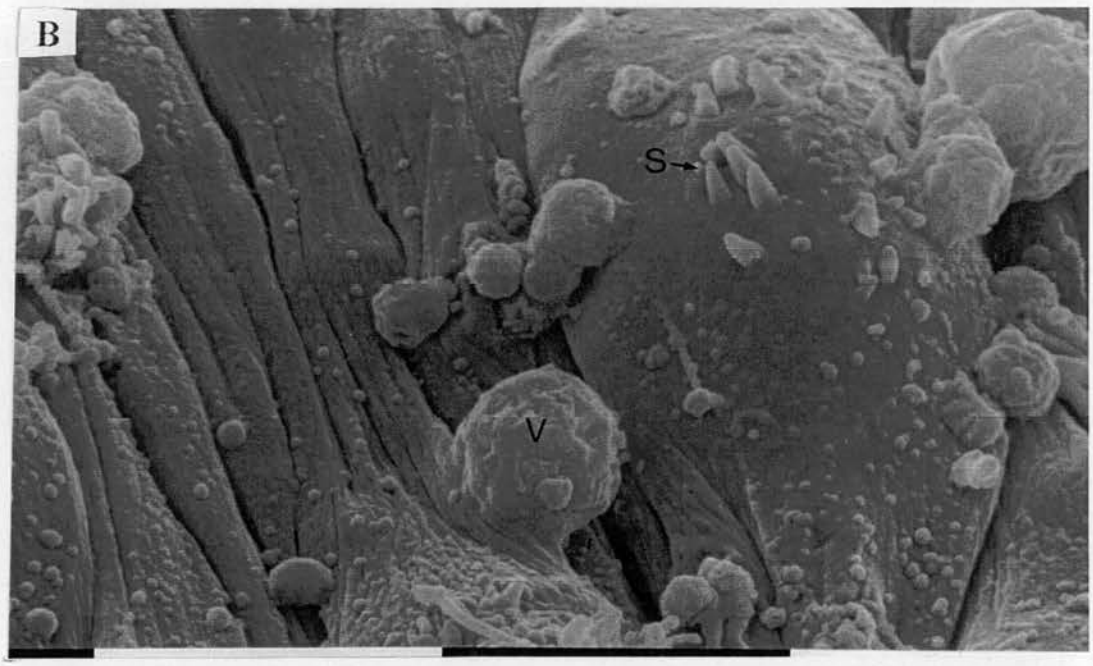

Figure 6.4

A: Adult female schistosome after 30 minutes of the vesicle forming protocol. Note ruptured vesicles (rv's) and crater like pits in outer tegumental membrane(p). Scale bar = 0.1 mm.

B: Adult male parasite after 30 minutes of the vesicle forming protocol. Note, spiny tubercles (t), membrane vesicles (v) and disrupted vesicles (dv) clearly arising from the outer tegument. Scale bar = 10 μm.

Figure 6.4

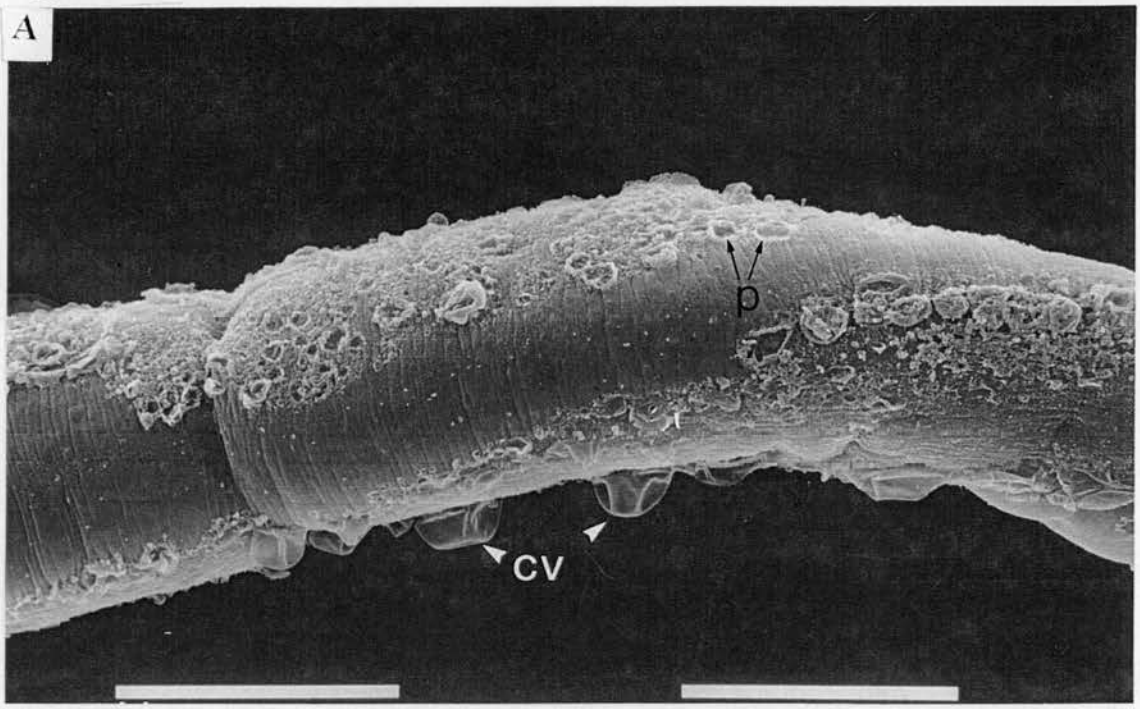

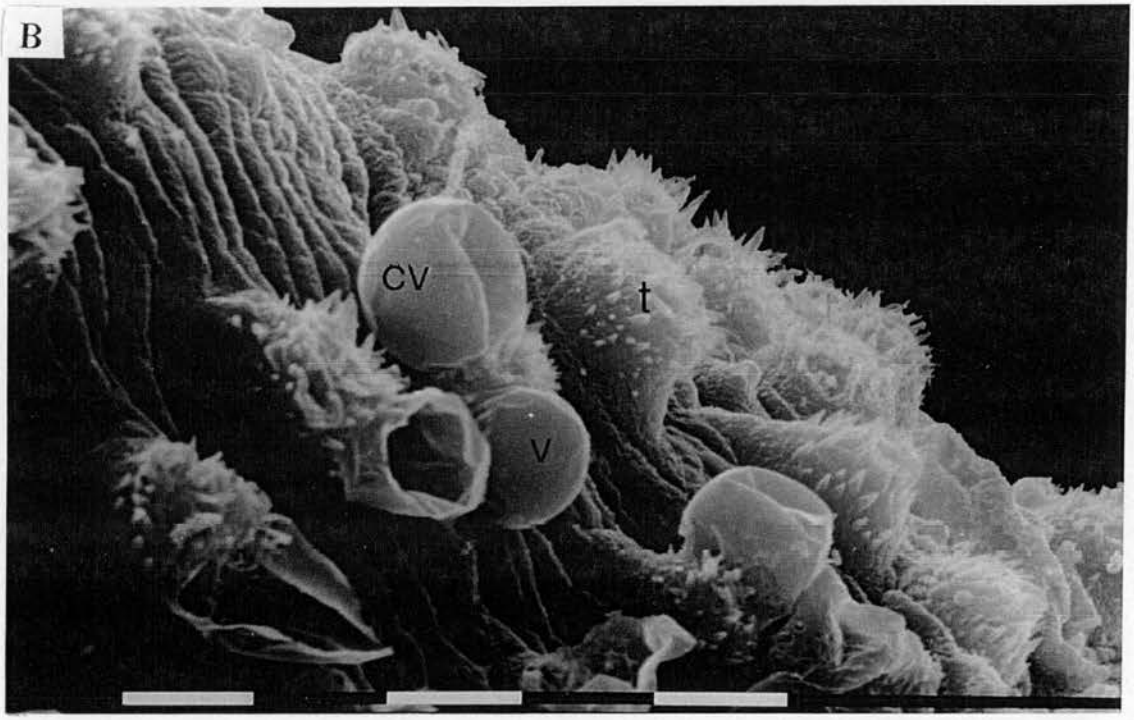

Figure 6.5 Parasites after 1 hour of the vesicle forming protocol

A: Paired adults showing intact (iv) and disrupted (dv) vesicles on both sexes. Also present are areas of severe tegumental disruption (td) on the male parasite. Scale bar = 1mm.

B: Adult male showing oral (os) and ventral (vs) suckers. Areas of tegumental disruption (td) and tegumental cracking (tc) can be observed. Intact vesicles (iv) and disrupted vesicles (dv) can be observed over the entire visible surface of the parasite, except for areas of severe tegumental disruption. Scale bar = 0.1 mm.

Figure 6.5

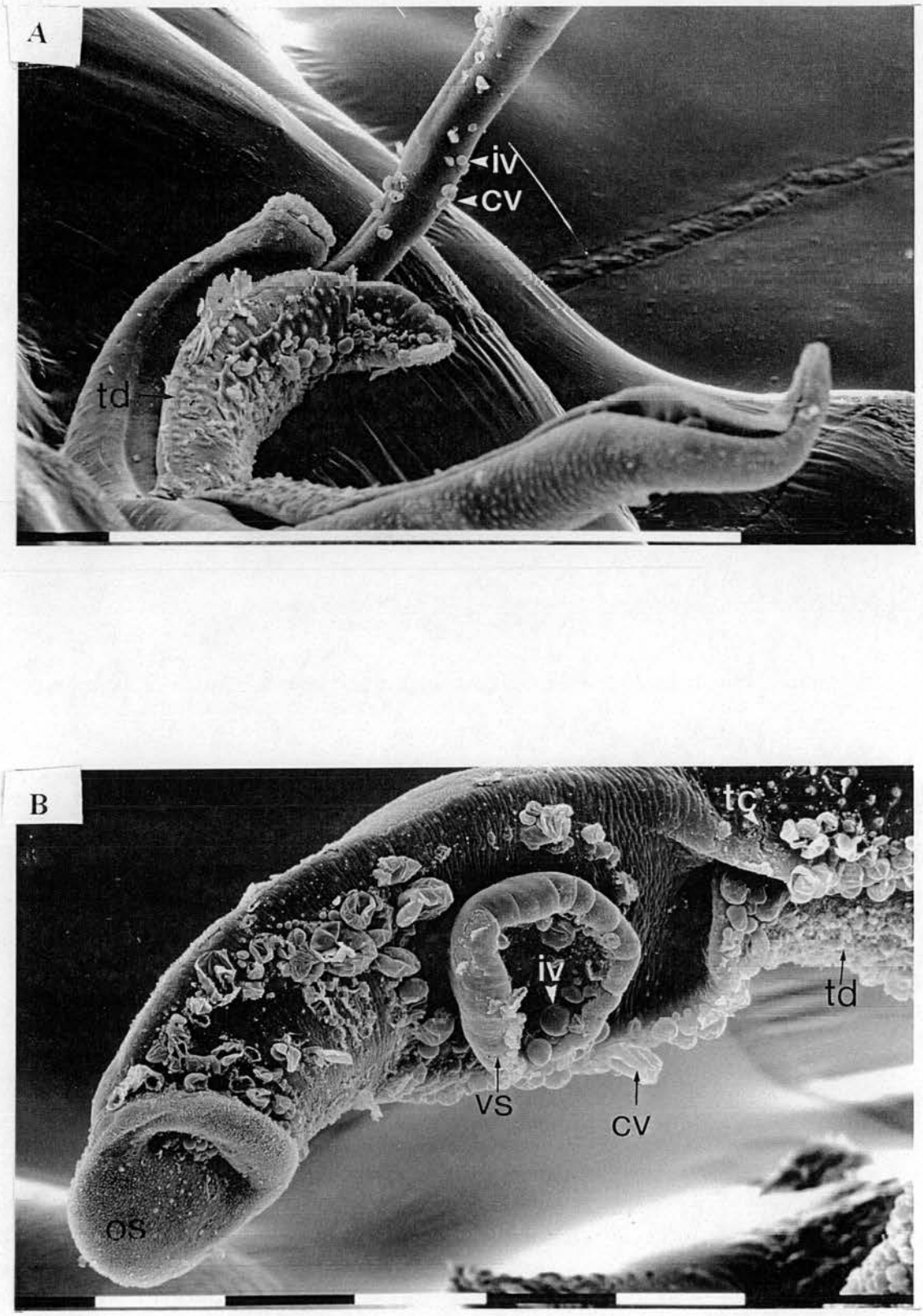

Figure 6.6 Parasites after 1 hour of the vesicle forming protocol

A: Intact vesicles (iv) and disrupted vesicles(dv). Note the clean, relatively smooth surface of intact vesicles. Scale bar = 10 μm.

B: Intact (iv) and disrupted (dv) vesicles on the parasite surface. Note the large number of membranous vesicles that can be obtained using the low pH treatment. Scale bar = 10 μm.

Figure 6.6

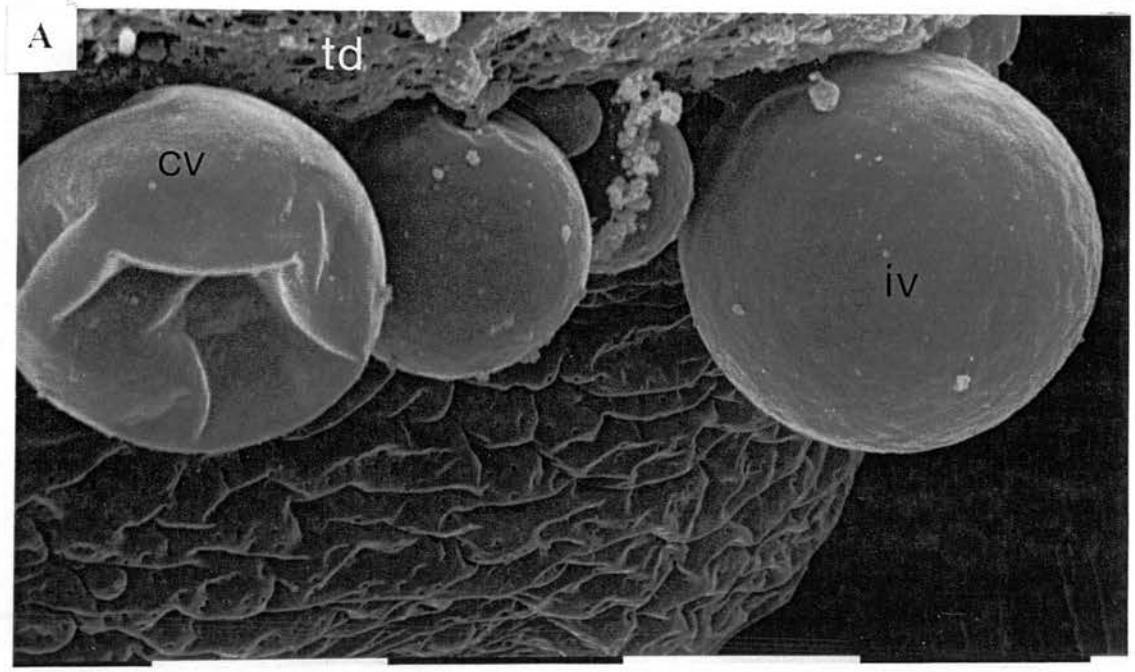

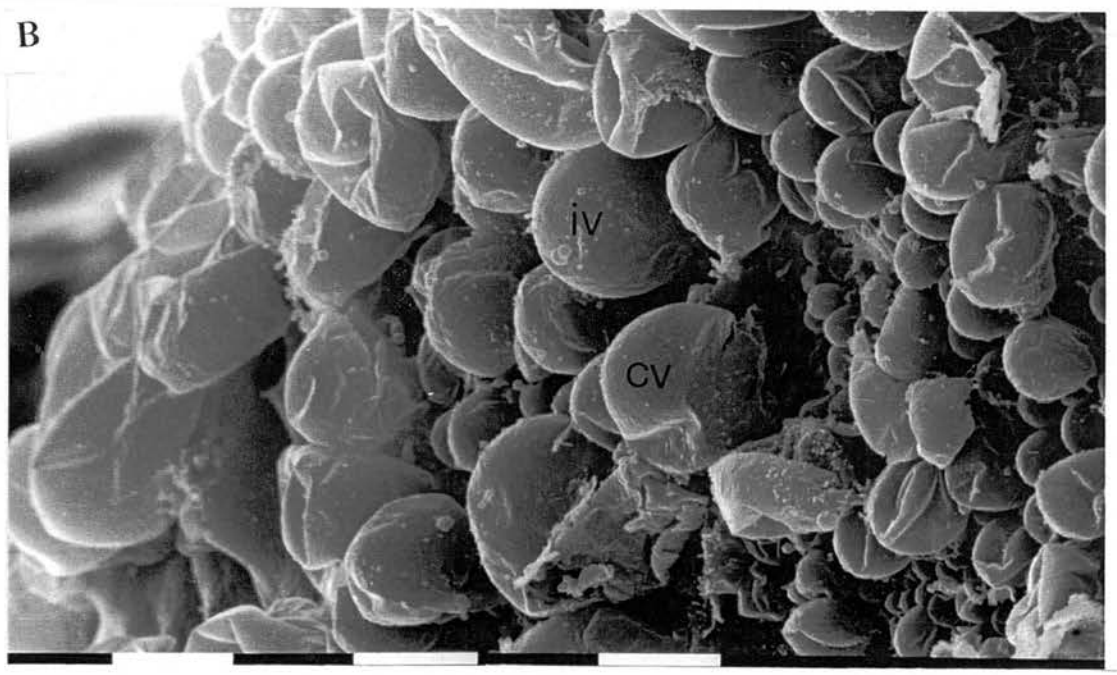

Transmission electron microscopy of the vesicle preparation

The effect of low pH media on the tegument of *Schistosoma mansoni* was also investigated using transmission electron microscopy. The effects of low pH treatment are shown in Figures 6.7 to 6.11. A control group of parasites was examined (Figure 6.7) and the tegument was found to possess the major anatomical components described in previous studies: including discoid bodies, membranous vesicles and surface pits (Silk, Spence and Gear, 1969; Smith, Reynolds and Lichtenberg, 1969; Wilson and Barnes, 1974; McLaren, 1980). After 15 minutes in VMEM media vesicles could be observed budding from the tegument of the parasite. The vesicles are clearly originating from the outer membranes of the tegument. After 15 minutes in VMEM the tegumental cytoplasm had become more floccular and diffuse in contrast to the control parasites. Parasites exposed to thirty minutes in VMEM also exhibit vesicles forming on the surface of the tegument (not shown), the tegumental cytoplasm has become more diffuse while the outer tegumental membranes appear to remain intact (Figure 6.9). There appears to be no obvious effect of a 30 minute VMEM incubation on the structure of the tissues underlying the tegument. The effect of a 1 hour low pH treatment is shown in Figure 6.10. Figure 6.10 shows that although the tegumental membrane appears to remain intact, the tegumental cytoplasm is severely disrupted. The cytoplasm contains electron dense material but this is interspersed with large electronlucent areas that apparently contain only fluid. The tissues underlying the tegument show no obvious effects of low pH treatment even after an hour in VMEM. Large vesicles can be observed in Figure 6.10, these appear to contain none of the constituents of the tegumental cytoplasm except for a thin layer of granular cytoplasm closely associated with the vesicle membrane. Figure 6.10 also demonstrates the extent of tegumental disruption after a prolonged (1 hour) low pH treatment. Figure 6.11 is a high power micrograph taken from a section through a vesicle. The vesicle was observed to retain the

multilamellar structure of the untreated tegument. In general the "double outer membrane" of the tegument was seldom defined clearly enough to determine the number of phospholipid bilayers present.

In summary, low pH treatment produces vesicles that originate from the outer tegumental membranes. VMEM also causes severe disruption to the tegumental cytoplasm as the incubation time increases. After thirty minutes of low pH treatment the tegumental cytoplasm is considerably more diffuse and floccular than in control parasites. The effect is more noticeable still after a 1 hour VMEM incubation. The underlying muscle layers display no obvious changes in appearance after low pH treatment. The basal membrane of the tegument appears to remain intact (Figure 6.9).

Figure 6.7

Control micrograph of the adult male (mag=x12500) containing the characteristic features of the tegument. The worm is bounded by the outer membrane (om) of the tegument which displays surface pits (sp). The tegumental cytoplasm contains discoid bodies (db) and membranous bodies (mb). The tegumental cytoplasm is separated from the underlying tissues by the basal membrane that displays numerous invaginations (iv). Underlying the basal membrane are the muscle layers (m). The tegumental cytoplasm is connected to the subtegumental cytons (cell bodies) by microtubule lined channels (c). Note the dense granular nature of the cytoplasm.

Figure 6.7

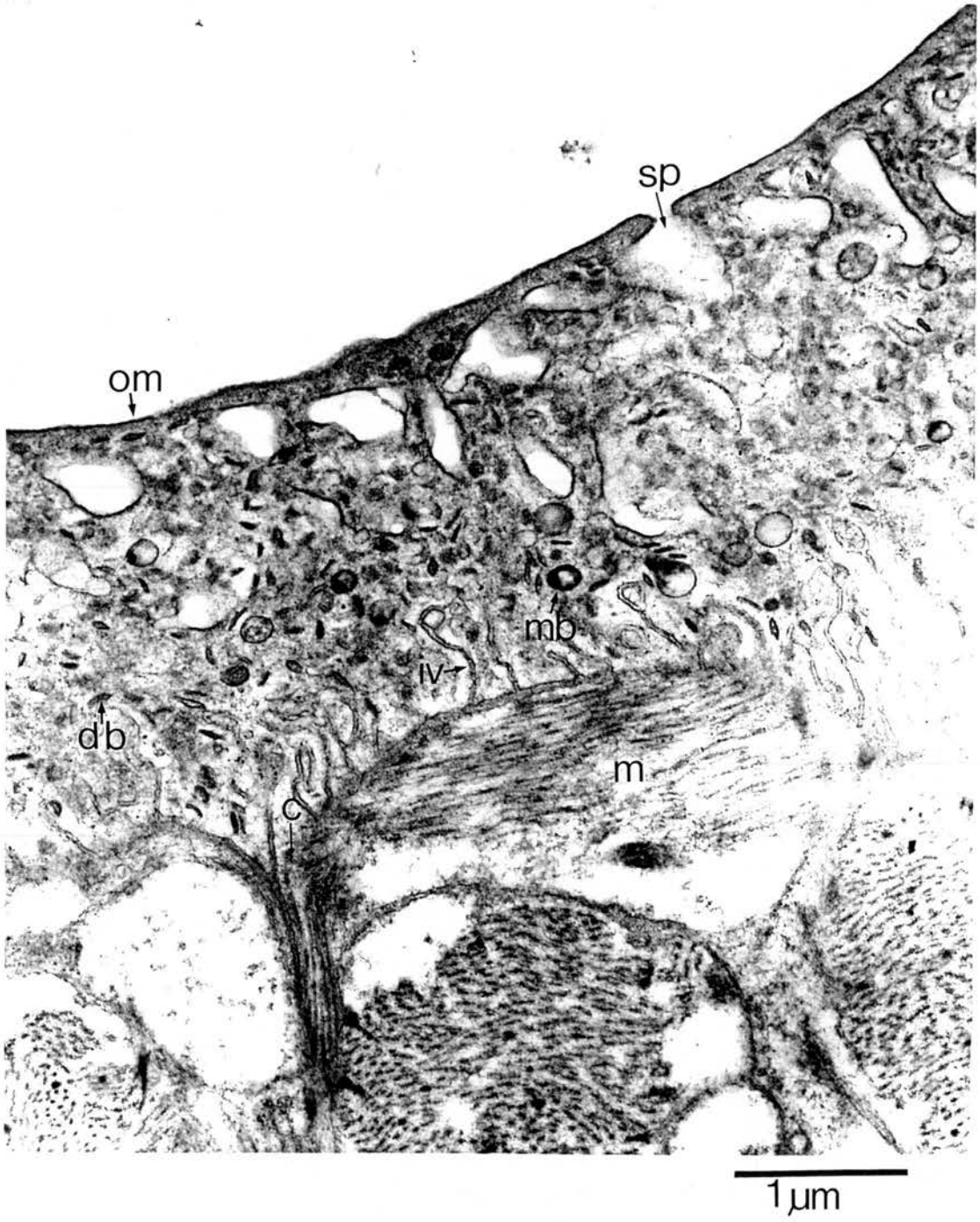

Figure 6.8

Micrograph of adult tegument after 15 minutes of vesicle forming protocol. The tegument contains all the features observed in the control micrograph including discoid bodies (db) and surface pits (sp). The outer membrane (om) of the tegument appears unchanged. Invaginations of the basal membrane (iv) can still be observed as can the underlying muscle layers (m): both structures appear relatively unaffected by 15 min. low pH treatment. The tegumental cytoplasm appears less dense and more floccular than in control parasites. Vacuoles (vac) can be observed in the basal region of the tegumental cytoplasm. Vesicles (v) can be observed "budding-off" from the outer tegumental membrane.

Figure 6.8

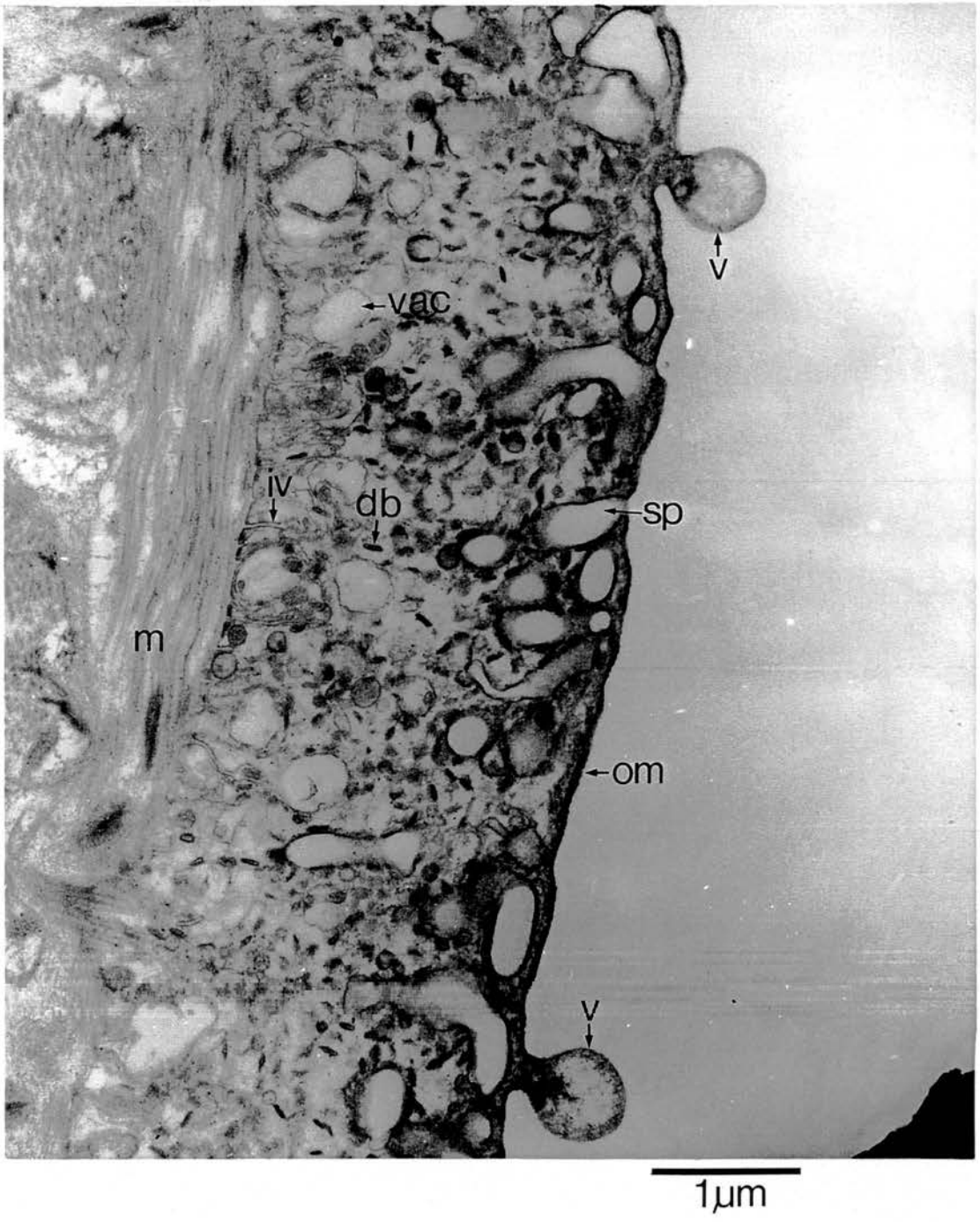

Figure 6.9

Tegument of adult parasite after 30 minutes of the vesicle forming protocol. The tegument remains intact, bounded on the outside by the outer membrane (om) and interiorly by the basal membrane, invaginations of which can still be observed (iv). The underlying muscle layers (m) remain unchanged in appearance by low pH treatment. The appearance of the tegumental cytoplasm has been substantially changed by 30 min. low pH treatment. Discoid bodies and membranous bodies are difficult to recognise. Areas of the tegument retain the dense granular cytoplasm (gc) observed in the control parasites. However the dense layers are separated by large diffuse regions (dr) of cytoplasm which contain no electron dense material.

Figure 6.9

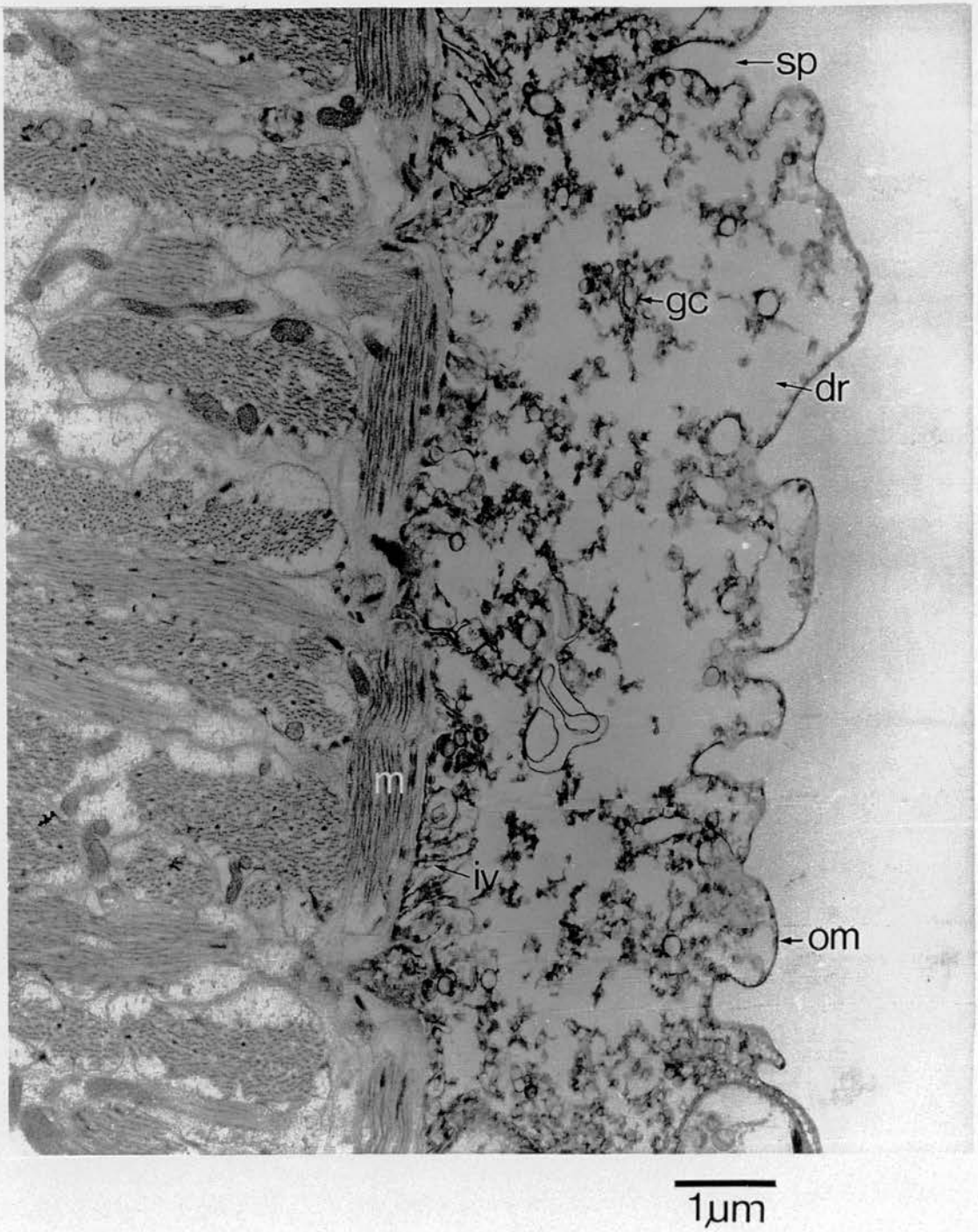

Figure 6.10

Adult parasite after 1 hour in the vesicle forming media. The outer membrane (om) of the tegument is still distinguishable. The underlying muscle (m) appears unchanged by low pH treatment. The tegumental cytoplasm is extremely diffuse with only small areas of electron dense granular material remaining. Three large membranous vesicles (v) can be observed. Several vesicles can be observed budding from the outer membrane of the tegument (vb). The vesicles appear to contain almost no electron dense material except a thin layer of granular cytoplasm (gc) associated with the enveloping membrane.

Figure 6.10

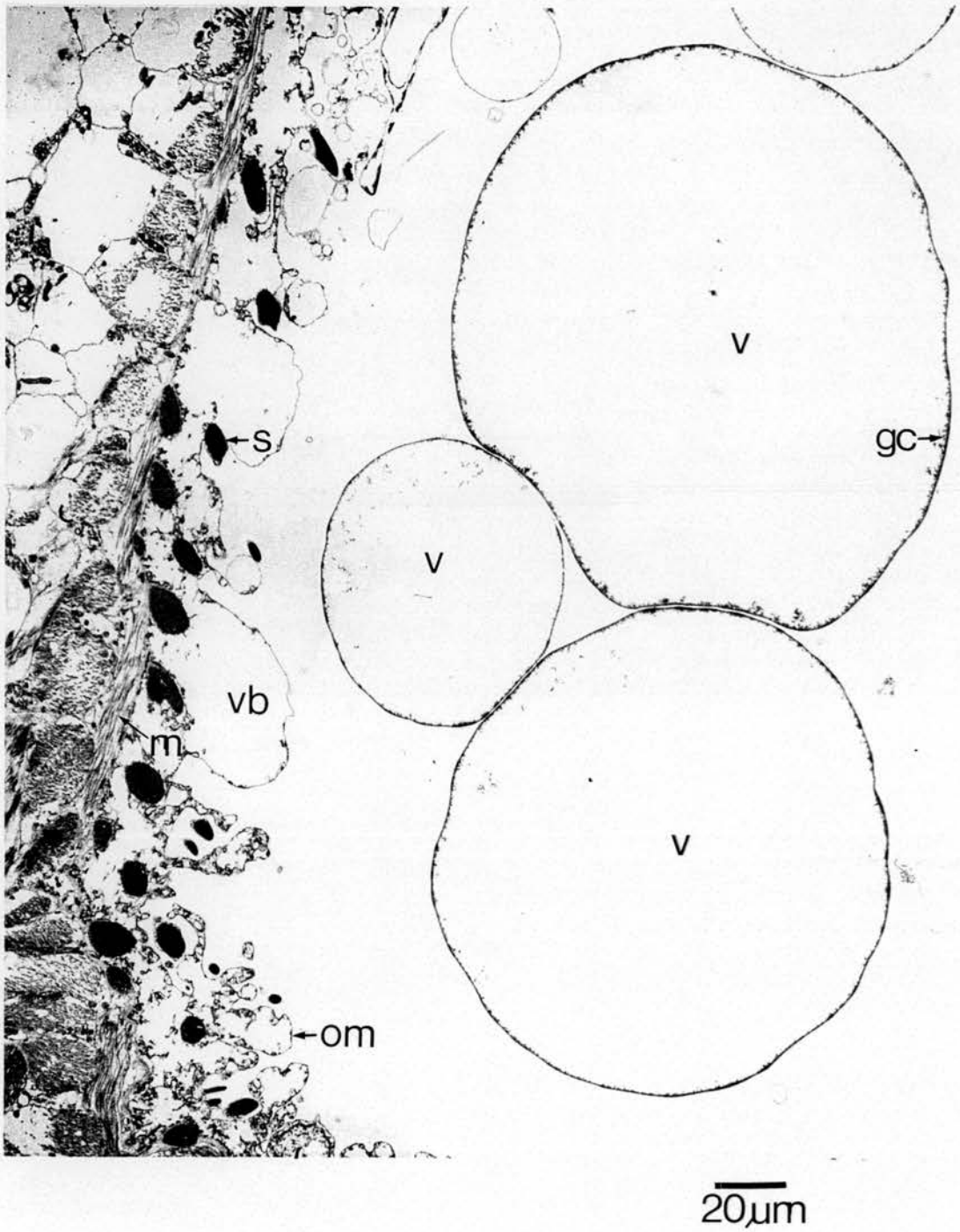

Figure 6.11

High power micrograph taken from a vesicle in Figure 6.7. The micrograph demonstrates that the vesicle formed by low pH treatment retains the unique multilaminate structure of the tegumental outer membrane (om).

Figure 6.11

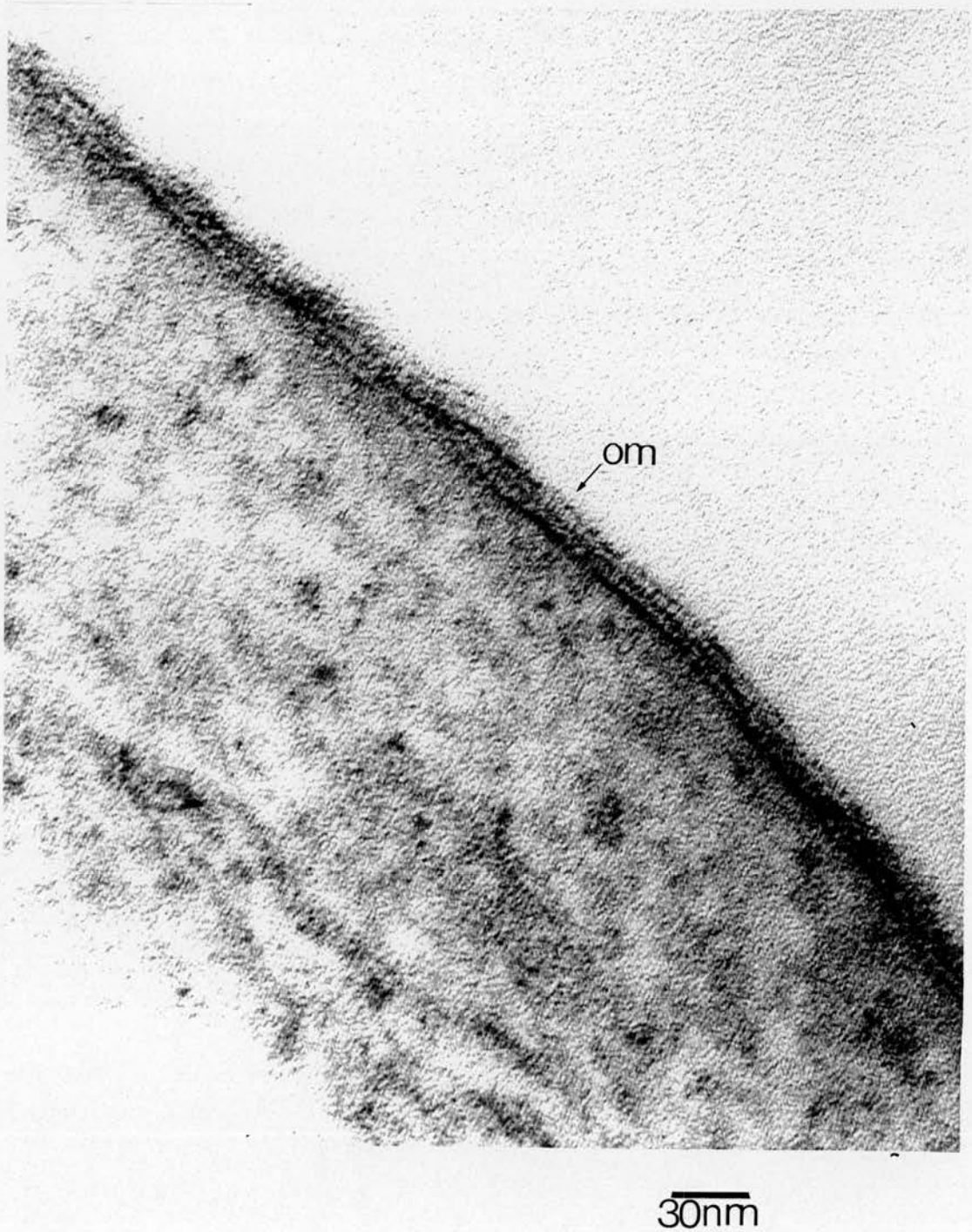

6.4 DISCUSSION

Effect of vesicle formation protocol on the parasite

The electron microscopy studies illustrate the effect on the tegument of treatment with low pH media. Incubation in VMEM has caused vesicles to bud from the outer membrane of the parasite tegument. The tegumental cytoplasm became increasingly floccular and diffuse as the incubation time was increased. The scanning microscopy illustrated that the outer membrane of the tegument became severely disrupted with longer incubations in low pH media. Vesicles were observed forming at all incubation times, also cracks in the tegument were also apparent after incubations of 30 minutes or longer. After a 1 hour incubation large areas of the tegumental outer membrane were observed to be stripped away. The parasites were not killed, or paralysed by the treatment as muscle contractions were observed in worms several hours after exposure to low pH. The transmission electron microscopy showed that the underlying muscle layers and other tissues remain relatively unaffected by exposure to low pH. The vesicle forming media only effects the tegument of the parasite. Prolonged incubations resulted in large areas of the outer tegumental membranes being entirely removed. Shorter treatments caused cracks to form in the tegumental membrane. The number of vesicles increased as the length of low pH treatment increased. However, observations during patch-clamp experiments showed that after a 15 minute treatment in VMEM vesicles continued to form for several hours in bathing solution of pH 7.2. This final observation demonstrates that the process of vesicle formation is initiated by low pH but continued exposure to the VMEM is not required. The mechanism by which low pH treatment induces vesicle formation is not known.

Other substances have been shown to cause the formation of vesicles from the outer membranes of parasite teguments however the vesicles appear different and the

substances frequently have other effects that differ from low pH treatment. Treatment of *Fasciola hepatica* with 10^{-3} M ouabain results in the formation of small "blebs" from the surface of the tegument (Skuce and Fairweather, 1989), the vesicles were substantially smaller than those observed on low pH treatment of adult schistosomes. Treatment of adult *Schistosoma mansoni* with praziquantel or its main metabolite causes surface lesions and "blebs" on the parasite tegument (Staudt, Schmahl, Blaschke, Mehlhorn, 1992). The parasites were incubated for 4 hours after which the vesicles were still extremely small (0.07-0.6 μm) compared with vesicles >50 μm in diameter observed after a 1 hr low pH treatment (Figure 6.10). Additionally praziquantel was observed to paralyse the parasites (Staudt *et al.* 1992) whilst rhythmic contractions were frequently observed several hours after low pH treatment. Incubation of adult *Schistosoma mansoni* in concanavalin A (con A) produced vesicles that superficially resembled those produced by low pH treatment (Simpson and McLaren, 1982). Incubation in con A resulted in vesicles 5-6 μm in diameter similar in size to those produced by shorter low pH treatments. Also the con A incubation produced a decrease in cytoplasmic density similar to the low pH treatment. However the con A treatment caused vacuolisation of the underlying muscles and deeper tissues that was not observed after low pH treatment. The vesicles and accompanying tegumental damage were a direct result consequence of lectin binding not a result of inhibition of a metabolic pathway (Simpson and McLaren, 1982). Low pH treatment (Figure 6.8) and con A incubation (Simpson and McLaren, 1982) both showed a degree of vacuolation at the basal region of the tegument. The vacuoles became less obvious as the low pH incubation time was increased and Simpson and McLaren (1982) have demonstrated that similar vacuoles can be observed in parasites incubated in normal RPMI media.

In summary, low pH incubation is one of several treatments that induce vesicle formation from the outer membrane of the parasite tegument. Observations demonstrate that low pH initiates the process of vesicle formation but the presence of a low pH environment was not required for the process to continue. Unlike treatment with praziquantel, low pH did not paralyse the parasites. The effect of low pH on the parasite tegument appears to have many similarities with the effects of con A. The exact mechanism by which low pH causes vesicle formation remains unclear. Low pH has been demonstrated to have dramatic effects on many proteins including ion-channels (Robertson and Martin, 1996). It is apparent that low pH upsets the osmoregulatory process in the tegument causing a net influx of water. The increase in pressure in the tegument causes the vesicles to bleb from the surface. Certain areas of the outer membrane of the parasite may be more susceptible to vesicle formation than others as domains of different fluidity have been reported (Kusel and Gordon, 1989). A more fluid region of membrane would be more likely to stretch to form a vesicle.

Source of vesicles

The results clearly demonstrate that incubation of adult schistosomes in low pH media (pH 3.5-4.0) at 37^0 C results in vesicles budding from the surface of the parasites. The number of vesicles produced could be increased by increasing the length of incubation. Small vesicles could be observed budding from the surface of the worms after a fifteen minute incubation. Incubation in low pH media for 2 hours resulted in a large number of vesicles budding from the worm surface. Initial scanning electron microscopy experiments showed vesicles on the surface of the parasite, however, their site of origin could not be determined accurately as the base of most vesicles could not be seen. The fluorescence studies demonstrated that a proportion (41%) of the vesicles were bounded by the outer bilayer of the outer tegumental double membrane demonstrating they originated from the outer membrane of the tegument (Foley *et al.* 1986). The fluorescence studies could not determine the site of origin of all the vesicles. The lack of fluorescence in some vesicles was attributed to leaching of the fluorescent probe or prolonged exposure to the bleaching properties of u.v. light. In many cases the vesicles were small and fluorescence could not be determined as the background fluorescence from the body of the worm was too intense. Transmission electron microscopy revealed that the vesicles formed from the outer membrane of the parasite tegument. There was no evidence of vesicles forming from any other source within the parasite. The appearance of the tissues underlying the tegument was compared between control parasites and those subjected to low pH treatment. The overall of appearance of the underlying muscles and tissues remained unaffected by exposure to low pH, no evidence of vesicles forming from the basal membrane of the tegument or the underlying tissue was observed.

Suitability for patch-clamping

The control scanning electron micrographs illustrate the uneven surface of the male schistosome. The female parasite possesses a much smoother surface (reviewed by McLaren, 1980). To date there are no reports of single-channel recordings from the tegument of the male schistosome. There have been reports of limited success obtaining single ion-channel records from adult females (Day *et al*, 1992b). The patch-clamp technique requires a seal between the glass pipette and the membrane of the cells to be studied of giga-ohm resistance. To achieve a seal of sufficient resistance the membrane to be studied is required to have a smooth, clean surface; in many preparations the membranes are artificially cleaned with enzymes prior to seal formation (Hamill *et al.* 1981). The lack of success in obtaining a giga-ohm seal from the male tegument reported by Day *et al,* (1992b) can be largely attributed to the uneven, spiny nature of the parasite surface (McLaren, 1980). An alternate method for obtaining seals of sufficient resistance from unsuitable preparations involves the formation of membrane vesicles from the specimen, *e.g.* single ion-channels have been recorded from membrane vesicles prepared from the somatic muscle cells of *Ascaris suum* (Dixon *et al,* 1993). The membrane vesicles prepared from the tegument of the adult schistosome appear very smooth and clean under the light microscope. The electron microscopy studies further show the smooth, clean surface of the vesicles. These studies demonstrate that the schistosome membrane vesicles produced by low pH treatment are suitable candidates for the patch-clamp technique.

Membrane Structure of vesicles

The membrane vesicles clearly arise from the outer tegument of the schistosome. The outer tegumental membrane of the schistosome is unusual in that it is composed of two bilayers in close association (Mclaren and Hockley, 1977) in contrast to the majority of eukaryotic cell membranes which are composed of a single bilayer. In effect, the tegument of the schistosome is bounded by two conventional membranes in close association. The transmission electron microscopy has shown that some of the vesicles possess the unusual, multilaminate, membrane structure found in the outer tegument, in the majority of vesicles poor fixation rendered the number of bilayers present in the vesicles unresolvable. The fluorescent probe used (AF18) inserts into bilayers but does not traverse them (Foley *et al.* 1986). Only the outer bilayer of the tegument was labelled with AF18 therefore the outer bilayer of the double membrane is present in at least 41% of the vesicles. The transmission electron microscopy studies gave no evidence of vesicles forming between the two bilayers or any separation of the two due to low pH treatment. Additionally the vesicles contained a thin layer of the granular tegumental cytoplasm close to the bounding membrane (Figure 6.10), previous studies have described a thin dense layer of granular cytoplasm underlying the inner bilayer of the double outer membrane of the parasite tegument (McLaren, 1980). It was concluded therefore that at least a proportion of the vesicles possess the double bilayer structure found in the native outer tegument. This unusual membrane arrangement has several interesting implications for any recordings of single ion-channels from the schistosome tegument; these are discussed in the next chapter.

CHAPTER 7: PATCH-CLAMP INVESTIGATION OF ION-CHANNELS IN VESICLES FROM *SCHISTOSOMA MANSONI* OUTER TEGUMENT.

7.1 INTRODUCTION

The patch-clamp technique allows the study of individual ion-channel types in biological membranes. At present schistosomiasis is treated with praziquantel, which although effective its mode of action remains unknown. Evidence suggests that praziquantel affects calcium homeostasis and therefore the drug may be acting on a specific ion-channel in the parasite tegument (Redman *et al,* 1996; Chapter 5). Clearly the study of the ion-channels present in the tegument of the parasite, and the effect of praziquantel on them, would help to elucidate the mechanism of praziquantel action. The aim of this section was to demonstrate that the vesicle preparation was suitable for patch-clamping and to demonstrate the presence of different ion-channel types within tegument derived membrane vesicles. This chapter describes observations on single-channel currents made from membrane vesicles produced by low pH treatment of adult schistosomes. The Materials and Methods section is outlined because the patch-clamp technique and vesicle preparation protocol are described in detail in Chapters 2 and 6 respectively. The main aim of this chapter was to demonstrate the suitability of the schistosome vesicle preparation for single-channel studies: all my attempts to apply any "sharp-electrode" methods to the vesicle preparation were unsuccessful because the vesicles always burst when impaled with the electrode.

The results section of the chapter begins with evidence of ion-channels grouped on the basis of ion selectivity. Ion selectivity was assessed by comparing experimentally obtained reversal potentials with those predicted by the Nernst equation (Hille, 1992). Evidence of a large-conductance non-selective cation

channel, in males, similar to the channel reported in female schistosomes (Day *et al*, 1992b) is presented. The results section continues with examples of experiments where the ion selectivity of the ion-channels present was not determined. The results also demonstrate that patch-clamping vesicles offers recordings of higher resolution than previous studies applied directly to the native membranes (Day *et al.* 1992b). The section concludes with a summary of the single-channel properties observed.

The discussion section of the chapter deals with the various channel types observed and their possible function. The unique membrane structure of the outer tegument may be conserved during vesicle formation (see chapter 6) and subsequent patch-clamp experiments. The implications of this are discussed and a hypothetical model is presented to aid the interpretation of several ambiguous experiments; to explain the high occurrence and large number of "subconductance states" seen in some recordings. Finally, the possible role of praziquantel as a channel modulator is considered.

7.2 MATERIALS AND METHODS

Patch-Clamp Experiments on Vesicle Preparation

The methods are outlined here, for a detailed description see Chapter 2 for the electrophysiological methods and Chapter 6 for details of the vesicle formation protocol. After undergoing the vesicle formation protocol, parasites were washed gently three times in GMEM and transferred to the recording chamber. The parasites were pinned onto Sylgard^{TM} and bathed in one of a number of solutions (Table 7.1). Pipettes were pulled, membrane patches were obtained and single-channel recordings made. Experiments were carried out using a range of bath and pipette solutions (Table 7.1). The majority of experiments were carried out using the isolated inside-out patch configuration (see Chapter 2) while a limited number employed the vesicle-

attached configuration. All recordings were obtained from vesicles originating from male parasites.

Single-channel recordings were obtained over a range of membrane potentials and the amplitudes of channel openings were used to construct a current-voltage plot. The single-channel conductances and reversal potentials were obtained from the line of best fit to the current-voltage plots. The Nernst equation (equation 1)(Hille, 1992) was used to calculate the predicted reversal potentials for ion-channels permeable to each ion species in the recording solutions.

$E_{Ion}=(RT\backslash F)\ ln\ [Ion]_o \backslash [Ion]_i$.....[1]

The Hille equation [1] for monovalent cations. Where E_{Ion} is the reversal potential for the ion species; R is the gas constant (1.987 cal K^{-1} mol^{-1}); T is temperature on the Kelvin scale; and F is Faradays constant ($9.648x10^4$ C mol^{-1}). *[Ion]* is the millimolar concentration of the ion species. The suffixes *i* and *o* refer to the inside (intracellular) and outside (extracellular) of the membrane patch. The reversal potential for any cation can be calculated by using the relevant concentrations. To calculate the predicted reversal potential for an anion species the equation must be altered: the millimolar concentration of ions on the inside (intracellular) is the numerator and the outside (extracellular) concentration the denominator.

In a number of experiments the observed reversal potential was significantly different to the reversal potentials predicted by the Nernst equation for a channel conducting a single ion species. In these cases a modified Goldman-Hodgkin-Katz equation (Hille, 1992)(equation 2) was used to assess the relative permeability of cations.

$E_{rev}=(RT\backslash F)\ ln\ (P_{Na}\ [Na]_o\ +P_K\ /P_{Na}[K]_o)\backslash(\ P_{Na}\ [Na]_i\ +\ P_K/P_{Na}\ [K]_i)$

.....[2]

The Goldman-Hodgkin-Katz equation *[2]*. Where E_{rev} is the reversal potential; *R, T* and *F* have their usual meanings; *[ ]* is the millimolar concentration of the particular ion species; the subscripts *i* and *o* refer to the inside (intracellular) and outside (extracellular) of the membrane patch; P_{Na} is the permeability of sodium ions and P_K the permeability of potassium. P_K/P_{na} is the relative permeability of potassium ions (relative to the permeability of sodium ions). The above equation can be modified to take Ca^{2+} permeability into consideration, the equation necessarily becomes more complex to take account of the divalent nature of calcium ions; equation 3 (adapted from Lewis, 1979).

$$E_{rev} = \frac{RT}{F} ln \frac{[Na]_o + \frac{P_K}{P_{Na}}\ [K]_o + \ 4P'\ \ [Ca]_o}{[Na]_i + \frac{P_K}{P_{Na}}\ [K]_i + \ 4P'\ \ [Ca]_i . e^{FE_{rev}/RT}} \quad .....[3]$$

$$P' = (P_{Ca}/P_{Na}) \left(\frac{1}{1+\ e^{FE_{rev}/RT}} \right) .....[4]$$

Where E_{rev} is the reversal potential; *R, T,e* and *F* have their usual meanings; *[ ]* is the millimolar concentration of the particular ion species; the subscripts *i* and *o* refer to the inside (intracellular) and outside (extracellular) of the membrane patch; P_{Na} is the permeability of sodium ions, P_K the permeability of potassium ions and P'_{Ca} is related to the permeability of calcium ions (P_{Ca}) by equation 4.

When the quality of channel records permitted, the probability of channel opening (P_{open}) was calculated (equation 5).

$P_{open} = (T_1+2T_2+3T_3+.....nT_n)(n \times total\ time)$.....*[5]*

Equation *[5]*, where P_{open}= probability of channel opening; T_n= time with n (and only n) channels open; n= total number of active channels in the patch; *total time*= duration of patch recording at fixed membrane potential.

Additional Electrophysiological Experiments

Attempts were made to apply conventional voltage-clamp and current-clamp techniques to the vesicle preparation. These were unsuccessful, attempts to impale a vesicle with a high resistance electrode resulted in the vesicle bursting. These experiments are not discussed further.

Table 7.1

Solution	Constituents (mM)	pH
"schistosome"	NaCl, 100; KCl, 20; $CaCl_2$, 3; $MgCl_2$, 2; Glucose 5; HEPES, 10.	pH to 7.4 with CsOH
High-Na	NaAcetate, 50; NaCl, 100; KCl, 20; $CaCl_2$, 2; HEPES, 5; Glucose, 5.	pH to 7.2 with NaOH
K-50	NaCl, 40; KCl, 50; $CaCl_2$, 50; HEPES, 5; Glucose, 5.	pH to 7.2 with KOH
Low-K	KCl, 5; NaCl, 125; $CaCl_2$, 0.4; $MgCl_2$, 0.4; HEPES, 10; ATP, 2.	pH to 7.4 with NaOH
High-K	NaCl, 25; KCl, 90; MgCl2, 2; Glucose, 20; HEPES, 10; L-Glutamine, 2.	pH to 7.4 with NaOH
Na-110	NaCl, 110; KCl, 5; $CaCl_2$, 2; Glucose, 20; HEPES, 10; L-Glutamine, 2.	pH to 7.4 with NaOH

Table 7.1: The concentrations (in mM) of the various solutions used in patch-clamp experiments on the schistosome derived membrane vesicles.

7.3 SCHISTOSOME RESULTS

From a sample of 295 pipettes, seals of resistance >0.5GΩ were obtained from 23% of pipettes while only 15% of pipettes gave seals of resistance >1 GΩ (suitable for single-channel recording). Of the membrane patches with resistances >1 GΩ 59% displayed evidence of ion-channel activity. Table 7.2 summarises the properties of the observed ion-channels described in this section. Nineteen current-voltage relationships were analysed. Ion-channels with conductances ranging between 7.7pS and 360pS were observed. On the basis of the observed reversal potential and equations *[1]* to *[4]* in the methods section the ionic selectivity of the channels was investigated. Evidence of channels selective for potassium (n=3), sodium (n=4), all cations (n=2) and Cl^- (n=1) will be presented. Additional experiments where the ion selectivity of the channels was uncertain (n=4) or could not be estimated (n=5) have also been included. The problems associated with identifying the properties of ion-channels within the tegument derived vesicle preparation have been listed.

Table 7.2

Channel Selectivity	No.	Conductance range (pS)	Comments
K^+	3	37.5-114	Highest conductance value may reflect the increase in K^+ concentration in the recording solutions.
Na^+	4	7.4-80	Variation in conductances may indicate more than one type of Na^+ channel present.
Cations	2	110-360	subconductance level of 210pS observed in one experiment.
Anion (Cl^-)	1	22.4-58.4	Conductance varies as the Cl^- concentration was increased during the experiment.
Partially characterised ion selectivity.	4	11.8-50.0	Not conducting K^+ alone or Na^+ alone.
Unknown	3	7.7-82.6	Interpretation of the current-voltage relationships uncertain.

Table 7.2

Table summarises the observed occurrence of each type of ion-channels. The channels are grouped according to their ion selectivity. The Table gives details of the number of observations and the range of conductances observed. Comments on each group of ion-channels are included in the final column.

Evidence for potassium selective ion-channels

Three experiments are presented containing current-voltage relationships where the observed reversal potential was closest to the predicted reversal potential for a channel permeable to potassium ions. All the experiments in this section were carried out using the isolated inside-out patch configuration.

Figure 7.1 illustrates a potassium selective ion-channel. The concentrations of each ion on either side of the membrane patch are given in Figure 7.1A. Single-channel records were obtained over a range of membrane potentials: example records are shown in Figure 7.1B. The amplitude of channel openings were plotted against membrane potential in Figure 7.1C. The line obtained by linear regression of the current-voltage relationship gave a slope conductance of 114pS and a reversal potential of -70.7mV. The reversal potentials predicted by the Nernst equation were: E_{Na}=7.97mV, E_{Cl}=44.3mV and E_K=-85.9mV. The observed reversal potential was clearly closest to that predicted for a potassium selective ion-channel.

In the experiment illustrated in Figure 7.2 single-channel events were obtained over a range of potentials. Up to three different amplitude levels were observed at some membrane potentials (Figure 7.2A). The channel amplitudes were plotted on a current-voltage plot and linear regression was used to fit a line to the smallest amplitude level (Figure 7.2B). The two larger channel amplitudes did not occur frequently enough over the membrane potentials tested to allow a current-voltage plot to be determined. The smallest of the channel amplitudes had a slope conductance of 37.5pS with a reversal potential of +24.4mV. The observed reversal potential was within 0.3mV of the reversal potential predicted for a potassium selective ion-channel. The Nernst equation predicted reversal potentials of

E_K=24.1mV, E_{Ca}=35.3mV, E_{Cl}=-10.8mV and E_{Na}=-33.6mV. It was concluded that the ion channel illustrated in Figure 7.2 was selective for potassium ions over sodium or chloride ions.

Another membrane patch yielded two distinct channel amplitudes (corresponding to two separate ion-channels) over the range of potentials tested. Current-voltage plots were constructed for each amplitude level and lines were fitted to the data using least squares regression. The recording solutions were identical to those used in Figure 7.2 and the Nernst equation predicted reversal potentials of: E_{Na}=-33.6mV, E_K=24.1mV, E_{Ca}=35.3mV and E_{Cl}=-10.8mV. One of the current-voltage relationships gave a slope conductance of 47.5 pS and a reversal potential of 15.8mV. The observed reversal potential suggested that the ion-channel was selective for potassium ions. The second current-voltage relationship gave a slope conductance of 53 pS and an observed reversal potential of -26.7mV. The observed reversal potential was closest to the predicted Nernst potential for sodium ions. It was concluded that the second current-voltage relationship represented an ion-channel selective for sodium ions. Further evidence for ion-channels selective for Na^+ ions is presented in the following section of this chapter.

Figure 7.1

A: Concentrations of ions on each side of the membrane patch. The bath contained a mixture of GMEM (Table 6.1, pp91) and 3M KCl. The pipette contained high-Na (Table 7.1, pp123) solution with an additional 2mM $CaCl_2$.

B: Examples of single-channel records obtained at -50mV and -85.3mV. In each case c refers to the channel in the closed state and o refers to the channel in the open state.

C: Current-voltage relationship constructed from channel amplitude versus membrane potential. Linear regression was used to fit a line to the observations and gave a slope conductance of 114 pS. The observed reversal potential was -70.7mV. The reversal potentials predicted by the Nernst equation are illustrated on the plot: E_K=-85.9mV, E_{Na}=7.97mV and E_{Cl}=44.3mV. The observed reversal potential was closest to the Nernst potential for a potassium selective ion-channel.

Figure 7.1

A

Ion [mM]	Bath (in)	Pipette (out)
Na	100	151
K	605	20
Ca	2	4
Cl	719	124
Acetate	0	50

B

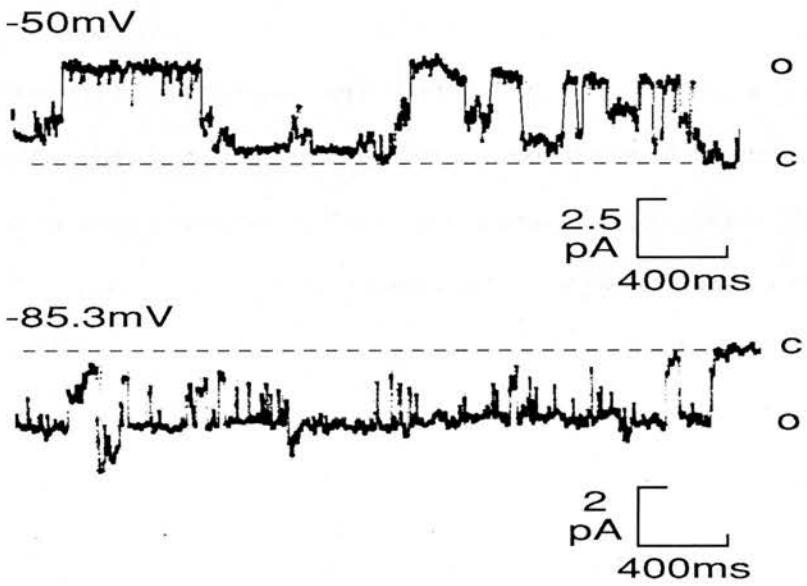

C

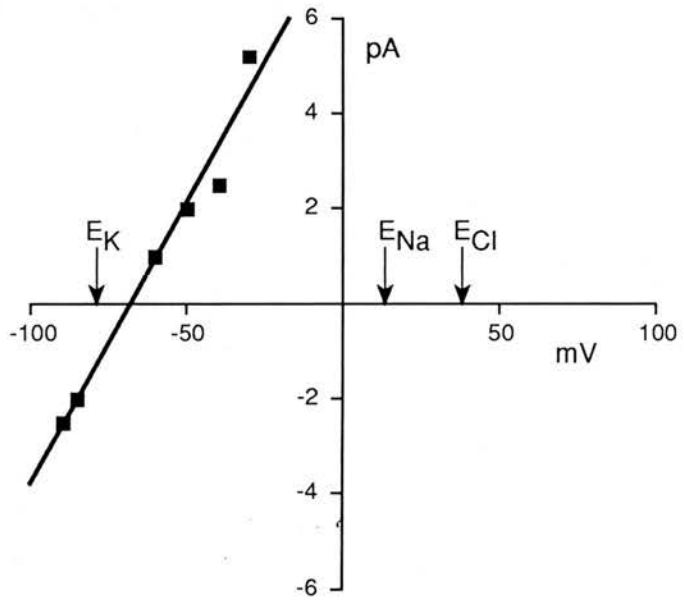

Figure 7.2

A: Examples of single-channel records at -40 and -60mV. There are clearly several (at least 3) different amplitude levels present. The levels used to construct the current voltage plot are labelled with dotted lines. Channel amplitude was calculated as the difference between Level 1 and Level 2.

B: Current-voltage relationship constructed from channel amplitudes at several different membrane potentials (■). The line obtained by linear regression gave a slope conductance of 37.5pS and a reversal potential of 24.4 mV. The bath contained high-Na solution and the pipette contained K-50 solution (constituents of each solution are given in Table 7.1, pp123). The reversal potentials predicted by the Nernst equation are illustrated on the plot: E_K=24.1mV, E_{Cl}=-10.8mV, E_{Ca}=35.3mV and E_{Na}=-33.6mV. The observed reversal potential was closest to the Nernst potential for a potassium selective ion-channel.

Figure 7.2

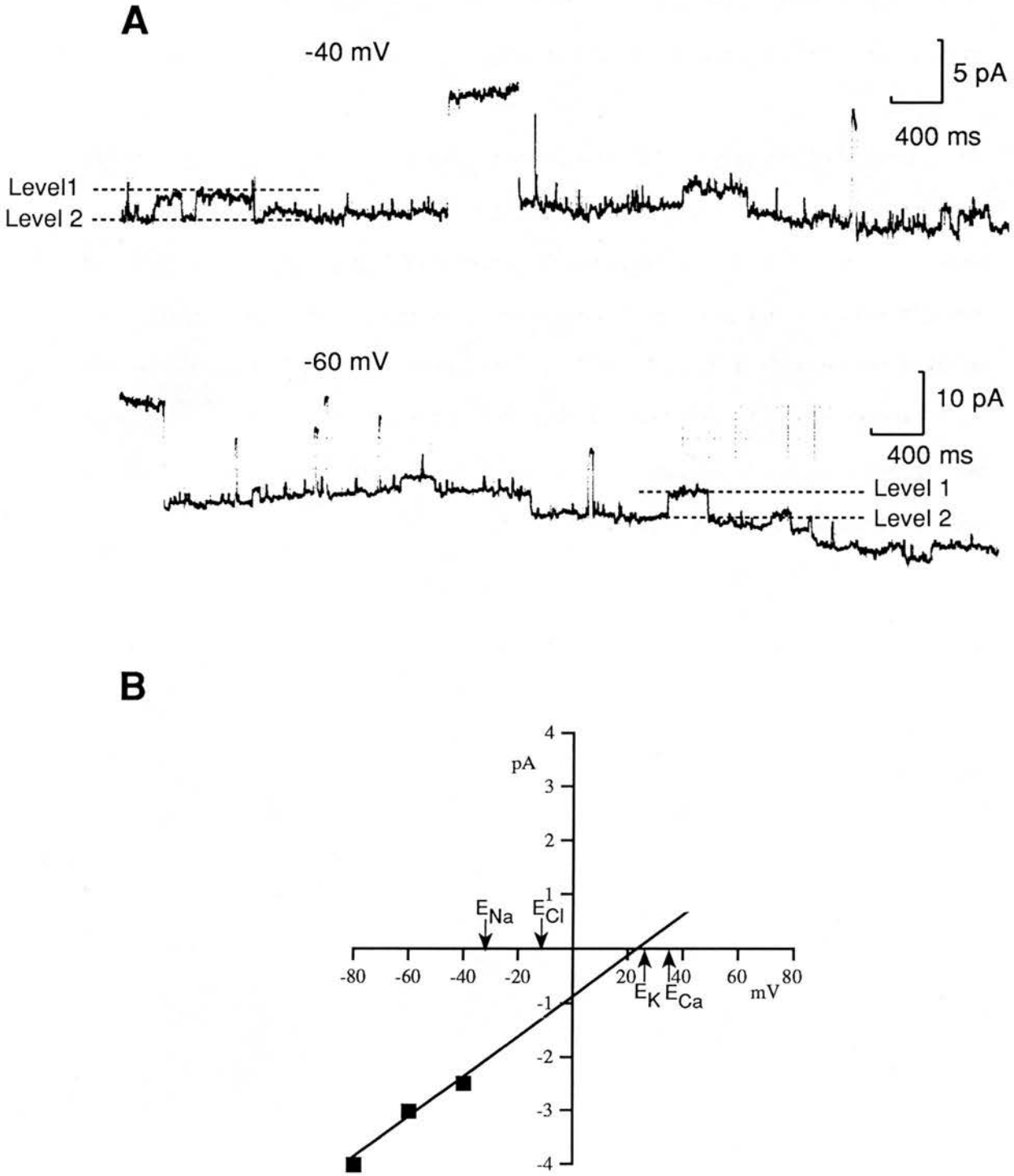
A
-40 mV
5 pA
400 ms
Level1
Level 2
-60 mV
10 pA
400 ms
Level 1
Level 2
B
pA
4
3
2
1
-1
-2
-3
-4
E_Na
E_Cl
-80
-60
-40
-20
20
40
60
80
mV
E_K
E_Ca

Evidence for sodium selective ion-channels

Figure 7.3 illustrates an ion-channel selective for sodium ions. The concentration of the ion species in the recording solutions is shown in Figure 7.3A. Initial recordings were made in the vesicle-attached configuration, the patch pipette was then pulled away from the vesicle surface and further single-channel recordings were made in the isolated inside-out patch configuration. A current-voltage relationship was constructed for the recordings made in the isolated inside-out patch configuration. The current-voltage relationship is shown in figure 7.3B. The line obtained by linear regression of the current-voltage relationship in the isolated inside-out configuration gave a conductance of 22.9pS and a reversal potential of 5.5mV. The observed reversal potential (5.5mV) was closest to the reversal potential predicted for a channel selective for Na ions over K^+, Ca^{2+}, or Cl^-. The predicted reversal potentials from the Nernst equation were E_{Na}=7.98mV, E_K=34.9, E_{Ca}=17.5mV, and E_{Cl}=-1.0mV.

Figure 7.3

A: The bath contained VMEM (see Table 6.1, pp91 for constituents) and the bath contained high-Na solution (see Table 7.1, pp123 for constituents). Concentrations of ion species on each side of the membrane patch; bath = intracellular, pipette = extracellular.

B: Current-voltage relationship for the isolated inside-out (□) configuration. The line obtained by linear regression gave a slope conductance of 22.9pS and a reversal potential of 5.5mV. The Nernst equation predicted reversal potentials of E_{Na}=7.98mV, E_K=34.9mV, E_{Ca}=17.5mV and E_{cl}=-1.0mV. Clearly the observed reversal potential is closest to the Nernst potential for a sodium selective ion-channel.

Figure 7.3

A

Ion [mM]	Bath (in)	Pipette (out)
Na	110	151
K	5	20
Ca	2	4
Cl	119	124
Acetate	0	50

B

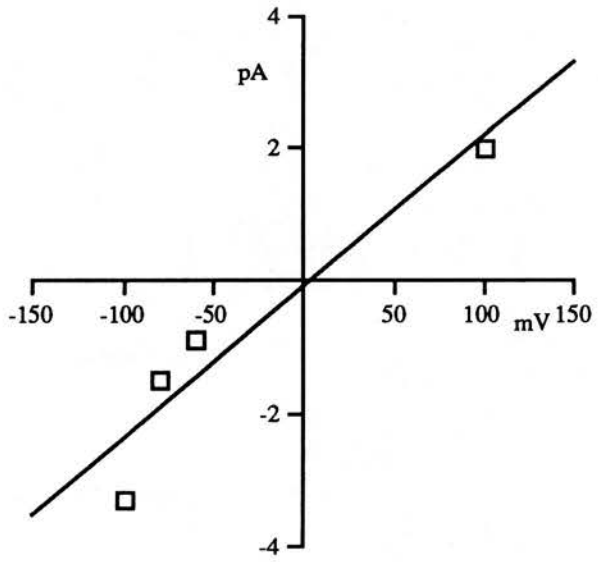

The experiment shown in Figure 7.4 used the isolated inside-out patch configuration. Single-channel recordings were made over a range of membrane potentials (for examples see Figure 7.4A). The amplitude of channel opening was plotted against membrane potential to give the current-voltage relationship shown in Figure 7.4B. The line obtained from the current-voltage plot by linear regression gave a conductance of 21.8pS and a reversal potential of 52.9mV. The observed reversal potential is closest to the reversal potential predicted for a sodium selective ion-channel. The Nernst equation predicted the reversal potentials for Na^+, K^+ and Cl^- to be 37.5mV, -73mV and 0mV respectively.

The experiment illustrated in Figure 7.5 was carried out using the isolated inside-out patch configuration. Single-channel recordings were made over a range of potentials, for examples see Figure 7.5A. The intracellular concentration of K^+ and Cl^- ions was then increased by adding a small volume of concentrated KCl to the bath. Further single-channel records were obtained over a range of potentials, for examples see Figure 7.5B. A current-voltage relationship was constructed for the channel openings prior to the addition of KCl and a further current-voltage relationship was constructed for the channel openings observed after the addition of the KCl. The current-voltage relationships (with lines fitted by linear regression) are shown on the same axis in Figure 7.5C. Prior to KCl addition, the line obtained by linear regression gave a conductance of 7.4pS and a reversal potential of 27mV. The Nernst equation predicts reversal potentials for channels selective to either Na, K or Cl of 37.5mV, -73mV and 0mV respectively. Clearly the observed reversal potential was closest to that predicted for an ion-channel selective for Na ions. After the addition of KCl the line obtained by linear regression from the current-voltage plot gave a conductance of 80.0pS and a reversal potential of 1.8 mV. The negative shift in the reversal potential of 25.2mV (from 27.0mV to 1.8mV) indicates the channel

present in this membrane patch had a selectivity for cations over anions. If the channel was selective for anions then the addition of KCl to the bath would cause a positive shift in the reversal potential. The increase in conductance demonstrates that although the channel is selective for Na^+ ions it will also conduct K^+ ions. Using the Goldman-Hodgkin-Katz equation and assuming a potassium permeability of 1 the relative sodium permeability was 10 prior to KCl addition and 7 after the addition of KCl, assuming a negligible Cl^- permeability in both cases.

Figure 7.4

A: Single-channel recordings made at the potentials indicated above the individual traces. All recordings were obtained at positive membrane potentials. For each channel record the labels c and o refer to the channel in the closed and open states respectively.

B: Current-voltage relationship constructed from the amplitude of openings observed at the potentials shown in **A**. The line obtained by linear regression gave a slope conductance of 21.8pS and a reversal potential of 52.9mV. The recording solutions used were high-K (bath) and Na-110 (pipette). Constituents of the recording solutions are given in Table 7.1 (pp123). The Nernst equation predicted reversal potentials of E_{Na}=37.5mV, E_K=-73mV and E_{Cl}=0mv. The reversal potentials predicted by the Nernst equation are illustrated on the plot. The observed reversal potential was closest to the Nernst potential for a sodium selective ion-channel.

Figure 7.4

A

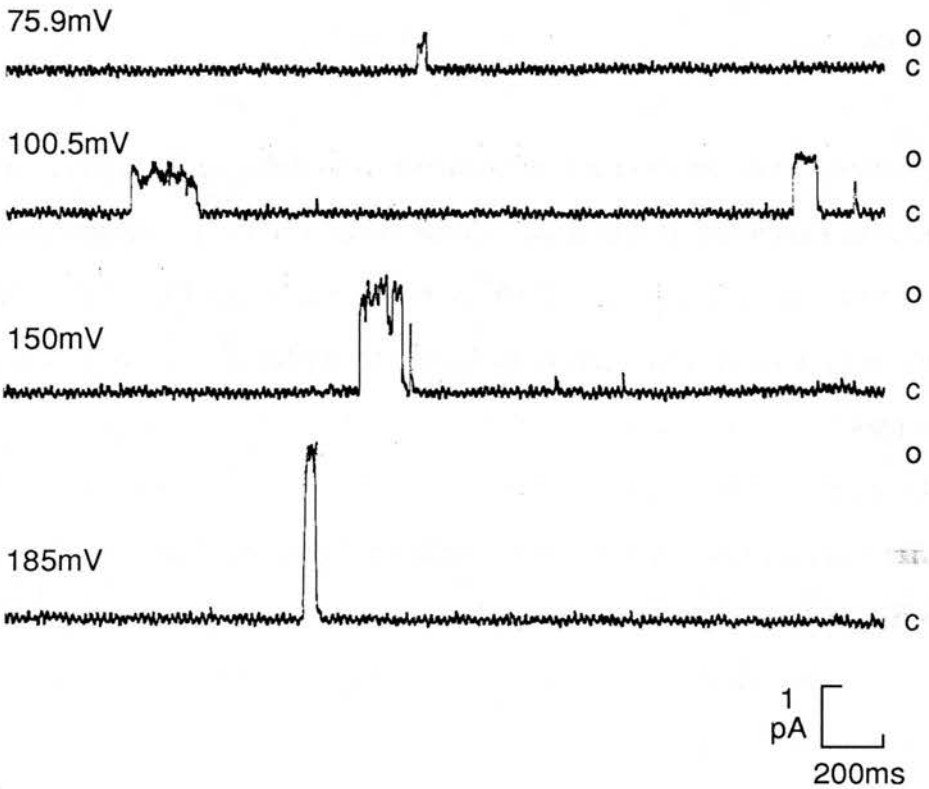
75.9mV
o
c
100.5mV
o
c
150mV
o
c
185mV
o
c
1
pA
200ms

B

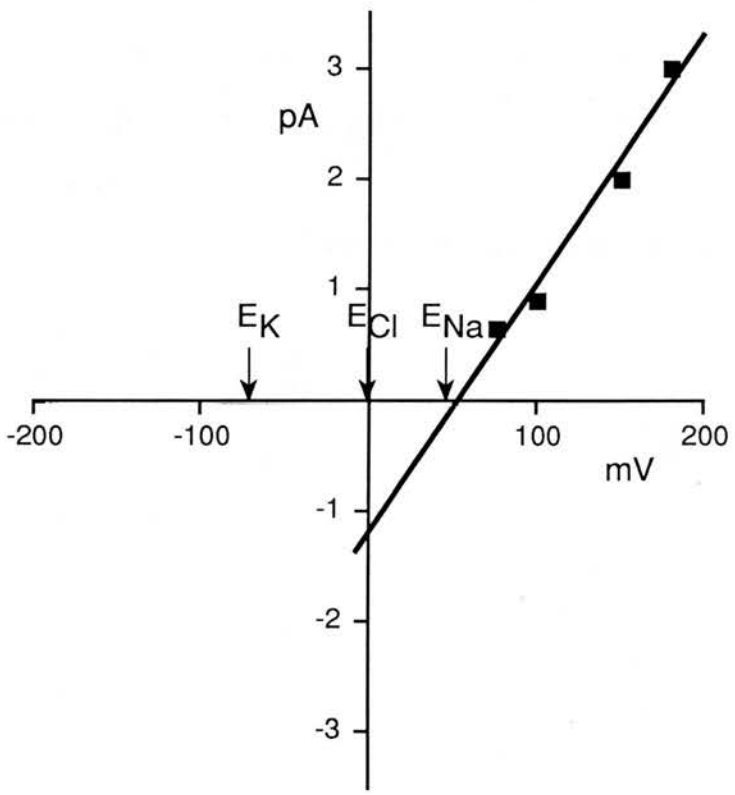
3
pA
2
1
E_K
E_Cl
E_Na
-200
-100
100
200
mV
-1
-2
-3

Figure 7.5

A: Example of single-channel records obtained at +140mV. Dotted lines labelled c and o refer to the closed and open state of the channel in the membrane patch. The bath contained high-K solution and the pipette contained Na-110 solution. Ionic concetrations of solutions are given in Table 7.1 (pp123)

B: Example of single-channel records obtained at -70 mV. Dotted lines labelled c and o refer to the closed and open state of the channel in the membrane patch. The pipette solution remained unchanged from A. Concentrated KCl (500µl 3M) was added to the bath solution to increase the intracellular concentration of potassium and chloride ions.

C: Current-voltage relationship constructed from the amplitude of channel openings prior to (□) and after (■) the addition of KCl to the bath. Prior to KCl addition the line obtained by linear regression gave a conductance of 7.4pS and a reversal potential of 27mV. Under these conditions the Nernst equation predicts reversal potentials of E_{Na}=37.5mV, E_K=-73mV and E_{Cl}=0mV. The observed reversal potential (27mV) is closest to the Nernst potential for a sodium selective ion-channel. After KCl addition the line obtained by linear regression gave a conductance of 80pS and a reversal potential of 1.8mV. The negative shift in reversal potential indicates the ion-channel was selective for cations over anions.

Figure 7.5

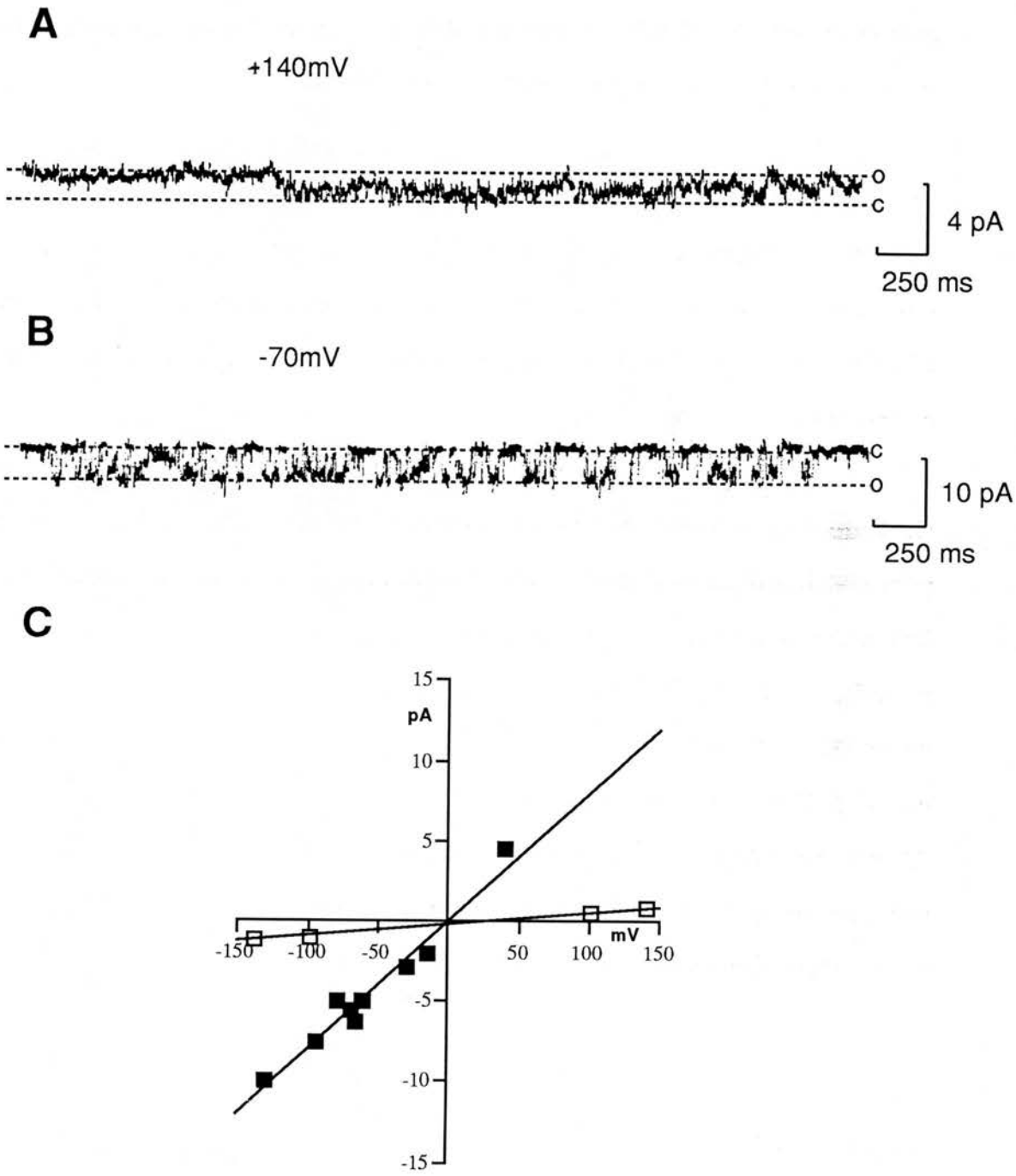
A
+140mV
o
c
4 pA
250 ms
B
-70mV
c
o
10 pA
250 ms
C
15
pA
10
5
-5
-10
-15
-150
-100
-50
50
100
150
mV

Evidence for a large conductance non-selective cation channel

A previous study has demonstrated the presence of an ion-channel in the outer membrane of the tegument of the female *S. mansoni* (Day *et al.,* 1992b). The channel had a mean conductance of 290pS and was selective for cations over anions. The channel had a very high probability of opening (P_{open}>0.9) over a range of potentials tested and appeared to display several subconductance levels. This section of the results presents evidence for the presence of a similar ion-channel in vesicles originating from the outer tegument of male *S. mansoni*. Single-channel events from various experiments were observed where the amplitude of channel openings are consistent with an ion-channel of very large conductance (~300pS), however, these events occurred too infrequently to allow current-voltage relationships to be constructed. The remainder of the section describes two experiments with 3 current-voltage plots that produced conductances between 110pS and 360pS. Both of the following experiments were carried out in the isolated inside-out patch configuration.

Figure 7.6 illustrates a membrane patch containing a single ion-channel displaying two amplitude levels. Single-channel recordings were made at three membrane potentials. At each membrane potential, at least two different amplitudes of channel opening were observed (Figure 7.6A). The amplitude of channel opening was plotted against membrane potential in Figure 7.6B. The lines obtained by linear regression of the two most frequently observed channel amplitudes gave conductances of 360pS and 210pS. The observed reversal potentials were 0mV and 2mV respectively. The Nernst equation predicted reversal potentials of E_{Na}=-33.6mV, E_K=24.1mV, E_{Ca}=35.5mV and E_{Cl}=-10.8mV. The Goldman-Hodgkin-Katz equation predicts a reversal potential for a channel equally permeable to sodium and potassium to be -17.7mV. Both channel amplitudes were observed to reverse close

to 0mV. The similarities in reversal potential suggest that the patch contains a single ion-channel displaying two conductance levels. The observed reversal potential may be explained by a channel that was non-selective for all ion species (anions and cations). If the channel was assumed to be cation selective, the observed 0mV reversal potential predicts a relative calcium permeability of 0.8 when the permeabilities for sodium and potassium ions were set to be 1 and the channel was assigned a negligible chloride permeability.

The experiment illustrated in Figure 7.7 used the isolated inside-out patch configuration. Single-channel records were obtained over a range of potentials an example of which is shown in Figure 7.7A. It was not possible to construct a current-voltage relationship because of the large number of different amplitude levels at each potential. The bath concentration of K^+ and Cl^- was increased by the addition of KCl (3M). Further single-channel recordings were made over a range of potentials (see Figure 7.7B for examples). The amplitude of channel openings, after the addition of the concentrated KCl, were plotted against membrane potential to give the current-voltage relationship shown in Figure 7.7C. The slope of the line gave a conductance of 110pS and a reversal potential of -30mV. The Nernst equation predicted reversal potentials of 37.3mV, -100mV and 19.0mV for Na^+, K^+ and Cl^- respectively. Clearly the observed reversal potential is not close to the predicted reversal potential for a single ion species. The Goldman-Hodgkin-Katz equation gave a reversal potential of -21.6mV for a channel equally permeable to sodium and potassium ions under these experimental conditions. The observed reversal potential may be explained by the channel being more permeable to K^+ ions than Na^+ ions. The observed reversal potential is closest to an ion-channel that is selective for cations over anions. The low calcium concentration of the solutions (any current carried by calcium would be very small) prevented any calculation of the relative

Ca^{2+} permeability of the channel. The reversal potential predicted for a non-selective "pore" was -1.2mV.

Figure 7.6

A: Single-channel records for -25mV and -50mV. For each trace the labels c and o refer to the closed and open state of the channel molecules. The two example traces for -25mV clearly demonstrate openings of different amplitude.

B: Current-voltage relationship for the two observed amplitude levels. Conductances were calculated at 210 (□) and 360 pS (■), with reversal potentials of 0mV and 2mV respectively. The similarity in reversal potentials suggests the patch contains a single ion-channel displaying two conductance levels. The bath contained high-Na solution and the pipette was filled with K-50 solution. Constituents of each solution are given in Table 7.1 (pp123). The Nernst equation predicts reversal potentials of E_{na}=-33.6, E_K=24.1mV, E_{Ca}=35.5 and E_{Cl}=-10.8mV. The reversal potentials predicted by the Nernst equation are illustrated on the plot. The observed reversal potentials are not close to any of those predicted by the Nernst equation for ion-channels permeable to a single ion species.

Figure 7.6

A

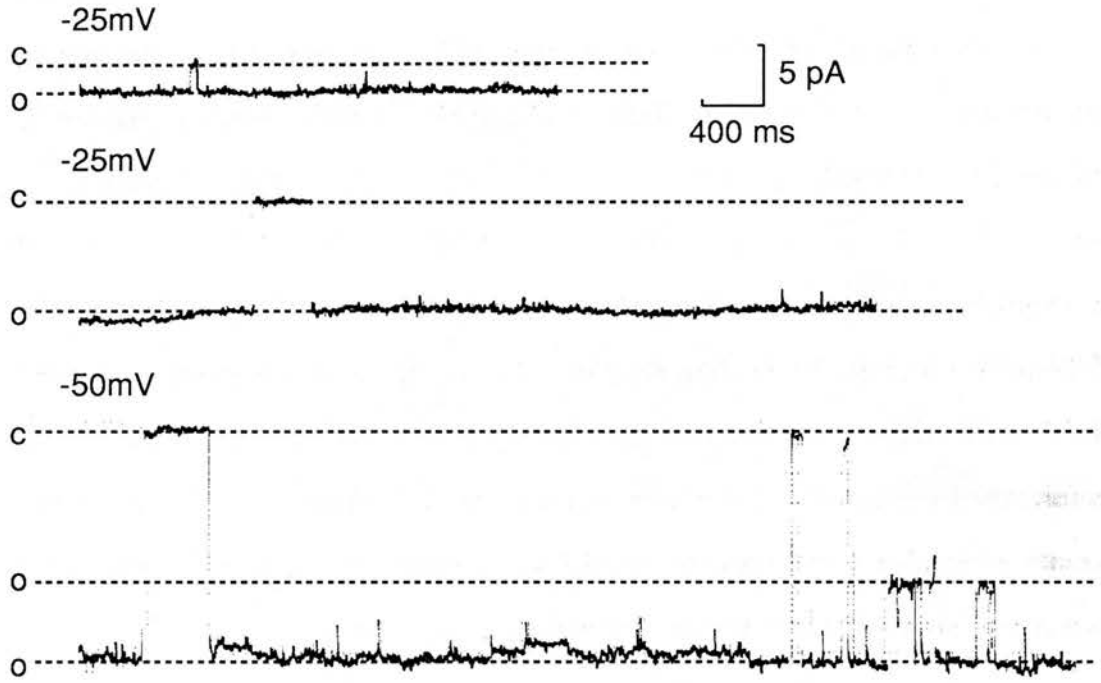
-25mV
c
o
5 pA
400 ms
-25mV
c
o
-50mV
c
o
o

B

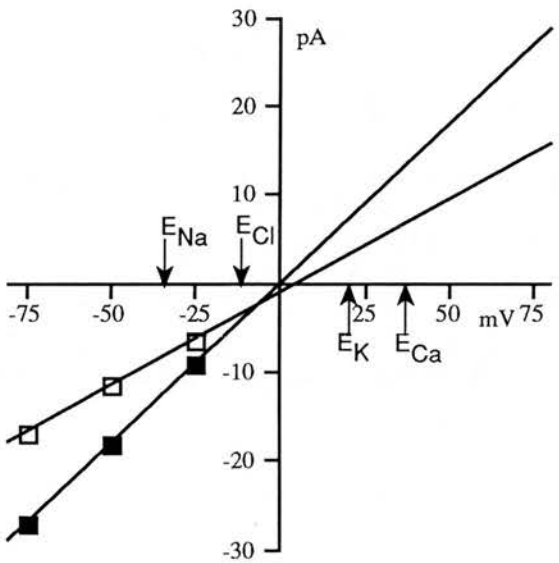
30
pA
20
10
E_Na
E_Cl
-75
-50
-25
25
50
mV
75
E_K
E_Ca
-10
-20
-30

Figure 7.7

A: Example of single-channel records obtained prior to the addition of 3M KCl. The dashed line labelled c refers to the "closed" state of the membrane patch, the label o refers to open, which in this case probably includes the opening of several different ion-channels. This is implied by the large number of different amplitude current steps in the record. The pipette contained Na-110 (Table 7.1, pp123) and the bath contained high-K solution (Table 7.1, pp123). Each solution contained an additional 10mM $CaCl_2$.

B: Examples of single-channel records at two membrane potentials after addition of 250µl of 3M KCl to the bathing solution. In the record at membrane potential -70mV the labels c and o refer to the channel molecule in the closed and open conformation respectively. The trace obtained at -100mV shows evidence of two channel molecules (with openings of the same amplitude) within the membrane patch. The label c refers to the no channels open, o_1 refers to only a single-channel open and 0_2 refers to two channel molecules in the open state at the same time.

C: Current-voltage relationship constructed from the amplitude of channel opening (■) after the addition of 3M KCl to the bath. The line obtained by linear regression gave a slope conductance of 110pS and a reversal potential of -30.0mV. The reversal potentials predicted by the Nernst equation are shown on the plot; E_K=-100mV, E_{Na}=37.3mV and E_{Cl}=19.0mV. The Goldman-Hodgkin-Katz equation predicted a reversal potential of -21.6mV for an ion-channel equally selective for Na^+ and K^+ ions. The observed reversal potential (-30mV) was closest to that predicted for an ion-channel equally selective for Na^+ and K^+ ions.

Figure 7.7

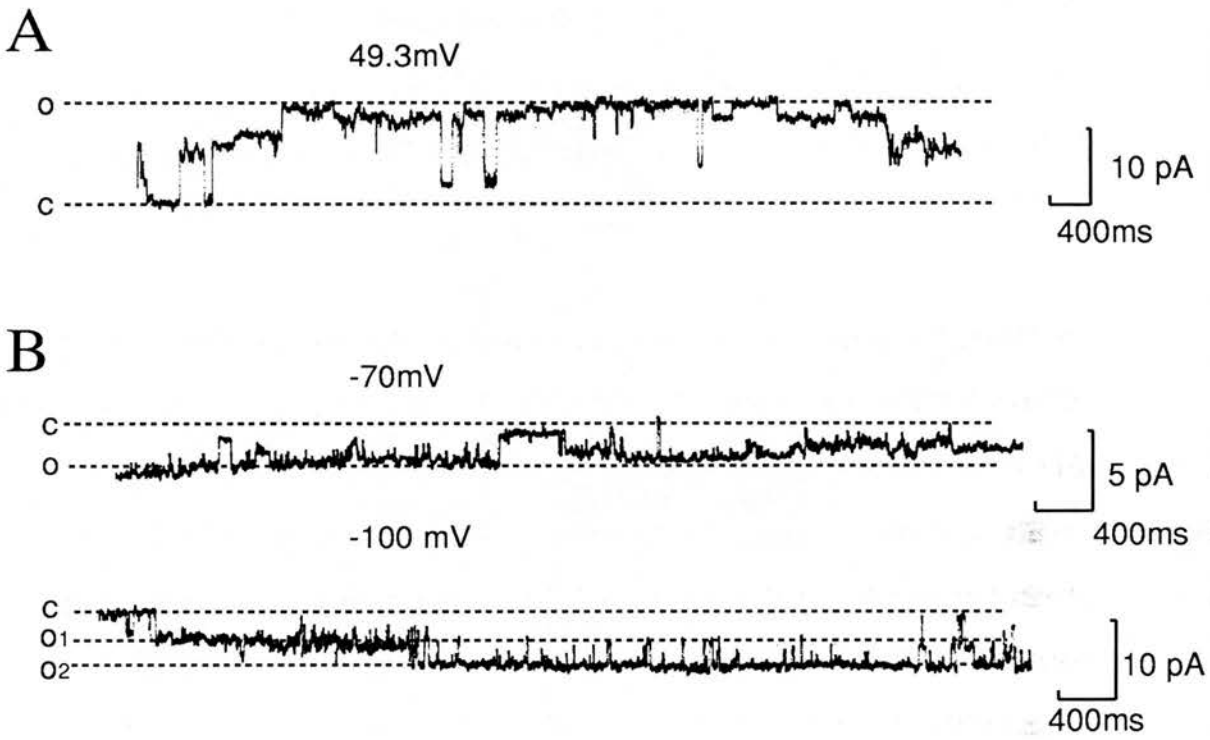
A
49.3mV
o
c
10 pA
400ms
B
-70mV
c
o
5 pA
400ms
-100 mV
c
o1
o2
10 pA
400ms

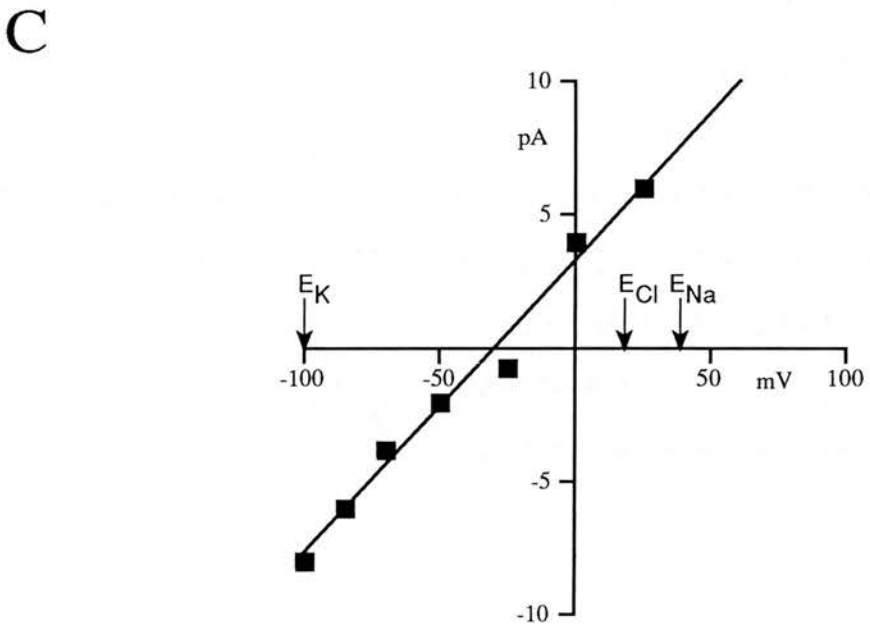
C
10
pA
5
-5
-10
E_K
E_Cl
E_Na
-100
-50
50
mV
100

Evidence of an anion selective channel

This section contains a single patch recording displaying channel amplitudes giving two current-voltage relationships. The experiment was carried out in the isolated inside-out patch configuration. The Nernst equation predicted the reversal potentials for Na^+, K^+ and Cl^- to be 37.5mV, -73mV and 0mV respectively. The Goldman-Hodgkin-Katz equation predicted a reversal potential of 0mV for a channel equally permeable to K and Na ions. Single-channel recordings were made over a range of membrane potentials, Figure 7.8A. A current-voltage plot of the channel amplitudes was constructed (Figure 7.8C); the line obtained by linear regression gave a conductance of 22.4pS and a reversal potential of -5.0mV. The ion selectivity of the channel could not be fully determined using the Nernst equation. The channel was selective for either Cl^- alone, equally selective for Na^+ and K^+ together or completely non-selective (for each possibility the predicted reversal potential was 0mV). The experiment was continued by adding KCl to the bathing solution (to increase the bath concentrations of K^+ and Cl^-). The addition of KCl to bath altered the reversal potentials predicted by the Nernst equation to E_{Cl}=23.9mV and E_K=-101.5mV. The predicted reversal potential for a channel equally permeable to Na and K ions was also altered to -24.3mV. Further single-channel recordings were made (for examples see Figure 7.9B) and their amplitude plotted against membrane potential in Figure 7.9C. The current-voltage relationship then gave a conductance of 58.4pS and a reversal potential of 10.2mV. The positive shift in observed reversal potential (of 15.2mV) is indicative of a channel that is selective for Cl^- ions (predicted shift of reversal potential=24.3mV). If the channel was selective for cations over anions then the addition of KCl to the bath would cause a negative shift in the observed reversal potential.

Figure 7.8

A: Single-channel records obtained at two membrane potentials prior to the addition of 3M KCl to the bath solution. In each record the dashed lines labelled c and o refer to the closed and open state of the channel molecule. The bath contained high-K solution (Table 7.1, pp123) and the pipette contained Na-110 solution (Table 7.1, pp123).

B: Single-channel records obtained at two membrane potentials after the addition of 3M KCl to the bath solution. In each record the dashed lines labelled c and o refer to the closed and open state of the channel molecule. Note the difference in amplitude between the channel records at -50mV in **A** compared with those for -50mV in **B**, the addition of KCl increases the amplitude of opening at -50mV.

C: Current-voltage relationship constructed for openings prior to KCl addition (■) and after KCl was added (□). The line obtained by linear regression prior to KCl being added gave a slope conductance of 22.4 pS and a reversal potential of -5.0 mV. The Nernst equation predicted the reversal potentials for Na^+, K^+ and Cl^- to be 37.5mV, -73mV and 0mV respectively. The Goldman-Hodgkin-Katz equation predicted a reversal potential of 0mV for a channel equally permeable to K and Na ions. The observed reversal potential was closest to that predicted for either a Cl^- selective ion-channel or an ion-channel equally selective for Na^+ and K^+. The line obtained by linear regression to openings observed after the addition of KCl gave a slope conductance of 58.4 pS and a reversal potential of 10.2 mV. The positive shift in observed reversal potential (of 15.2mV) is indicative of a channel that is selective for anions over cations.

Figure 7.8

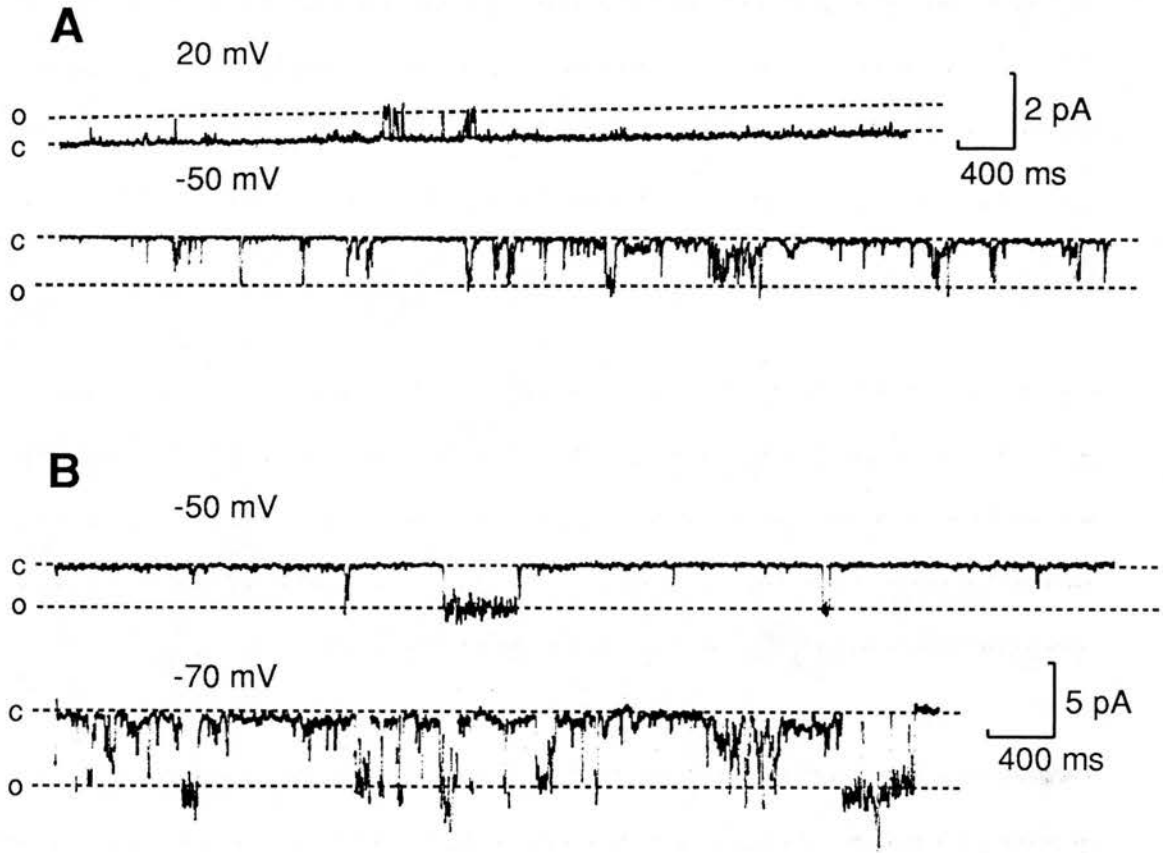
A
20 mV
o
c
2 pA
400 ms
-50 mV
c
o
B
-50 mV
c
o
-70 mV
c
o
5 pA
400 ms

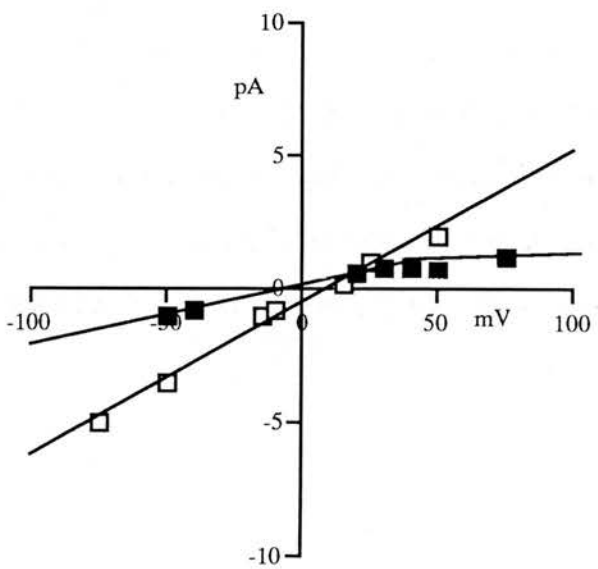
C
10
pA
5
0
-5
-10
-100
-50
0
50
mV
100

Experiments with partially characterised ion selectivity

Three experiments are presented containing 4 current-voltage relationships. The observed reversal potential did not give a conclusive indication as to which ions the channels present were conducting. All the experiments in this section were carried out with membrane patches in the inside-out configuration.

Figures 7.9 illustrates an experiment where the Nernst equation predicted reversal potentials for Na^+, K^+ and Cl^- of 37.5mV, -73mV and 0mV respectively. The Goldman-Hodgkin-Katz equation also predicted a reversal potential of 0mV for ion-channels equally permeable to sodium and potassium ions and for ion-channels that were totally non-selective. Examples of single-channel records are shown in Figure 7.9A. The amplitude of the channel events is plotted against voltage in Figure 7.9B: the observed reversal potential was -10mV and the line obtained by linear regression gave a slope conductance of 50pS. Clearly the observed reversal potential was closest to the reversal potential predicted for a Cl^- selective channel; however the predicted reversal potentials for a channel permeable equally to Na^+ and K^+ or a channel permeable to all ions were also 0mV.

Figure 7.10 illustrates the result of another experiment. Examination of the channel records revealed two separate amplitude levels over the range of membrane potentials tested. The current-voltage relationship in Figure 7.10 has the lines obtained by linear regression for both of the observed channel amplitudes: slope conductances were 40.0pS for the larger amplitude openings and 13.0pS for the smaller. The reversal potentials were 0.4mV and -5.1mV respectively. The quality of the recordings prevented any kinetic analysis. The similarities between the reversal potentials and the lack of information on single-channel kinetics prevents any conclusion as to whether the differing amplitude levels are separate channels or

different conductance levels of the same channel. The Nernst equation predicted reversal potentials for Na^+, K^+ and Cl^- of 37.5mV, -73mV and 0mV respectively. The Goldman-Hodgkin-Katz equation also predicted a reversal potential of 0mV for ion-channels equally permeable to sodium and potassium ions and for ion-channels that were totally non-selective. Clearly the observed reversal potentials (0.4mV and -5.1mV) were closest to the predicted reversal potential of 0mV. As with the previous experiment it was impossible to determine which ion species the channel(s) were permeable to either Cl^- alone, Na^+ and K^+ equally or whether they were totally non-selective.

The experiment illustrated in Figure 7.11 was carried out using similar solutions as the previous experiment.. Alteration of the solutions did not affect any of the predicted reversal potentials quoted in the previous paragraph. Figure 7.11A shows representative single-channel records at two membrane potentials. The current-voltage relationship is shown in Figure 7.11B; the observed reversal potential was 5.7mV and the line obtained by linear regression gave a slope conductance of 11.8pS. As with the previous experiment the observed reversal potential was closest to the reversal potential predicted for a channel permeable to Cl^- alone or permeable to K^+ and Na^+ equally, or completely non-selective for all ion species present.

Using the Nernst and Goldman-Hodgkin-Katz equations, it was impossible to determine the exact ion selectivity of the channels in this section: they were selective for either Cl^- alone, equally selective for Na^+ and K^+ together or completely non-selective. However the observed reversal potentials eliminated the possibility that the channels are permeable to potassium ions only or sodium ions only.

Figure 7.9

A: Examples of single-channel records at two negative membrane potentials. In each case the channel is closed at the level indicated by the dashed line labelled c. The open level is indicated by the dashed line labelled o.

B: The current-voltage relationship constructed by plotting amplitude of channel opening against membrane potential. The line obtained by linear regression of the data gave a slope conductance of 50pS and a reversal potential of -10 mV. During the experiment the bath contained high-K solution and the pipette was filled with Na-110 solution. Table 7.1 (pp123) lists the constituents of each solution. The Nernst equation predicted reversal potentials of E_{Na}=37.5mV, E_K=-73.0mV and E_{Cl}=0mV. The Nernst potentials are indicated on the plot. The Goldman-Hodgkin-Katz equation predicted a reversal potential of 0mV for ion-channels equally permeable to Na^+ and K^+ ions and for ion-channels that were totally non-selective. The observed reversal potential (-10mV) is closest to the reversal potential predicted for either a Cl^- selective ion-channel, a channel equally selective for Na^+ and K^+ or a totally non-selective ion-channel.

Figure 7.9

A

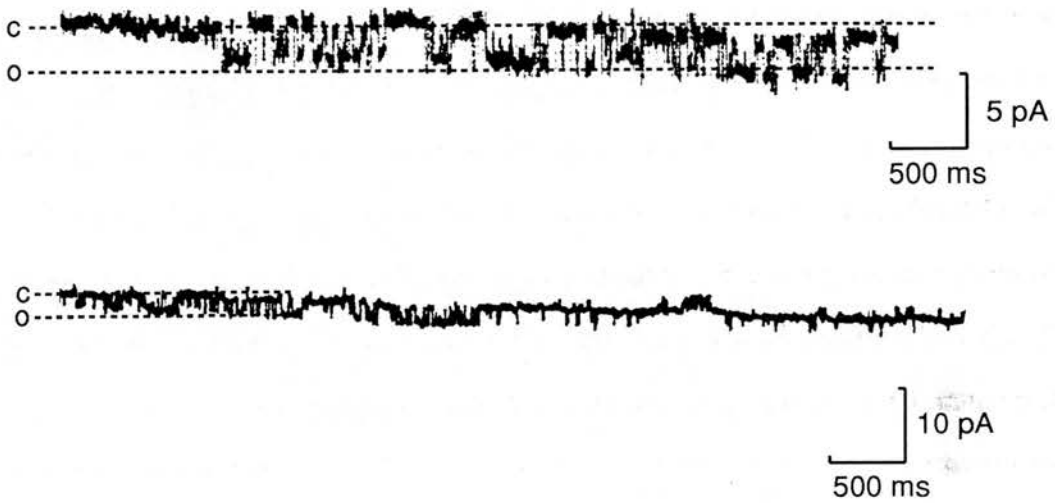
c
o
5 pA
500 ms
c
o
10 pA
500 ms

B

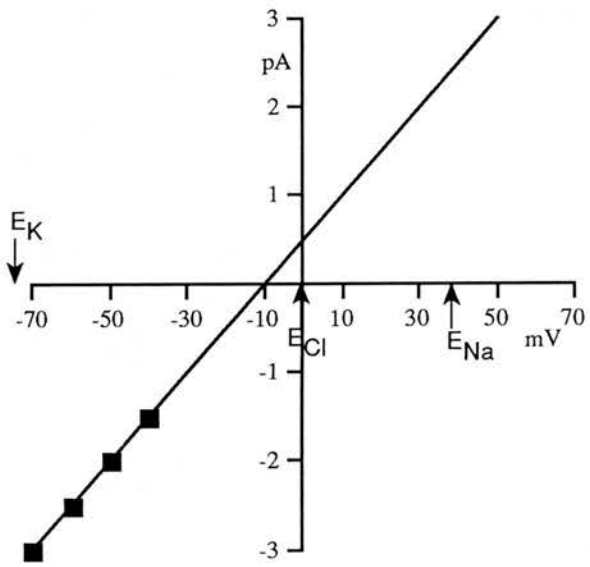
3
pA
2
1
E_K
-70
-50
-30
-10
10
30
50
70
mV
E_Cl
E_Na
-1
-2
-3

Figure 7.10

Current-voltage relationships from single-channel records displaying two distinct amplitude levels (from the experiment dated 4\10\94). Linear regression was used to fit lines to each amplitude level. The smaller openings (■) gave a slope conductance of 13 pS and a reversal potential of -5.1mV. The line obtained by linear regression of the larger openings (□) gave a slope conductance of 40.0 pS and a reversal potential of 0.4 mV. The bath and pipette were filled with high-K solution and Na-110 solution respectively (for constituents see Table 7.1, pp123). The reversal potentials predicted by the Nernst equation are illustrated on the plot: E_{Na}=37.5mV, E_K=-73.0mV and E_{Cl}=0mV. Additionally the Goldman-Hodgkin-Katz equation predicted a reversal potential of 0mV for ion-channels equally permeable to Na^+ and K^+ ions and for ion-channels that were totally non-selective. The observed reversal potentials (-5.1mV and 0.4mV) are closest to the 0mV predicted reversal potential.

Figure 7.10

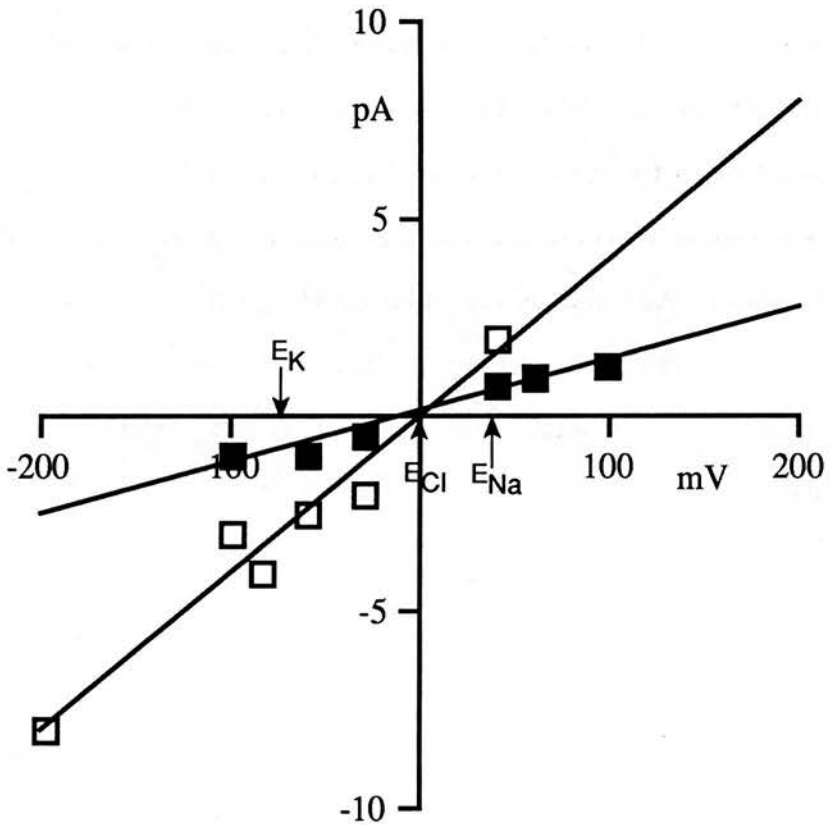

Figure 7.11

A: Single-channel records obtained at membrane potentials of 40 and -39 mV. There appeared to be several conductance levels present, at each potential the largest of these was measured. The level for channel openings and closures are indicated on the records by the dashed lines labelled o and c respectively.

B: Current-voltage relationship constructed from the amplitude of channel openings. The line obtained by linear regression gave a slope conductance of 11.8 pS and a reversal potential of 5.7 mV. The bath and pipette were filled with high-K solution and Na-110 solution respectively (for constituents see Table 7.1, pp123). The solutions were modified by the addition of 10mM $CaCl_2$. The reversal potentials predicted by the Nernst equation are illustrated on the plot: E_{Na}=37.5mV, E_K=-73.0mV and E_{Cl}=0mV. Additionally the Goldman-Hodgkin-Katz equation predicted a reversal potential of 0mV for ion-channels equally permeable to Na^+ and K^+ ions and for ion-channels that were totally non-selective. The observed reversal potential (5.7mV) was closest to the 0mV predicted reversal potential.

Figure 7.11

A

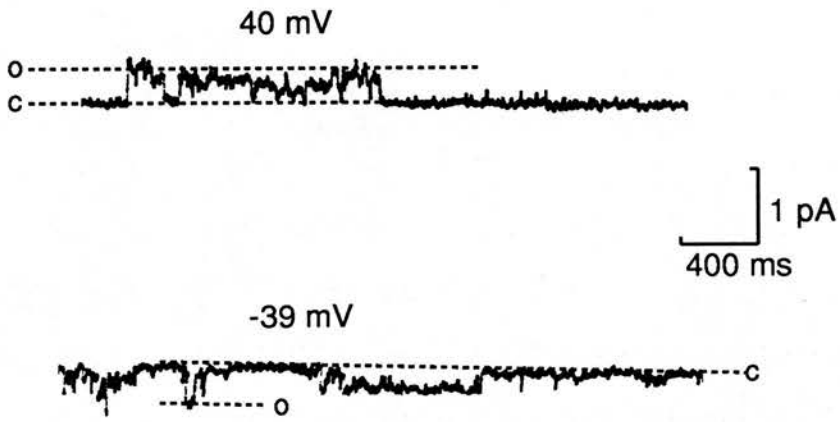

B

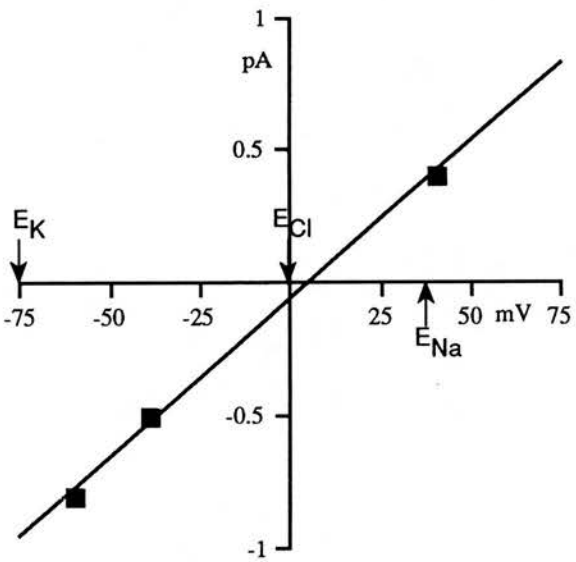

Experiments with ion selectivity not determined

In these experiments solutions of identical concentrations were used on each side of the membrane patch. It was therefore impossible to obtain any information on the ionic selectivity of the channels present in the membrane patches. The conductance of the channels in the membrane patches was calculated, additionally a single membrane patch gave records of sufficient quality to allow a calculation of the probability of channel opening over a range of membrane potentials.

The experiment illustrated in Figure 7.12 was carried out in the vesicle-attached configuration. The concentrations of each ion species in the recording solution are given in Figure 7.12A. Since the concentrations of each ion species were identical on each side of the membrane patch no determination of the ion selectivity of the channel could be made. Examples of single-channel records are given in Figure 7.12B. The amplitude of channel opening was plotted against membrane potential to give a current-voltage relationship (data not shown). The line obtained by linear regression through these points gave a slope conductance of 7.7pS and a reversal potential of -0.05mV; the reversal potential was close to zero indicating that the gross ion concentration inside the membrane vesicle was the same as the bathing solution. The linear nature of the current-voltage plot gives no evidence of rectification at positive or negative membrane potentials. The relationship between the probability of channel opening (P_{open}) and membrane potential is shown in Figure 7.12C. The channel in this patch had a much higher probability of opening at depolarised membrane potentials compared with hyperpolarised membrane potentials. The membrane potentials tested exceeded normal physiological limits: this was necessary to resolve the small amplitude of channel openings presented by such a low slope conductance.

The experiment illustrated in Figure 7.13 was carried out using the isolated inside-out patch configuration. As in the previous experiment no determination of the ion selectivity of channels present was possible. Sample records of single-channel openings are shown in Figure 7.13A with the current voltage relationships for the two most commonly observed conductance levels given in Figure 7.13B. The two levels of openings gave conductances of 82.6pS and 17.8pS, with reversal potentials of-10.0mV and 32.2mV respectively. The channel records were difficult to analyse as several other levels of channel opening were frequently observed. The two main conductance levels present showed different characteristics in there opening behaviour suggesting that in this patch there are at least two separate ion-channel types. In addition the smaller of the two conductances displayed rectification at negative membrane potentials, reinforcing the implication that two channel types are present rather than a single ion-channel type displaying multiple conductance states.

Figure 7.12 Experiment no.1 25\6\93

A: Concentrations of each ion species in the bath and pipette solutions. The recording solution was "schistosome" solution (for constituents see Table 7.1, pp123).

B: Examples of single-channel records at 100mV and -100mV. Labels c and o refer to the closed and open state of the channel respectively.

C: Histogram showing the relationship between membrane potential and probability of channel opening (P_{open}).

Figure 7.12

A

Ion Species	Na	K	Cl	Mg	Ca
Concentration (mM)	100	20	130	2	3

B

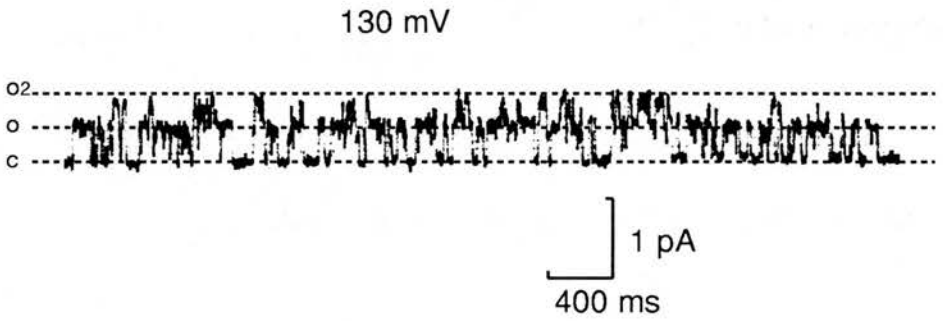

C

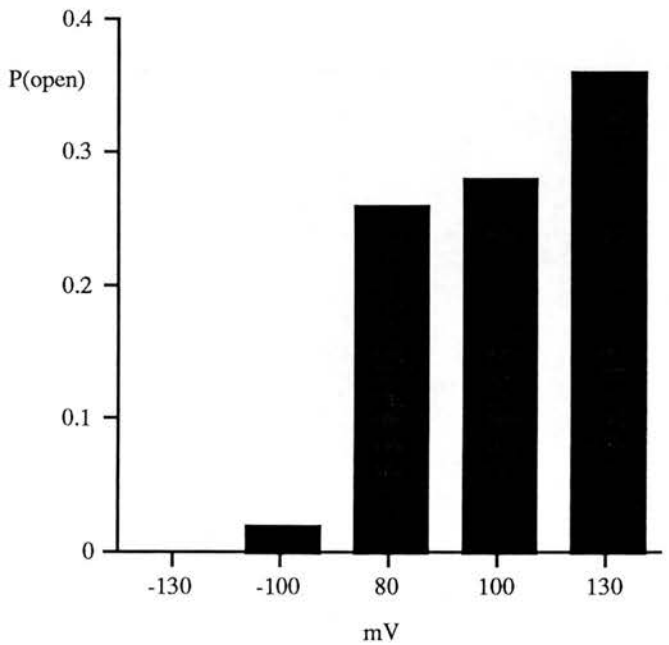

Figure 7.13

A: Single-channel records at 90mV and -78.4mV, showing the two most commonly observed conductance levels. Labels c and o refer to the closed and open confirmation of the channel molecules present. The recording solution was "schistosome" solution (for constituents see Table 7.1, pp123)

B: Amplitude of channel openings plotted against membrane potential for the two most commonly observed conductance levels. The two levels gave a slope conductances of 82.6pS (■) and 19.1pS (●) respectively and reversal potentials of -10.1mV (■) and 32.2mV (●) respectively. The smaller unitary conductance displayed rectification at hyperpolarise membrane potentials; slope conductance was therefore calculated over the range 90mV to -61.3mV inclusive.

Figure 7.13

A

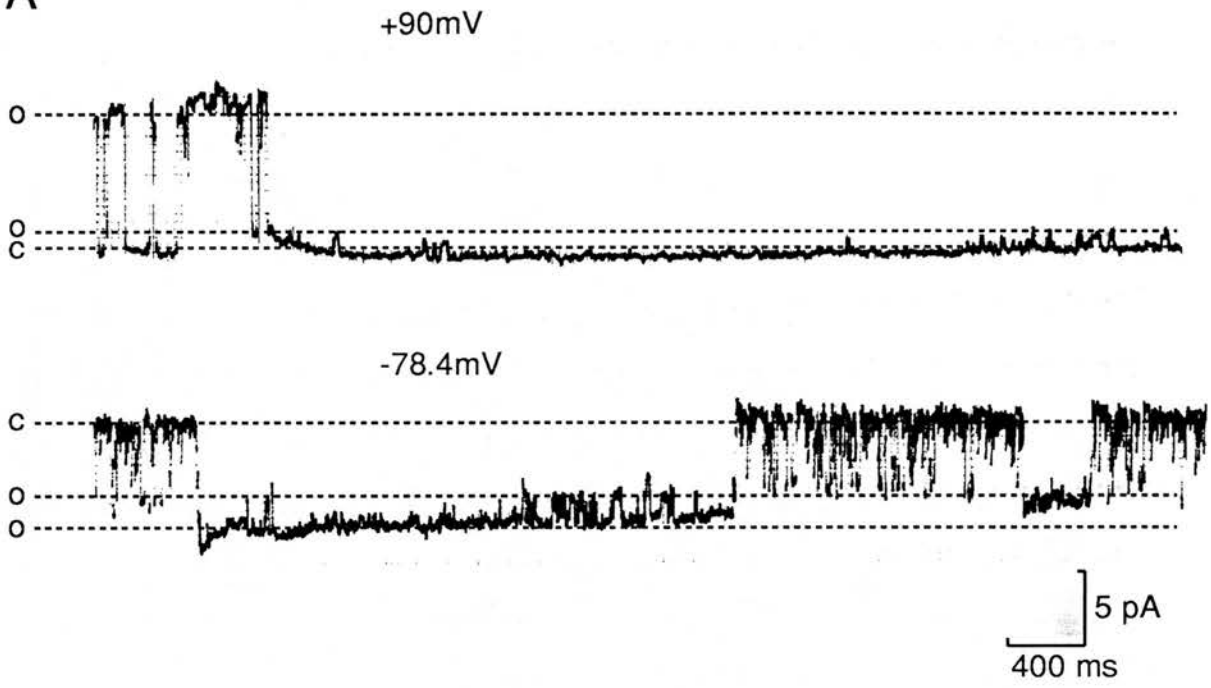

B

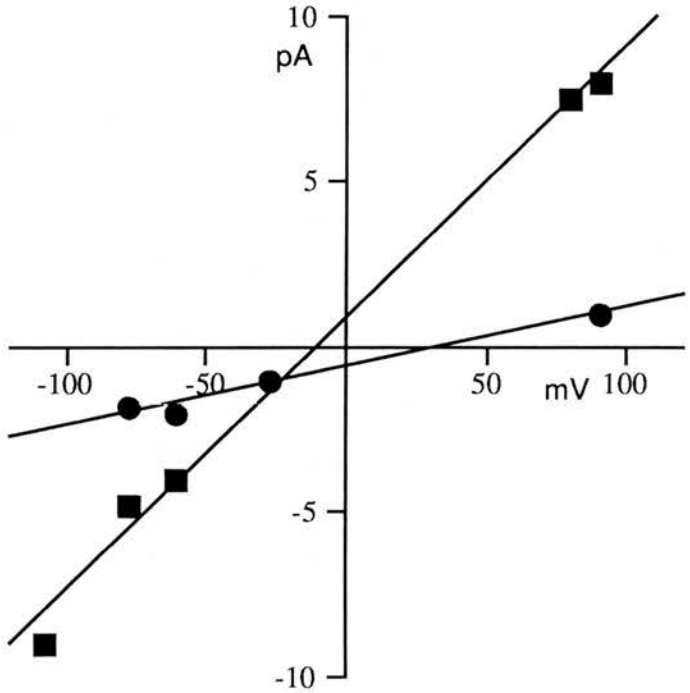

Some problems associated with identifying single-channel conductances and ion selectivities.

In a number of experiments it was possible to observe obvious single-channel openings and closings, but attempts to plot the current-voltage relationships in these experiments were unsuccessful. The lack of success was attributed to three factors (often occurring in combination): 1) in some cases the small amplitude of the currents prevented an accurate estimate of single-channel amplitude; 2) the possibility that the openings observed at different potentials were not the same ion-channel but were due to several ion-channel types within the membrane patch; 3) the seal quality deteriorated before channel amplitudes could be recorded over a sufficient range of potentials to allow the construction of a current-voltage relationship. This section gives four examples of such experiments.

The experiment illustrated in Figure 7.14 was carried out using a symmetrical solution on each side of the membrane patch (for concentrations of ions present see Figure 7.12A); making comment on the ion selectivity of the channel(s) present impossible. In this instance the experiment was carried out using the isolated inside-out patch configuration. The channel records shown in Figure 7.14A demonstrate that there are at least two different amplitudes of channel event at the membrane potentials tested. The amplitudes of the two main states were plotted against membrane potential on the current-voltage relationship given in Figure 7.14B. Since the ionic concentrations were identical on each side of the membrane patch then the predicted reversal potential for any ion-channel (regardless of its ionic selectivity) is 0 mV. The current-voltage plot in Figure 7.14B shows the amplitude of the observed single-channel events: linear regression gave rise to estimated reversal potentials of 90mV and 122mV. It appeared that there was more than one ion-channel type present in the membrane patch because, at each of the potentials recorded, two

different amplitudes of events were observed. The results from this experiment were not analysed further as it was not possible to identify which of the observed single-channel events were from the same ion-channel. Clearly assumptions about channel events based on a single membrane model do not apply. The possibility that the membrane patch contained both of the bilayers of the outer tegument is discussed later in Section 7.4 and appendix II.

Figure 7.15A shows an experiment carried out using the isolated inside-out patch configuration.. The recordings show obvious single-channel events but no estimate for conductance or reversal potential was possible. Figure 7.16B shows an isolated inside-out patch, recordings were obtained at only two potentials before the seal resistance deteriorated to an unusable level. As in the previous experiment, the experiment illustrated in Figure 7.16C was carried out using an isolated inside-out membrane patch. The single-channel records demonstrate two distinct channel amplitudes at a fixed membrane potential. The channel openings appear to have very different characteristics suggesting they are representative of two separate ion-channel types present in the same membrane patch. Addition of KCl to the bath (to increase the bath concentration of K^+ and Cl^-) resulted in a deterioration in the seal quality; it was still possible to observe single-channel events (Figure 7.15D) but the poor resolution prevented any estimates of conductance or reversal potential.

Figure 7.14

A: Examples of single-channel records at +150mV and +199mV, labels c and o refer to the channel in the closed and open state respectively. The recordings were made with "schistosome" solution in the bath and pipette (for constituents see Table 7.1, pp123)

B: Amplitude of channel openings plotted against membrane potential for single-channel events observed. The experiment was carried out using symmetrical solutions therefore for any ion-channel present the reversal potential would be 0mV. The results rendered it impossible to fit lines (using linear regression) to the data points to give a reversal potential of close to 0mV.

Figure 7.14

A

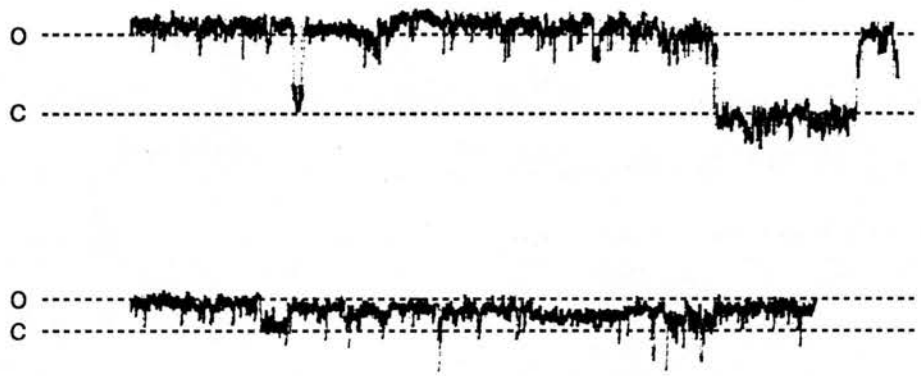

B

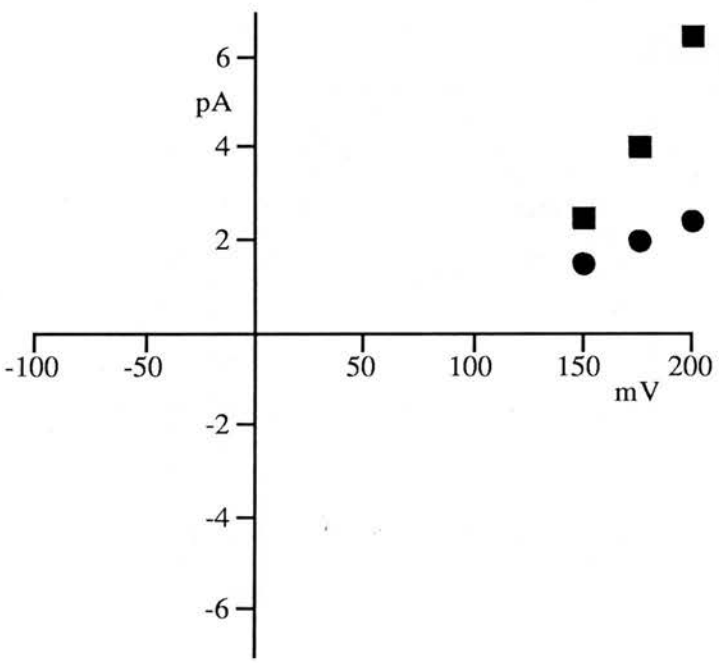

Figure 7.15 Examples of single-channel recordings from a number of experiments. The labels c and o on the channel records refer to the closed and open conformation of the channel.

A: Examples of single-channel events at +40.3mV and -40.1mV from the experiment dated 1\3\94 no.2. In both cases the amplitude of channel opening is approximately 1pA. The pipette was filled with high-K (Table 7.1, pp123) solution and the outside of the patch was bathed in VMEM (Table 6.1, pp92). The seal deteriorated before recordings could be made at other membrane potentials.

B: Examples of single-channel events at +20.1mV and -30.0mV from the experiment dated 1\3\95. The bath contained high-K solution while the pipette contained Na-110 solution (constituents of solutions are given in Table 7.1, pp123). Both solutions were modified by the addition of 10mM $CaCl_2$.

C: Single-channel events at +175 mV from the experiment dated 18\4\95. Two clear amplitude levels are present, labelled *a* and *b*. The amplitude level *a* is approx. 0.15pA in size and the long "burst" of openings illustrated is 400ms in duration; amplitude level *b* is approx. 0.7pA in size and the observed openings were of much shorter duration. The apparent difference in kinetics and suggests that the openings represent two distinct ion-channel types rather than subconductance levels of the same channel. The bath contained high-K solution while the pipette contained Na-110 solution (constituents of solutions are given in Table 7.1, pp123).

D: Single-channel events at +175 mV from the experiment dated 18\4\95 after the addition of KCl to the bath to increase the concentrations of K^+ and Cl^- at the intracellular surface of the membrane patch. Channel openings can be observed but cannot be separated into two separate levels. The addition of KCl resulted in a rapid deterioration of seal quality and further meaningful recordings were impossible to obtain.

Figure 7.15

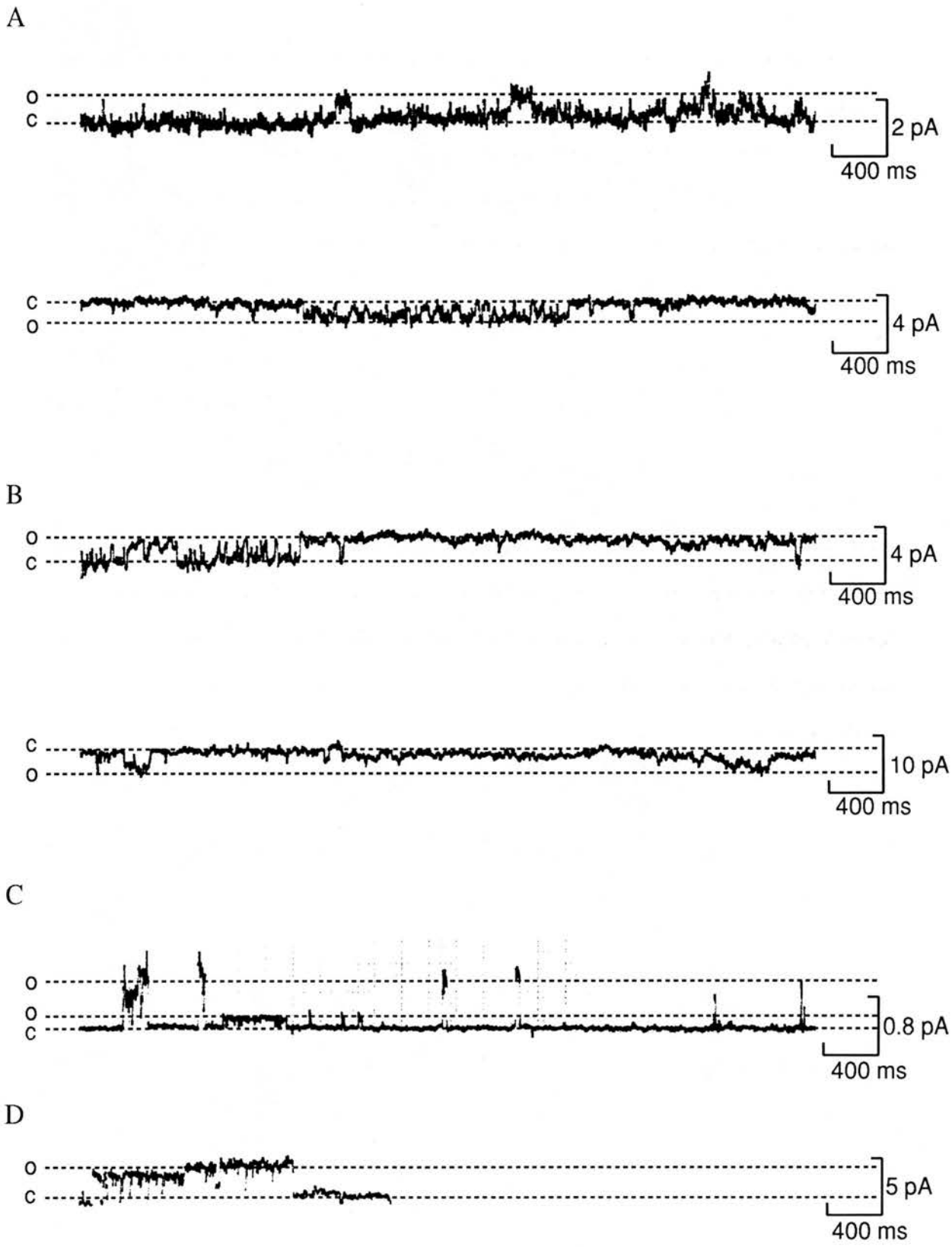
A
o
c
2 pA
400 ms
c
o
4 pA
400 ms
B
o
c
4 pA
400 ms
c
o
10 pA
400 ms
C
o
o
c
0.8 pA
400 ms
D
o
c
5 pA
400 ms

7.4 DISCUSSION

Suitability of vesicles for patch recording

The vesicle preparation has been shown to allow the recording of single-channel currents from the schistosome tegument (Robertson, Martin and Kusel, 1996). However to investigate the ion-channels in a membrane preparation successfully the frequency of obtaining giga-ohm resistance patches must be high enough to allow a reasonable amount of data to be obtained. Previous patch-clamp experiments using a muscle derived membrane preparation from *Ascaris suum* have given a frequency of sealing of ~33%(Chapter 3); the sealing frequency for the schistosome vesicle preparation was lower at ~15%. However in the *Ascaris* vesicle preparation only ~25% of membrane patches displayed channel activity compared with ~59% of schistosome membrane patches. Overall the frequency of obtaining membrane patches with resolvable ion-channels present was low and future work should initially concentrate on increasing the frequency with which giga-ohm resistance seals can be obtained. To date this is the first report of single-channel recording from the tegument of adult male *Schistosoma mansoni*, the frequency of sealing was low (15%) but better than the 10% frequency reported from a patch-clamp study using the smoother tegument of the female (Day *et al,* 1992b).

Specific types of ion-channel present

The results demonstrate the presence of ion-channels in the membrane vesicle preparation. The observed ion-channels varied in conductance (7.4pS to 360pS) and ion-selectivity (determined on the basis of reversal potential). The results were grouped on the basis of ion selectivity and are discussed below.

Potassium selective ion-channels

The adult male schistosome maintains an electrical potential of around -60mV across the outer membrane of the tegument (Pax *et al,* 1987). The parasite tegument appears to act as a potassium electrode with the intracellular $[K^+]$ maintained at much higher concentrations than the extracellular $[K^+]$. A Na-K pump is believed to contribute to the membrane potential but inhibition of the pump by ouabain only depolarises the membrane by around -20mV (Fetterer *et al.* 1981). Clearly potassium selective ion-channels have a role to play in maintenance of the potential across the tegument. In my study, three membrane patches displayed ion-channels selective for K^+ ions. The conductances were 37.5pS, 47.5pS and 114pS. The largest conductance value was obtained using a high K^+ concentration bathing solution. The high bath K^+ concentration could account for the increased conductance. The two experiments with similar conductances were carried out using a more physiological potassium concentration. There have been no previous reports of potassium channels in the *S. mansoni* tegument although potassium selective currents have been observed in isolated muscle cells (Day *et al,* 1993). A voltage insensitive potassium channel similar to a maxi-K channel with a conductance of 195pS has been recorded from muscle fibres (Blair *et al,* 1991). A *Shaker*-related voltage-gated potassium channel gene has been cloned from the parasite and expressed in *Xenopus* oocytes (Kim *et al,* 1995). The tegument of protoscoleces of *Echinococcus granulosus* possess a potassium selective ion-channel with a

conductance of 244pS (Grosman and Reisin, 1995). All these observations are consistent with the presence of K channels in the tegument of trematode parasites

Non-selective cation channels

Two experiments illustrated in this thesis described ion-channels selective for cations over anions. The first experiment had a main conductance of 360pS and a subconductance state of 210pS. If the channel was given an equal K^+ and Na^+ permeability of 1, the Goldman-Hodgkin-Katz equation revealed estimation of the *pCa/pNa* ratio to be 0.8. The large conductance of the channel and the presence of a subconductance level are similar to the properties of the non-selective cation channel in females observed by Day *et al* (1992b) who observed a 290pS channel with subconductance levels approximately 95pS apart. However, Day *et al* (1992b) made no estimate of the relative Ca^{2+} permeability of the channel, the *pNa/pK* ratio varied between 0.7 and 1.1 in the absence of a significant calcium concentration.

The second patch (illustrated in Figure 7.7) contained a channel that was selective for cations over anions with a slope conductance of 110pS. The relatively low slope conductance may indicate that I was observing a subconductance level rather than the ion-channel opening to its full conductance. In addition a number of membrane patches displayed occasional large amplitude channel openings that were consistent with the presence of a large conductance channel (for example see Figure 7.11A) but openings and closures were too infrequent to allow a current-voltage relationship to be plotted. The results demonstrate the presence of a large-conductance non-selective cation channel in the male tegument with similar properties to the ion-channel described in the female tegument (Day *et al*, 1992b), which may have a relatively high (0.8) *pCa/pNa* ratio. Recent studies from the tegument of *Echinococcus granulosus* have also revealed a high conductance cation selective

ion-channel: the channel had a conductance of 107pS and a high (>0.9) probability of opening, the P_{Ca}/P_{Na} was approximately 0.4 (Grosman and Reisin, 1995)

Sodium selective ion-channels

The sodium activity (concentration) of the tegumental cytoplasm has been estimated at approximately 30mM which is substantially lower than the extracellular sodium concentration (Pax *et al.* 1987). The imbalance in sodium ion concentration across the tegument results in a continuous influx of sodium across the tegument which is believed to be offset by the active extrusion of Na^+ ions by the Na-K pump. The sodium channel blocker amiloride causes a hyperpolarisation of the tegument of *E. granulosus* indicating the presence of sodium selective ion-channels in the tegument of that species (Ibarra and Reisin, 1994). The results presented in this thesis describe four patches where the ion-channels present were selective for sodium ions. The conductances ranged from 7.4pS to 80pS. The high conductance value of 80pS was obtained from a membrane patch exposed to a high (non-physiological) bath concentration of ions. The conductances (under more physiological ion concentrations) ranged from 7.4pS to 53pS. Channel events were observed at positive and negative membrane potentials in three of the four membrane patches. The sodium selective ion-channel with a conductance of 21.8pS was only observed to open at positive membrane potentials. The differences in conductance and voltage sensitivity between membrane patches indicate that there are more than one type of sodium selective ion-channel in tegument derived vesicles.

Chloride selective ion-channels

A single patch recording of chloride selective ion-channels is presented. The observed positive shift in the reversal potential on the addition of concentrated potassium chloride to the bath solution was strong evidence for a chloride selective

channel: a channel selective for cations would exhibit a negative shift in the reversal potential. The lower conductance value of 22.4pS obtained prior to the addition of 3M KCl gives an indication of the channel conductance under physiological conditions. Previous studies have concentrated on the effect of cations on the resting potential of the tegument (Fetterer, Pax, Bennett, 1980b) whilst anions have been ignored. The tegument of *E. granulosus* is believed to have a relatively high chloride permeabiltiy (Ibarra and Reisin, 1994). Other preparations have demonstrated the importance of chloride selective ion-channels in stabilising the membrane potential (for review see Franciolini and Petris 1990).

Experiments with unknown ion selectivity

Four membrane patches contained ion channels with conductances ranging from 11.8pS to 50.0pS and observed reversal potential values (close to 0mV) that could not be definitively interpreted. The composition of the solutions used resulted in 0mV reversal potential values for different channel types with different ion-selectivities. The 0mV reversal potential predicted the ion-channels present to be either chloride selective, equally selective for potassium and sodium ions, or totally non-selective. However on the basis of the observed reversal potential the ion-channels in the four experiments can be excluded from the Na-selective and K-selective groups of ion-channel.

The final group of five experiments were carried out using symmetrical recording solutions which prevented estimation of ion-selectivity. The conductances in these experiments ranged from 7.7pS to 82.6pS. No attempt was made to assess the possible function of these channels as there ion selectivity remains unknown.

Summary

The results demonstrate the presence of a range of ion-channel types in vesicles derived from the outer tegument of male *Schistosoma mansoni.* The channels present varied in conductance (7.4pS to 360pS) and ion selectivity. Evidence has been presented of ion-channels selective for potassium ions, chloride ions and sodium ions. Additionally a large conductance cation selective channel previously described in female parasites (Day *et al,* 1992b) was observed in vesicles derived from male worms.

Interpretation of noisy recordings: the double membrane model

In a number of experiments the analysis was limited to the conclusion that ion-channels were present in the membrane patch. Two major factors prevented further analysis: firstly, in several records the level of background noise was too high to permit estimation of channel amplitude; secondly, in several experiments a large number of "subconductance" levels were observed making it impossible to determine channel amplitude. Another feature of some recordings was a "rounding" of channel events caused by capacitance: in isolated patches from conventional membranes this phenomenon indicates that the isolated patch has resealed to form a vesicle on the pipette tip.

Sources of noise in conventional membrane preparations

In conventional membrane preparations a high level of background noise can be explained by either poor seal resistance or by an inherently noisy membrane. In the schistosome vesicle preparation the level of background noise was observed to be independent of the seal resistance indicating that seal quality alone would not explain the variations in noise level. Also, since the noise level varied between patches, not all of the background noise could be accounted for by an inherently noisy membrane. The presence in some patches of a large number of current steps, termed "subconductance" levels could indicate either: (1) a large number of different ion-channel types in the membrane patch; or (2) ion-channels in the patch displaying true "subconductance" levels (Tank *et al.*, 1982).

The preceding paragraph is an explanation of how noisy records and subconductance levels can appear in a conventional membrane preparation composed of a single bilayer. The tegument vesicle preparation can offer another possible explanation

why these observations occurred; this explanation is considered in the rest of this chapter.

Unique property of the outer tegument.

The outer membrane of the schistosome tegument, unlike more conventional membranes, possesses two phospholipid bilayers in close association (McLaren and Hockley, 1973). In other words the outer "membrane" of the tegument is, in reality, two conventional membranes very close together. Chapter 6 demonstrates that some of the vesicles produced by low pH treatment retain this unique membrane arrangement. Electrophysiological experiments have shown that the outer tegument of the parasite is selective for certain ions indicating that ion-channels are present in the membranes of the outer tegument. However it is not known whether these ion-channels are located in the outer or inner bilayer or both. If the channels are located in both bilayers and both remain intact on isolation of the membrane patch then the current records may appear different to those obtained from more conventional membrane patches. Mitochondria also possess a "double membrane" and ion channels have been isolated from both of the bilyers present. At first it was believed that the outer bilayer of the mitochondria was a non-selective sieve (containing large conductance channels with little or no selectivity). The inner bilayer maintained the electrical potential necessary for mitochondrial functioning. More recent findings (of small conductance channels in the outer bilayer) have suggested that the arrangement of ion channels and maintenance of the membrane potential are more complex (for review see Mannella, 1992).

Model of the schistosome double Bilayer.

Figure 7.16A shows a hypothetical model of the schistosome outer tegument with two ion-channels located in both the inner and outer bilayers. The channels in the

inner bilayer have a conductance of 20pS and those in the outer bilayer have a conductance of 100pS. The ion-channels in the model are assumed to have identical ion selectivity and display no rectification. The model is held at a membrane potential of -50mV. Figure 7.16B is a circuit diagram of the model: ion-channels are represented as resistors whilst the channel gates are represented as switches. Figure 7.16C shows a predicted current trace obtained and shows how it would change when each of the channels in the membrane patch opens or closes. It is apparent from Figure 7.16C that the membrane with the smallest conductance limits the size of the current flowing. If the model has one channel open in each of the two membranes then opening of another 100pS channel in the outer membrane only causes a small increase in the current flowing whilst opening of another 20pS channel in the inner membrane almost doubles the amount of current passed. The hypothetical current trace in Figure 7.16C demonstrates the difficulty in interpreting the channel records with a relatively simple arrangement of channels. Table 7.3 summarises the total conductance of the model for each combination of channel openings and closures. The total conductance of the patch was calculated by using equations *[6]* and *[7]*.

$$G_{Inner}=(G_{Im}+G_{ic1}+G_{ic2}.....G_{icn}).....[6]$$

Equation *[6]* was used to calculate the overall conductance of each of the inner bilayer where: G_{Inner} was the conductance of the bilayer; n was the number of ion-channels in the bilayer; G_{ic1}, G_{ic2}, are the conductances of the individual ion-channels present; G_{Im} is the conductance of the inner phospholipid membrane. The overall conductance of the outer bilayer can be calculated using the same equation by substituting the appropriate conductance values for the ion-channels present.

$$\frac{1}{G_{Tot}} = \left(\frac{1}{G_{Inner}} + \frac{1}{G_{Outer}} \right) \quad \text{.....[7]}$$

Equation *[7]* was used to calculate the overall conductance of the double bilayer where: G_{Tot} was the total conductance of the double bilayer; G_{inner} was the conductance of the inner bilayer; and G_{outer} was the total conductance of the outer bilayer. The model assumes that both of the phospholipid bilayers have formed a high resistance seal with the pipette glass; other possible consequences for the bilayers in the tegument double membrane during sealing and isolation of a membrane patch are described in detail in appendix II.

Figure 7.16

A: Hypothetical model of ion-channels in an isolated patch pulled from the "double membrane" of the schistosome outer tegument. The outer bilayer contains two ion-channels each with a conductance of 100pS. The inner bilayer contains two channels each with a conductance of 20pS. The patch was held at a membrane potential of -50mV. The model assumes that all ion-channels in the patch have identical ion selectivities, display no rectification, and exhibit no subconductance levels.

B: A circuit diagram of the membrane patch model shown in **A**. The ion-channels in the patch are represented by resistors while the channel gates are represented by switches.

C: A theoretical trace from the membrane patch model showing the various current steps occurring as different ion-channels in the patch open and close. Various changes in current are labelled (*i*) to (*viii*) which correspond to the opening or closing of specific ion-channels in the model. The trace begins with none of the channels in the patch open (*i*). A 100pS channel in the outer bilayer opens (*ii*); no current flows. A 20pS channel in the inner bilayer opens (*iii*) and a current of -0.84pA flows. At (*iv*) a second 20pS channel in the inner bilayer opens allowing a current of -1.43pA to flow. At (*v*) the second 100pS channel in the outer bilayer opens, at this point all the channels in the patch are open, and a current of -1.67pA flows. At (*vi*) a 20pS channel closes and the current is reduced to -0.91pA. One of the 100pS channels in the outer bilayer closes at (*vii*) reducing the current to -0.84pA. At (*viii*) the second 100pS channel closes and no current can flow across the patch. The theoretical trace shown includes all the possible current levels allowed by the model. However, the trace does not show all the possible steps between these levels. The trace clearly demonstrates how complex channel records could become when recording across the tegument "double membrane".

Figure 7.16

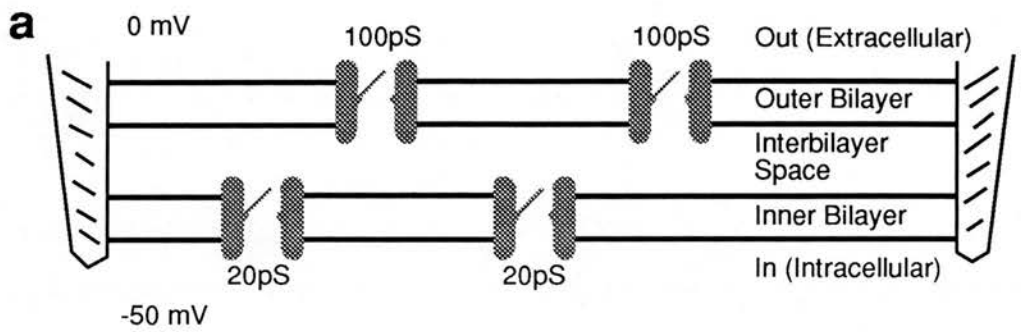
a
0 mV
100pS
100pS
Out (Extracellular)
Outer Bilayer
Interbilayer Space
Inner Bilayer
In (Intracellular)
20pS
20pS
-50 mV

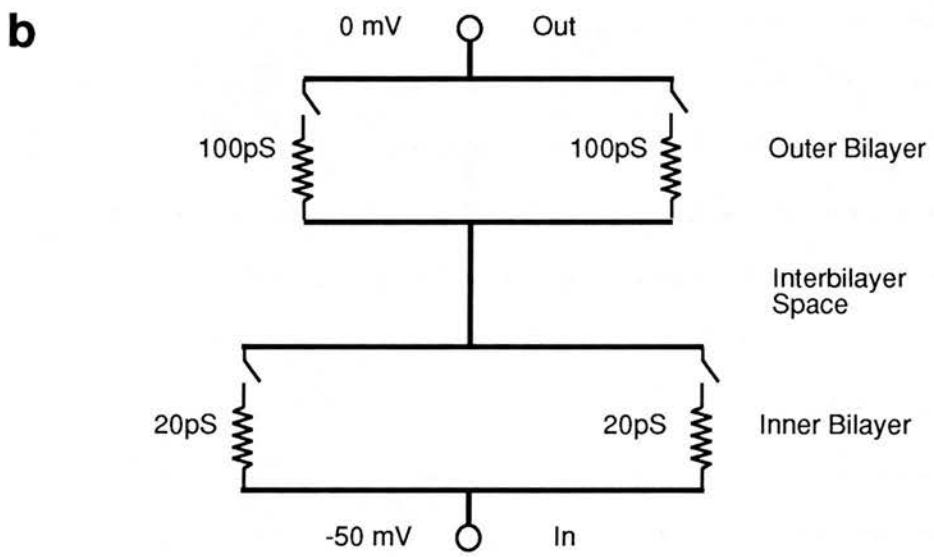
b
0 mV
Out
100pS
100pS
Outer Bilayer
Interbilayer Space
20pS
20pS
Inner Bilayer
-50 mV
In

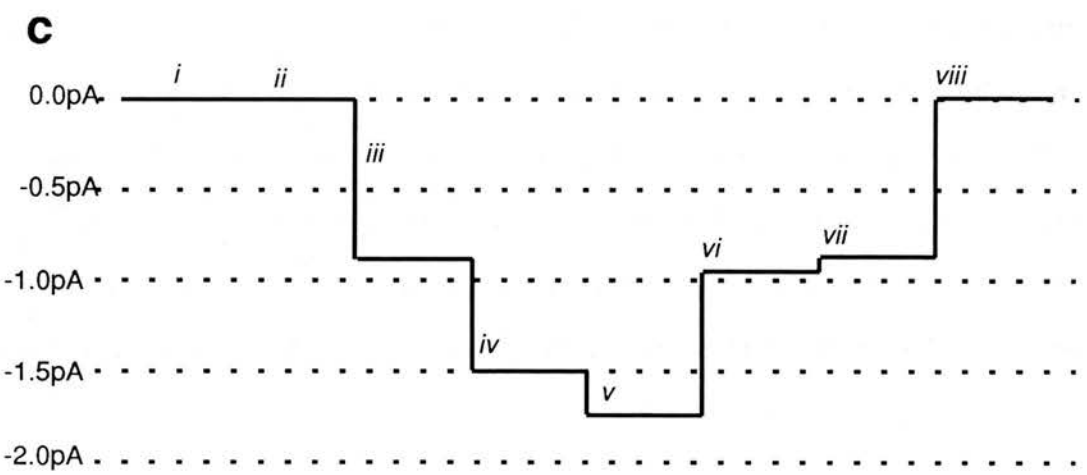
c
0.0pA
-0.5pA
-1.0pA
-1.5pA
-2.0pA
i
ii
iii
iv
v
vi
vii
viii

Table 7.3

Bilayer	Outer		Inner		Patch Conductance (pS)	Current Flowing at -50mV (pA)
Channel Conductance	100pS	100pS	20pS	20pS		
	O	C	C	C	0	0
Channels	O	C	O	C	16.7	-0.84
Open (O) or	O	O	O	C	18.2	-0.91
Closed (C)	O	O	O	O	33.3	-1.67
	O	C	O	O	28.6	-1.43
	C	C	O	O	0	0

Table 7.3

The table demonstrates the four possible conductances of the "double membrane" patch model (excluding 0pA). The table also gives values for the current flowing through the patch at -50mV for each of the conductance levels.

Limitations of the Model

The model of the "double membrane" of the outer tegument is necessarily oversimplified. I have assumed a uniform conductance for the channels within each bilayer and also that all the channels present have an identical ion selectivity. Biological membranes commonly contain several ion-channel types with varying conductances and ion selectivities. Incorporation of these factors into the tegument "double membrane" model would increase the possible number of current steps. In the model there are five possible current levels (including 0mV) for any single potential (Table 7.3). If, to make the model more realistic, each of the four ion-channels were assigned a different conductance then the number of observable current levels would increase to nine.

The model also takes no account of the distance between ion-channels in the inner and outer membranes. The model could be made more complex by the incorporation of a resistor in series between the two bilayers. The resistance between two channels in separate bilayers is dependent on the distance they are apart; the larger the distance then the greater the resistance. It has been estimated that the bilayers in the schistosome "double membrane" are 7nm apart (McLaren and Hockley, 1973). Clearly the smallest distance between the channels in the separate bilayers is 7nm *i.e.* the channels are located one directly below the other in the membrane patch. A typical isolated patch has an estimated area of $\approx 9\mu m^2$ that is not in contact with the pipette glass (Sakmann and Neher, 1983): therefore it is also possible that ion-channels in the two bilayers may be separated by a distance of up to 3μm. The shape of a membrane patch is approximately circular, therefore the largest distance between two points is equal to the diameter of the circle. A patch with an area of $\approx 9\mu m^2$ has an approximate diameter of 3μm. The possible range of distances

separating channels in the two bilayers (7nm to 3μm) would also affect the amplitude of the current steps.

The double membrane model: possible problems interpreting channel records

The model shown in Figure 7.15 gives five possible current levels (Table 7.3). If the channels in the model were incorporated into a single bilayer (as in conventional membranes) then the number of current levels would be nine. This observation implies that the double membrane model has fewer possible current levels and would be easier to interpret. However, in the conventional membrane each individual current step is uniform and directly related to the conductance of a channel. At -50mV the opening of a 100pS channel, regardless of the open\closed state of the other channels in the patch, always gives an increase in current of 5pA. In the double membrane model the opening of a 100pS can give: no increase in current; an increase of 0.84pA; an increase of 1.43pA; an increase of 0.07pA; or an increase of 0.24pA. The increase in current is dependent on the open or closed states of the other ion-channels in the patch. Clearly there is no simple relationship between the amplitude of a current step and the conductance of the channel that opens to cause it. The difficulty of interpreting the channel records would also be increased as there is no way to reliably estimate the number of channels in a membrane patch.

The experimental results in Figure 7.14 could not be interpreted by using a conventional model of a membrane patch: the predicted reversal potential for all ion-channels was 0 mV while linear regression of the data gave reversal potentials >50 mV. The observations could be explained by the proposed model. In the double membrane model the amplitude of channel opening is not related to the channel conductance simply by Ohms law because the amplitude of channel opening depends on the conductance of the other ion-channels present in the additional bilayer.

CHAPTER 8: GENERAL DISCUSSION AND FUTURE WORK.

8.1 Vesicle preparations allow the study of ion-channels in parasitic Helminths.

The patch-clamp technique is a powerful tool for investigating the properties of ion-channels. The noise level of the recording is limited by its requirement for giga-ohm resistance seals between the pipette glass and the membrane of interest (Hamill *et. al.* 1981). Many cell membranes do not possess a surface suitable for forming high resistance seals: the *Ascaris* somatic muscle cell is covered in a collagen matrix that renders seal formation impossible; the outer membrane of the schistosome tegument is extremely uneven and (in the case of males) covered in a large number of spines from which it is impossible to obtain high resistance seals (McLaren, 1980). Low pH treatment of the schistosome results in vesicles forming from the double outer membrane of the tegument that are suitable for patch-clamping (Robertson, Martin, Kusel, 1996; 1997) while treatment of *Ascaris* muscle flaps with collagenase results in muscle cell vesicles that are also suitable for patch-clamping (Robertson and Martin, 1996).

8.2 The large conductance Ca-dependent chloride channel in *Ascaris suum.*

Physiological Significance.

The large conductance Ca-dependent chloride channel has been hypothesised to perform an excretory role (Valkanov *et al.* 1994). Briefly, the channel was observed to conduct the carboxylic anions that are the end products of anaerobic respiration in the somatic muscle cell. The findings in Section I of the thesis do not disagree with that hypothesis. The effect in changes of pH on each side of the membrane was investigated (Robertson and Martin, 1996). While pH changes had no significant effects on the conductance of the channel it had a dramatic effect on channel gating. Briefly, decreased extracellular pH increased the probability of channel opening

(P_{open}) at negative membrane potentials. Alterations in the intracellular pH had more dramatic effects. An increase in the intracellular pH raised P_{open} at each of the membrane potentials tested. A decrease in intracellular pH decreased P_{open} at negative membrane potentials and increased P_{open} at positive membrane potentials. The effective gating charge of the channel was calculated under each of the experimental conditions. Reduced intracellular pH had the most dramatic effect on the gating charge: a reduction in pH changed the polarity of the effecting gating charge from negative (-3e) under control conditions to positive (+1.8e) when the intracellular pH was reduced to 6.0. These results led to the construction of a model to describe channel gating. The model contained several histidine residues on the channel gate; on reduced pH these residues were protonated thus changing the sign of the effective gating charge. The observed pH sensitivity was at first surprising. However, respiration in *Ascaris* produces protons as well as the carboxylic anions that the channel conducts. The presence of an active proton pump in the muscle cell would lead to an increased intracellular pH, the change in pH would increase the probability of channel opening and allow more waste anions to leave the cell.

A possible target site for new anthelminthics.

The Ca-dependent chloride channel from *Ascaris* muscle cells does not fit easily into any of the proposed classes of chloride channel (see Chapter 1 for review). The lack of similarities between the Ca-dependent chloride channel and other chloride channels suggests that it differs from the chloride selective channels found in the host. Clearly, any difference between parasite and host is a possible anthelminthic target site as theoretically any drug that affects a parasite specific target will have no detrimental effects on the host. Additionally, the Ca-dependent chloride channel is the most commonly observed chloride channel in membrane vesicles prepared from

the somatic muscle cells of *Ascaris* (R.J. Martin, Unpublished observations). These facts together with the proposed excretory role of the channel (Valkanov *et al,* 1994) make the Ca-dependent chloride channel a suitable target for future anthelminthics.

Future Work.

The unique properties and hypothesised function of the Ca-dependent chloride channel render it a suitable target for future anthelminthics. Future work could investigate the ability of various compounds to block the channel. However, the work presented in this thesis (Section I; Robertson and Martin, 1996) and previous work on the Ca-dependent chloride channel (Thorn and Martin, 1987) have been hampered by the occurrence of channel run-down. I suggest that future studies should initially concentrate on investigating channel run-down with an aim to allow recordings of longer duration to be obtained. A greater understanding of how this phenomenon occurs (and how to prevent it) could increase the success of studies aimed to find novel compounds that block the Ca-dependent chloride channel. Channel activity has been shown to be dependent on intracellular Ca^{2+} concentrations but run-down still occurs regardless of Ca^{2+} concentration (Thorn, 1987 PhD thesis). The phenomenon of channel run-down has been reviewed recently (Becq, 1996) and initial work could concentrate on examining the effect of PKA and phosphatase inhibitors on channel run-down; in the CFTR chloride channel run-down is caused by dephosphorylation of the channel molecule by endogenous phosphatases (reviewed by Becq, 1996).

8.3 Ion-channels in the outer tegument of *Schistosoma mansoni.*

The work presented in Section II of the thesis demonstrates a new preparation that allows the recording of ion-channels from the outer tegumental membranes of adult male *Schistosoma mansoni* (Robertson, Martin and Kusel, 1996; Robertson, Martin

and Kusel, 1997). To date there has been little information on the ion-channel types present in the schistosome tegument because of the difficulty of obtaining high-resistance seals from the membranes. The outer tegument of the schistosome is in direct contact with the host and is thought to be the main site of nutrient absorption for the parasite. There is a membrane potential of approximately -60 mV across the tegument implying the presence of ion-channels in the outer "double membrane". The uneven surface of the adult parasite has made patch-clamp studies difficult. To date only one paper has been published on patch-clamp studies of the outer tegumental membrane of the parasite (Day *et al,* 1991). The authors describe a large-conductance non-selective cation channel in female parasites; the authors also state that obtaining high resistance seals was difficult and could only be accomplished in female parasites, they were unable to obtain seals from adult males. Chapter 6 of the thesis demonstrates that membranous vesicles can be produced from the double outer membrane of the schistosome by low pH treatment, while Chapter 7 demonstrates that these vesicles are suitable for patch-clamping.

Ion-channels present in the tegument: possible functions

The results of Chapter 7 demonstrate that the patch-clamp technique can be successfully applied to tegument derived membrane vesicles formed by low pH treatment. The development of this preparation offers the opportunity to study the ion-channel types present in the outer tegument of *S. mansoni*. The initial results of patch-clamp study are presented in Chapter 7; the results indicate that there are several different types of ion-channel present with differing conductances and ionic selectivities (based on reversal potential measurements). Evidence has been presented for different ion-channels, selective for either potassium, sodium or chloride ions. This is the first direct evidence to date of such ion-channels from the tegument of adult schistosomes. Patch-clamp experiments on the tegument derived

vesicles have also demonstrated the presence of the large-conductance non-selective cation channel in male parasites; the channel had previously only been observed in female parasites (Day *et al.* 1991). Additionally, results indicate that the large-conductance non-selective cation channel is also permeable to calcium ions. Potassium selective ion-channels may play a role in the maintenance of the resting membrane potential across the tegument. In many preparations chloride selective channels play an important role in and secretion (Kuriyama *et al.,* 1995). The possible role of sodium selective ion-channels remains unclear.

Implications for the mode of praziquantel action.

Recent reviews on the possible mode of praziquantel action have emphasised the importance in changes in the parasites calcium concentrations during drug action (Redman *et al,* 1996; Day *et al,* 1992b). Treatment of the parasites causes an influx of calcium across the tegument and depolarisation of the tegument. The influx of calcium ions suggests that praziquantel opens an ion-channel located in the outer membrane of the tegument that allows calcium to enter the worm. The results of the patch-clamp studies (Chapter 7) suggest that the large-conductance non-selective cation channel found in the tegument is permeable to calcium ions and is therefore a possible site of praziquantel action. However, more work on the vesicle preparation is required to classify the ion-channels types present in the outer tegument and how they are affected by praziquantel.

Future work.

The work on *Schistosoma mansoni* presented in this thesis (Section II) demonstrates that vesicles produced by low pH treatment of the parasite offer a new means of studying ion-channels in the outer membrane of the parasite. The study has demonstrated that there are several different ion-channel types present which vary in

conductance and ionic selectivity. Clearly vesicle preparations allow single-channel study of membranes that were previously unsuitable for patch-clamp experiments. Future studies should classify in more detail the properties of the ion-channel types present in the outer membrane of the schistosome tegument and possible investigate the effects of praziquantel on any ion-channels observed.

A proportion (at least 41%) of the vesicles produced by low pH treatment contain the unusual "double outer membrane" found in the schistosome tegument (Chapter 6). An alternative method to form vesicles from the "double outer membrane" is treatment with concanavalin A (Simpson and McLaren, 1982). Any future studies could compare the suitability for patch-clamping (*i.e.* the frequency of obtaining giga-ohm resistance seals) of vesicles produced by low pH and concanavalin A treatment.

Finally, the question of whether isolated inside-out patches from vesicles contain the double outer membrane or are composed of a single bilayer should be addressed. The electrical model in Appendix II shows how single-channel records obtained from a "double membrane" patch could differ from recordings made from a single membrane. An alternative method to investigate the problem would be to use amphotericin B. Any isolated patch suspected to contain the "double membrane" could have amphotericin B added to the bathing solution. Amphotericin B is used in electrophysiological experiments to perforate a cell-attached membrane patch to allow whole cell recordings (Rae, Cooper, Gates, Watsky, 1991; Hill, Martin, Miller, 1996). Amphotericin B would perforate the inner bilayer but as it does not traverse bilayers the remaining bilayer (outer) would remain unaffected. In a "double membrane" patch, recordings obtained after perforation by Amphotericin B would have similar properties to recordings obtained from a single membrane as the

resistance of the inner bilayer would have been substantially reduced by Amphotericin B perforation.

Bibliography

Abath, F.G.C., Werkhauser, R.C. 1996. The tegument of *Schistosoma mansoni:* functional and immunological features. *Parasite Immunol.* **18:**15-20.

Andrews, P.,Thomas, H., Pohlke, R., Seubert, J. 1983. Praziquantel. *Med. Res. Rev.* **3:**147-200.

Becq, F. 1996. Ionic channel run down in excised membrane patches. *Biochim. Biophys. ACTA.* **1286:**53-63.

Blair, K.L., Bennett, J.L., Pax, R.A. 1992. Praziquantel: physiological evidence for its site(s) of action in magnesium-paralysed *Schistosoma mansoni. Parasitology.* **104:**59-66.

Blair, K.L., Bennett, J.L., Pax, R.A. 1993. Serotonin and acetylcholine: further analysis of praziquantel-induced contraction of magnesium-paralysed *Schistosoma mansoni. Parasitology.* **000:**1-9.

Blair, K.L., Day, T.A., Lewis, M.C., Bennett, J.L., Pax, R.A. 1991. Studies on muscle cells isolated from *Schistosoma mansoni:* a Ca-dependent K^+ channel. *Parasitology.* **102:**251-258.

Blatz, A.L. 1990. Chloride channels in skeletal muscle. *In* Chloride Channels and Carriers in Nerve, Muscle and Glial Cells, ed. by Alvarez-Leefmans, F.J. and Russell, pp.407-419. (Plenum Press, New York).

Blatz, A.L., Magelby, K.L. 1983. Single voltage-dependent chloride-selective channels of large conductance in cultured rat muscle. *Biophys. J.* **43:**237-241.

Brading, A.F., Caldwell, P.C. 1964. The effect of ions on the resting potentials of muscle cells in *Ascaris lumbricoides*. *J. Physiol.* **173:**36P.

Brading, A.F., Caldwell, P.C. 1971. The resting membrane potential of the somatic muscle cells of *Ascaris lumbricoides. J. Physiol.* **217:**605-624.

Bricker, C.S., Pax, R.A., Bennet, J.L. 1982 Microelectrode studies of the tegument and sub-tegumental compartments of male *Schistosoma mansoni*- anatomical location of sources of electrical potential. *Parasitology.* **85:**149.

Bormann, J., Hamill, O.P., Sackmann, B. 1987. Mechanisms of anion permeation through channels gated by glycine and γ-aminobutyric acid in mouse cultured spinal neurons. *J. Physiol.* **385:**243-286.

Bruce, J.L., Pezzlo, F., Yajima, Y., McCarty, J.E. 1971. An electron microscope study of *Schistosoma mansoni* migration through mouse tissue: ultrastructure of the gut during hepatoportal phase migration. *Exp. Parasitol.* **30:**165-173.

Caldwell, P.C., Ellory, J.C. 1968. Ion movements in somatic muscle cells of *Ascaris lumbricoides. J. Physiol.* **197:**75-76P.

Camancho, M., Alsford, S., Jones, A., Agnew, A. 1995. Nicotinic acetylcholine receptors on the surface of the blood fluke *Schistosoma. Mol. Biochem. Parasitol.* **71:**127-134.

Cappe de Baillon, P. 1911. Etude sur les fibres musculaires d'*Ascaris*. La Cellule. **27:**165-211.

Castle, N.A., Haylett, D.G., Jenkinson, D.H. 1989. Toxins in the characterisation of potassium channels. *Trends in Neurosci.* **12:**59-65.

Cioli, D., Pica-Mattoccia, L., Archer, S. 1993. Drug resistance in schistosomes, *Parasitol. Today.* **9:**162-166.

Crompton, D.W.T. 1988. The Prevalence of Ascariasis. *Parasitol. Today* **4:**162-169.

Crompton, D.W.T., Nesheim, M.C., Pawlowski, Z.S. 1989. Ascariasis and its prevention and control. (London, New York and Philadelphia: Taylor and Francis).

Cully, D.F., Vassilatis, D.K., Liu, K.K., Paress, P.S., Vanderploeg, L.H.T., Schaeffer, J.M. 1994. Cloning of an avermectin-sensitive glutamate-gated chloride channel from *Caenorhabditis elegans*. *Nature.* **371:**707-711.

Day, T.A., Bennett, J.L., Pax, R.A. 1992. Praziquantel: The Enigmatic Antiparasitic. *Parasitol. Today* **8:**342-344.

Day, T.A., Bennett, J.L., Pax, R.A. 1992. *Schistosoma mansoni*: Patch-Clamp Study of a Nonselective Cation Channel in the Outer Tegument of Females. *Exp. Parasitol.* **74:**348-356.

Day, T.A., Maule, A.G., Shaw, C., Halton, D.W., Moore, S., Bennett, J.L., Pax, R.A. 1994. Platyhelminth FMRFamide-related peptides (FaRPs) contract *Schistosoma mansoni* (Trematode: Digenea) muscle fibres *in vitro. Parasitology.* **109:**455-459.

Day, T.A., Orr, N., Bennet, J.L., Pax, R.A. 1993. Voltage-gated currents in muscle cells of *Schistosoma mansoni. Parasitology.* **106:**471-477.

Day, T.A., Kim, E., Bennett, J.L., Pax, R.A. 1995. Analysis of the kinetics and voltage-dependency of transient and delayed K^+ currents in muscle-fibres isolated from the flatworm *Schistosoma mansoni. Comp Biochem & Physiol. A-Physiology.* **111:**79-87.

Del Castillo, J., Morales, T., Sanchez, V. 1963. Action of piperazine on the neuromuscular system of *Ascaris*. *Nature.* **200:**706.

Del Castillo, J., De Mellow, W.C., Morales, T. 1964. Influence of Some Ions on the Membrane Potential of *Ascaris* Muscle. *J. Gen. Physiol.* **48:**129-140.

Del Castillo, J., De Mellow, W.C., Morales, T. 1964b. Inhibitory action of γ-aminobutyric acid on *Ascaris* muscle. *Experientia.* **20:**141-143.

Del Castillo, J., Rivera, A., Soloranzo, S., Serrato, J. 1989. Some aspects of the neuromuscular system of *Ascaris*. *Q. J. Exp. Physiol.* **74:**1071-1087.

De Harven, E. 1967. Methods in electron microscopic cytology. In: *Methods in Cancer Research,* Vol. 1 (Edited by Buch, H.) pp3-44. Academic press, New York.

Dixon, D.M., Martin, R.J. 1993. Patch-clamp and Chloride Channels in *Ascaris suum*. *Parasitol. Today.* **9:**341-344.

Dixon, D.M., Valkanov, M., Martin, R.J. 1993. A Patch-Clamp Study of the Ionic Selectivity of the Large Conductance, Ca-Activated Chloride Channel in Muscle Vesicles Prepared from *Ascaris suum*. *J. Membrane Biol.* **131:**143-149.

Doenhoff, M.J., Modha, J., Lamertucci, J.R. 1988. Anti-schistosome chemotherapy enhanced by antibodies specific for a parasite esterase. *Parasitology.* **65:**507-510.

Duittoz, A.H. 1990. Pharmacology of GABA receptors in *Ascaris suum* muscle : an electrophysiological study. (PhD Thesis, University of Edinburgh).

Duittoz, A.H., Martin, R.J. 1991. Effects of SR95103 on GABA-activated single-channel currents from *Ascaris suum* muscle. *Comp. Biochem. and Physiol. C-Pharmacology Toxicology and Endocrinology.* **98:**423-432.

Fallon, P.G., Sturrock, R.F., Niang, C.M., Doenhoff, M.J. 1995. Diminished susceptibility to Praziquantel in a Senegal isolate of *Schistosoma mansoni. Am. J. Trop. Med. Hyg.* **53:**61-62.

Fallon, P.G., Doenhoff, M.J. 1994. Drug-resistant schistosomiasis: resistance to praziquantel and oxaminiquine induced in *Schistosoma mansoni* mice is drug specific. *Am. J. Trop. Med. Hyg.* **51:**83-88.

Fallon, P.G., Mcneice, C., Probert, A.J., Doenhoff, M.J. 1994. Quantification of praziquantel-induced damage on the surface of adult *Schistosoma mansoni* worms: estimation of esterase and alkaline phosphatase activity. *Parasitol. Res..* **80:**623-625.

Fallon P.G., Tao, L-F., Ismail, M.L., Bennett, J.L. 1996. Schistosome Resistance to Praziquantel: Fact or Artefact? *Parasitol. Today.* **12:**316-320.

Fallon, P.G., Cooper, R.O., Probert, A.T., Doenhoff, M.J. 1992. Immune-dependent chemotherapy of schistosomiasis. *Parasitology.* **105:**S41-S48.

Fetterer, R.H., Pax, R.A., Bennett, J.L. 1980a. Praziquantel, potassium and 2,4-dinitrophenol: analysis of their action on the musculature of *Schistosoma mansoni. Eur. J. Pharmacol.* **64:**31-38.

Fetterer, R.H., Pax, R.A., Bennett, J.L. 1980b. *Schistosoma mansoni*: characterisation of the electrical potential from the tegument of adult males. *Exp. Parasitol.* **49:**353-365.

Fetterer, R.H., Pax, R.A., Bennett, J.L. 1981. Na $^{+}$-K^{+} transport, motility and tegumental membrane potential in adult male *Schistosoma mansoni. Parasitology.* **82:**97-109.

Foley, M., MacGregor, A.N., Kusel, J.R., Garland, P.B., Downie, T., Moore, I. 1986. The lateral diffusion of lipid probes in the surfaces of *Schistosoma mansoni. J. Cell Biology* **B103:**807-818.

Franciollini, F., Petris, A. 1990. Chloride channels of biological membranes. *Biochemica and Biophysica Acta.* **1031:**247-259.

Goeze, J.A.E. 1782. *Versuch einer Naturgeschichte der Eingeweidewurmer thierischer Korper* (Blankenburg).

Gönnert, R. 1955. Schistosomiasis-studien I. Beiträge zur anatomie und histologie von *Schistosoma mansoni. Zeitschrift für Tropenmedizin und Parasitologie.* **6:**18-33.

Gray, P.T.A., Bevan, S., Ritchie, J.M. 1984. High conductance anion-selective channels in rat cultured Schwann cells. *Proc. R. Soc. B. London* **221:**395-409.

Grosman, C., Reisin, I.L. 1995. *Echinococcus granulosus:* Partial characterisation of the conductive properties of two cation channels from protoscoleces of the Ovine strain, reconstituted on planar lipid bilayers. *Exp. Parasitol.* **81:**546-555.

Hamill, O.P., Marty, A., Neher, E., Sakmann, B., Sigworth, F.J. 1981. Improved Patch-Clamp Techniques for High-Resolution Current Recording from Cells and Cell-Free Membrane Patches. *Pflügers Arch.* **391:**85-100

Hanke, W., Miller, C. 1983. Single Chloride Channels from *Torpedo* Electroplax. *J. Gen. Physiol.* **82:**25-45.

Harnett, W., Kusel, J.R. 1986. Increased exposure of parasite antigens at the surface of adult male *Schistosoma mansoni* exposed to praziquantel *in vitro*. *Parasitology.* **61:**401-405.

Harnett, W. 1988. The anthelminthic action of Praziquantel. *Parasitol. Today.* **4:**144-146.

Harpur, R.P. 1963. Maintenance of *Ascaris lumbricoides in vitro*-II. Changes in muscle and ovary carbohydrates. *Canad. J. Biochem. Physiol.* **41:**1673-1689.

Harris, J.E., Crofton, H.D. 1957. Structure and function in the nematodes: internal pressure and cuticular structure in *Ascaris. J. Exp. Biol.* **34:**116-130.

Hill, P.B., Martin, R.J., Miller, H.R.P. 1996. Charecterisation of whole-cell currents in mucosal and connective tissue mast cells using amphotericin B. *Pflugers Arch.* **432:**986-994.

Hille, B. 1968. Charges and potentials at the nerve surface: Divalent ions and pH. *J. Gen. Physiol.* **51:**221-236.

Hille, B., Woodhull, A.M., Shapiro, B.I. 1975. Negative surface charge near sodium channels of nerve: divalent ions, monovalent ions, and pH. *Phil. Trans. R. Soc. Lond.* **270:**301-318.

Hille,B. 1992. Ionic channels of excitable membranes 2nd ed. *Sinauer Associates, Sunderland, Mass.*

Hobson, A.D., Stephenson,W., Beadle, L.C. 1952. Studies on the physiology of *ascaris lumbricoides. J. Exp. Biol.* **29:**22-29.

Hockley, D.J., McLaren, D.J. 1973. *Schistosoma mansoni*: changes in the outer membrane of the tegument during development from cercaria to adult worm. *Int. J. Parasitol.* **3:**13-25.

Holden-Dye, L., Hewitt, G.M., Wann, K.T., Krogsgaard-Larsen, P., Walker, R.J. 1988. Studies involving avermectin and the γ-aminobutyric acid (GABA) receptor of *Ascaris suum* muscle. *Pesticide Science.* **24:**231-245.

Ibarra, C., Reisin, I.L. *Echinococcus granulosus* -Characterisation of the electrical potential of the syncytial tegument of protoscoleces incubated *in vitro* -effect of inhibitors. *Exp. Parasitol.* **78:**400-409.

Jarman, M. 1959. Electric activity of muscle cells of *Ascaris* muscle. *Nature.* **184:**1244.

Kim,E., Day, T.A., Bennett, J.L., Pax, R.A. 1995. Cloning and functional expression of a *Shaker*-related voltage-gated potassium channel gene from *Schistosoma mansoni* (Trematoda: Digenea). *Parasitology.* **110:**171-180.

Kolb, H.A., Brown, C.D., Murer, H. 1985. Identification of a voltage-dependent anion channel in the apical membrane of a Cl^--secretory epithelium (MDCK). *Pflügers Arch.* **403:**262-265.

Kostyuk, P.G., Shuba,Ya.M., Savchenko, A.N. 1988. Three types of calcium channels in mouse sensory neurones. *Pflügers Arch.* **411:**661-669.

Kostyuk, P., Verkhratsky, A. 1994. Calcium stores in neurones and glia. *Neurosci.* **63:**381-404.

Kuriyama, H., Kitamura, K., Nabata, H. 1995. Pharmacological and physiological significance of ion-channels and factors that modulate them in vascular tissues. *Pharmacol. Rev.* **47:**387-573.

Kusel, J.R., Gordon, J.F. 1989 Biophysical properties of the schistosome surface and their relevnce to its properties under immune and drug attack. *Parasitol. Immunol.* **11:**431-451.

Lancet editorial; 6th May 1989; Ascariasis; 997-998.

Lane, C.A., Pax, R.A., Bennett, J.L. 1987. L-Glutamine: an amino acid required for maintenance of the tegumental membrane potential of *Schistosoma mansoni. Parasitology.* **94:**233-242.

Lewis, C.A. 1979. Ion-Concentration Dependence of the Reversal Potential and the Single Channel Conductance of Ion-channels at the Frog Neuromuscular Junction. *J. Physiol.* **286:**417-445.

Lewis, P.R., Shute, C.C.D. 1966. The distribution of cholinesterase in cholinergic neurons demonstrated with the electron microscope. *J. Cell Sci.* **1:**381-390.

Lima, S.F., Vieira, L.Q., Harder, A., Kusel,J.R. 1994. Altered behaviour of carbohydrate-bound molecules and lipids in areas of the tegument of adult *Schistosoma mansoni* worms damaged by praziquantel. *Parasitology* **109:**469-477.

Linnaeus, C. 1758. *Systema Naturae I* (Holmiae: Laurentii Salvii).

Logothetis, D.E., Movahedi, S., Satler, C., Lindpainter, K., Nadal-Ginard, B. 1992. Incremental Reductions of Positive Charge within the S4 Region of a Voltage-Gated K^+ Channel Result on Corresponding Decreases in Gating Charge. *Neuron.* **8:**531-540.

MacGregor, A.N., Kusel, J.R., Wlson, R.A. 1988. Isolation and characterisation of discoid granules from the tegument of adult *Schistosoma mansoni. Parasitol. Res.* **74:**250-254.

Madison, D., Malenka, R.C., Nicoll, R.A. 1986. Phorbol esters block a voltage-sensitive chloride current in hippocampal pyramidal cells. *Nature.* **321:**695-697.

Martin, R.J. 1980. The effect of GABA on the input conductance and membrane potential of *Ascaris* muscle. *Br. J. Pharmacol.* **71:**99-106.

Martin, R.J. 1982. Electrophysiological effects of piperazine and diethyl carbamizine on *Ascaris suum* somatic muscle. *Br. J. Pharmacol.* **84:**445-461.

Martin, R.J. 1985. γ-aminobutyric acid- and piperazine-activated single-channel currents from *Ascaris suum* body muscle. *Br. J. Pharmacol.* **84:**445-461.

Martin, R.J. 1993. Neuromuscular Transmission in Nematode Parasites and Antinematodal Drug Action. *Pharmac. Ther.* **58:**13-50.

Martin, R.J., Thorn, P., Gration, K.A.F., Harrow, I.D. 1992. Voltage-activated currents in somatic muscle of the nematode parasite *Ascaris suum. J. exp. Biol.* **173:**75-90.

Martin, R.J. and Valkanov, M. 1996. Effects of Acetylcholine on a slow voltage-activated non-selective cation current mediated by non-nicotinic receptors on isolated *Ascaris* muscle bags. *Exp. Physiol.* **81:**909-925.

Martin, R.J. and Valkanov, M., Dale, V.M.E., Robertson, A., Murray, I. 1996. Electrophysiology of *Ascaris* muscle and anti-nematodal drug action. *Parasitology.* **113:**S137-S156.

Maule, A.G., Bowman, J.W., Thompson, D.P., Marks, N.J., Friedman, , A.R., Geary, T.G. 1996. FMRFamide-related peptides (FaRPs) in nematodes: occurrence and neuromuscular physiology. *Parasitology.* **113:**S119-S136.

Mayer, M.L., Owen, D.G., Barker, J.L. 1990. Calcium-dependent chloride currents in vertebrate central neurons. *In* Chloride Channels and Carriers in Nerve, Muscle and Glial Cells. ed. by Alvarez-Leefmans, F.J. and Russell, pp.407-419. (Plenum Press, New York).

McLaren, D.J., Hockley, D.J. 1977. Blood flukes have a double outer membrane. *Nature*. **269:**147-149.

McLaren, D.J. 1980. *Schistosoma mansoni*: The parasite surface in relation to host immunity. In: Tropical Medicine Research Studies, Vol. 1, (ed. K.N. Brown), Chichester Research Studies Press. John Wiley.

Olsen, L.S., Kelley, G.W., Sen, H.G. 1958. Longevity and egg-production of *Ascaris suum. Transactions of the American Microscopical Society.* **77:**380-383.

Papazian, D.M., Timpe, L.C., Jan, Y.N., Jan, L.Y. 1991. Alteration of voltage dependence of *Shaker* potassium channel by mutations in the S4 sequence. *Nature.* **349:**305-310.

Parri, H.R., Holden-Dye, L., Walker, R.J. 1991. Studies on the Ionic Selectivity of the GABA-Operated Chloride Channel on the Somatic Muscle Bag Cells of the Parasitic Nematode *Ascaris suum. Exp. Physiol.* **76:**597-606.

Pax, R.A., Bennett, J.L. 1990. Studies on intrategumental pH and its regulation in adult male *Schistosoma mansoni. Parasitology.* **101:**219-226.

Pax, R.A., Chen, G-Z., Bennett, J.L. 1987. *Schistosoma mansoni*: Measurement of Na^+ Ion Activity in the Tegument and the Extracellular Spaces Using Ion-Selective Microelectrodes. *Exp. Parasitol.* **64:**219-227.

Pax, R.A., Fetterer, R., Bennett, J.L. 1979. Effects of Fluoxetine and Imipramine on male *Schistosoma mansoni. Comp. Biochem. Physiol.* **64C:**123-127.

Pax, R.A., Siefker, C., Bennett, J.L. 1984. *Schistosoma mansoni*: Differences in Acetylcholine, Dopamine, and Serotonin control of circular and longitudinal parasite muscles. *Exp. Parasitol.* **58:**314-324.

Pennington, A.J., Martin, R.J. 1990. A patch-clamp study of acetylcholine-activated ion-channels in *Ascaris suum* muscle. *J. exp. Biol.* **154:**201-221.

Rae, J., Cooper, K., Gates, P., Watsky, M. 1991. Low access resistance perforated patch recordings using amphotericin B. *J. Neurosci. Methods.* **37:**15-26.

Rao, G.S.J., Wariso, B.A., Cook, H.W.H., Harris, B.G. 1987. Reaction of *Ascaris suum* phosphofructokinase with diethylpyrocarbonate. *J. Biol. Chem.* **262:**14068-14073.

Redman, C.A., Robertson, A., Fallon, P.G., Modha, J., Kusel, J.R., Doenhoff, M.J., Martin, R.J. 1996. Praziquantel: an urgent and exciting challenge. *Parasitol Today.* **12:**14-20.

Robertson, A. P., Martin, R.J., Kusel, J.R. 1996. Single-channel recordings from tegument-derived vesicles of *Schistosoma mansoni*. *J. Physiol.* **495P:**33P-34P

Robertson, A. P., Martin, R.J., Kusel, J.R. 1997. A vesicle preparation for resolving single channel currents in tegument of male *Schistosoma mansoni*. *Parasitology.* **114:***(In Press).*

Rosenbluth, J. 1963. Fine structure of body muscle cells and neuromuscular junction in *Ascaris lumbricoides. J. Cell Biol.* **25:**495-515.

Rosenbluth, J. 1973. Obliquely striated muscle .; In; The Stucture and Function of the Muscle, Vol 1, Structure. (Academic Press; New York and London; 391-395).

Sakmann, B., Neher, E. Geometric Paremeters of Pipettes and Membrane Patches. In: Single-channel Recording, pp 37-51, (eds. Sakmann and Neher), Plenum, New York.

Saz, H.J., Weil, A. 1962. Pathway of formation of α-methyl valerate by *Ascaris lumbricoides*. *J. Biol. Chem.* **237:**2053-2056.

Saz, H.J. 1981. Energy metabolisms of parasitic helminths-adaptations to parasitism. *Ann. rev. physiol.* **43:**323-341.

Schneider, G.T., Cook, D.I., Gaga, P.W., Young, J.A. 1985. Voltage sensitive, high-conductance chloride channels in the luminal membrane of cultured pulmonary alveolar (type II) cells. *Pflügers Arch.* **404:**354-357.

Senft, A.W., Gilber, W.B. 1977. *Schistosoma mansoni* tegumental appendages: scanning microscopy following thiocarbohydrazide-osmium preparation. *Am. J. Trop. Med. Hyg.* **26:**1169-1177.

Silk, M.H., Spence, I.M., Gear, J.H.S. 1969. Ultrastructural studies of the blood fluke-*Schistosoma mansoni*. I The integument. *S. Afr. J. med. Sci.* **34:**1-10.

Silk, M.H., Spence, I.M. 1969. Ultrastructural studies of the blood fluke-*Schistosoma mansoni*. II The musculature. *S. Afr. J. med. Sci.* **34:**11-20.

Simpson, A.J.G., McLaren, D.J. 1982. *Schistosoma mansoni*: Tegumental Damage as a Consequence of Lectin Binding. *Exp. Parasitol.* **53:**105-116.

Skuce, P.J., Fairweather, I. 1989. *Fasciola hepatica:* the effect of the sodium ionophore monesin on the adult tegument. *Parasitol. Res.* **75:**223-232.

Smith, J.H., Reynolds, E.S., Lichtenberg, F. von. 1969. The integument of *Schistosoma mansoni. Am. J. Trop. Med. Hyg.* **18:**28-49.

Smith, M.H., Lee, D.L. 1963. Metabolism of haemoglobin and haematin compounds in *Ascaris lumbricoides. Proceedings of the Royal Society of London B.* **157:**234-257.

Smithers, S.R., Terry, R.J. 1965. Infection of laboratory hosts with cercariae of *Schistosoma mansoni* and the recovery of adult worms. *Parasitology* **55:**695-700.

Soulsby, E.J.L. 1965. Textbook of veterinary clinical parasitology; Vol. 1 Helminths. Blackwell Scientific Publications, Oxford. pp184-185.

Staudt, U., Schmahl, G., Blaschke, G., Mehlhorn, H. 1992. Light and scanning electron microscopy studies on the effects of the enantiomers of praziquantel and its metabolite on *Schistosoma mansoni*. *Parasitol. Res.* **78:**392-397.

Storey, G.W., Phillips, R.A. 1985. The survival of parasite eggs throughout the soil profile. *Parasitology.* **91:**585-590.

Stretton, A.O.W. 1976. Anatomy and development of the somatic musculature of the nematode *Ascaris*. *J.Exp. Biol.* **64:**773-788.

Stümer, W., Conti, F., Suzuki, H., Wang, X., Noda, M., Yahagi, N., Kubo, H., Numa, S. 1989. Structural parts involved in activation and inactivation of he sodium channel. *Nature.* **339:**597-603.

Tank, D.W., Miller, C., Webb, W.W. 1982. Isolated-patch recording from liposomes containing functionally reconstituted channels from *Torpedo* electroplax. *Proc. Natl. Acad. Sci. USA.* **79:**7749-7753.

Thomas, R.C. 1984. Experimental Displacement of Intracellular pH and the Mechanism of it's Subsequent Recovery. *J. Physiol.* **354:**3P-22P.

Thomas, H., Gönnert, R., Pohlke, R., Seubert, J. 1975. A new compound against adult tapeworms. *Proceedings of the 7th International Conference of the World Association for the Advancement of Veterinary Parasitology.* Abstract 51.

Thompson, D.P., Pax, R.A., Bennett, J.L. 1982. Microelectrode studies of the tegument and sub-tegumental compartments of male *Schistosoma mansoni*: analysis of electrophysiological properties. *Parasitology* **85:**163-178.

Thorn, P. 1987. Ionic currents in the somatic muscle cells of *Ascaris suum*. PhD Thesis, University of Edinburgh.

Thorn, P., Martin, R.J. 1987. A High-Conductance Calcium-Dependent Chloride Channel of *Ascaris suum* Muscle. *Q. J. Exp. Physiol.* **72:**31-49.

Tielens, A.G.M., van der Bergh, S.G. Aerobic and anaerobic energy metabolism in the life cycle of parasitic helminths. *In* Surviving hypoxia mechanisms of control and adaptation. *CRC Press, London.* Eds Hochachka, P.W., Lutz, P.L., Sick, T., Rosenthal, M., van der Thillart, G. 1993.

Tielens, A.G.M. 1994. Energy generation in parasitic helminths. *Parasitol. Today.* **10:**346-352.

Tyson, E. 1683. *Lumbricus teres,* or some anatomical observations on the roundworm bred in human bodies. *Philosophical Transactions of the Royal Society of London.* **13:**152-161.

Valkanov, M.A., Martin, R.J. 1995. A chloride channel in *Ascaris suum* selectively conducts dicarboxylic anion products of glucose fermentation and suggests a role in removal of waste organic anions. *J. membrane Biol.* **148**41-49.

Valkanov, M., Martin, R.J., Dixon, D.M. 1994. The Ca-Activated Chloride Channel of *Ascaris suum* Conducts Volatile Fatty Acids Produced by Anaerobic Respiration: A Parch-Clamp Study. *J. Membrane Biol.* **138:**133-141.

Wakelin, D. 1984. Schistosomes. Concominant immunity and immunopathology. In *Immunity to parasites*, How animals control parasite infections. (Wakelin , D.) Chapter 6:74-93. *Edward Arnold.*

Weisblat, D.A., Byerly, L., Russel, R.L. 1976. Ionic mechanisms of electrical activity in somatic muscle of the nematode *Ascaris lumbricoides. J. Comp. Physiol.* **111:**93-113.

Wilson, R.A., Barnes, P.E. 1974. The tegument of *Schistosoma mansoni*: observations on the formation, structure and composition of cytoplasmic inclusions in relation to tegument function. *Parasitology.* **68:**239-258.

Wolde Mussie, E., Vande Waa, J., Pax, R.A., Fetterer, R., Bennett, J.L. 1982. *Schistosoma mansoni:* Calcium efflux and effects of calcium-free media on responses of the adult male musculature to praziquantel and other agents inducing contraction. *Exp. Parasitol.* **53:**270-278.

Wood, I.B., Pankarich, J.A., Berger, H. 1963. Effect of *Ascaris suum* on pigs . *J. Parasitol.* Supplement, **49:**45.

Young, G.P.H., Young, J.D.E., Deshpande, A.K., Goldstein, M., Koide, S.S., Cohn, Z.A. 1984. A Ca^{2+}-activated channel from *Xenopus laevis* oocyte membranes reconstituted into planar bilayers. *Proc. Nat. Acad. Sci. USA.* **81:**5155-5159.

Zagotta, W.N., Aldrich, R.W. 1990. Voltage-dependent gating of *Shaker* A-type channels in Drosophila muscle. *J. Gen. Physiol.* **95:**29-60.

Appendix I: Probability of channel opening (P_{open}) from individual experiments at each potential under each of the experimental conditions. P_{open} was calculated using the equation described in Chapter 2 (Materials and Methods).

mV.	Control	Acid Bath	Alkali Bath	Acid Pipette
-40	**0.00303** **0.126** **0.149** **0.2997** **0.4578**	**0.000375** **0.053** **0.004346** **0.00165**	**0.5094** **0.12** **0.332** **0.2735**	**0.45** **0.317** **0.207** **0.543**
-30	**0.0609** **0.2457** **0.3172** **0.3451** **0.4824**	**0.004374** **0.088** **0.013** **0.00131**	**0.4854** **0.1272** **0.477** **0.328**	**0.514** **0.5338** **0.4906** **0.4683**
-20	**0.182** **0.01795** **0.1772** **0.3692** **0.5676**	**0.0517** **0.136** **0.1226** **0.0222**	**0.5665** **0.2003** **0.402** **0.45**	**0.565** **0.623** **0.396** **0.4286**
-10	**0.193** **0.108** **0.2572** **0.3274** **0.3433**	**0.112** **0.202** **0.0802** **0.00393**	**0.3623** **0.22** **0.4325** **0.25**	**0.632** **0.4877** **0.193** **0.1855**
10	**0.0754** **0.000155** **0.0492** **0.1054** **0.2651**	**0.2172** **0.166** **0.00805** **0.00266**	**0.2715** **0.1544** **0.2995** **0.2122**	**0.021** **0.2934** **0.0976** **0.0793**
20	**0.0107** **0.000526** **0.003598** **0.1472** **0.1153**	**0.525** **0.3904** **0.4618** **0.316**	**0.2855** **0.0733** **0.316** **0.02632**	**0.299** **0.019** **0.034** **0.0459**
30	**0.000251** **0.000799** **0.004349** **0.0986** **0.03033**	**0.1692** **0.504** **0.2887** **0.131**	**0.0657** **0.0305** **0.152** **0.0606**	**0.088** **0.078** **0.0077** **0.0572**
40	**0** **0.000283** **0.005314** **0.0725** **0.0537**	**0.215** **0.4685** **0.2729** **0.184**	**0.1464** **0.00495** **0.2231** **0.0163**	**0** **0.004073** **0.0063** **0.05706**

Appendix II: An electrical model of ion-channels in the tegument of *Schistosoma mansoni*

Throughout Section II of the thesis (experiments on *S. mansoni*) there are frequent referrals to the unusual arrangement of phospholipid bilayers that constitute the "double outer membrane" of the schistosome tegument. A simple model was presented in Chapter 7 that describes effects of the membrane arrangement on single-channel currents. This appendix deals in more detail with the possible arrangement of ion-channels in the "double outer membrane" and how results obtained using the patch-clamp technique would differ from results obtained using more conventional membranes (containing a single bilayer). In single membrane patch recordings the amplitude of channel opening is linearly related to the channel conductance and the driving force. The presence or absence of other ion-channels in the membrane patch and their conductance state (opened or closed) has no effect on channel amplitude and the linear (ohmic) relationship to the driving force.

The "double outer membrane" of the schistosome tegument.

The outer membrane of the schistosome tegument is in fact two phospholipid bilayers in close association, in other words, two distinct membranes. The two membranes are around 7 nm apart. The parasite maintains a potential difference across the "double membrane"; ion-channels have been recorded from the "double membrane" of the outer tegument. To date, no one has determined if ion-channels are present in one or both of the phospholipid bilayers. If the membrane potential across the tegument is maintained by ion-channels in only one of the bilayers then the other bilayer must have a high permeability for all ions (*i.e.* it must present a low resistance pathway for all ions). Recordings obtained from such an arrangement would be similar to conventional single-channel recordings as the amount of current flowing would be determined only by the bilayer responsible for maintaining the membrane potential. If the ion-channels are located in both of the phospholipid bilayers then the implications for single-channel recordings are more complex and are discussed below.

Possible physical properties of isolated inside-out patches from the outer tegument

Chapter 6 demonstrates that a proportion of the membrane vesicles produced by low pH treatment retain both phospholipid bilayers of the outer tegument. The majority of experiments used membrane patches in the isolated inside-out configuration. Figure 1 summarises the possible consequences of sealing onto the double bilayer and then isolating the resulting membrane patch. There are three possible membrane arrangements in isolated patches pulled from the "double outer membrane". The first possibility is that on isolation only the outer bilayer (in contact with the pipette glass) is isolated (Fig. 1C right); such a patch would produce single-channel records that were indistinguishable from a conventional isolated patch. The second possibility is that both bilayers are removed on isolation of the patch, however only the outer bilayer forms a high resistance seal with the pipette glass (Fig. 1C left). Again such a patch would produce single-channel records very similar to those obtained from a conventional preparation. The third possibility is outlined in Figure 1D. Briefly, a seal is formed between the pipette glass and the outer bilayer, both bilayers are removed on isolation, then with time the "loose" ends of the bilayers fuse together. The result bears many similarities to the vesicles that often form on pipette tips when a conventional membrane patch is isolated. The type of patch outlined in Figure 1D would produce single-channel records that were substantially different from those obtained from a conventional isolated inside-out patch: the rest of this appendix considers the type of records that could be expected from such a patch and the relationship between the possible observations and the properties of the ion-channels present.

Electrical model of a "double membrane" patch

Figure 2 is an electrical model of the patch configuration shown in Figure 1D. The model was modified from that suggested by Hamill *et. al.* (1981) to represent an isolated patch in a conventional preparation that had re-sealed to form a vesicle on the pipette tip. The model shows two ion-channels in each of the bilayers of the patch for simplicity, there could be many more.

Figure 1: Diagram representing some of the possible consequences of forming an isolated inside-out patch from the "double membrane" of the schistosome outer tegument. **A:** Diagram representing the inner and outer phospholipid bilayers of the outer tegument. **B:** A fire polished glass patch pipette has been placed on the membrane surface and gentle suction applied. The result is a giga-ohm resistance seal between the pipette glass and the outer bilayer of the "double outer" membrane. **C:** The patch pipette has been moved away from the "double membrane", removing (and isolating) a patch of the "double membrane". It is possible that on isolation only the outer of the two phospholipid bilayers is removed (right), alternatively both of the bilayers may have been removed (left). In either eventuality, the membrane patch would produce records similar to patches pulled from a conventional membrane because the potential difference is across a single bilayer. In the patch with two bilayers present the inner bilayer has not formed a high resistance seal with the pipette thus there is a low resistance pathway to the bathing solution. **D:** The isolated patch contains both of the bilayers that constitute the double membrane of the schistosome outer tegument. With time the loose ends of the bilayer fuse together to form a structure that bears some similarities to the vesicles that frequently form on pipette tips after isolation of membrane patches pulled from conventional membrane preparations. The patch structure represented in **D** would possess different properties from a conventional membrane patch.

Figure 1

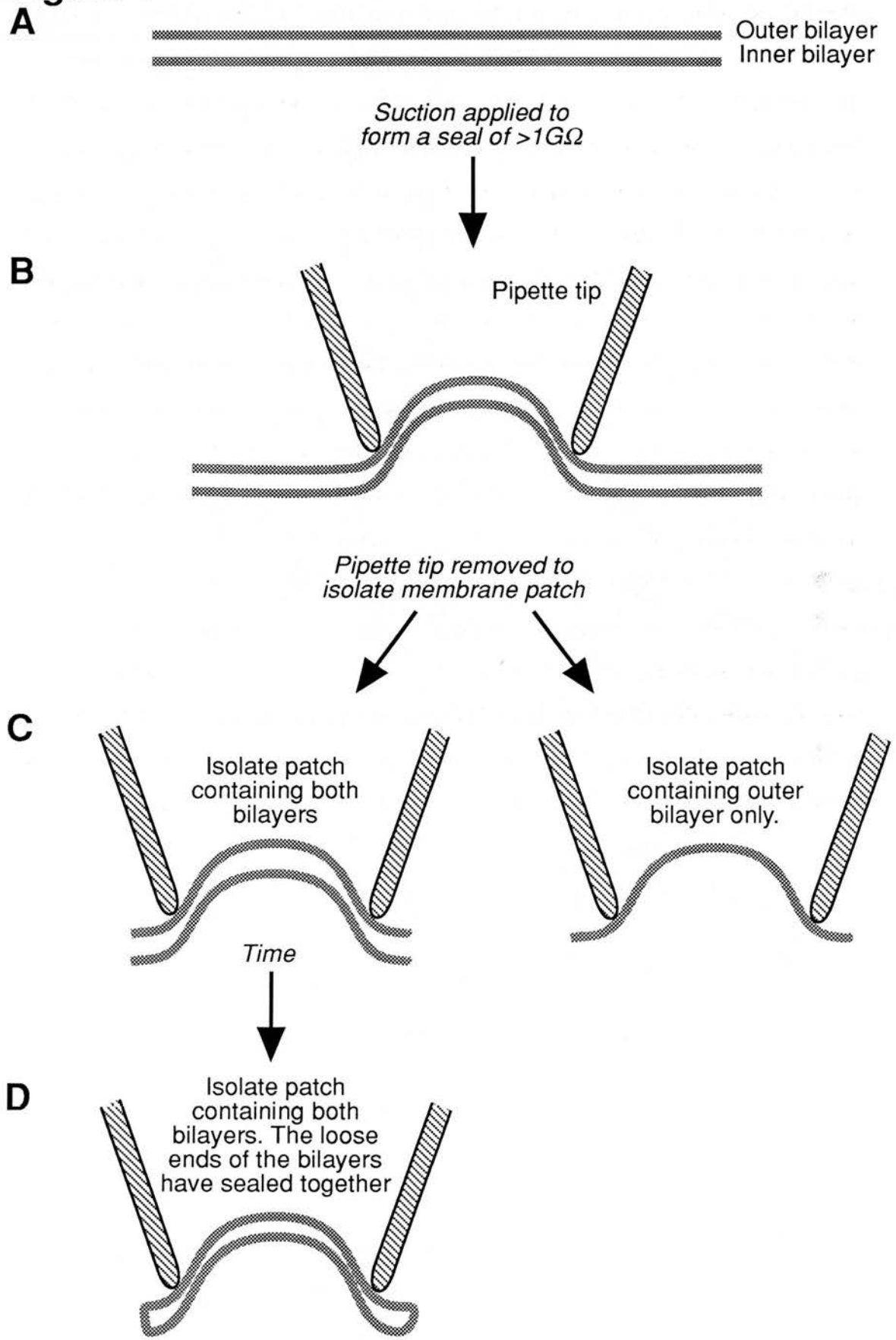
A
Outer bilayer
Inner bilayer
Suction applied to
form a seal of >1GΩ
B
Pipette tip
Pipette tip removed to
isolate membrane patch
C
Isolate patch
containing both
bilayers
Isolate patch
containing outer
bilayer only.
Time
D
Isolate patch
containing both
bilayers. The loose
ends of the bilayers
have sealed together

Figure 2: Electrical model of the patch configuration shown in Figure 1D. The potential across the patch is fixed by the patch amplifier (which also measures the current flowing). The outer and inner bilayers of the "double membrane" are represented by RC circuits in series. For the outer bilayer the RC circuit is composed of: a resistor of fixed value representing the resistance of the bilayer (R_{om}); two further resistors in parallel (each bearing switches) representing the ion-channels in the bilayer (R_{oc1} and R_{oc2}) ; and a capacitor representing the capacitance of the bilayer (C_o) . The inner bilayer is represented by a similar circuit.

Figure 2

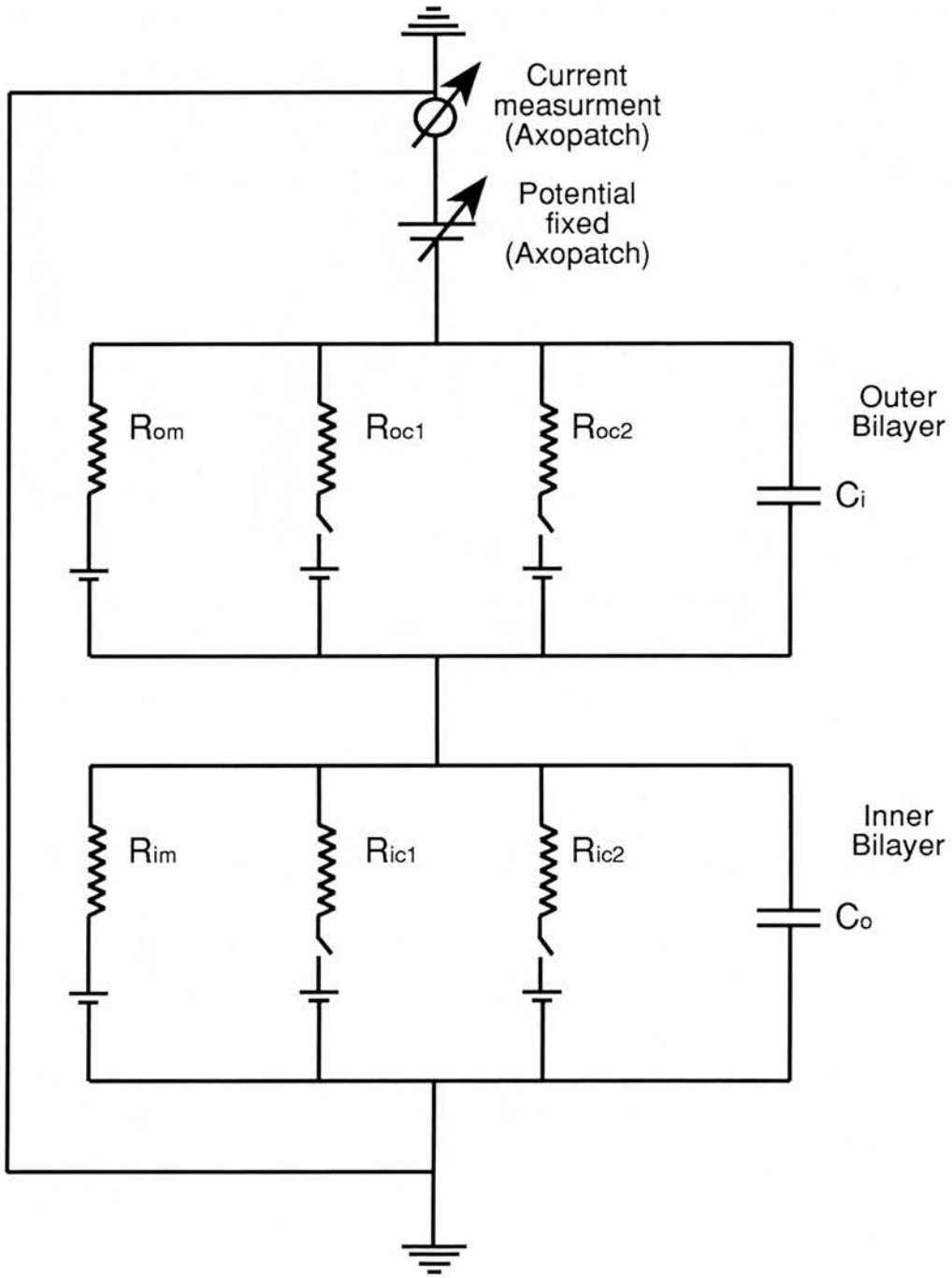
Current
measurment
(Axopatch)
Potential
fixed
(Axopatch)
Rom
Roc1
Roc2
Outer
Bilayer
Ci
Rim
Ric1
Ric2
Inner
Bilayer
Co

Equations used and assumptions made in calculations from the model

The calculate how the records obtained from the electrical model would relate to the single-channel properties of the ion-channels in the model the following equations were used:

$$\frac{1}{R_{Inner}} = \frac{1}{R_{im}} + \frac{1}{R_{ic1}} + \frac{1}{R_{ic2}} + \ldots \frac{1}{R_{icn}} \quad \ldots\ldots [1]$$

Equation 1 was used to calculate the overall resistance of a bilayer. Where R_{Inner} was the total resistance of the inner bilayer. R_{im} is the resistance of the inner membrane. R_{ic1} , R_{ic2} , R_{icn} are the resistances of the individual ion-channels in the membrane patch, and n is the number of ion-channels in the membrane patch. The total resistance of the outer bilayer can be calculated by using the same equation by substituting the appropriate values for ion channel resistances.

$$R_{Tot} = R_{Inner} + R_{Outer} \quad \ldots\ldots [2]$$

Equation 2 was used to calculate the overall resistance of the double membrane patch where: R_{Tot} was the total resistance of the "double membrane" patch, R_{Inner} was the resistance of the inner bilayer of the "double membrane" patch, and R_{Outer} was the resistance of the outer bilayer of the "double membrane" patch.

$$G_{app} = R_I^2 / \left(\left(R_I + R_O \right) \left(R_C . R_O + R_C . R_I + R_I . R_O \right) \right) \quad \ldots\ldots [3]$$

Equation 3 was used to calculate the apparent conductance (G_{app}) of a channel in the inner bilayer of a "double membrane" patch. Where R_I is the resistance of the inner bilayer (including all the ion-channels that are open) and R_O is the resistance of the outer bilayer (including all the ion-channels that are open). R_C is the resistance of the ion-channel whose apparent conductance is being estimated. The above equation gives the apparent conductance value for a channel in the inner bilayer, to calculate

the apparent conductance of a channel in the outer bilayer the term R_I^2 has to be replaced with R_O^2 .

$$\tau = R_O \| R_I \| R_C \| (C_I + C_O) \quad \text{.....[4]}$$

Equation 4 was used to calculate the time constant (τ) for the channel in equation 3. The terms R_I, R_O and R_C are described above. C_O and C_I are the capacitance values for the outer and inner bilayers respectively.

The above equations were used to examine how the apparent conductances of the channels present in the electrical model varied with the open\closed states the other ion-channels in the model. The total amount of current flowing across the model at -50 mV was also calculated. The time constants of events were also calculated. To use the above equations several assumptions were required and these are listed below.

The batteries illustrated in the electrical model have all been set with a zero voltage when the total membrane current was calculated. The channels in the outer bilayer were all assumed to have identical conductance values of 100 pS. The channels in the inner bilayer were also assumed to have identical conductance values, in this case 20 pS. The resistance of each of the phospholipid bilayers was estimated as 100 GΩ. The values for capacitance were estimated from an assumed bilayer area of 5 μm^2 and an assumed capacitance of 1 $\mu F\backslash cm^2$. These assumptions give a total capacitance ($C_I + C_O$) of 0.1 pF. The estimates of patch area, capacitance, and membrane resistance were all obtained from Hamill *et al* (1981). The calculations were carried out on a theoretical membrane patch containing ten channels in each of the phospholipid bilayers.

Electrical potential across the model

For simplicity the calculations in this appendix assumed symmetrical ionic concentrations and also that the channels present had identical ionic selectivities. However, the electrical potential across the model would be affected by differences in ionic concentration on each side of the membrane patch and also by the ionic selectivity of the channels present. If the ionic concentrations across the "double membrane" change, the membrane potential across the double bilayer would be the sum of the potentials across each of the individual bilayers. The potential across each bilayer would be determined by the conductances, ionic selectivities, ion gradients and number of the different channel types present; as in more conventional membranes (Hille, 1992)

Results from the Model

The results of the calculations are illustrated in Figure 3 (apparent conductances and current flowing across the membrane) and Figure 4 (Tau values). The model shows several interesting differences between the theoretical "double membrane" patch and a patch from a conventional membrane. Figure 3A demonstrates that the apparent conductance of an ion-channel in "double membrane" patch is dependent on the number of open channels in the patch. In a conventional membrane this is not the case where the apparent conductance is not altered by the number of open channels in the patch. Figure 3B illustrates how the total current across the "double membrane" patch changes with the number of open channels. As in a conventional membrane, the current flowing across the "double membrane" patch increases as the number of open channels increases. Unlike a conventional membrane the relationship is not linear. Figure 4 demonstrates how the time constant (τ) for a channel changes depending on the number of other channels that are open. From the model the time constants range between 0.42 ms and 0.07 ms. The τ value decreases (in a non-linear manner) as the number of open channels increases.

The electrical model can explain apparently nonsensical results.

The experiment illustrated in Figure 7.15 was obtained from an isolated patch with identical concentrations of ions on each side of the membrane. Attempts to place lines of best fit through the data resulted in extremely positive (>50 mV) reversal potentials. With identical ion concentrations the reversal potential must be 0 mV. The large positive reversal potentials can be explained by the model. As Figure 3 demonstrates the apparent conductance of a channel is affected by the number of ion-channels open in each bilayer. The apparent non-zero reversal potential could result from changes in the apparent conductance of the channel due to the opening or closing of the other ion-channels present in the membrane patch.

Figure 3: Apparent conductances and total current flowing across a model "double membrane" patch.

Numerical values obtained from the electrical model shown in Figure 2. For the calculations the "double membrane" patch was assigned 10 ion-channels in each bilayer. All the channels in the inner bilayer had identical conductances of 20 pS. All the channels in the outer bilayer had identical conductances of 100 pS. For simplicity, it was assumed that all the ion-channels in the patch had identical ion selectivities. The bilayers were each assigned a resistance of 100 MΩ.

A: Graph showing how the apparent conductance of a 100 pS channel in the outer bilayer of a "double membrane" patch varies with the number of open channels in the inner and outer bilayers. The points on the graph represent the apparent conductance of the channel. The y-axis gives the apparent conductance in pS. The x-axis gives the number of channels open in the outer bilayer. n is the number of channels open in the inner bilayer. The relationship shows that the apparent conductance of a channel in the outer bilayer increases as the number of open channels in the inner bilayer increases. The apparent conductance of the same channel falls as the number of open channels in the outer bilayer increases. Neither of these relationships is linear. In a conventional patch (containing a single membrane) the apparent conductance of the channels does not change and is independent of the number of open channels present.

B: Graph showing the relationship between the amount of current flowing across the "double membrane" patch at -50 mV and the number of open channels in both membranes. The y-axis gives the total amount of current flowing. The x-axis gives the number of channels open in the inner bilayer of the patch while n is the number of channels open in the outer bilayer of the patch. Thus the total current flowing increases with the number of open channels. The relationship is not linear; in contrast to a conventional membrane patch.

Figure 3

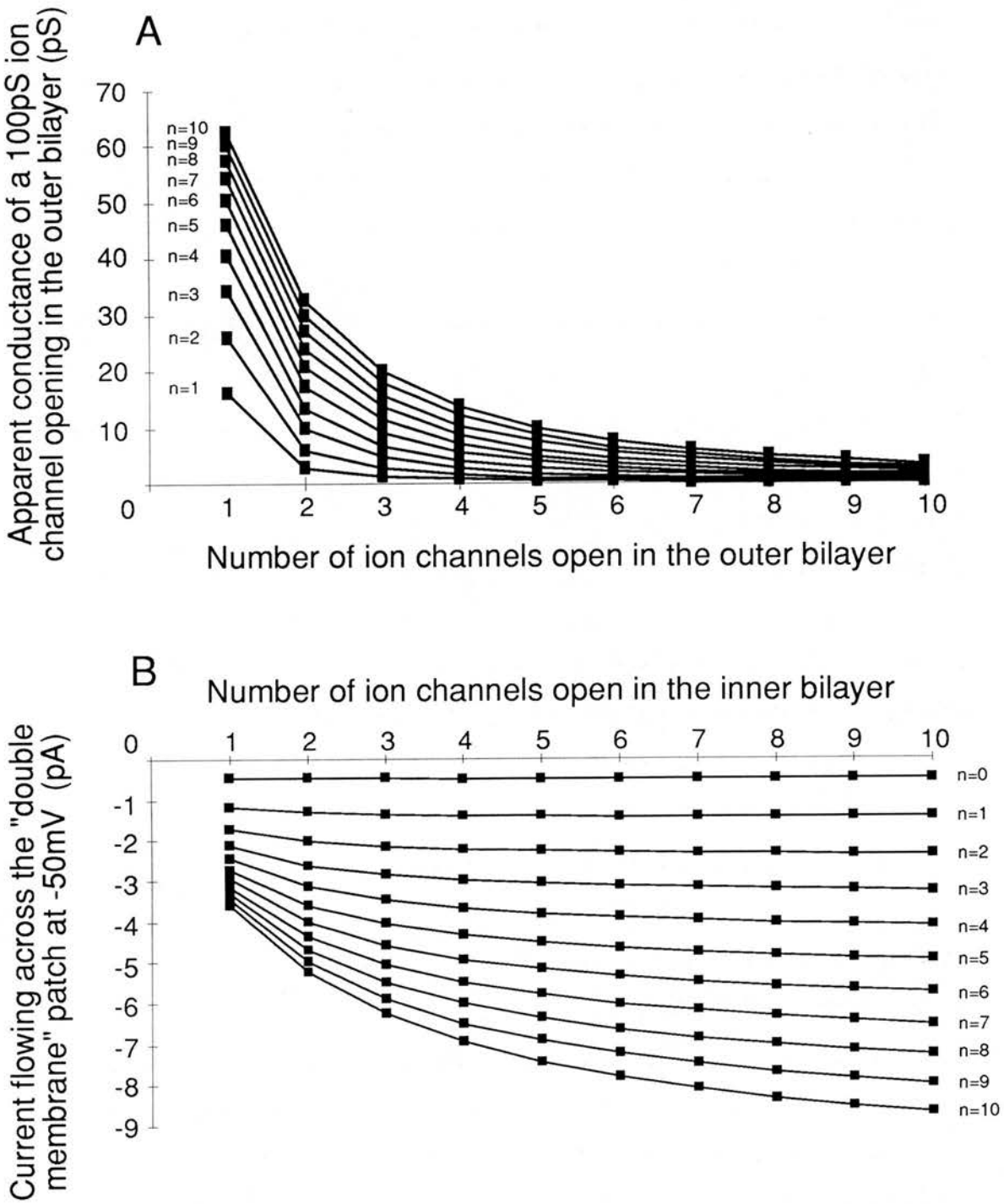
A
Apparent conductance of a 100pS ion channel opening in the outer bilayer (pS)
70
60
50
40
30
20
10
0
n=10
n=9
n=8
n=7
n=6
n=5
n=4
n=3
n=2
n=1
1
2
3
4
5
6
7
8
9
10
Number of ion channels open in the outer bilayer
B
Number of ion channels open in the inner bilayer
Current flowing across the "double membrane" patch at -50mV (pA)
0
-1
-2
-3
-4
-5
-6
-7
-8
-9
n=0
n=1
n=2
n=3
n=4
n=5
n=6
n=7
n=8
n=9
n=10

Figure 4: Tau values for a 100 pS channel in the membrane model

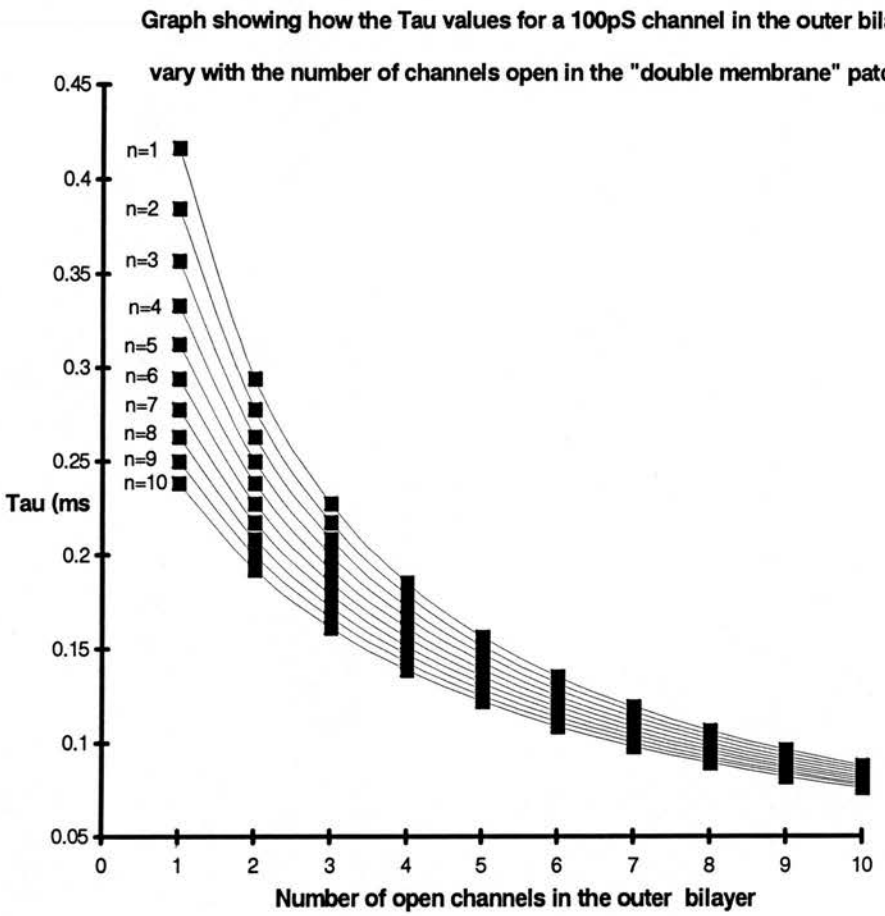

Figure 4: Graph demonstrating how the time constant (Tau) varies with the number of channels open in the membrane patch. Tau becomes shorter as the number of open channels increases, regardless of which bilayer the channels are located in. Tau ranges from a high of ≅ 0.42 ms (with only one channel in each bilayer open) to a low of ≅ 0.07 ms (with ten channels open in each of the bilayers).

Appendix III: Publications arising from this study.

A: Published Abstracts

1. Robertson, A. P., Martin, R.J., Kusel, J.R. 1996. Single-channel recordings from tegument-derived vesicles of *Schistosoma mansoni*. *J. Physiol.* **495P:**33P-34P.

B: Papers

2. Robertson, A.P., Martin, R.J. 1996. Effects of pH on a high conductance Ca-dependent chloride channel: a patch-clamp study in *Ascaris suum.* *Parasitology* **113:**191-198.

3. Robertson, A. P., Martin, R.J., Kusel, J.R. 1997. A vesicle preparation for resolving single channel currents in tegument of male *Schistosoma mansoni*. *Parasitology.* **114:***(In Press).*

C: Review Articles

6. Martin, R.J., Valkanov, M.A., Dale, V.M.E., Robertson, A., Murray, I. 1996. Electrophysiology of *Ascaris* muscle and anti-nematodal drug action. *Parasitology.* **113:**S137-S156.

5. Redman, C.A., Robertson, A., Fallon, P.G., Modha, J., Kusel, J.R., Doenhoff, M.J., Martin, R.J. 1996. Praziquantel: an urgent and exciting challenge. *Parasitol. Today.* **12:**14-20.

6. Martin, R.J., Bjorn, H., Robertson, A.P. 1997 Target sites of anthelminthics. *Parasitology.* **114:***(In Press).*

REFERENCES

vden, C., Sithigorngul, P., Brackley, P., Guastella, J. & Stretton, A.O.W. (1993). *J. Comp. Neurol.* **333**, 455–468.
ıle, A.G., Shaw, C. Bowman, J.W., Halton, D.W., Thompson, D.P., Thim, L., Kubiak, T.M., Martin, R.A. & Geary, T.G. (1995). *Peptides* **16**, 87–93.
ri, H.R., Holden-Dye, L. & Walker, R.J. (1991). *Exp. Physiol.* **76**, 597–606.

Glutamate and L-aspartate increase input nductance of *Ascaris suum* pharyngeal muscle

. Murray and R.J. Martin

partment of Preclinical Veterinary Sciences, R(D)SVS, mmerhall, University of Edinburgh, Edinburgh 9 1QT

Ascaris suum is a large intestinal nematode parasite of s and sometimes humans. Avermectins are a group of ibiotic anthelmintics used to treat infections of such matodes in domestic animals and man. Cully *et al.* (1994) e cloned and expressed a glutamate-gated Cl^- channel m *C. elegans*, sensitive to the avermectins. The presence a glutamate-gated Cl^- channel, sensitive to an avermectin, s also been demonstrated in pharyngeal muscle of *Ascaris um* (Martin, 1996).

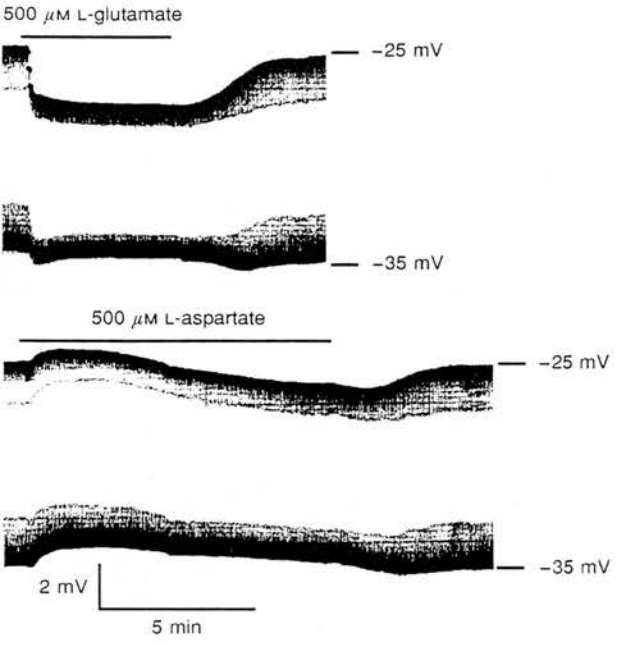

Fig. 1. Effect of 500 μM L-glutamate and 500 μM L-aspartate on input conductance of an *Ascaris* pharyngeal preparation. Methods: Martin (1996). The traces are potential records in response to hyperpolarizing current pulses (1·5 μA, 1 s, 0·5 Hz (not shown)).

We have now examined the effects of L-glutamate ($n = 4$) d L-aspartate ($n = 4$) on input conductance of *Ascaris* aryngeal muscle using a two-microelectrode current-mp technique. Bath-applied L-glutamate produced a reversible hyperpolarization and increase in conductance; L-aspartate produced an initial depolarization followed by a hyperpolarization and increase in conductance (Fig. 1). The conductance dose–response relationships were sigmoid with G_{max} of 134 and 56·1 μS, ED_{50} of 318 and 973 μM and n_H of 1·1 and 2·0 for glutamate and aspartate, respectively.

Our results show that receptors present in the *Ascaris* pharyngeal muscle are different from the expressed receptors of Cully *et al.* (1994), which are insensitive to L-aspartate.

Iain Murray holds an MRC studentship.

REFERENCES

Cully, D.F., Vassilatis, D.K., Liu, K.K., Paress, P.S., Van der Ploeg, L.H.T., Schaeffer, J.M. & Arena, J.P. (1994). *Nature* **371**, 707–711.
Martin, R.J. (1996). *Parasitology* **112**, 247–252.

Single-channel recordings from tegument-derived vesicles of *Schistosoma mansoni*

A.P. Robertson, R.J. Martin and J.R. Kusel*

*Department of Preclinical Veterinary Sciences, R(D)SVS, University of Edinburgh, Edinburgh EH9 1QH and *Department of Biochemistry, University of Glasgow, Hillhead, Glasgow*

Schistosomiasis is a widespread tropical disease of man caused by the trematode *Schistosoma mansoni*. The disease is usually treated with praziquantel, a highly effective drug with few side effects. The exact mechanism by which praziquantel kills the parasite has yet to be determined (for review, see Redman *et al.* 1996). Praziquantel causes an influx of calcium across the parasite tegument, suggesting that the drug may act on a specific ion channel within the tegument. We have developed a method for forming membrane vesicles from the schistosome tegument that allows the application of the patch-clamp technique.

Treatment of *S. mansoni* in low pH media (Gibco BHK-21 adjusted to pH 3·75 with 5 M HCl) for 15–30 min resulted in the formation of membrane vesicles from the tegument. In order to check the origin and structure of the vesicles, parasites were pre-treated with 4-aminofluoroscein to label the outer tegumental membrane and examined using fluorescence microscopy. The results showed that some of the vesicles originated from the outer tegumental membrane. Scanning electron microscopy revealed that the vesicles possessed a smooth surface suitable for applying the patch-clamp technique. Transmission electron microscopy demonstrated that some vesicles possessed the double bilayer found in the outer tegument of the adult schistosome.

Our patch-clamp recordings showed the presence of a large conductance (290 pS), non-selective cation channel with similarities to those channels previously described by Day *et*

also found evidence of a high-conductance
ium-selective channel (Fig. 1) and a smaller
pS) sodium-selective channel.

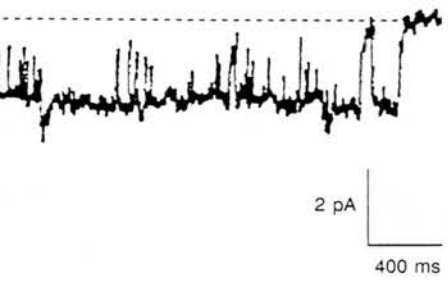

les of single-channel openings from an isolated
h, at −85 mV. The patch shows a K^+-selective
l potential was −70 mV (predicted Nernst E_K was

t further study of the ion channels present in
e tegumental membrane will lead to a
which ion channel may be responsible for the
duced by praziquantel treatment.

s supported by a BBSRC studentship and the

REFERENCES

et, J.L. & Pax, R.A. (1992). *Exp. Parasitol.* **74**,

obertson, A.P., Fallon, P.G., Modha, J., Kusel, J.R.,
. & Martin, R.J. (1996). *Parasitol. Today* **12**,

ninium lactate on electrical activity in neuron of *Lymnaea stagnalis, in vitro*

ell, C.R. McCrohan, K.N. White and

*logical Sciences, University of Manchester, 3 9PT and *Rayne Institute, St Thomas' on SE1 7EH*

is ubiquitous in the environment and
availability of aluminium is influenced by pH
to which it is bound. The neurotoxicity of
ate, a water-soluble compound at neutral pH,
n an identified molluscan neuron, cell RPD1
gnalis. Intracellular recordings were made in
ntral nervous system maintained in Mops-
at pH 7·4. Aluminium lactate and sodium
) were applied extracellularly to give final
of 100 and 300 μM, respectively.
vas usually silent under control conditions.
aluminium lactate ($n = 6$) occurred after a
s. The cell was depolarized by up to 20 mV.
excitatory synaptic inputs increased in
d amplitude, indicating activation of presynaptic neurons. Activity was induced in RPD1, usually in the form of bursts of action potentials occurring at a maximum frequency of 10–44 per minute and containing between two and nine spikes. Spike amplitude and duration within bursts were 72·5 ± 0·5 mV (mean ± S.E.M.) and 4·9 ± 0·2 ms, respectively, compared with 79·8 ± 1·0 mV and 4·2 ± 0·3 ms in control. Spike afterhyperpolarization was reduced between spikes in bursts. In half of the preparations, significant spike broadening subsequently occurred after 4–10 min; some action potentials had durations of up to 3 s.

Application of sodium lactate produced no response in four out of six preparations. However, in two preparations a small depolarization was seen, lasting 15–90 s and leading to a train of spikes. This might be attributable to a short lasting decrease in intracellular pH induced by lactate (De Hemptinne *et al.* 1983). No changes in spike shape were observed.

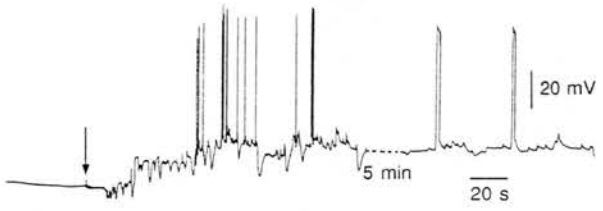

Fig. 1. Effect of aluminium lactate superfusion (100 μM; arrow) on electrical activity of RPD1 neuron.

Aluminium lactate is clearly bioavailable at neutral pH, producing repeatable effects on electrical activity. The changes in spike shape are consistent with a reduction in K^+ conductance, although other actions cannot be ruled out.

REFERENCE

De Hemptinne, A., Marrannes, R. & Vanheel, B. (1983). *Am. J. Physiol.* **245**, C178–183.

Voltage-activated ionic currents from isolated squid giant axon Schwann cells

Euan R. Brown *, Isao Inoue † and Izuo Tsutsui ‡

**The Marine Biological Association Laboratory, Plymouth, †Institute for Enzyme Research, Tokushima University, Tokushima, Japan and ‡N.I.P.S., Okazaki, Japan*

The squid giant axon and associated Schwann cells are an excellent *in situ* system to study neuron–glial interactions (Abbott *et al.* 1995). However, it has not been possible to obtain detailed information about Schwann cell membrane properties. We have developed a method for isolating giant axon Schwann cells and subjecting them to whole-cell voltage clamp.

Squid (*Loligo forbesi*) were decapitated and giant axons cleaned of small fibres in Ca^{2+}-free artificial seawater (ASW,

ffects of pH on a high conductance Ca-dependent hloride channel: a patch-clamp study in *Ascaris suum*

P. ROBERTSON* *and* R. J. MARTIN

partment of Preclinical Veterinary Sciences, R.(D.) S.V.S., Summerhall, University of Edinburgh, inburgh EH9 1QH

ceived 2 November 1995; revised 6 February 1996; accepted 28 February 1996)

MMARY

sma membrane vesicles prepared from the bag region of the somatic muscle cells of the parasitic nematode *Ascaris suum* ntain high conductance, voltage sensitive, Ca-dependent chloride channels, suggested to be involved in the excretion carboxylic acids produced by the anaerobic respiration of glucose (Valkanov, Martin & Dixon, 1994). The effect of ered pH on this channel was investigated using the patch-clamp technique and isolated inside-out membrane patches. anges in pH had little effect on channel conductances and only a small effect on reversal potentials. Under control nditions (symmetrical pH 7·2) the channel had the highest probability of opening at ~ -35 mV (the resting membrane tential of the cell). At positive membrane potentials the probability of opening decreased. The Boltzmann equation was ed to describe the relationship between membrane potential and probability of channel opening, and to calculate the ective gating charge. Reduction of external pH produced an increase in the probability of channel opening at hyper-larized membrane potentials. An increase in internal pH caused a voltage-independent increase in the probability of nnel opening and made the effective gating charge less negative. The effect of reducing internal pH was marked: the nnel then opened most frequently at positive membrane potentials and the probability of opening at -35 mV was atly reduced. The decrease in internal pH changed the polarity of the effective gating charge. A simple model was nstructed to describe the effects of pH on channel gating.

y words: patch-clamp, *Ascaris suum*, Cl^- channel, pH, effective gating charge.

TRODUCTION

preparation from the somatic muscle cells of the rcine parasitic nematode *Ascaris suum* has been veloped which is suitable for electrophysiological dy (Jarman, 1959; Martin, 1980). Previous dies have shown that the relatively low resting tential of the cell, ~ -35 mV, is insensitive to anges in the extracellular potassium concentration, t is dramatically affected by changes in extra-llular chloride concentrations, thus demonstrating elatively high chloride permeability (Del Castillo, Mellow & Morales, 1964; Brading & Caldwell, 71). Permeability ratios for K, Na and Cl of 1:4:7 pectively have been reported (Caldwell & Ellory, 68). Patch-clamp studies on membrane vesicles epared from the bag region of the somatic muscle l have demonstrated the presence of 3 types of oride channel. The largest and most commonly served of these is a high conductance Ca-pendent chloride channel (140 pS in 140 mM Cl ution; Thorn & Martin (1987)). Previously, chlor- channels have been assigned to 4 categories on basis of their properties (Franciolini & Petris, 37) however, the *Ascaris* Ca-dependent chloride nnel does not readily fit in to any of these.

Corresponding author.
: 0131 650 6094. E-mail: alanr@lab0.vet.ed.ac.uk.

The ionic selectivity of the high conductance Ca-dependent chloride channel has been determined (Dixon, Valkanov & Martin, 1993; Valkanov, Martin & Dixon, 1994; Valkanov & Martin, 1995) and the ability of this channel to conduct the long-chain fatty acids, which are products of anaerobic respiration in *Ascaris*, has been demonstrated. This has led to the suggestion that the channel may be involved in the removal of these waste products from the cell (Valkanov *et al.* 1994).

In a review of muscle chloride channels, Bretag (1987) described several different channels where the conductance or gating was altered by changes in pH. Respiration in *Ascaris* muscles results in the production of protons and long-chain fatty acyl waste products (Saz & Weil, 1962). In this study we have looked at the effect of pH on the Ca-dependent chloride channel to gain a clearer insight into the mechanism of this channel's gating and its physiological function.

MATERIALS AND METHODS

Preparation of muscle vesicles

Specimens of *Ascaris suum* were collected from the local slaughter house at weekly intervals and maintained at 34 °C in Locke's solution (changed daily)

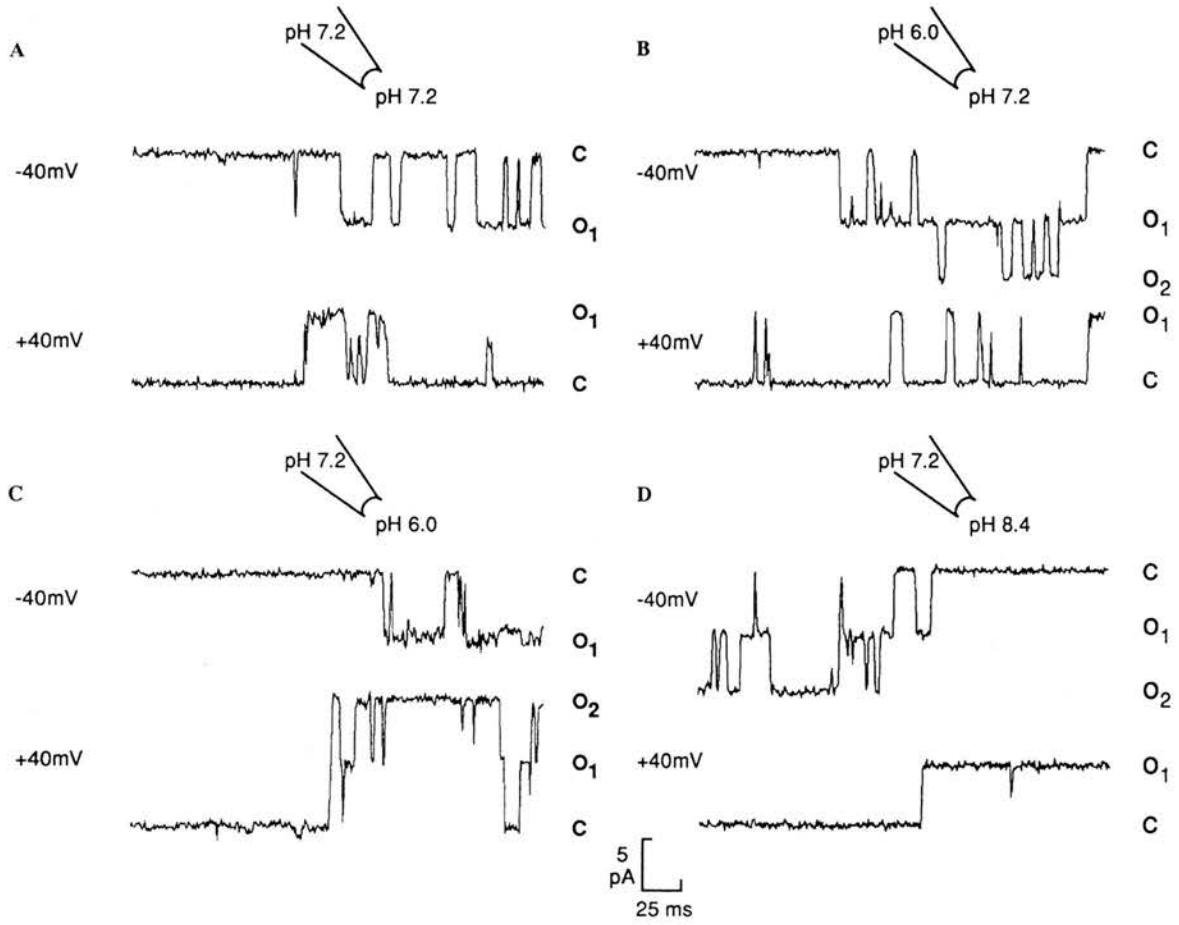

Fig. 1. Inward (−40 mV) and outward (+40 mV) currents in isolated inside-out patches under each of the experimental conditions. (A) Control; bath pH = 7·2, pipette pH = 7·2. (B) Bath pH = 7·2, pipette pH = 6·0. (C) Ba pH = 6·0, pipette pH = 7·2. (D) Bath pH = 8·4, pipette pH = 7·2.

for up to 4 days. The anterior 5 cm of the worm was discarded, the next 2 cm section of worm was removed and cut along one lateral line. The resulting flap was pinned cuticle side down onto Sylgard and the gut removed. The preparation was washed (3 times) with warm (37 °C) extracellular solution, composed of (mM): NaCl, 35; $Na(C_2H_3O_2)$, 105; KCl, 2; $MgCl_2$, 2; HEPES, 10; glucose, 3; ascorbic acid, 2; EGTA, 1; pH adjusted to 7·2 using NaOH. The washed flap was then incubated in enzyme solution (0·5 mg/ml collagenase in EGTA-free extracellular solution) for 10 min at 37 °C. Following enzyme treatment and 3 washes with extracellular solution the flap was incubated at 37 °C in extracellular solution. Approximately 1 h after collagenase treatment vesicles could be observed 'budding off' the bag region of the muscle cell membrane. The vesicles were harvested using a Pasteur pipette and transferred to the recording chamber.

Recording set-up

Patch pipettes with resistances of 1–3 MΩ (Garner glass 7052) and coated with Sylgard to improve frequency responses were used. Single-channel recordings were made using inside-out patches muscle membrane with seal resistances > 1 G Currents were monitored using a LIST EPC current–voltage converter, filtered at 1 kHz (3 d by an 8-pole Bessel-type filter, viewed on an o cilloscope (HITACHI VC-6025) and recorded on Racal Thermionic Store Four FM tape recorder.

Experimental procedure

All experiments were carried out at room tem perature (15–20 °C). Vesicles in the recordi chamber were mounted on the stage of a Nik TMS-PH3 inverted light microscope and viewed × 200 magnification under phase-contrast. T chamber was grounded using an agar bridge.

The bath and pipette solutions were composed (mM): CsCl, 140; $Mg(CH_3COO)_2$, 2; $Ca(CH_3COO$ 1; HEPES, 10; adjusted to the desired pH wi CsOH. Experiments were carried out with pipet solutions of pH (pH^o) 7·2 and bath solutions wi pH (pH^i) at either 6·0, 7·2 or 8·4. The pHs of t bath solution and pipette solution were constant f each patch experiment. Using isolated inside-o membrane patches the pipette solution is in conta

with the extracellular surface of the membrane patch and the bath solution in contact with the intracellular surface of the membrane. Additional experiments involved a pipette solution pH of 6·0 and the bath solution pH of 7·2. For each patch, current records were obtained for potentials of −40, −30, −20, −10, +10 20, 30 and 40 mV.

Analysis

Records were analysed using an IBM PC2/70 computer and the PAT, version 6.1, single-channel analysis programme (John Dempster, Strathclyde University). Current–voltage plots were constructed to obtain slope conductances and reversal potentials of the currents. The probability of channel opening was calculated for each potential using the following equation:

$$P_{open} = (T_1 + 2T_2 + 3T_3, \ldots, + n \times T_n)/(n \times total\ time), \quad (1)$$

where P_{open} = probability of channel opening; T_n = time with n (and only n) channels open; n = the total number of channels in the patch; total time = duration of patch recording. T_n was calculated from the area under the peak of an all points current amplitude histogram corresponding to n (and only n) channels being open.

To minimize the effect of any rundown, a positive and then a negative potential was studied sequentially. A typical sequence was +40, −40, +10, −10, +20, −20, +30 and 30 mV. Only experiments where full sequences were obtained were used in the analysis. Channels opening to subconductance levels were classified as closed: only channel openings to the full conductance level were classified as open. Inspection of channel records revealed that subconductance levels were almost entirely absent at high values of P_{open}. At low P_{open} values (e.g. positive membrane potentials under control conditions) subconductance levels were more common; care was taken to avoid the opening of several channels to subconductance levels being interpreted as the opening of a smaller number of channels to the full conductance level.

Effective gating charge

The Boltzmann equation (2) was fitted by non-linear least squares regression to the P_{open}-voltage relationship with a FORTRAN program utilizing the NAG E04CCF subroutine, and was used to obtain values for the 'effective gating charge' of the channel under the various experimental conditions.

$$P_{open} = P_{max}/[1 + Exp\{(V_{half} - V)/V_{slope}\}], \quad (2)$$

where P_{max} is the maximum value of P_{open} (proportion of time the channel is open) allowed by the equation, V is the membrane potential in mV, V_{half} is the voltage at which the function is half its maximum value and V_{slope} is the slope factor. The 'effective gating charge' was calculated using:

$$effective\ gating\ charge = (kT/ze)/V_{slope}, \quad (3)$$

where k is Boltzmann's constant, T is absolute temperature on the Kelvin scale, z is the valence of the permeant ion and e is the elementary charge. kT/ze under experimental conditions was 24 mV (Hille, 1992).

Statistics

Statistical significance was assessed using analysis of variance. Additionally the reversal potential values for each experimental condition were compared with the control values using the Mann–Whitney test.

RESULTS

Vesicles were prepared daily and used within 5 h of enzyme treatment, after which time the preparation deteriorated to an extent where giga-seal formation was unlikely. Giga-seals were obtained from ~ 33 % of attempts with new patch pipettes but channel activity was detected in only ~ 25 % of all giga-seals. Not more than 15 % of seals displaying channels retained activity for long enough for sufficient recordings to be made.

Figure 1 shows representative channel recordings at −40 and +40 mV from patches under each of the experimental conditions examined. The records suggest that the proportion of time the channel is open is greater at hyperpolarized membrane potentials compared to positive membrane potentials except where there is a reduction in pH^i to 6·0. Under all experimental conditions the current–voltage relationship was linear (not shown) with, under control conditions (symmetric pH 7·2), a mean conductance of 149·0 pS and a mean reversal potential of 0·9 mV (Table 1). The changes in pH tested on each side of the membrane had no statistically significant effect on the conductance of the channel. For example pH 8·4/7·2 (intracellular/extracellular) gave a mean conductance of 146·0 pS and a mean reversal potential of 0·7 mV (Table 1). However, there was a small, but statistically significant ($0{\cdot}05 > P > 0{\cdot}02$), effect of pH on the reversal potentials using analysis of variance. Comparison of the values for each experimental condition using the Mann–Whitney test showed that only the condition $pH^o = 6{\cdot}0/pH^i = 7{\cdot}2$ differed significantly from the control value ($P < 0{\cdot}05$).

Effect of pH on probability of channel opening

The effect of pH on the P_{open}-voltage relationship was highly significant, $P < 0{\cdot}0001$ when all data

Table 1. Mean conductance ± S.E.M. and mean reversal potential ± S.E.M. for each pH condition

(N = number of patch experiments.)

	Bath pH(pH^i)	Pipette pH (pH^o)	N	Mean conductance ± S.E.M. (pS)	Mean reversal potential ± S.E.M. (mV)
Control	7·2	7·2	5	149·0 ± 5·8	+0·9 ± 0·4
Intracellular acid	6·0	7·2	4	168·2 ± 4·5	+0·5 ± 0·4
Intracellular alkali	8·4	7·2	4	146·0 ± 9·0	+0·7 ± 0·2
Extracellular acid	7·2	6·0	4	139·3 ± 4·0	+2·2 ± 0·3

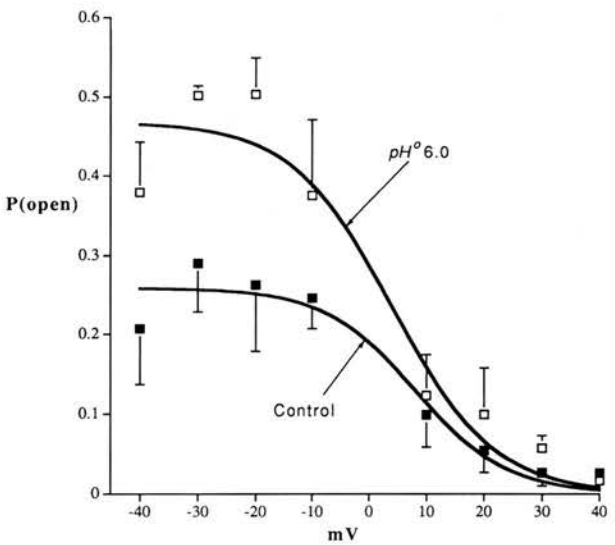

Fig. 2. Effect of acid pH^o on the P_{open}/membrane potential relationship. P_{open} values ± S.E.M. Control (■): pH^o 7·2, pH^i 7·2 (n = 5). Test (□): pH^o 6·0, pH^i 7·2 (n = 4). Lines of best fit were obtained for both data sets from the Boltzmann equation.

points were compared using analysis of variance. Figure 2 shows the mean P_{open} ± S.E.M. values when the pH at the extracellular surface of the membrane patch (pH^o) was reduced to 6·0. Control values are presented for comparison. The control plot shows that the channel is most likely to be open around the resting membrane potential of the cell, (−30 to −40 mV) with the mean P_{open} for −40 and −30 mV being 0·21 and 0·29 respectively. In contrast, P_{open} at +40 mV is much smaller with a mean value of 0·01. Previous studies have produced similar results for a symmetrical pH of 7·6 and a chloride concentration of ~ 175 mM (Thorn & Martin, 1987). The reduced pH^o produced a marked increase in P_{open} over the range of hyperpolarized membrane potentials tested: P_{open} −30 mV = 0·50 at pH^o = 6·0. There also appeared to be a small increase in P_{open} at most positive membrane potentials: pH^o 7·2, P_{open} + 30 mV = 0·03; pH^o 6·0, P_{open} + 30 mV = 0·06. The slope of the line generated by the best fit to the Boltzmann equation showed that the effective gating charge wa negative for both the control conditions and reduced pH^o (Table 2).

The effects of an increase in pH at the intracellula surface of the membrane patch (pH^i) are shown i Fig. 3 with the control values presented for com parison. The slopes of the fits to the Boltzmann equation indicate no change in sign of the 'effectiv gating charge' associated with an increase in pH^i However, the increase in pH^i produced a vertica shift in the P_{open}-voltage plot with P_{open} values a −30 mV and +30 mV of 0·29 and 0·03 respectivel for pH^i = 7·2; and 0·35 and 0·07 for pH^i = 8·4.

Figure 4 shows the effect of reducing pH^i: Fig. 4 shows the values obtained for mean P_{open} when pH was reduced to 6·0. The mean P_{open} values for each o the potentials tested under the control condition (symmetrical pH 7·2) are shown in Fig. 4B. Th results show that a fall in pH^i produced a reductio in P_{open} at hyperpolarized potentials (pH^i 7·2 P_{open} a −30 mV was 0·29; pH^i 6·0 P_{open} at −30 mV wa 0·03). At positive membrane potentials P_{open} i increased when pH^i is reduced: under contro conditions P_{open} at +30 mV was 0·03; this rises to P_{open} of 0·27 when pH^i = 6·0. The slope of the lin obtained from the Boltzmann equation is positiv (Table 2), indicating that the 'effective gatin charge' had become positive when pH^i was reduced

The effective gating charge and pH

Table 2 shows the values for the parameters of th Boltzmann equation obtained under the various pH conditions. The effective gating charge for th control conditions was −3·0 electron charges and i the minimum charge that is moved across th potential drop during the transition C⇔O. Th estimate of the total charge will be low if th moveable charged groups in the channel travel onl part of the way across the potential field. The result show that there is little change in the effective gatin charge between the control conditions (−3 e) an reduced pH^o conditions (−2·7 e). The large chang

Table 2. Values of P_{max}, V_{half} and V_{max} obtained from the Boltzmann fits and the 'effective gating charge' for each pH condition

	Bath pH (pH^i)	Pipette pH (pH^o)	P_{max}	V_{half}	V_{slope}	Effective gating charge
Control	7·2	7·2	0·26	8·0	−8·0	−3·0
Intracellular acid	6·0	7·2	0·34	2·6	13·1	+1·8
Intracellular alkali	8·4	7·2	0·36	18·9	−12·9	−1·9
Extracellular acid	7·2	6·0	0·47	4·0	−8·8	−2·7

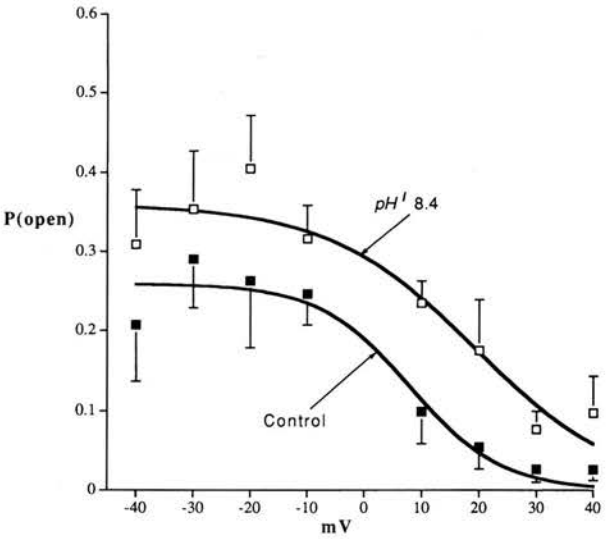

Fig. 3. Effect of alkali pH^i on the P_{open}/membrane potential relationship. P_{open} values ± S.E.M. Control (■): pH^o 7·2, pH^i 7·2 ($n = 5$). Test (□): pH^o 7·2, pH^i 8·4 ($n = 4$). Lines of best fit were obtained for both data sets from the Boltzmann equation.

associated with decreased pH^i, which gave an 'effective gating charge' of +1·8 e, may have been caused by the protonation of several amino acids on the gate of the channel protein.

V_{half} shifted from +8·0 mV (control) to +18·9 mV with the increased pH^i; decreased pH^i moved V_{half} along the voltage axis to +2·6 mV. Both of these horizontal shifts indicate a possible screening/neutralization of a negative surface charge on the intracellular face of the membrane (Hille, 1992). However, the negative movement of V_{half} from 8·0 mV (control) to 4·0 mV when pH^o was decreased cannot be explained by protons interacting with a negative surface charge on the extracellular face of the membrane: the increase in external [H^+] would produce a positive shift in V_{half} if protons were screening a negative surface charge.

Equation (2) also estimates the maximum values, P_{max}, of the P_{open} data sets. Under control conditions P_{max} was 0·26. Each of the experimental conditions shows increases in the value of P_{max}, when compared to the control. When the pH^i was reduced, P_{max} rose to 0·34; an increase in pH^i raised P_{max} to 0·36. A reduction of pH^o gave the largest increase in P_{max} to a value of 0·47.

DISCUSSION

The results show that changes in pH have no significant effect on single-channel conductances. The relationship between P_{open} and membrane potential, described by a Boltzmann equation, was significantly altered by changes in pH. The mechanisms involved in the pH sensitivity of this channel are considered and the physiological significance of the effects of pH is discussed.

Effect of pH on surface potential

Altered pH can lead to changes in surface charge that result in shifts in voltage dependence: negative shifts occur on increased extracellular pH and positive shifts occur on increased intracellular pH (Hille, 1992). For example, extracellular acidification to pH 4·5 leads to a +25 mV shift in the Na activation curve, whilst an increase in extracellular pH to 10 gives a −8 mV shift (Hille, 1968).

The significant positive shift in reversal potential on extracellular acidification in the *Ascaris* chloride channel (Table 1) implies that protons are altering the surface potential in a similar manner. The changes observed in V_{half} (Table 2) on altered pH^i are also consistent with proton concentration altering surface potential. The shift in V_{half} from the control value on reduced pH^o is not predicted by pH effects on surface potential; the shift in V_{half} implies that protons are interacting directly with the channel molecule.

Channel model and pH sensitivity of gating

Figure 5 shows a minimal model that explains the observed effects of pH on our *Ascaris* chloride

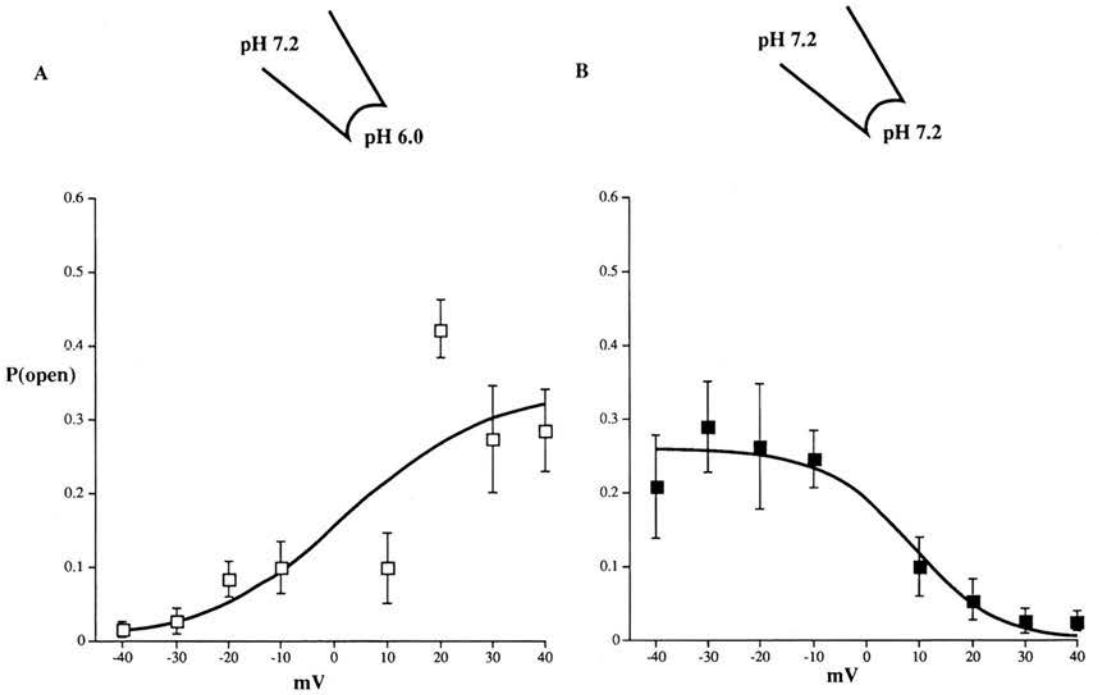

Fig. 4. (A) Relationship between mean $P_{open} \pm$S.E.M. and membrane potential with $pH^i = 6{\cdot}0$ ($n = 4$) (B) Relationship between mean $P_{open} \pm$S.E.M. and membrane potential under symmetrical pH 7·2 conditions ($n = 5$). Lines of best fit were obtained for both data sets from the Boltzmann equation.

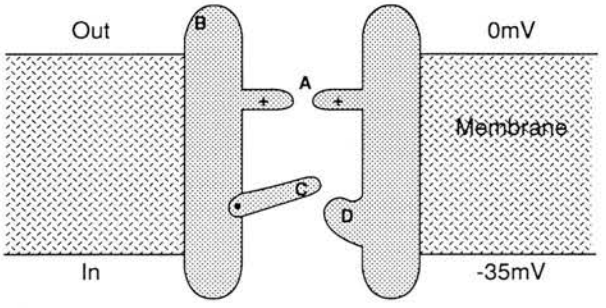

Fig. 5. A simple model of the Ca-dependent chloride channel under control conditions. (A) Selectivity filter of the channel. (B) Proton binding site on the extracellular surface of the channel molecule, proton binding increases P_{open}. (C) Voltage sensor or 'gate', under control conditions bears a charge of -3 e. Decreased pH^i causes binding of protons to imidazolium side-chains of histidine molecules which results in a change in the charge on the 'gate' to $+1{\cdot}8$ e. (D) Positively charged site, binds to a negative charge on channel 'gate' (site C).

channel. The selectivity filter (site A) may possess one or two cationic binding sites (Dixon *et al.* 1993); the lack of variation in the single-channel conductances suggests altered [H^+] has no effect on these sites within the pH range tested.

Extracellular acidification produced increases in P_{open} without affecting gating charge, indicating the presence of a site (site B) only approachable from the extracellular solution.

Under symmetrical pH 7·2 conditions the voltage sensor (site C) has an overall charge of -3 e (Table 2). Interestingly, the gating charge on *Torpedo* chloride channels is smaller, at $+1$ e (Hanke & Miller, 1983) whilst Na, Ca and K channels have larger gating charges of between $+4$ e and $+6$ e (Zagotta & Aldrich, 1990). The dramatic effects that changes in pH^i have on gating charge indicate that the voltage sensor are located intracellularly to the selectivity filter.

The charge on the voltage sensor is sensitive to pH^i (in the range 7·2 to 6·0) and becomes positive at pH 6·0. The *pKa* values of amino acids suggest that only histidine has the appropriate properties to achieve the change in gating charge; the *pKa*'s of other amino acids lie outside the pH range tested. It is therefore suggested that histidine is one of the constituent amino acids of the voltage sensor. The number of histidines that can be protonated is at least 5 (to allow for the change in gating charge from -3 e to $+2$ e); but probably more, for two reasons. First, if the voltage sensor only moves partway across the membrane electric field (as the channel opens) the measured gating charge is less than the actual number of charges present on the channel 'gate' (Hille, 1992). Secondly, studies on K^+ channels have shown that not all the charges on the voltage sensor contribute equally to the effective gating charge (Papazian *et al.* 1991; Logothetis *et al.* 1992).

Site D (Fig. 5) is required to explain the increase in P_{open} with the increase in pH^i. It is suggested that the site located at D normally contains a positively charged residue that forms an ion pair with one of the negative charges on the voltage sensor, similar to suggestions made for Na channels (Stühmer *et al.*

1989). The positively charged residue would lose its proton at high pH, facilitating the opening of the gate and explaining the observed increase in P_{open} at increased pH^i.

Limitations of the model

The above minimal model explains the effects of the pH values tested on the Ca-dependent chloride channel, but there are obvious limitations to this simple model. The Boltzmann model employed only allows for a single step between channel opening ⇔ closing, whereas previous studies have shown several open and closed states (Thorn & Martin, 1987) demonstrating that the gating process is more complex. Our model also shows the 'effective gating charge' located on a single 'gate' whereas, in K^+ channels, activation is brought about by 4 identical gating charges acting independently (Zagotta & Aldrich, 1980). The gating charges in the Ca-activated chloride channel may also act independently.

Physiological significance

Our results show that the Ca-dependent chloride channel is dramatically affected by changes in pH. At a symmetrical pH of 7·2 the channel has a relatively high P_{open} at the resting membrane potential of the cell; when the pH on the intracellular side of the membrane (pH^i) is reduced to 6·0 channel opening is virtually abolished. We have hypothesized that the protonation state of several histidine residues in the channel molecule play an important part in this pH sensitivity. It is interesting that one of the glycolytic enzymes (phosphofructokinase) in *Ascaris* muscle also displays pH sensitivity (Rao *et al.* 1987), due to the protonation of histidine residues present within the enzyme.

In *Ascaris* the anaerobic respiration of glycogen gives rise to carboxylic acids as waste products (Saz & Weil, 1962). The pH of the muscle cell cytoplasm is reported as 7·37 (Del Castillo *et al.* 1989), while the *pKa* values of the waste carboxylic anions have an upper limit of 4·7. At physiological pHs the waste carboxylic acids are $> 99{\cdot}2\,\%$ ionized suggesting that passive diffusion of the uncharged acid across the muscle cell membrane is an unlikely method of excretion. Under symmetrical (pH 7·2) conditions the Ca-dependent chloride channel is permeable to the waste carboxylic anions (Valkanov *et al.* 1994) and has its highest P_{open} around the resting membrane potential of the cell; these observations led to the hypothesis that the channel was responsible for the excretion of waste carboxylic anions (Valkanov *et al.* 1994). Anaerobic respiration in *Ascaris* also results in the production of protons which must be removed from the cell. The presence of an active ionic pump mechanism in the muscle cell has been suggested (Brading & Caldwell, 1971). If there is an active proton pump in the bag membrane, its action would lead to an increased pH^i and an increase in the ionized:unionized concentration ratio of carboxylic anions. In turn the raised pH^i favours opening of the Ca-dependent Cl channel. Thus the pH sensitivity of the channel may facilitate the excretion of waste anions.

A.P.R. was funded by a BBSRC Research Studentship.

REFERENCES

BRETAG, A. H. (1987). Muscle chloride channels. *Physiological Reviews* **67**, 618–714.

BRADING, A. F. & CALDWELL, P. C. (1971). The resting membrane potential of somatic muscle cells of *Ascaris lumbricoides*. *Journal of Physiology* **27**, 605–624.

CALDWELL, P. C. & ELLORY, J. C. (1968). Ion movements in somatic muscle cells of *Ascaris lumbricoides*. *Journal of Physiology* **197**, 75–76P.

DEL CASTILLO, J., DE MELLOW, W. C. & MORALES, T. (1964). Influence of some ions on the membrane potential of *Ascaris* muscle. *Journal of General Physiology* **48**, 129–140.

DEL CASTILLO, J., RIVERA, A., SOLORZANO, S. & SERRATO, J. (1989). Some aspects of the neuromuscular system of *Ascaris*. *Quarterly Journal of Experimental Physiology* **74**, 1071–1087.

DIXON, D. M., VALKANOV, M. & MARTIN, R. J. (1993). A patch-clamp study of the ionic selectivity of the large conductance, Ca-activated chloride channel in muscle vesicles prepared from *Ascaris suum*. *Journal of Membrane Biology* **131**, 143–149.

FRANCIOLINI, F. & PETRIS, A. (1988). Chloride channels of biological membranes. *Archives of Biochemistry and Biophysics* **261**, 97–102.

HANKE, H. & MILLER, C. (1983). Single chloride channels from *Torpedo* electroplax; activation by protons. *Journal of General Physiology* **82**, 25–45.

HILLE, B. (1968). Charges and potentials at the nerve surface: Divalent ions and pH. *Journal of General Physiology* **51**, 221–236.

HILLE, B. (1992). *Ionic Channels of Excitable Membranes*. 2nd Edn. Sinauer Associates, Sunderland, Mass.

JARMAN, M. (1959). Electric activity in muscle cells of *Ascaris* muscle. *Nature, London* **184**, 1244.

LOGOTHETIS, D. E., MOVAHEDI, S., SATLER, C., LINDPAINTER, K., NADAL-GINARD, B. (1992). Incremental reductions of positive charge within the S4 region of a voltage-gated K^+ channel result in corresponding decrease in gating charge. *Neuron* **8**, 531–540.

MARTIN, R. J. (1980). The effect of GABA on the input conductance and membrane potential of *Ascaris* muscle. *British Journal of Pharmacology* **71**, 99–106.

PAPAZIAN, D. M., TIMPE, L. C., JAN, Y. N. & JAN, L. Y. (1991). Alteration of voltage-dependence of *Shaker* potassium channel by mutations in the S4 sequence. *Nature, London* **349**, 305–310.

RAO, G. S. J., WARISO, B. A., COOK, H. W. H. & HARRIS, B. G.

(1987). Reaction of *Ascaris suum* phosphofructokinase with diethylpyrocarbonate. *Journal of Biological Chemistry* **262**, 14068–14073.

SAZ, H. J. & WEIL, A. (1962). Pathway of formation of α-methyl valerate by *Ascaris lumbricoides*. *Journal of Biological Chemistry* **237**, 2053–2056.

STÜHMER, W., CONTI, F., SUZUKI, H., WANG, X., NODA, M., YAHAGI, N., KUBO, H. & NUMA, S. (1989). Structural parts involved in activation of the sodium channel. *Nature, London* **339**, 597–603.

THORN, P. & MARTIN, R. J. (1987). A high-conductance calcium-dependent chloride channel in *Ascaris suum* muscle. *Quarterly Journal of Experimental Physiology* **72**, 31–49.

VALKANOV, M., MARTIN, R. J. & DIXON, D. M. (1994). The Ca-activated chloride channel of *Ascaris suum* conducts volatile fatty acids produced by anaerobic respiration: a patch-clamp study. *Journal of Membrane Biology* **138**, 133–141.

VALKANOV, M. & MARTIN, R. J. (1995). A Cl channel in *Ascaris suum* selectively conducts dicarboxylic anion products of glucose fermentation and suggests a role in removal of waste organic anions. *Journal of Membrane Biology* **148**, 41–49.

ZAGOTTA, W. N. & ALDRICH, R. W. (1990). Voltage-dependent gating of *Shaker* A-type channels in *Drosophila* muscle. *Journal of General Physiology* **95**, 29–60.

A vesicle preparation for resolving single-channel currents in tegument of male *Schistosoma mansoni*

A. P. ROBERTSON[2], R. J. MARTIN[1]* *and* J. R. KUSEL[2]

[1] *Department of Preclinical Veterinary Sciences, R.(D.)S.V.S., Summerhall, University of Edinburgh, Edinburgh EH9 3QH*
[2] *Division of Biochemistry and Molecular Biology, Davidson Building, University of Glasgow, Glasgow G12 8QQ*

(*Received 21 December 1996; revised 21 February 1997; accepted 21 February 1997*)

SUMMARY

A tegumental vesicle preparation from adult male *Schistosoma mansoni* was developed that allows the resolution of single ion-channel currents. Adult male schistosomes were exposed to a low pH (3·75) medium for a period of approximately 30 min at 37 °C. During this period smooth vesicles formed from the tegument. Fluorescence microscopy following staining of the tegument with the dye, 5-*N*-[octadecanoyl]aminofluorescein (AF-18), transmission electron microscopy and scanning electron microscopy revealed that the vesicles were produced from the outer tegumental membrane. The fluorescence studies showed the presence of the double bilayer structure of the outer membrane in > 41 % of the vesicles. These studies suggested that the preparation is suitable for single-channel recording with the patch-clamp technique. Cell-attached and isolated inside-out patch recordings of ion-channel activity were obtained with giga-ohm resistance seals. Different types of ion-channel were recorded from tegumental vesicles from male schistosomes, illustrating the potential of the technique. The channels observed included: a non-selective cation channel (360 pS); a K^+ channel (with a conductance of 115 pS in high bath-K conditions); and a Cl^- selective channel (20 pS). The currents of these ion-channels may cross the double bilayer of the outer tegumental membrane.

Key words: *Schistosoma mansoni*, tegument, vesicles, patch-clamp, ion-channels.

INTRODUCTION

The surface anatomy of *Schistosoma mansoni* is not smooth but irregular, making the patch-clamp study of single ion-channel activity in the tegument difficult (Day, Bennett & Pax, 1992). The complex morphology of the tegument has been described by Gönnert (1955), Smith, Reynolds & Lichtenberg (1969), Hockley & McLaren (1973), Wilson & Barnes (1974), McLaren & Hockley (1977) and Senft & Gilber (1977). The dorsal tegumental surface of the adult male bears a large number of crypts, and dome-shaped structures known as tubercles that have a large number of pointed spines. The female tegument is smoother.

The complex surface topography of the adult schistosome has so far only permitted low resistance patch recordings of a high conductance channel from the tegument of the female (Day *et al.* 1992). The channel is a non-selective cation channel with a main conductance of 295 pS that appears to arise from the cooperative opening of several ion-channels with a unitary conductance of 95 pS. In this paper we describe the preparation of a smooth tegumental vesicle from the male schistosome, suitable for patch-clamp studies. We show that this method is capable of recording channels with high resolution, allowing additional, smaller conductance, channels to be resolved.

* Corresponding author: Department of Preclinical Veterinary Sciences, R.(D).S.V.S., Summerhall, University of Edinburgh, Edinburgh EH9 3QH. Tel: +131 650 6094/5. Fax: +131 650 6576. E-mail: R.J.MARTIN@ed.ac.uk

MATERIALS AND METHODS

Source of Schistosoma mansoni

BALB/c mice with mature infections of a Puerto Rican strain of *Schistosoma mansoni* were killed by cervical dislocation. The animals were then dissected to expose the thoracic and abdominal cavities. The portal vein was cut close to the liver and 50 ml of *G*lasgow *M*inimal *E*ssential *M*edium (*GMEM*: GibcoBRL BHK21 Cat. No. N12541-025) at 37 °C injected into the heart. The perfusion of medium through the circulation ejected mature worms from the incised portal vein. Schistostomes were collected on fine gauze and transferred to Petri dishes containing GMEM (37 °C). Parasites were washed 3 times in GMEM and maintained in an incubator at 37 °C until required. GMEM was prepared daily to minimize bacterial contamination. Routinely, parasites were used for experiments within 4 h of harvesting from the mice.

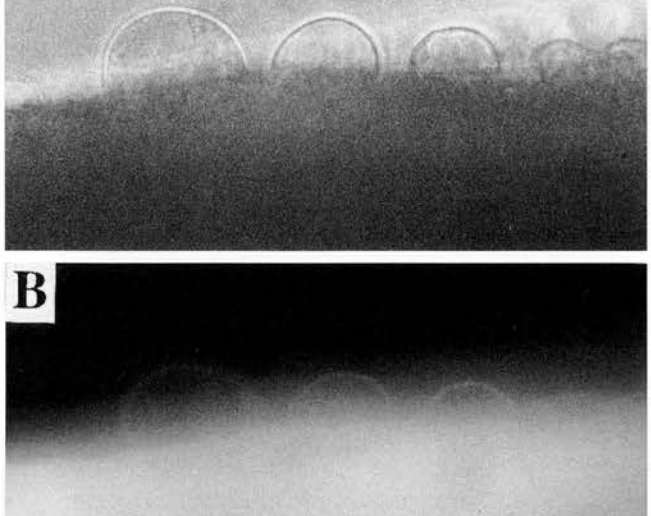

Fig. 1. (A) Phase-contrast photomicrograph of a male *Schistosoma mansoni* showing the membrane vesicles on the surface of the worm. (B) FITC fluorescence micrograph of the same field of view as (A). Note the presence of the fluorescent vesicles.

Vesicle formation

Parasites were transferred from GMEM to a Petri dish containing 5–10 ml of the low pH (3·75) *VMEM* (*V*esicle *M*inimal *E*ssential *M*edium: produced by addition of 5 M HCl to GMEM) and incubated at 37 °C for time-periods between 15 min and 2 h. An inverted light microscope, Nikon TMS-PH3, at ×200 magnification, was used to observe the 'budding' of vesicles seen on the surface of the parasite after 15–30 min.

Initiation of the process of vesicle formation was dependent on the low pH of VMEM: the optimum pH range for vesicle initiation was 3·5–4·0, with few vesicles being formed with media outside this range. The process of vesicle formation was not dependent on the continued presence of VMEM; an incubation of 30 min was sufficient to initiate vesicle formation, with the process of vesicle formation occurring after the worms had been returned to solutions at pH 7·4.

Fluorescent vesicle studies

Eight male schistosomes were removed from mice and maintained in GMEM. The parasites were divided into 3 groups: UC, SC and SV. Group UC ($n = 2$), the unstained control, was incubated in GMEM for 15 min, washed 5 times in GMEM, then incubated in VMEM for 2 h, followed by 5 washes in GMEM and maintained in GMEM for examination. Group SC ($n = 3$), the stained control, was incubated in 10 μM 5-*N*-[octadecanoylamino]fluorescein (AF 18) for 15 min, washed 5 times in GMEM and maintained for examination in GMEM. Group SV ($n = 3$), the stained vesiculated preparation, was incubated in 10 μM AF-18 for 15 min, then washed 5 times with GMEM and placed in VMEM for 2 h followed by 5 washes in GMEM and maintained in GMEM.

Parasites from each group were mounted on well slides in GMEM and examined using bright field and then fluorescence microscopy using a Leitz Ortholux II microscope, mercury lamp and FITC filters. Parasites from the unstained control group, UC, showed no autofluorescence and were not examined further. Bright field photomicrographs and fluorescence photomicrographs were taken of the stained control and stained vesiculated groups, SC and SV, with a Wild MPS51 camera and Fujichrome 100 film.

Scanning electron microscopy of vesicles

Thirteen male schistosomes were divided into 4 groups and incubated in VMEM for time-periods of either 0 min ($n = 3$), 15 min ($n = 4$), 30 min ($n = 4$) or 1 h ($n = 2$). The parasites were then fixed for a minimum of 3 h in 3% glutaraldehyde in 0·1 M sodium cacodylate buffer (pH 7·4). Fixation was followed by 3 × 20 min washes in sodium cacodylate buffer, pH 7·4, and then 1% osmium tetroxide solution (in 0·1 M sodium cacodylate buffer, pH 7·4) in a 1–2 h post-fixation step. Parasites were then washed for 30 min in distilled water. Dehydration used increasing concentrations of acetone (50–100%) taking 30 min steps. Specimens were dried using carbon dioxide and a critical-point drier (Polaron E3000 SIICPD) and sputter coated with 20 nm gold/palladium (60/40) in an Emscope SC500 sputter coater. Parasites were viewed under a Philips 505 scanning electron microscope.

Transmission electron microscopy

Thirty-one male schistosomes were divided into 4 groups and incubated in VMEM for time-periods of 0 min ($n = 5$), 15 min ($n = 3$), 30 min ($n = 6$) and 1 h ($n = 17$); and were processed for transmission electron microscopy using the method described by Hockley & McLaren (1973). The parasites were triple fixed. Initial fixation was in 2% (v/v) glutaraldehyde in a cacodylate buffer containing 0·05 M sodium cacodylate and 2 mM calcium acetate, pH 7·4. The worms remained in the glutaraldehyde fixative for 5 h at 4 °C and were then washed 3 times in ice-cold Lewis/Shute buffer. For the second fixation step the parasites were placed in 1% (w/v) osmium tetroxide in Lewis/Shute buffer for 2 h at 4 °C followed by 10 washes in ice-cold de-ionized distilled

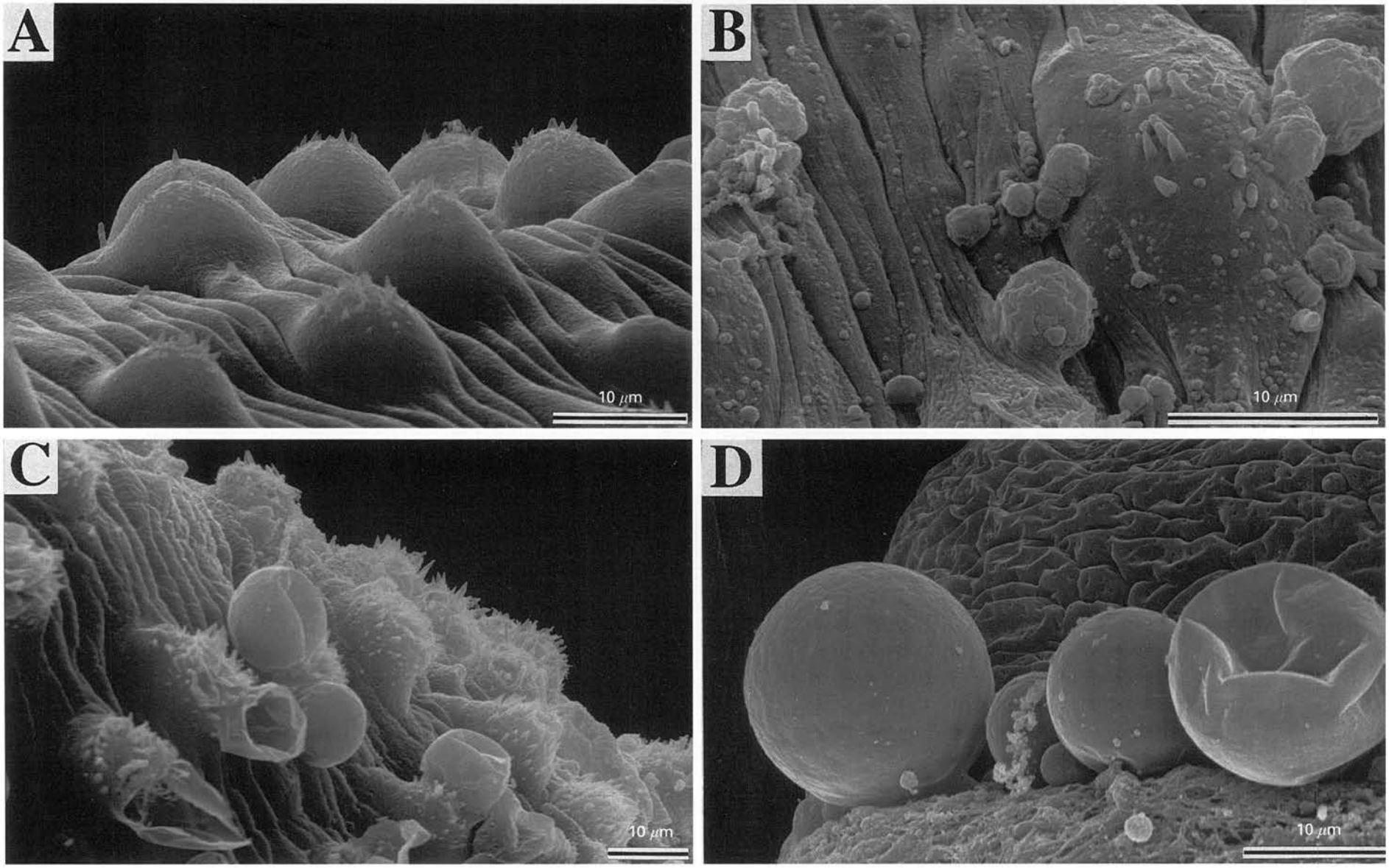

Fig. 2. Scanning electron micrographs. (A) Control scanning micrograph of adult male schistosome showing hill-shaped tubercles topped with spines and the convoluted surface of the tegumental membrane between tubercles. (B) Surface of an adult male after a 15 min treatment in VMEM (vesicle forming medium) at 37 °C. Surface of male parasite showing vesicles budding from the tegumental surface. (C) Adult schistosome after 30 min of the vesicle-forming protocol. Note ruptured vesicles. (D) Parasites after 1 h of the vesicle-forming protocol showing the presence of larger vesicles and the loss of tegumental membrane in the upper section of the micrograph.

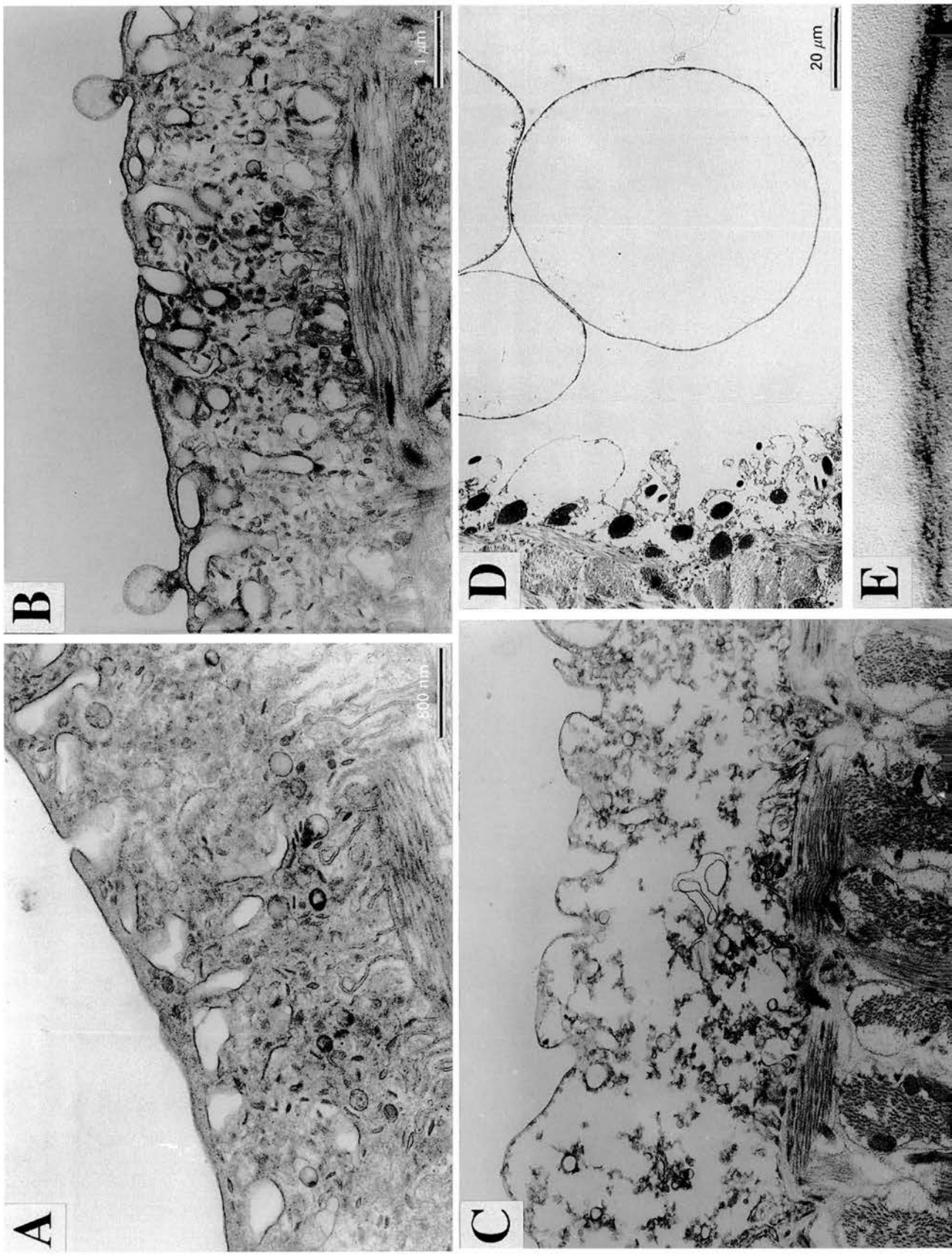
A
500 nm
B
1 μm
C
D
20 μm
E

water. Finally the parasites were placed in a 0·5% aqueous solution of uranyl acetate, pH 5, containing 45 mg/ml sucrose for 1·5 h at 4 °C in total darkness. The worms were then washed 3 times in ice-cold deionized distilled water.

Specimens were dehydrated in a series of incubations in increasing concentrations of ethanol: 25, 50 and 75% each for 10 min. Parasites were then resuspended in 100% ethanol and embedded in Araldite. Sections were cut with a Diatome diamond knife and stained using uranyl acetate and lead citrate. Sections were examined using a Philips EM 400 electron microscope.

Patch-clamp experiments from vesicle preparations

Vesiculated schistosomes were washed gently 3 times in GMEM and transferred to the recording chamber at room temperature, viewed with a Nikon TMS inverted microscope and pinned onto Sylgard™ that lined the recording chamber.

Patch-pipettes were made from Garner glass microcapillary tubing (Cat. no. 7052) and pulled to a resistance of about 1 MΩ when filled with pipette solutions. Single-channel currents were recorded after making a giga-seal between the patch-pipette and the vesicle membrane using a List EPC-7 patch amplifier, filtered at 1 kHz using a laboratory-built 8-pole Bessel filter and permanent records made on a Racal Thermionic Store 4 FM tape recorder with a speed of 7·5 inches/sec. All recordings were obtained from vesicles originating from male parasites.

Unless stated otherwise the bath solution contained (mM): NaCl, 25; KCl, 90; $MgCl_2$, 2; glucose, 20; HEPES, 10; L-glutamine, 2, with the pH adjusted to 7·4 with NaOH. The pipette solution contained (mM): NaCl, 110; KCl, 5; $CaCl_2$, 2; glucose, 20; HEPES, 10; L-glutamine, 2 with the pH adjusted to 7·4 with NaOH.

The single-channel data were analysed by playing the taped records of channel activity into a CED 1401 interface and analysed using an RM 486 PC using Pat 6.0 software (Dempster, Strathclyde University) to measure the channel amplitudes. The slope conductance of the channel I/V plots were estimated by least squares regression and the reversal potential determined by extrapolation or interpolation. The relative permeabilities of the ions were calculated from the reversal potentials using the Goldman–Hodgkin–Katz equation (Hille, 1992).

RESULTS

Fluorescence microscopy of the vesicle preparations

AF-18 was selected for staining the tegument because it inserts into the outer bilayer of the schistosome tegumental membrane but does not enter the inner bilayer (Foley *et al.* 1986). The unstained control schistosome group (UC) showed no autofluorescence so that the level of fluorescence was dramatically less than that present in the stained control group (SC) incubated in AF-18 without undergoing the vesicle-forming protocol. The strong fluorescence of group SC demonstrated the efficacy of our staining technique.

Fig. 1 shows a phase-contrast and a fluorescence photomicrograph of vesicles produced from the stained vesiculated group (SV). The intensity of fluorescence varied from vesicle to vesicle with 41% (7 from a sample of 17) showing clear detectable fluorescence. The presence of the stained fluorescent vesicles demonstrates the presence of the outer bilayer of the tegument in at least a good proportion of the vesicles. The vesicles which did not fluoresce may not possess the outer bilayer of the tegument or the level of fluorescence may have been too low to detect.

Scanning electron microscopy of the vesicles

Unvesiculated control male schistosomes were examined using scanning electron microscopy. The tegument of the schistosomes displayed the typical morphological characteristics of the species including the spiny tubercles as shown in Fig. 2A.

Incubation for 15 min in VMEM resulted in small vesicles budding from the surface of the parasite (Fig. 2B). Low pH treatment for 15 min caused little damage or disruption to the tegument other than the production of the small vesicles.

Treatment with VMEM for 30 min resulted in the formation of larger and more numerous vesicles in the schistosome. Again the vesicles were derived from the outer tegument but more of the vesicles

Fig. 3. Transmission electron micrograph (TEM). (A) Control TEM through the tegument of an adult male showing the tegumental outer membrane, surface pits and channels from the surface pits. Note the relatively dense nature of the tegumental cytoplasm. (B) Micrograph of adult tegument after 15 min of vesicle-forming protocol. Vesicles can be observed budding-off from the outer tegumental membrane. The tegument contains all the features observed in the control micrograph. (C) Tegument of adult parasite after 30 min of the vesicle-forming protocol. All the main features of the tegument can be distinguished but the tegument has become more floccular and appears less dense. (D) Adult parasite after 1 h in the vesicle-forming medium. Note the dispersion of the contents of the tegumental cytoplasm. The underlying membranes and muscle layers appear to be unaffected by the 1 h treatment with low pH media. (E) Control micrograph showing the unique heptalaminate (double bilayer) structure of the outer membrane.

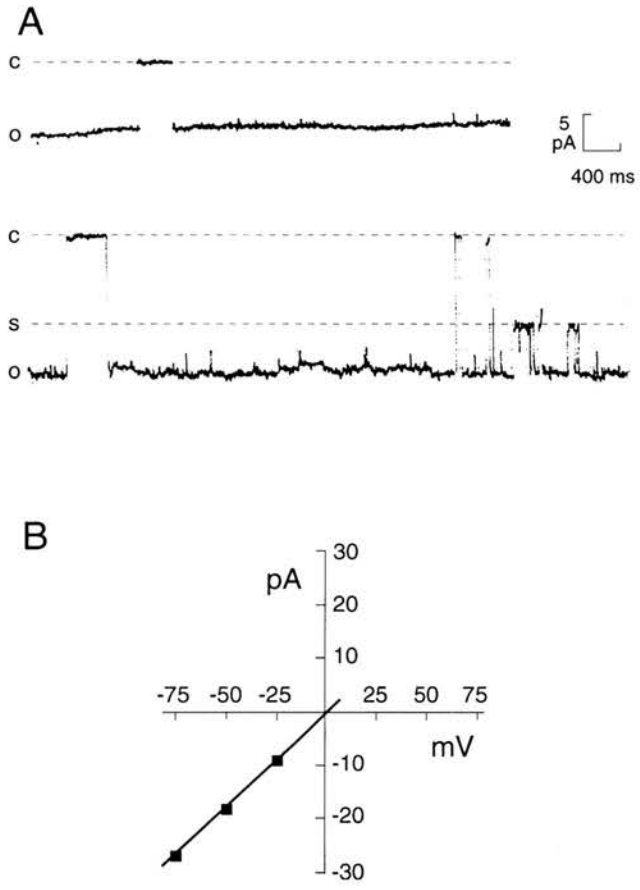

Fig. 4. Non-selective cation channel. Isolated inside-out patch. (A) Single-channel records at −25 mV and −50 mV. C and O refer to the closed and open state of the channel molecules; S indicates the level of the subconductance state. (B) I/V relationship. Slope conductance: 360 pS (■). Reversal potential: 0 mV. Pipette solution (mM): NaCl, 40; KCl, 50; $CaCl_2$, 50; HEPES, 5; glucose, 5. pH adjusted to 7·2 with KOH. Bath solution (mM): Na^+ acetate, 50; NaCl, 100; KCl, 20; $CaCl_2$, 2; HEPES, 5; glucose, 5. pH adjusted to 7·2 with NaOH.

were ruptured after the 30 min VMEM treatment (Fig. 2C).

After 1 h treatment in VMEM, the vesicles were larger as shown in Fig. 2D. The parasite tegument was severely disrupted by the prolonged exposure to low pH; cracks were observed and areas of the outer tegument were stripped away.

Transmission electron microscopy of the vesicle

The effect of low pH treatment on the tegument of male *S. mansoni* was also investigated using transmission electron microscopy. Fig. 3A shows the control appearance of the tegument before low pH treatment. After 15 min in the VMEM, vesicles could be observed budding from the outer layer of the tegument (Fig. 3B).

The cytoplasm of the tegument gradually became more floccular and diffuse after 15 min in VMEM and by 1 h (Fig. 3C and D) the tegumental cytoplasm had become much more diffuse and damaged with large vesicles present. It is pointed out, however, that even at 1 h, the underlying muscle layers displayed no noticeable changes in appearance, with the basal membrane of the tegument remaining intact (Fig. 3D). At much higher magnification, it was found that some of the vesicles possessed the double bilayer of the outer tegument (Fig. 3E). However, it is pointed out that the resolution of the vesicle membranes did not permit the presence of the double bilayer to be discerned in most of the vesicles.

Suitability of vesicle preparation for patch-clamp formation

Although the vesicles appeared to be smooth and suitable for patch-clamp recording, we found that not all the vesicles permitted giga-seal formation. A total of 265 patch pipettes was applied to the vesicle membrane and 61 (23 %) produced seals > 0·5 GΩ and of these, 39 (15 %) produced seals > 1 GΩ. In the sample that produced seals > 1 GΩ, we were able to discern clear channel activity in 23 patches. The following description of channel activity is based on an analysis of those 23 patches. The patches were obtained from 21 adult male parasites.

A large conductance non-selective cation channel

The report of Day *et al.* (1992) describes the presence of a non-selective cation channel with a high conductance (295 pS) in the outer membrane of the tegument of female *S. mansoni*. The channel was selective for cations and showed regularly spaced subconductance steps of 95 pS. We found a similar channel in 5 patches recorded from vesicles originating from the outer tegument of male *S. mansoni*.

Fig. 4 shows channel currents and I/V plots from such a high conductance channel made from an inside-out patch from a male parasite. The slope conductance of the mainstate conductance was 360 pS with a reversal potential near 0 mV. In addition to the mainstate, the channel also shows the presence of a subconductance level making conductance steps of *ca.* 100 pS (Fig. 4A). The predicted Nernst potentials under the recording conditions used in Fig. 4 were: E_{Na} −33·6 mV, E_K +24·1 mV, E_{ca} +35·5 mV and E_{Cl} −10·8 mV, showing that this channel was not selectively permeable to just 1 ion, because the channel reversal potential did not match the Nernst potential of any single ion present.

The non-selective cation channel described by Day *et al.* (1992) was equally permeable to Na^+ and K^+ with the pNa/pK ratio estimated to be 0·7–1·1 in the absence of significant concentrations of Ca^{2+}. The observed reversal potential in Fig. 4B cannot be explained by the channel only being permeable to

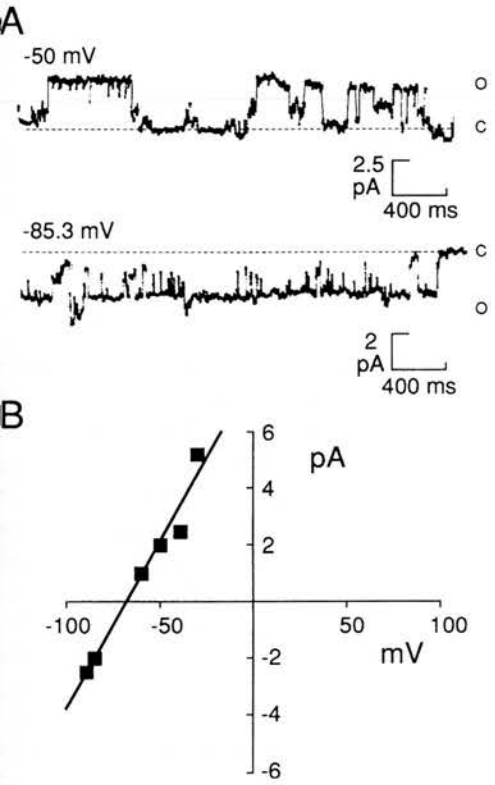

Fig. 5. A potassium-selective channel. Isolated inside-out patch. (A) Single-channel records at membrane potentials of −50 mV (−2·7 pA) and −85·3 mV (−2·2 pA). C and O refer to the open and closed levels of the ion-channel. (B) I/V relationship constructed by plotting amplitude of channel opening against trans-patch potential. The slope conductance: 114 pS. Reversal potential: −71 mV. Pipette solution (mM): NaCl, 100; KCl, 20; $CaCl_2$, 4; HEPES, 5; glucose, 5. pH adjusted to 7·2 with NaOH. Bath solution (mM): NaCl, 100; KCl, 605; $CaCl_2$, 2; HEPES, 5; glucose, 5. pH adjusted to 7·2 with NaOH. E_K −86 mV.

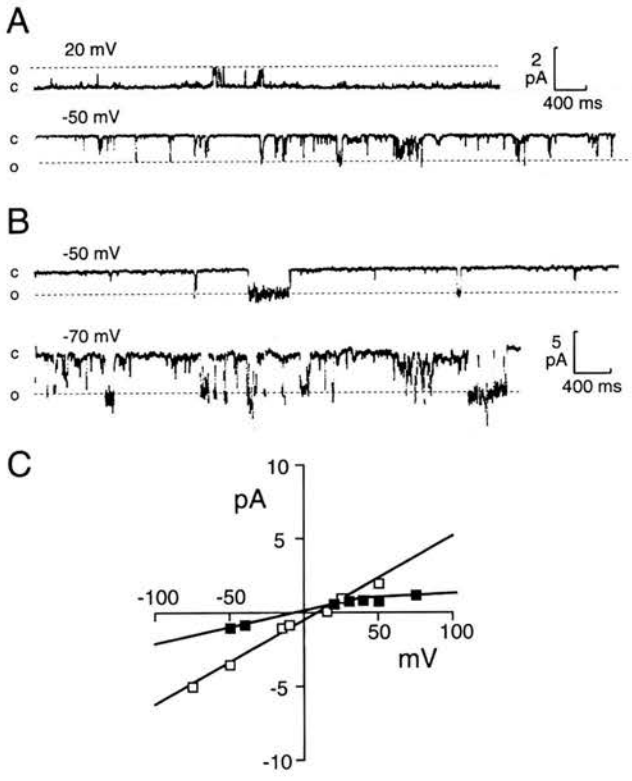

Fig. 6. A Cl^--selective channel and I/V plot. Isolated inside-out patch. (A) Single-channel records obtained at 2 membrane potentials prior to the addition of 3 M KCl to the bath solution. C and O refer to the closed and open state of the channel molecule. Pipette solution (mM): NaCl, 110; KCl, 5; $CaCl_2$, 2; glucose, 20; HEPES, 10; L-glutamine, 2. pH adjusted to 7·4 with NaOH. Bath solution (mM): NaCl, 25; KCl, 90; $MgCl_2$, 2; glucose, 20; HEPES, 10; L-glutamine, 2. pH adjusted to 7·4 with NaOH. E_{Na} −37 mV, E_K −73 mV, and E_{Cl} 0 mV. (B) Single-channel records obtained at 2 membrane potentials after the addition of KCl to the bath solution changing the Cl^- concentration from 119 to 307 mM. In each record the dashed lines labelled C and O refer to the closed and open state of the channel molecule. Note that addition of KCl increases the amplitude of opening at −50 mV. An increase in the concentration of Cl^- in the bath (added KCl) from 119 to 307 mM would produce a shift of E_{Cl} from 0 to +23 mV and a change in E_K from −73 to −101 mV. (C) I/V plot constructed for openings before KCl addition (■) and after KCl was added (□). Note that the plot before KCl addition showed significant inward rectification. The reversal potential was, therefore, estimated by linear regression using the 2 values just above and the 2 values below the reversal potential. Prior to KCl being added, the slope conductance was 22 pS with a reversal potential of −5 mV. The linear regression for the best fit to openings observed after the addition of KCl gave a slope conductance of 58 pS and a reversal potential of +10 mV.

monovalent cations (i.e. impermeable to Ca^{2+}) because a reversal potential of −19 mV is predicted. It may, however, be explained if the channel is also permeable to Ca^{2+}: a reversal potential of 0 mV with the solutions present in Fig. 4 is predicted with a pNA/pK of 1 and a pCa/pK ratio of 0·8. We point out that the calculation of reversal potentials in the presence of the divalent Ca cation is more complex (Lewis, 1979). We have not yet carried out experiments in which the Ca^{2+} concentration was changed to observe the effects on reversal potential.

Evidence for K^+ selective ion-channels

Three isolated patch recordings were made from K^+-selective channels. Fig. 5 shows an example of 1 of these channel currents and its I/V plot. The slope conductance of the channel (with a high bath-K concentration) was 114 pS with a reversal potential of −71 mV. The Nernst reversal potential predicted for the ions used in Fig. 5 were: E_{Na} +8 mV, E_{Cl} +44 mV and E_K −86 mV. The channel was identified as being selective for K^+ ions because the predicted E_K was closest to the observed reversal potential. Two other ion-channels were also identified as being K^+ selective on the basis of their

reversal potentials. They had slope conductances of 38 pS (observed reversal potential +24 mV; predicted reversal potential +24 mV) and 48 pS (observed reversal potential +16 mV; predicted reversal potential +24 mV) with the solutions described in the legend of Fig. 4.

Evidence of a Cl^- selective channel

Fig. 6 shows examples of 'noisy' channel currents that were recorded from a inside-out patch. The I/V plot (Fig. 6C), under the recording conditions where the Nernst reversal potentials were: E_{Na} −37 mV, E_K −73 mV, and E_{cl} 0 mV was not linear and showed significant inward rectification. In order to estimate the reversal potential we used the 2 outward current values seen at potential just more positive than the reversal potential and the 2 inward current values at the negative potentials. Simple regression gave a reversal potential of −5 mV and a slope conductance of 22 pS. An increase in the concentration of Cl^- in the bath (added KCl) from 119 to 307 mM produced a nearly linear I/V plot with an increase in the slope conductance to 58 pS and a positive shift in the reversal potential to +10 mV. The positive shift in reversal potential is indicative of a channel that is selective for Cl^- ions over K^+ ions but is less than the predicted Nernst Cl^- potential of +23 mV, suggesting that the channel also has a low permeability to K^+ ions. Addition of KCl to a purely K^+-selective channel would produce a negative shift in the observed reversal potential.

Four other ion-channels recorded from under similar conditions before the addition of KCl had similar slope conductances (mean ± S.E.: 28·7 ± 9·6 pS, $n = 4$) and reversal potentials near 0 mV (mean ± S.E. −2·3 ± 3·4 mV, $n = 4$). The values of the conductances and reversal potentials were consistent with these channels also being permeable to Cl^-.

DISCUSSION

Effect of vesicle formation protocol on the parasite

The electron microscopy studies illustrate the effect on the tegument of treatment with low pH media. The parasites were not killed by the treatment as muscle contractions were observed in worms several hours after exposure to low pH. The transmission electron microscopy showed that the underlying muscle layers and other tissues remain relatively unaffected by exposure to low pH. The vesicle-forming media only affect the tegument of the parasite. Prolonged incubations resulted in large areas of the outer tegumental membranes being entirely removed. Shorter treatments caused fissures in the tegumental membrane. The number of vesicles increased as the duration of low pH treatment increased. However, observations during patch-clamp experiments showed that after a 15-min treatment in VMEM, vesicles continued to form for several hours in a bathing solution of pH 7·2. This final observation demonstrates the the process of vesicle formation is initiated by low pH but continued exposure to the VMEM is not required. The mechanism by which low pH treatment induces vesicle formation is not known.

Source of vesicles

Initial scanning electron microscopy experiments showed vesicles on the surface of the parasite. The fluorescence studies demonstrated that a proportion of the vesicles were bound by the outer bilayer of the outer tegumental double membrane. The lack of fluorescence in some vesicles may be due to leaching of AF-18 from the vesicles or that some regions of the surface membrane are inaccessible to the probe. In many cases the vesicles were small and fluorescence could not be determined as the background fluorescence from the body of the worm was too intense. Transmission electron microscopy revealed that the vesicles formed from the outer membrane of the parasite tegument. There was no evidence of vesicles forming from any other source within the parasite so it was concluded that the membrane vesicles arise from the outer tegument of the schistosome.

Membrane structure of vesicles

The outer tegumental membrane of the schistosome is unusual, in that it is composed of 2 bilayers in close association (McLaren & Hockley, 1977) in contrast to the majority of cell membranes that are composed of a single bilayer. In effect, the tegument of the schistosome is bound by 2 conventional membranes in close association. Transmission electron microscopy has shown that some of the vesicles possess the usual heptalaminate membrane structure found in the outer tegument; in other vesicles the number of bilayers present in the vesicles was unresolvable. Additionally, the fluorescent probe, octadecanoylaminofluorescein (AF-18), inserts into bilayers but does not traverse them (Foley *et al.* 1986). Only the outer bilayer of the tegument was labelled with AF-18, therefore the outer bilayer of the double membrane is present in a good proportion (*ca.* 40%) of the vesicles. The transmission electron microscopy studies gave no evidence of vesicles forming from the outer of the 2 bilayers or any separation of the 2 bilayers due to low pH treatment. We conclude therefore that at least a proportion of the vesicles possess the double bilayer structure found in the native outer tegument. This unusual membrane arrangement has several interesting implications for any recordings of single ion-channels from the schistosome tegument.

Suitability of vesicle for patch-clamp experiments

The control scanning electron micrographs illustrate the uneven surface of the male schistosome. The female parasite possesses a much smoother surface. To date there are no reports of single-channel recordings from the tegument of the male schistosome. There has been a report of some success obtaining single ion-channel records from adult females (Day *et al.* 1992). The patch-clamp technique requires a seal between the glass pipette and the membrane of the cells to be studied to be > 1 GΩ in resistance. To achieve a seal of sufficient resistance, the membrane to be studied is required to have a smooth, clean surface; in many preparations the membranes are artifically cleaned with enzymes prior to seal formation. The lack of prior success in obtaining a giga-ohm seal from the male tegument can be largely attributed to the uneven, spiny nature of the parasite surface. An alternative method for making suitable membrane preparations involves the formation of membrane vesicles from the specimen: single ion-channels have been recorded from membrane vesicles prepared from the somatic muscle cells of *Ascaris suum* (Martin, Kusel & Pennington, 1992). The membrane vesicles prepared from the tegument of the adult schistosome appear very smooth and clean under the light microscope. The electron microscopy studies also show the smooth, clean surface of the vesicles. These studies demonstrate that the schistosome membrane vesicles produced by low pH treatment are suitable candidates for the patch-clamp technique.

We found that approximately 15% of patch-pipettes formed giga-seals after applying gentle suction to the patch-pipette. This level of success with the schistosome vesicles is still lower than with many cells in tissue culture. The 15% seal success rate is an improvement on that achieved by Day *et al.* (1992) who were not able to make recordings from the male schistosome and achieved less than a 10% success rate from the female without achieving good giga-seals. Nonetheless, we still found sealing onto the membrane harder than cells in tissue culture and this may be due to the continued presence of the extensive glycocalyx and the complex multilaminate nature of the outer membrane (Stein & Lumsden, 1973).

In about 60% (23 of 39) of the giga-ohm patch recordings, single-channel current steps could be resolved but, in the remainder, the current record was very noisy and single-channel currents could not be resolved. It was assumed that the simultaneous opening of a large number of ion-channels produced this noise because the seal resistance of the patch-pipette was greater than 1 GΩ.

We often observed channel currents that stepped between the closed and mainstate conductance level and in addition showed what appeared to be many subconductance levels. The origin of the subconductance levels may relate to the structure of the ion-channel. It may also relate to the presence of the double bilayer across the membrane with ion-channels present in the inner and outer membrane. If such an arrangement does obtain, then the currents observed to cross the patch of membrane will be determined by a network of channels in parallel in the same membrane bilayer and by the channels in series across the 2 bilayer membranes. Despite these difficulties we were able to obtain giga-seal patches and were able to resolve channel currents with conductances as small as 10 pS. We were also able to observe a non-selective cation channel, a K^+-selective channel and a Cl^--selective channel.

The schistosome tegument vesicle preparation, then, offers a technique for resolving single-channel currents and offers an approach for studying physiological and pharmacological effects on their ion-channels.

REFERENCES

DAY, T. A., BENNETT, J. L. & PAX, R. A. (1992). *Schistosoma mansoni*: patch-clamp study of a non-selective cation channel in the outer tegument of females. *Experimental Parasitology* **74**, 348–356.

FOLEY, M., MACGREGOR, A. N., KUSEL, J. R., GARLAND, P. B., DOWNIE, T. & MOORE, I. (1986). The lateral diffusion of lipid probes in the surfaces of *Schistosoma mansoni*. *Journal of Cell Biology* **B103**, 807–818.

GÖNNERT, R. (1955). Schistosomiasis-Studien I. Beiträge zur Anatomie und Histologie von *Schistosoma mansoni*. *Zeitschrift für Tropenmedizin und Parasitologie* **6**, 18–33.

HILLE, B. (1992). *Ionic Channels of Excitable Membranes*, 2nd edn. Sinauer Associates, Sunderland, Mass.

HOCKLEY, D. J. & MCLAREN, D. J. (1973). *Schistosoma mansoni*: changes in the outer membrane of the tegument during development from cercaria to adult worm. *International Journal for Parasitology* **3**, 13–25.

LEWIS, C. A. (1979). Ion-concentration dependence of the reversal potential and the single channel conductance of ion-channels at the frog neuromuscular junction. *Journal of Physiology* **286**, 417–445.

MARTIN, R. J., KUSEL, J. R. & PENNINGTON, A. J. (1990). Surface properties of membrane vesicles prepared from muscle cells of *Ascaris suum*. *Journal of Parasitology* **76**, 340–348.

MCLAREN, D. J. & HOCKLEY, D. J. (1977). Blood flukes have a double outer membrane. *Nature, London* **269**, 147–149.

SENFT, A. W. & GILBER, W. B. (1977). *Schistosoma mansoni* tegumental appendages: scanning microscopy following thiocarbohydrazide–osmium preparation. *American Journal of Tropical Medicine and Hygene* **26**, 1169–1177.

SMITH, J. H., REYNOLDS, E. S. & LICHTENBERG, F. VON (1969). The integument of *Schistosoma mansoni*. *American Journal of Tropical Medicine and Hygene* **18**, 28–49.

STEIN, P. C. & LUMSDEN, R. D. (1973). *Schistosoma*

mansoni: tropochemical features of cercariae, schistosomula, and adults. *Experimental Parasitology* **33**, 499–514.

WILSON, R. A. & BARNES, P. E. (1974). The tegument of *Schistosoma mansoni*: observations on the formation, structure and composition of cytoplasmic inclusions in relation to tegument function. *Parasitology* **68**, 239–258.

Praziquantel:
An Urgent and Exciting Challenge

C.A. Redman, A. Robertson, P.G. Fallon, J. Modha, J.R. Kusel, M.J. Doenhoff and R.J. Martin

The anthelmintic drug praziquantel has proved useful in the treatment of schistosomiasis. The precise mechanism by which praziquantel kills the parasites has yet to be elucidated. Here, John Kusel and colleagues review the current theories on praziquantel action and suggest future avenues for research, which becomes urgent in the light of some reports of drug resistance.

Schistosomiasis is widespread in tropical areas and continues to spread rapidly, as recent outbreaks in Senegal have shown[1]. No vaccine exists for human populations, although vaccine candidates have been proposed[2]. Treatment of the disease worldwide relies very heavily on praziquantel (PZQ), a highly effective drug with few side effects[3]. The effectiveness of this drug against schistosomes, and against other helminths, is well documented[3,4], but the precise mechanisms by which the drug affects the parasite have yet to be elucidated[5]. Recent reports from Senegal suggest that this drug is not always very effective and that resistant strains may have developed[6]. An excellent article on PZQ has just been published[7].

PZQ-sensitive sites

PZQ acts within the tegument and muscle cells of the schistosome. The structure of the tegument is shown in Fig. 1; the surface membrane is represented as a highly complex double bilayer, the lipids and proteins of which may be organized into domains of differing properties and composition[8,9]. Variation has been observed in the distribution and the extent of the damage to the surface of adult parasites with respect to species, sex and individuals[10,11]. Differences between juvenile and adult[12–15] and male and female worms of *S. mansoni* have been observed[11,16]. These differences in susceptibility suggest membrane composition may be an important factor in PZQ-induced damage. Differences in membrane properties and phospholipid composition have been reported for different ages/sexes of *S. mansoni*[14,17,18]. However, other explanations, such as possible differences in distribution of PZQ-sensitive sites, must be considered.

PZQ induces a Ca^{2+} influx across the tegument, thought to be vital in the drug's effect, causing an immediate muscular contraction[19]. Bathing parasites in Ca^{2+}-free medium blocks this PZQ-induced contraction[20–23]. The effect of such treatment is not immediate, however, requiring more than ten minutes to take effect. This is explained by the draining of sequestered Ca^{2+} from pools in the worm. Evidence suggests that the tegument of the worm contains PZQ-sensitive sites. This is from work carried out on normal worms and worms which have had their tegument removed[24]. PZQ-induced contraction was found to be biphasic in normal parasites when incubated in high-Mg^{2+} medium, while only the larger, second contraction was observed in detegumented worms. The presence of these PZQ-sensitive sites in the surface would explain why the tegument is so susceptible to damage by PZQ. However, the tegument is electrically coupled to muscle cells, so that a rise in intrategumental Ca^{2+} might lead to increased Ca^{2+} in the sarcoplasmic reticulum which could lead to contraction[25]. The electrical coupling between the tegument and the muscle cells would explain why any physical or chemical change in the schistosome environment, affecting the tegument, will produce changes in the muscle cells. This means that external agents, such as PZQ, may produce muscle contraction by interacting with tegument rather than muscle cells directly.

The anatomical basis for the coupling between the tegument and muscle cells could be junctional complexes between the tegument and muscle cells[26] (Fig. 1)[27]. These PZQ-sensitive sites may also occur in muscle cells. This conclusion is based on observations on detegumented schistosomes that still contract in response to PZQ application, as well as initial observations on dissociated muscle fibres which contract when exposed to low concentrations of PZQ[24].

The relationship between PZQ and Ca^{2+} influx would suggest that sites of action are Ca^{2+}-permeable

Christopher Redman, Jayant Modha and **John Kusel** are at the Davidson Building, Division of Biochemistry and Molecular Biology, Institute of Biological and Life Sciences, The University of Glasgow, Glasgow, UK G12 8QQ. Padraig Fallon and Michael Doenhoff are at the School of Biological Sciences, University of Wales, Bangor, UK LL57 2UW. Alan Robertson and Richard Martin are at the Department of Physiology, Royal (Dick) Veterinary School, Edinburgh University, Summerhall, Edinburgh, UK EH9 1QH.
Tel: +44 141 330 4621. Fax: +44 141 330 4620, e-mail: gbca66@udcf.gla.ac.uk

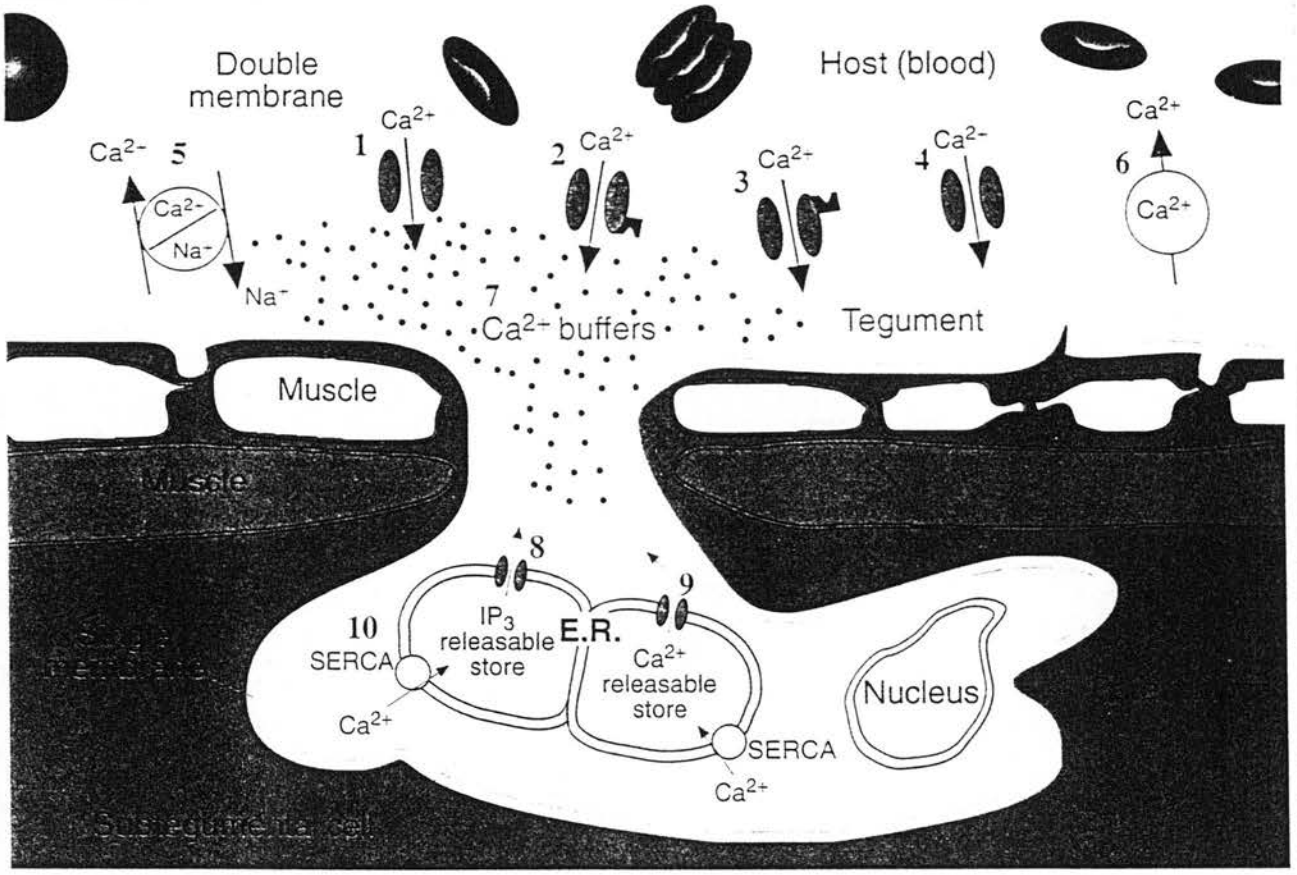

Fig. 1. Diagram representing the *Schistosoma* tegument, underlying muscle layers and parenchyma, and showing the three electrical compartments recognized by an advancing micropipette. (1)–(10) are common cellular factors/components responsible for modulating intracellular [Ca^{2+}]: (1) second messenger-gated Ca^{2+} channel; (2) calcium release activated Ca^{2+} channel; (3) agonist-gated Ca^{2+} channel; (4) voltage-gated Ca^{2+} channel. PZQ increasing the P_{open} of (1)–(4) could account for the observed influx of Ca^{2+} across the tegument. (5) Na^{-}/Ca^{2+} exchange pump; (6) Ca^{2+} pump, inhibition of either (5) or (6) by PZQ could lead to an increase in intrategumental [Ca^{2+}]; (7) reduction in buffering capacity induced by PZQ would lead to an increase in the free [Ca^{2+}]. PZQ can also induce effects when the parasite is bathed in Ca^{2+}-free media, suggesting the drug also interacts with intracellular calcium stores (found in rough endoplasmic reticulum); (8) and (9) are release channels for Ca^{2+} stores, sensitive to inositol triphosphate and Ca^{2+}, respectively. PZQ may cause either of these types of channel to open and release calcium from these stores. (10) SERCA (sarco endoplasmic reticulum calcium) pumps responsible for filling the intracellular calcium stores. Inhibition of SERCA pumps by PZQ is a possibility. Factors (1) to (10) will be present in the muscle cells of the parasite, thus accounting for the action of the drug on tegumented worms. However, there are pathways of low electrical resistance between tegument and muscle cell (11), and from muscle cell to muscle cell (12), which may be conduits for PZQ action. (1)–(6) could also face onto extracellular spaces. Factors (1)–(6) are shown spanning the double membrane of the *Schistosoma* outer tegument as their specific location in this structure has not been determined. (Diagram modified from Ref. 27.)

ion channels in the membranes of the tegument and muscle cells[24] (Fig. 1). Ca^{2+}-influx may be blocked by Mg^{2+} or La^{3+}, but not Ni^{2+}, Co^{2+} or the Ca^{2+} channel blocker D-600 (Refs 21,22). These channels must be pharmacologically distinct from the host Ca^{2+} channels, otherwise PZQ would be toxic to the host and not therapeutically effective. High Mg^{2+}/Ca^{2+} medium decreases PZQ-induced vacuolation[28], suggesting that either Mg^{2+} affects on Ca^{2+} influx, perhaps by inhibiting Ca^{2+} ion channels, or it inhibits vacuolation. However, these putative ion channels have yet to be observed physiologically. The biphasic PZQ tetanic contraction of the parasite may be due to two or more populations of Ca^{2+} ion channels, perhaps of different types (Fig. 1).

The electrical properties of dissociated muscle cells have also been studied using whole-cell voltage clamp[5]. Three types of muscle cell, and two types of voltage-activated outward K^{+} currents were identified. All three types of cell possessed the delayed rectifier-like K^{+} current, but only two of the muscle cell types possessed the rapidly inactivating 'A' K^{+} current. These dissociated muscle cells contract by bathing in high external K^{+}, which suggests the presence of voltage-activated Ca^{2+} currents. They also contract in response to PZQ. Interestingly, no voltage-activated inward currents were detected despite the evidence of voltage-activated Ca^{2+} currents present in these cells. The failure to detect any voltage-activated currents may relate to the whole cell voltage-clamp technique used, which involves breaking into the cell and presumably dialysing the contents of the cell: Ca^{2+} currents easily run down in small cells and require all voltage-activated outward currents to be blocked before they can be seen. A detailed investigation of the voltage-activated inward currents and the influence of PZQ using different methods to isolate the muscle cells seems a rational next step.

Table 1. Schistosoma mansoni tegumental antigens exposed on the worm surface by praziquantel

Antigen	Molecular mass (kDa)	Praziquantel-exposed[a]	Antibody-enhanced killing	Refs
Nonspecific esterase	27	IIF ENZ	Yes	33
Tubercle glycoprotein	200	IIF	Yes	34,35
Alkaline phosphatase	67–260 (polymeric)	IIF ENZ (females)	Yes	34,36
Actin	43	IIF	NT[b]	37
Sm23	23	IIF	NT	38
Acetylcholinesterase	(polymeric)	IIF	NT	39

[a]Exposure demonstrated by indirect immunofluorescence (IIF) or by quantitative enzyme assays (ENZ). [b]NT, not yet tested.

Antigen exposure

In animal models, curative doses of PZQ result in the exposure of antigens[29] and binding and penetration of host defence cells into the worm after 17 h (Refs 19,30,31). The end result is the formation of granulomas in which the worms are broken down after 14–18 days. However, at subcurative dose of PZQ the worms appear to be able to repair the tegumental lesions[19].

It has been shown that the host immune system plays an important role in PZQ-induced parasite death, *in vivo*[32]. A number of worm tegumental antigens that are exposed by PZQ have been identified (Table 1)[33–39]. The majority of these antigens are glycoproteins, consistent with the finding that carbohydrates are exposed on the surface of PZQ-damaged worms[33,40]. However, it may be that, once exposed, these molecules are shed from the surface[40]. The synergistic activity of PZQ plus antibody is attributed to the antibody binding to specific exposed epitopes and thereby immunologically enhancing worm death[32,33]. Perhaps these specific antibodies allow an immune-based action to take place against PZQ-induced epitopes before the worm is able to repair the areas of damage. The specific antibodies are able to induce increased macrophage binding to the worm surface within two hours, *in vitro* (C. Graham, unpublished).

Alternatively the antibody-mediated enhancement of mortality of drug-treated worms may be a result of antibodies inhibiting PZQ-exposed enzymes, as has been demonstrated for alkaline phosphatase[36]. In view of the possible role alkaline phosphatase plays in nutrient uptake[41], inhibition of this enzyme by the antibody may impede critical metabolic processes of the worm. Such processes would be important if the worm were to repair PZQ-induced damage.

It is of interest that the majority of PZQ-exposed *S. mansoni* antigens (the 200 kDa tubercle glycoprotein, acetylcholinesterase, alkaline phosphatase and Sm23) have been shown to be attached to the membrane via glycosylphosphatidylinositol (GPI) anchors[38,42,43], perhaps on the inner membrane, as has been suggested for the acetylcholine receptor[39]. These proteins can be released from the worm surface by bacterial phosphatidylinositol-specific phospholipase C (PIPLC)[42–44]. It has been proposed that the GPI-anchor may facilitate the selective release of that protein by a phospholipase[45]. A GPI-specific phospholipase D (GPIPLD) activity has been detected in *S. mansoni*, either endogenous or adsorbed onto the surface from the host plasma[46]. It might be envisaged that GPIPLD in the membrane could cause release of the GPI-linked antigens, exposed by PZQ[45] (Fig. 2). An increase in alkaline phosphatase activity on the

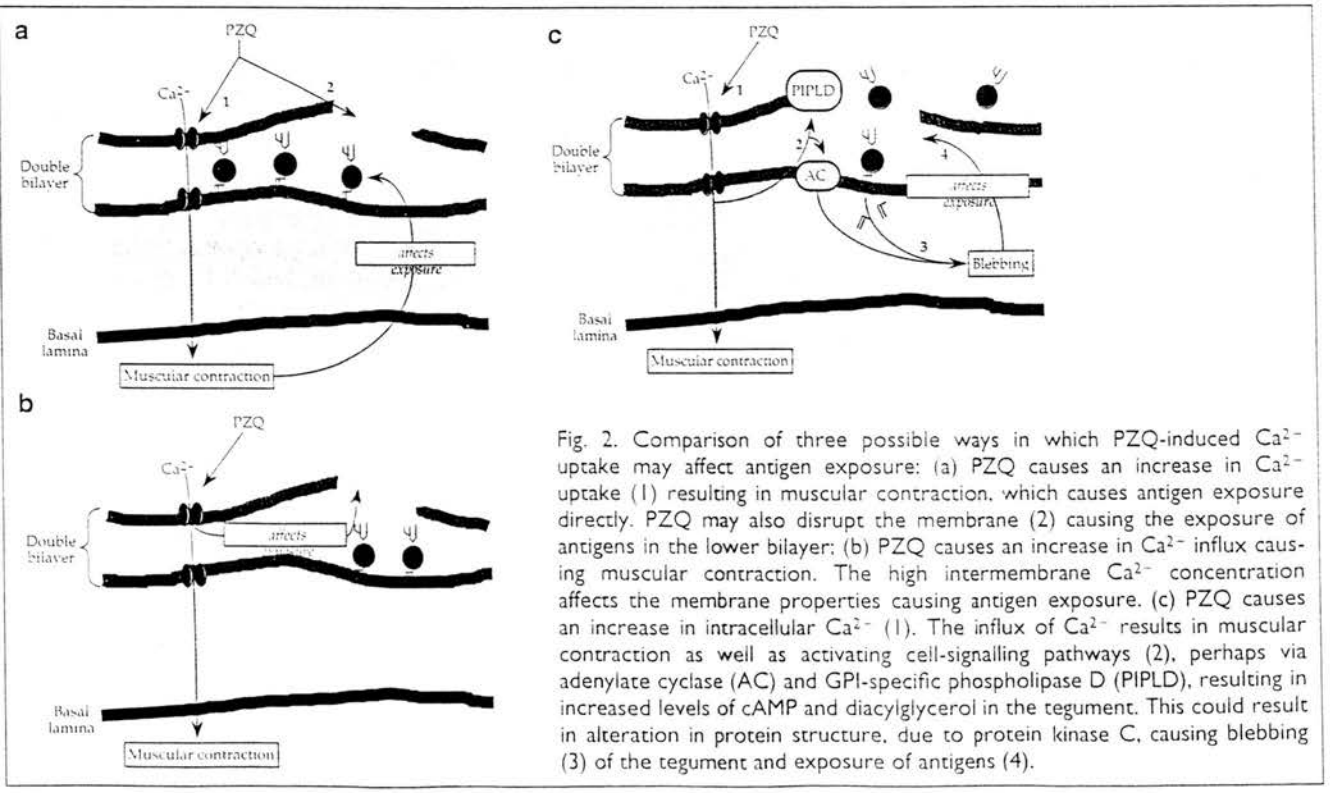

Fig. 2. Comparison of three possible ways in which PZQ-induced Ca^{2+} uptake may affect antigen exposure: (a) PZQ causes an increase in Ca^{2+} uptake (1) resulting in muscular contraction, which causes antigen exposure directly. PZQ may also disrupt the membrane (2) causing the exposure of antigens in the lower bilayer; (b) PZQ causes an increase in Ca^{2+} influx causing muscular contraction. The high intermembrane Ca^{2+} concentration affects the membrane properties causing antigen exposure. (c) PZQ causes an increase in intracellular Ca^{2+} (1). The influx of Ca^{2+} results in muscular contraction as well as activating cell-signalling pathways (2), perhaps via adenylate cyclase (AC) and GPI-specific phospholipase D (PIPLD), resulting in increased levels of cAMP and diacylglycerol in the tegument. This could result in alteration in protein structure, due to protein kinase C, causing blebbing (3) of the tegument and exposure of antigens (4).

Table 2. Summary of experiments[a] that may elucidate crucial questions

Question	Experimental procedure	Possible outcome of experiment; problems with interpretation
(1) What kind of Ca^{2+} channel is sensitive to PZQ?	Incubate worms with those inhibitors[34,35] that block Ca^{2+} channels (Fig. 1), and observe effects when PZQ is added.	Some channels may be very different from mammalian channels: inhibitors may not be effective.
(2) Does Ca^{2+} (in absence of PZQ) induce antigen exposure?	Load worms with 'caged' Ca^{2+} (Refs 56,57), and photoactivate[b]; measure antigen exposure.	If Ca^{2+} release increases antigen exposure, Fig. 2a is invalid.
(3) Does PZQ induce antigen exposure via Ca^{2+}?	Load worms with 'caged' Ca^{2+} chelator (diazo-2) and treat with PZQ after photoactivation; measure antigen exposure.	Ca^{2+} sequestration should prevent antigen exposure, if Figs 2b and 2c are valid.
(4) Where are the Ca^{2+} stores within the parasite?	Load worms with fluorescent Ca^{2+} reporting compound (fluo-3) and treat with PZQ.	Ca^{2+}-rich vesicles and stores should be apparent by fluorescence or confocal microscopy; these may deplete with PZQ treatment.
(5) Are PZQ-sensitive Ca^{2+} channels located in the surface membrane?	Patch-clamp studies on isolated membrane vesicles[38].	Ca^{2+} channels, once identified, may respond to PZQ in isolated membranes.
(6) Can radioactive derivative of PZQ be used to crosslink PZQ-sensitive site?	Photoactivable PZQ derivative might be synthesized, and incubated with the worm.	Photoactivation and crosslinking to receptor might identify binding protein on SDS PAGE (see Ref. 59 for an example using chloroquine).
(7) Can antigens that synergize with the immune system be located in the membrane fraction?	Fractionate isolated surface membrane into detergent-soluble and -insoluble fractions: look for distribution of relevant antigens (Table 1).	GPI-linked proteins often found in detergent-insoluble membrane domain. Photobleaching studies might confirm 'immobile' character in living worms.
(8) Do antigens synergizing with the immune system become released from the parasite after PZQ treatment?	After PZQ treatment *in vitro*, measure release of GPI-anchored antigens from the surface of the medium.	Those synergizing may not be released: release may be seen only with non-synergizing antigens.
(9) What is the nature of the surface membrane repair after PZQ treatment?	Measure uptake of exogenous lipid, and parasite synthesis of lipid and protein by membrane after PZQ damage.	Compare with other kinds of damage (eg. by basic protein) and especially PZQ-resistant forms. Rates of HSP70 synthesis increase.
(10) What is the nature of the variability to PZQ action over the worm's surface?	Fluorescent PZQ could be used to observe distribution of PZQ binding sites. Fluorescent PZQ might be synthesized.	Antibodies to PZQ-sensitive sites would be valuable if Question 6 was answered with identification of a protein.
(11) Can PZQ induce Ca^{2+} influx in the absence of Ca^{2+} channels[60]?	Prepare membrane vesicles which, by patch clamp, have no Ca^{2+} channels. Observe effects of PZQ.	PZQ may alter membrane lipid properties to allow Ca^{2+} influx.

[a] In all experiments suggested, both PZQ-sensitive and -resistant strains of *Schistosoma mansoni* should be compared.
[b] 'Caged' compounds and fluorescent derivatives can be obtained or custom synthesized by Molecular Probes, Eugene, Oregon, USA.

surface of the parasite after PZQ exposure[38] suggests that this enzyme may not be released into the plasma, by either endogenous or exogenous phospholipases. Synergism between PZQ and the immune system may be seen with antibodies against those antigens which remain in the membrane after PZQ treatment. The antibody isotype will also be important in recruiting secondary effector mechanisms.

Drug resistance

Progress in the understanding of the mode of action of a drug may be made by comparative studies on drug-resistant and -susceptible isolates. By comparison with microbial infection, however, suitable definition of drug resistance may be more difficult to formulate for parasitic infections, and for schistosomiasis in particular, because of the variation in susceptibility of different maturation stages and sexes of the parasite to the drugs in question. For example, post-larval but immature schistosomes not previously exposed to schistosomicidal drugs have a 'natural resistance' or 'tolerance' to doses that will kill older worms[12], and PZQ in particular is more effective against female than against male worms under certain circumstances[19,36].

In contrast to such inherent resistance that depends on geographic origin, maturational state or sex, 'true resistance' to a schistosomicidal drug has been defined as a genetically transmitted loss of sensitivity in a parasitic population that was previously sensitive to that drug[45]. By this definition, a recently described, selectively bred laboratory isolate of *S. mansoni*[47] that was insusceptible to doses of PZQ that killed unselected isolates would appear to be expressing 'true

stance'. Comparison of the properties of this resist- isolate, and of isolates from Senegal which are) putatively insusceptible to PZQ may help in cidating the mode of action of this drug and the ure of the resistance. There are several possible ianations for resistance in human populations and electively bred isolates. It may be that drug insus- tibility is due to a delay in maturation of the para- , resulting in prolongation of the immature state ich is 'naturally resistant' or 'tolerant' to the drug. e mutation or absence of a PZQ-receptor protein[5], l the modulation of the expression, exposure or nunogenicity of the specific proteins which render normal parasites susceptible to immunologically icted damage are other possibilities. Insusceptibil- in Senegal may be due to the absence of antibodies inst those surface antigens that have been shown to ergize with the immune system after PZQ treatment ble 1).

embrane fluidity and metabolism

When we consider the effects of PZQ on the double ayered surface membrane, it is possible to envisage y rapid (occurring in the first few minutes) and ger-term (over several hours) effects. A very rapid crease in membrane fluidity was observed when adecanoylamino-fluorescein (AF18) was used as a obe in photobleaching experiments[18]. The fluidity another fluorescent probe, PKH2 (Sigma) increased er PZQ treatment. This may indicate that AF18 and H2 enter different domains. Domains in the sur- e membrane have been observed by several work- [8,9,48]. It may be possible that PZQ preferentially erts into particular domains, as opposed to general ertion. In mammalian cells, certain domains have en found to be rich in cholesterol, sphingomyelin d GPI-linked proteins[48,49]. The GPI-linked antigens at are exposed after PZQ treatment in *S. mansoni* ay occur in such domains. It has been observed that e action of GPIPLD, such as that found on the rface of *S. mansoni*[46], may be affected by the physi- l state of the bilayer in which the substrates are cated[50]. Alternatively the antigens, such as alkaline osphatase[32], may be orientated in the membrane ch that the anchor is protected from the GPIPLD tivity. It is important to find out whether or not ese GPI-anchored antigens are released from the embrane *in vivo*.

If antigens were released by a phospholipase, *in o*, then a rise in intracellular diacylglycerol may cur[46] (Fig. 2). Phorbol esters, which activate protein nase C, were shown to cause vacuolation of the orm surface[50]. This vacuolation was believed to in- olve the signal transduction pathway, perhaps via acylglycerol[51]. It may be that the PZQ-induced Ca^{2+} flux causes the activation of protein kinase C, by acti- tion of a phospholipase, as in other systems[52,53]. The nosphorylation of proteins by protein kinase C could estabilize the tegument, causing the vacuolation and ntigen exposure[51] (Fig. 2c).

Several, longer-term effects of PZQ have been bserved. *In vitro* studies analysing the binding of uorescent lectins to PZQ-damaged regions of the arasite surface show carbohydrate moieties to have gh rates of lateral diffusion, suggesting possible edding of these antigens[18]. As discussed above, this may involve phospholipase activity. PZQ also stimulates heat shock protein 70 (HSP70) synthesis and secretion over a 24 h period (N. Wardy, PhD Thesis, University of Glasgow, 1994). HSP70 is likely to be important in membrane repair, but its secretion may stimulate the immune response of the host, and play a role in the immune dependence of chemotherapy. Lipid uptake is also decreased by PZQ, as measured by AF18 insertion. This effect over a period of days might result in a diminished ability of the worm to repair regions of PZQ-induced damage.

Future perspectives

Figure 2 suggests some possible consequences of an increase in tegumental Ca^{2+} ion concentration. (1) The increase in Ca^{2+} causes muscular contraction, while tegumental damage and antigen exposure is a separate consequence of PZQ binding to the surface membrane; (2) an increase in Ca^{2+} causes both contraction and antigen exposure; (3) a signalling pathway is triggered by an increase in Ca^{2+}, involving activation of adenylate cyclase (Type I) or phospholipase D, leading to cytoskeletal changes and antigen exposure. Experiments can be designed to investigate these possibilities. Comparison of susceptible and resistant parasites could reveal more about the mechanism of PZQ activity. The use of the *R* (−) (active) and *S* (−) (inactive) stereoisomers of PZQ in experiments would reveal whether or not the effects observed are relevant to the activity of PZQ.

Table 2 gives a brief summary of some experiments[54–60] that may answer some crucial questions. Questions 1, 5, 6 and 10 are directed to the identification of the PZQ site; Questions 2 and 3 to the role of Ca^{2+} in antigen exposure; Question 4 to the location of Ca^{2+} stores; and Questions 7–9 to the location and properties of synergizing antigens in the surface membrane. It is possible that PZQ can perturb the surface membrane[60] as a primary event[7] and that Ca^{2+} influx is a consequence of this perturbation. Question 11 is directed to this. Answers to these questions should (1) determine whether or not there is a PZQ site, (2) define the role of Ca^{2+} in inducing antigen exposure, and (3) help to determine the physiological basis for resistance. If there is a PZQ-specific binding protein, its gene can be identified as has been done with the ivermectin binding protein in *C. elegans*[61]. A recent paper reports the binding of PZQ with *S. japonicum* glutathione-*S*-transferase[62].

Acknowledgements

We would like to thank the Wellcome Trust and the BBSRC for support. We would also like to thank Donato Cioli for advice and for enabling us to read his article on PZQ (Ref. 7) prior to publication. Alison Agnew and Marcela Camacho for allowing us to read Ref. 39 prior to publication, and Adam Harder for advice and critical discussion.

References

1 Stelma, F.F. *et al.* (1993) **Epidemiology of *Schistosoma mansoni* infections in a recently exposed community in northern Senegal.** *Am. J. Trop. Med. Hyg.* 49, 701–706

2 Grezel, D. *et al.* (1993) **Protective immunity induced in rat schistosomaiasis by single dose of the SM28GST recombinant antigen: effector mechanisms involving IgE and IgA antibodies.** *Eur. J. Immunol.* 23, 454–460

3 Andrews, P. *et al.* (1983) **Praziquantel.** *Med. Res. Rev.* 3, 147–200

4 Harnett, W. (1988) **The anthelmintic action of praziquantel.** *Parasitology Today* 4, 144–146

5 Day, T.A., Bennett, J.L. and Pax, R.A. (1992) Praziquantel: the enigmatic antiparasitic. *Parasitology Today* 8, 342–344
6 Fallon, P.G., Sturrock, R.F. *et al.* (1995) Diminished susceptibility to Praziquantel in a Senegal isolate of *Schistosoma mansoni*. *Am. J. Trop. Med. Hyg.* 53, 61–62
7 Cioli, D. *et al.* Antischistosomal drugs, past, present...and future? *Pharmacol. Ther.* (in press)
8 Kusel, J.R. and Gordon, J.F. (1989) Biophysical properties of the schistosome surface and their relevance to its properties under immune and drug attack. *Parasitol. Immunol.* 11, 431–451
9 Caulfield, J.P. *et al.* (1991) Low density lipoproteins bound to *Schistosoma mansoni* do not alter the lateral diffusion or shedding of lipids in the outer surface membrane. *J. Cell Sci.* 98, 167–173
10 Becker, B. *et al.* (1980) Light and electron microscopic studies on the effect of praziquantel on *Schistosoma mansoni, Dicrocoelium dendriticum* and *Fasciola hepatica* (Trematoda) *in vitro*. *Z. Parasitenkunde* 63, 113–128
11 Shaw, J.R. and Erasmus, D.A. (1983) *Schistosoma mansoni*: the effects of a subcurative dose of praziquantel on the ultrastructure of worms *in vivo*. *Z. Parasitenkunde* 69, 73–90
12 Sabah, A.A. *et al.* (1986) *Schistosoma mansoni*: chemotherapy of infections of different ages. *Exp. Parasitol.* 61, 294–303
13 Flisser, A. *et al.* (1990) *Schistosoma mansoni*: enhanced efficacy of praziquantel treatment in immune mice. *Parasitol. Immunol.* 11, 319–328
14 Rumjanek, F.D. (1987) in *Biochemistry and Physiology in the Biology of Schistosomes, from Genes to Latrines* (Rollinson, D. and Simpson, A.J., eds), pp 163–183, Academic Press
15 Xiao, S-H. *et al.* (1984) Praziquantel induced vesicle formation in the tegument of male *Schistosoma mansoni* is calcium dependent. *J. Parasitol.* 70, 177–179
16 Modha, J. *et al.* (1990) Immune dependence of schistosomicidal chemotherapy: an ultrastructural study of *Schistosoma mansoni* adult worms exposed to praziquantel and immune serum *in vivo*. *Parasitol. Immunol.* 12, 321–324
17 Vial, H.J. (1985) Renewel of the membrane complex of *Schistosoma mansoni* is closely associated with lipid metabolism. *Mol. Biochem. Parasitol.* 17, 203–218
18 Lima, S. *et al.* (1994) Effects of culture and praziquantel on membrane fluidity parameters of adult *Schistosoma mansoni*. *Parasitology* 109, 57–65
19 Mehlhorn, H. *et al.* (1981) *In vivo* and *in vitro* experiments on the effect of praziquantel on *Schistosoma mansoni*: a light and electron microscopic study. *Arzneimittel Forschung* 31, 344–354
20 Pax, R.A. *et al.* (1984) *Schistosoma mansoni*: differences in acetylcholine, dopamine and serotonin control of circular and longitudinal parasite muscles. *Exp. Parasitol.* 58, 314–324
21 Fetterer, R.H. *et al.* (1980) *Schistosoma mansoni*: characterization of the electrical potential from the tegument of adult males. *Exp. Parasitol.* 49, 353–365
22 Wolde-Mussie, E. *et al.* (1982) *Schistosoma mansoni*: calcium efflux and the effects of calcium-free media on the responses of the adult male musculature to praziquantel and other agants inducing contraction. *Exp. Parasitol.* 53, 270–278
23 Pax, R.A. *et al.* (1979) Effects of fluoxetine and imipramine on male *Schistosoma mansoni*. *Comp. Biochem. Physiol.* 64, 123–126
24 Blair, K.L. *et al.* (1994) *Schistosoma mansoni*: myogenic characteristics of phorbol ester induced muscle contraction. *Exp. Parasitol.* 78, 302–316
25 Thompson, D.P. *et al.* (1982) Microelectrode studies of the tegument and subtegumental compartments of the male *Schistosoma mansoni*: an analysis of electrophysiological properties. *Parasitology* 85, 163–178
26 Silk, M.A. and Spence, I.M. (1969) Ultrastructural studies of the blood fluke *Schistosoma mansoni*. III. The nervous tissue and sensory structures. *S. A. J. Med. Sci.* 34, 11–20
27 Kostyuk, P. and Verkhratsky, A. (1994) Calcium store in neurons and glia. *Neurosci.* 63, 381–404
28 Bricker, C.S. *et al.* (1983) The relationship between tegumental disruption and muscle contraction in *Schistosoma mansoni* exposed to various compounds. *Z. Parasitenkunde* 69, 61–71
29 Harnett, W. and Kusel, J.R. (1986) Increased exposure of parasite antigens at the surface of adult male *Schistosoma mansoni* exposed to praziquantel *in vitro*. *Parasitology* 93, 401–405
30 Brindley, P.J. and Sher, A. (1987) The chemotherapeutic effect of praziquantel against *Schistosoma mansoni* is dependent on host antibody response. *J. Immunol.* 136, 215–220
31 Doenhoff, M. *et al.* (1987) Evidence for an immune-dependent action of praziquantel on *Schistosoma mansoni* in mice. *Trans. R. Soc. Trop. Med. Hyg.* 81, 947–951
32 Fallon, P.G. *et al.* (1992) Immune-dependent chemotherapy of schistosomiasis. *Parasitology* 105, S41–S48
33 Doenhoff, M. *et al.* (1988) Anti-schistosome chemotherapy enhanced by antibodies specific for a parasite esterase. *Immunology* 65, 507–510
34 Brindley, P.J. *et al.* (1989) Role of the host antibody in the chemotherapeutic action of praziquantel against *Schistosoma mansoni*: identification of target antigens. *Mol. Biochem. Parasitol.* 34, 99–108
35 Tanaka, T. *et al.* (1993) *Schistosoma*: a 200 kDa chemotherapeutic target antigen is differentially localized in African vs Oriental species. *Exp. Parasitol.* 76, 293–301
36 Fallon, P.G. *et al.* (1994) Quantification of praziquantel-induced damage on the surface of adult *Schistosoma mansoni* worms: estimation of esterase and alkaline phosphatase activity. *Parasitol. Res.* 80, 623–625
37 Linder, E. and Thors, C. (1992) *Schistosoma mansoni*: praziquantel-induced tegumental lesion exposes actin of surface spines and allows binding of actin depolarizing factor gelsolin. *Parasitology* 105, 71–78
38 Koster, B. and Strand, M. (1994) *Schistosoma mansoni*, immunolocalization of 2 different fucose-containing carbohydrate epitopes. *Parasitology* 108, 433–446
39 Camacho, M. *et al.* (1995) Nicotinic acetylcholine receptors on the surface of the blood fluke *Schistosoma mansoni*. *Mol. Biochem. Parasitol.* 71, 127–134
40 Lima, S. *et al.* (1994) Altered behaviour of carbohydrate-bound molecules and lipids in areas of the tegument of adult *Schistosoma mansoni* worms damaged by praziquantel. *Parasitology* 109, 469–477
41 McLaren, D. (1980) in *Schistosoma mansoni: the Parasite Surface in Relation to Host Immunity* (Brown, K.N., ed.), pp 1–27, Research Studies Press
42 Espinoza, B. *et al.* (1991) Acetylcholinesterase from *Schistosoma mansoni*: immunological characterization. *Immunol. Lett.* 28, 167–174
43 Sauma, S. and Strand, M. (1990) Identification and characterisation of glycosylphosphatidylinositol-linked *Schistosoma mansoni* adult worm immunogens. *Mol. Biochem. Parasitol.* 38, 199–210
44 Espinoza, B. *et al.* (1991) Phosphatidylinositol-specific phospholipase C induces biosynthesis of acetylcholinesterase via diacylglycerol in *Schistosoma mansoni*. *Eur. J. Biochem.* 195, 863–870
45 Cioli, D. *et al.* (1993) Drug resistance in schistosomes. *Parasitology Today* 9, 162–166
46 Hawn, T.R. and Strand, M. (1993) Detection and partial characterization of glycophosphatidylinositol-specific phospholipase activities from *Fasciola hepatica* and *Schistosoma mansoni*. *Mol. Biochem. Parasitol.* 59, 73–82
47 Fallon, P.G. and Doenhoff, M.J. (1994) Drug-resistant schistosomiasis: resistance to praziquantel and oxamniqine induced in *Schistosoma mansoni* in mice is drug specific. *Am. J. Trop. Med. Hyg.* 51, 83–88
48 Mayor, S. *et al.* (1994) Sequestration of glycosylphosphatidylinositol-anchored proteins in caveolae triggered by crosslinking. *Science* 264, 1948–1951
49 Ferguson, M.A.J. (1994) What can GPI do for you? *Parasitology Today* 10, 48–52
50 Low, M.G. and Huang, K.S. (1991) Factors affecting the ability of glycosylphosphatidylinositol-specific phospholipase D to degrade membrane anchors of cell surface proteins. *Biochem. J.* 279, 483–493
51 Wiest, P.M. *et al.* (1992) *Schistosoma mansoni*: characterization of phosphoinositide response. *Exp. Parasitol.* 74, 38–45
52 Sugiya, H. and Furuyama, S. (1990) Sphingosine increases inositol triphosphate in rat parotid acinar-cells by a mechanism that is independent of protein kinase C but dependent on extracellular calcium. *Cell Calcium* 11, 469–475
53 Berridge, M.J. and Irvine, R.F. (1984) Inositol triphosphate, a novel second messenger in cellular signalling transduction. *Nature* 312, 315
54 Hosey, M.M. and Lazdunski, M. (1988) Calcium channels: molecular pharmacology, structure and regulation. *J. Membr. Biol.* 104, 81–105
55 Somlyo, A.P. and Somlyo, A.V. (1994) Signal transduction and regulation in smooth muscle. *Nature* 372, 231–236
56 McCray, J.A. and Trentham, D.R. (1989) Properties and uses of photoreactive compounds. *Annu. Rev. Biophys. Biophys. Chem.* 18, 239–270
57 Sands, W. and Kusel, J.R. (1992) Changes in the lateral diffusion

of fluorescent lipid analogues in the surface membrane of adult male *Schistosoma mansoni*. *Mol. Biochem. Parasitol.* 53, 233–242

Dixon, D.M. and Martin, R.J. (1993) Patch clamp and chloride channels in *Ascaris suum*. *Parasitology Today* 9, 341–344

Foley, M. et al. (1994) Photoaffinity labelling of chloroquine-binding proteins in *Plasmodium falciparum*. *J. Biol. Chem.* 269, 9655–9661

Harder, A. et al. (1985) Influence of praziquantel and Ca^{2+} on the bilayer-isotropic-hexagonal transition of model membranes. *Mol. Biochem. Parasitol.* 14, 55–69

Cully, D.F. et al. (1994) Cloning of an avermectin-sensitive glutamate-gated chloride channel from *Caenorhabditis elegans*. *Nature* 371, 707–711

McTigue, M.A. et al. (1995) Crystal structure of a schistosomal drug and vaccine target: glutathione-S-transferase from *Schistosoma japonica* and its complex with the leading antischistosomal drug Praziquantel. *J. Mol. Biol.* 246, 21–27

Electrophysiology of *Ascaris* muscle and anti-nematodal drug action

R. J. MARTIN, M. A. VALKANOV, V. M. E. DALE, A. P. ROBERTSON *and* I. MURRAY

Department of Preclinical Veterinary Sciences, R.(D.)S.V.S., Summerhall, University of Edinburgh, Edinburgh, EH9 1QH, UK

SUMMARY

Three groups of anthelmintic drugs act directly and selectively on muscle membrane receptors of parasitic nematodes. These groups of anthelmintics are: (1) *The Nicotinic Agonists* (levamisole, pyrantel, morantel and oxantel) that act on acetylcholine receptors of nematode somatic muscle; (2) *The GABA Agonist*, piperazine, that acts on nematode muscle GABA receptors; and (3) *The Avermectins* that open glutamate gated Cl^- channels on nematode pharyngeal muscle. The electrophysiology and pharmacology of muscle and neuromuscular transmission the nematode parasite, *Ascaris suum*, is outlined and effects of anthelmintics that interfere with transmission described. Resistance to anthelmintics has appeared in some parasitic nematodes but the mechanisms of this resistance remain to be determined.

Key words: Electrophysiology, *Ascaris suum*, muscle, pharynx, levamisole, pyrantel, morantel, oxantel, piperazine, milbemycin, avermectins.

INTRODUCTION

One nematode parasite that is often used to study the mode of action of anthelmintic drugs is *Ascaris suum*, a large 30 cm nematode that can be recovered from the intestine of pigs. It has the advantage that it can be collected from the abattoir on a weekly basis and maintained in a warm saline solution for about five days. The large size of its muscle and nerve cells means that it is amenable to electrophysiological study. The electrophysiological actions of a number of anthelmintics, like levamisole, piperazine and avermectins have been studied using preparations from *Ascaris*.

This account outlines the electrophysiology and pharmacology of neuromuscular transmission in *Ascaris* and describes effects of anthelmintic drugs that act on its ion-channels.

THE ANATOMY AND PHYSIOLOGY OF THE SOMATIC NEUROMUSCULAR SYSTEM OF *ASCARIS*

The nervous system

Goldshmidt (1908; 1909) recognized that there were only a small number of neurones present in *Ascaris* (about 250) and found that these neurones have the same structure and position in each animal. A similar organization is found throughout nematodes (White *et al.* 1976, 1986).

There are two main nerve cords that originate from a cranial pharyngeal nerve ring and run along the length of the body: the dorsal nerve cord and the ventral nerve cord (Fig. 1A). The cell bodies of all motor neurones are found in the ventral nerve cord and communicate with the dorsal nerve cord via commissures that contain one or two motor neurone axons, Fig. 1B.

The anatomy of the motorneurone system has been examined by Stretton *et al.* (1978). The commissures connecting the dorsal and ventral nerve cords form a pattern which repeats itself along the length of the body. The pattern consists of three right hand commissures and one left hand commissure; this pattern is used to define a segment. Fig. 1B illustrates one segment: there are 11 motor neurones present in the segment. In addition to the motorneurones, there are also interneurones present in the nerve cords. The 11 motorneurones of each segment are divided into 7 anatomical types according to the distribution of their axons and dendrites. Three of the motorneurones (DI, DE2 and DE3) occur only once in each segment, but the other four types (DE1, VI, V1 and V2) occur twice in each segment.

The physiological role of each type of the motorneurone was also determined by Stretton *et al.* (1978) by selective electrical stimulation of single motorneurones and recording of the response in the muscle field of the motorneurone. This study showed that DI and VI were inhibitory and the DE1, DE2, DE3, V1 and V2 were, or were likely to be, excitatory.

Subsequently, histochemical studies demonstrated the presence of the enzyme choline acetyltransferase in the axons of DE1, DE2, DE3, V1 and V2, further supporting the view that acetylcholine is the excitatory transmitter in these neurones (Johnson & Stretton, 1985). Histochemical techniques have

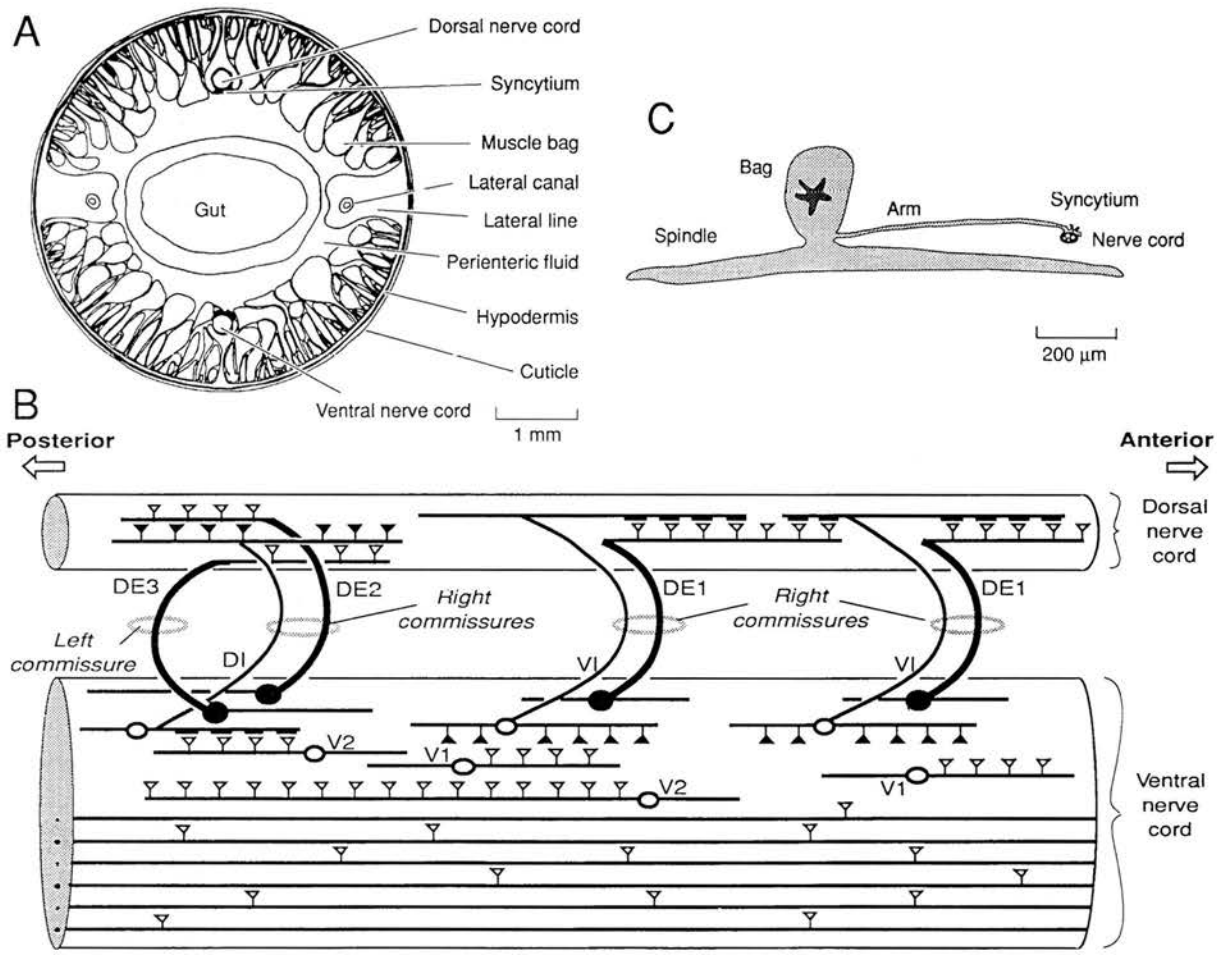

Fig. 1. Diagrams of the somatic neuromuscular structures of *Ascaris suum*. (A) Cross section through the anterior body wall. (B) Diagram of the anatomical organization of the dorsal and ventral nerve cord in one 'segment' of *Ascaris*. 11 motorneurones are present in each segment. 6 large interneurones run the length of the ventral cord. There are 7 anatomical types of motorneurones: dorsal excitatory, DE1, DE2 & DE3; dorsal inhibitory, DI; ventral inhibitory, VI; ventral excitatory, V1 & V2. All cell bodies of the motorneurones are in the ventral cord. (C) Diagram of the structure of a somatic muscle cell and the location of the neuromuscular junction at the syncytium.

also demonstrated GABA-immunoreactivity in the motor neurones, DI and VI (Johnson & Stretton, 1987; Guastella, Johnson & Stretton, 1991; Guastella & Stretton, 1991), a finding that is consistent with GABA being the inhibitory transmitter. In addition to the transmitters acetylcholine and GABA, it is likely that co-transmitters are also present in the motorneurones (Stretton *et al.* 1991). The most abundant are immunologically similar to FMRFamide. A number of these have been isolated from *Ascaris* and have been characterized (Stretton *et al.* 1991), the first was named AF1, *Ascaris* FMRFamide-like 1 (Cowden, Stretton & Davis, 1989), the second was named AF2 (Cowden & Stretton, 1993).

The anatomy of somatic muscle

Schneider (1895) was one of the earliest to describe the body muscle of *Ascaris* but the peculiar structure of the muscle cells with processes of the muscle cell passing to the nervous system rather than a process of the nervous system passing to the muscle cell meant that there was considerable debate about this between the early scientists (Goldschmidt, 1908, 1909; Cappe de Baillon, 1911).

Fig. 1A & C shows the location and structure of *Ascaris* somatic muscle cells. Each cell is composed of: (1) the contractile spindle region which lies under the hypodermis; (2) the enlarged balloon-shaped structure which contains the nucleus and many glycogen granules and is referred to as the bag region; (3) the arm which usually arises at the base of the bag region and which is a thin process that passes from the muscle cell to the syncytium where it breaks up into a number of fine processes known as fingers. The neuromuscular junctions are formed between the longitudinal axons of the motorneurones and the syncytium by extensions of the longitudinal axons that break through the hypodermal chalice to approach the syncytium (Rosenbluth, 1965). There are two types of synaptic vesicles: 40 nM clear vesicles, clustered around the presynaptic membrane and dense-cored vesicles that are 80–100 nM in

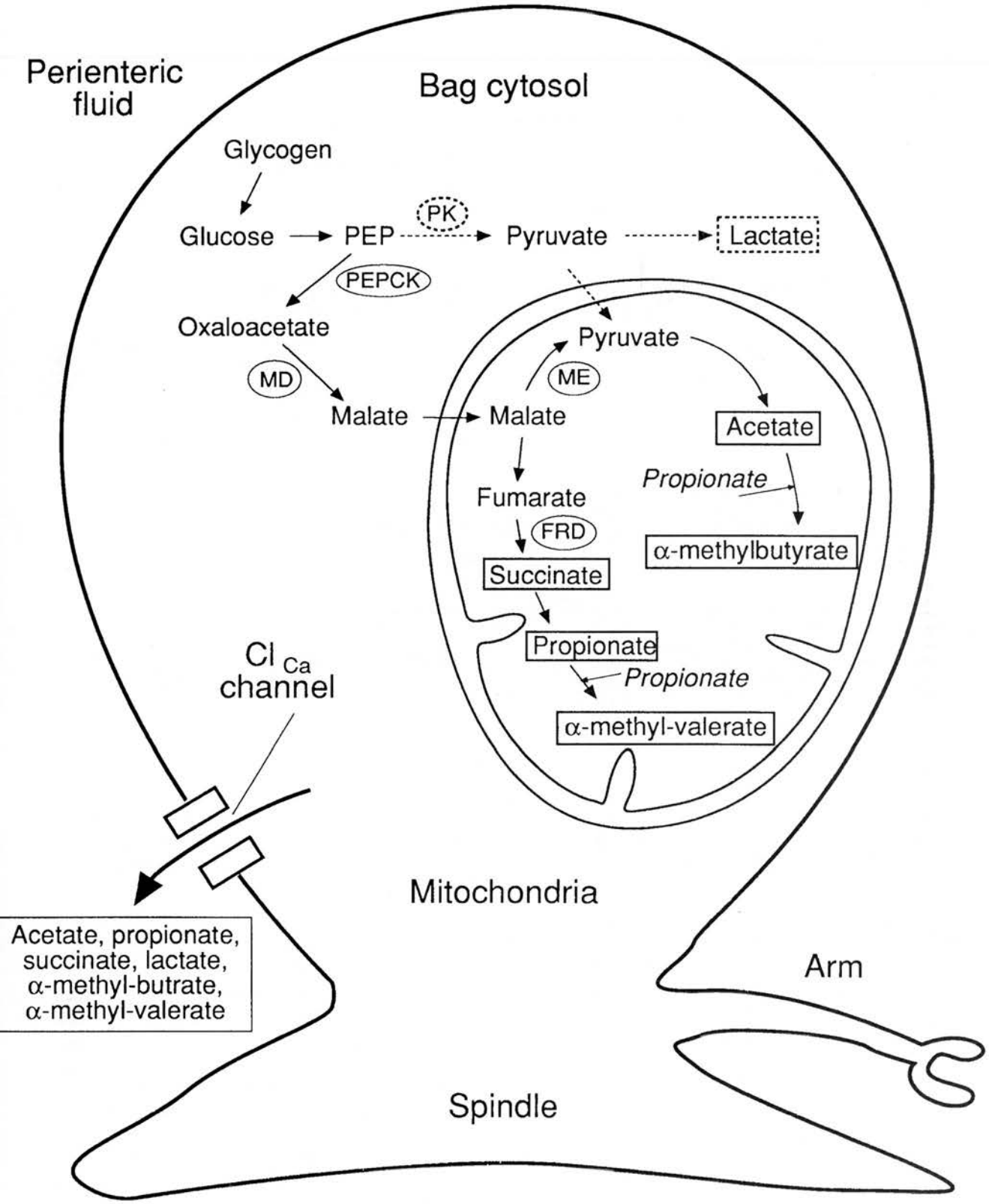

Fig. 2. Diagram of the breakdown pathway of glycogen in the cytoplasm and mitochondria in *Ascaris*. The end-products like succinate, propionate, acetate, α-methylbutyrate, α–methyl valerate are shown in a rectangular box outside the cell in the perienteric fluid and in a rectangular box at the original site of their production. PEP, phosho-enol pyruvate; PK, pyruvate kinase; PEPCK, phosho-enol pyruvate carboxy kinase; MD, malate dehydrogenase; ME, malic enzyme; FRD, fumarate reductase. The pathway outlined by the dashed arrows is absent or only present at a low level. One route for excretion through the muscle membrane is through the Ca^{2+}-activated Cl^- channel.

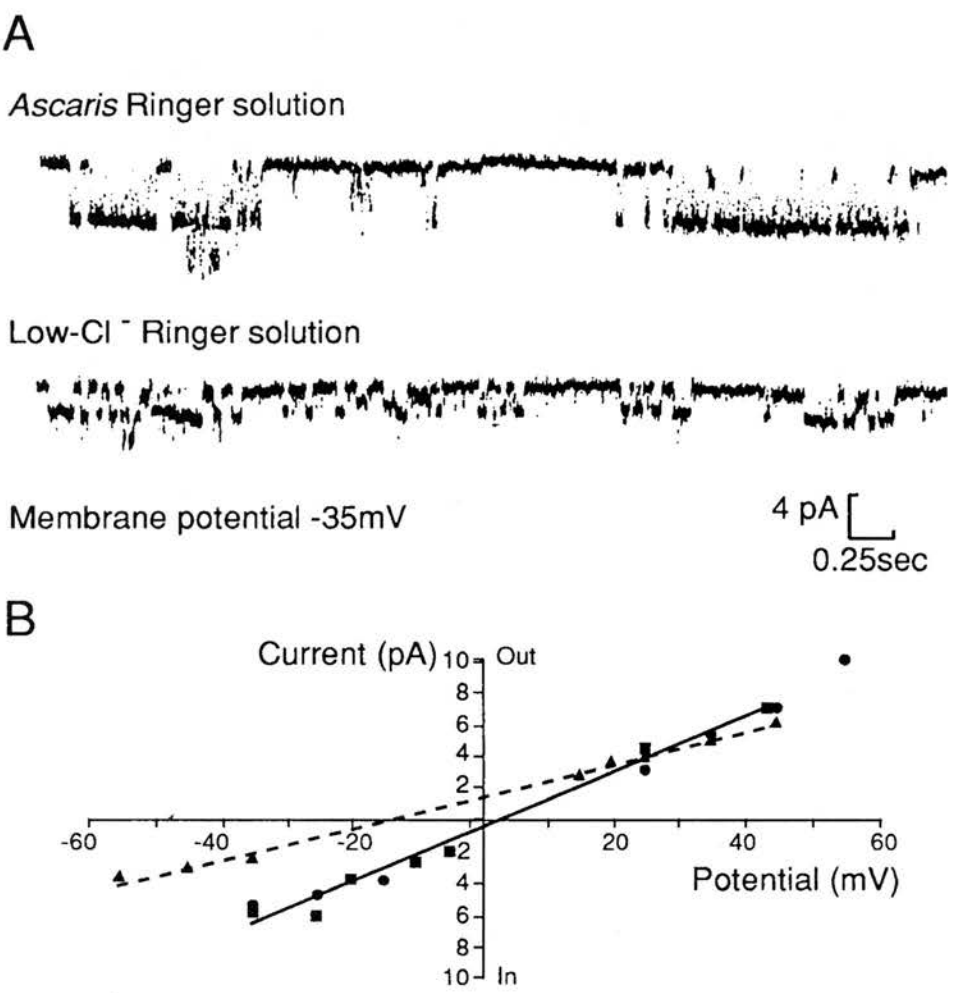

Fig. 3. Ca^{2+}-activated Cl^- channel currents recorded in an isolated inside-out patch. (A) The top trace shows a recording at −35 mV in the presence of symmetrical Cl^- solutions; the lower trace shows channel currents recorded from the same patch and at the same membrane potential but after replacing the bath solution with a low-Cl^- solution. (B) the I/V plot shows the relationship between current amplitude and voltage in symmetrical Cl^- (▲) and in the presence of reduced bath-Cl^- (■ & ●). The reduced Cl^- causes a hyperpolarizing shift in the zero current potential and a reduction in the slope conductance of the channel. It shows that the channel conducts Cl^-.

diameter. Apart from regions in the head of *Ascaris*, only the dorsal muscles are connected to the dorsal nerve cord and only the ventral muscle is connected to the ventral nerve cord. This arrangement is a reflection of the fact that muscle contraction is only possible in the dorsal-ventral plane and that the dorsal muscle contracts while the ventral muscle relaxes and *vice versa*.

ELECTROPHYSIOLOGY OF SOMATIC MUSCLE

Membrane potential

Intracellular records of the membrane potential of *Ascaris* were made soon after the development of glass micropipettes (Jarman, 1959); he described a resting potential of about −30 mV on which was superimposed regular spike-like depolarizations. The ionic basis of the resting membrane potential was then investigated by Del Castillo, de Mello & Morales (1964) and Brading & Caldwell (1971). Both of these studies concluded that extracellular K^+ had little effect on potential in contrast to the effect of Cl^-. Brading & Caldwell (1971) suggested that an active pump, possibly moving carboxylic acids across the membrane, might explain the behaviour of the membrane potential.

Permeability of Ca^{2+}-dependent Cl^- channels in the bag membrane and excretion of organic anions

The composition of the peri-enteric fluid, that surrounds the *Ascaris* muscle cells, has been examined by Hobson *et al.*, (1952*a*, *b*); Saz & Weil (1962); Tsang & Saz (1973). They showed that the peri-enteric fluid contains low concentrations of Cl^- but high concentrations of carboxylic acids (acetate, propionate, succinate, 2-methylbutyrate and 2-methylvalerate) that are produced inside the muscle cells from anaerobic fermentation of glucose (Fig. 2).

The bag membrane has been shown to contain a high density of Ca^{2+}-dependent Cl^- channels that have conductances of 100–200 pS (Fig. 3; Martin

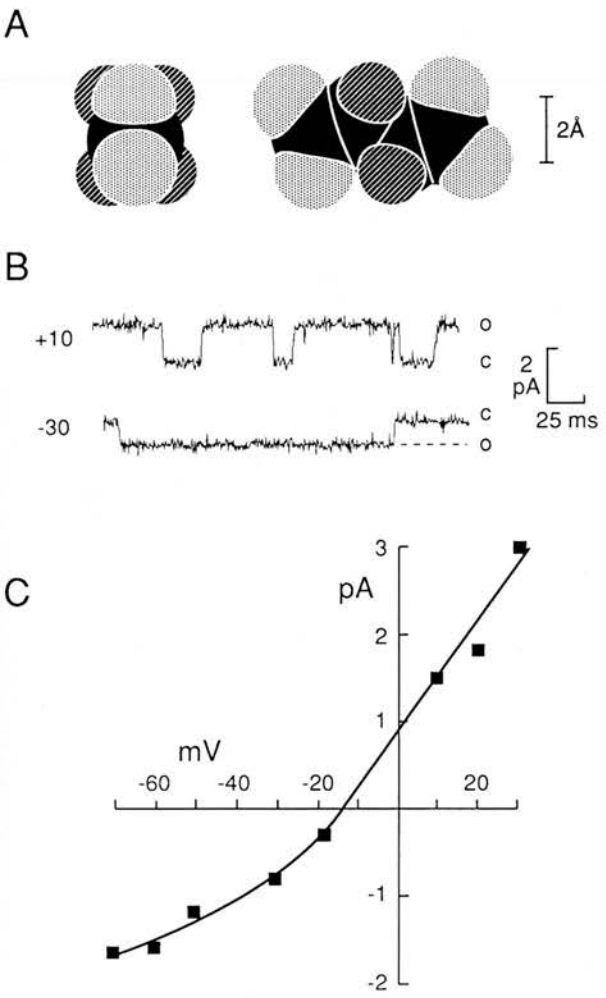

Fig. 4. (A) Space-filling model of the end view and side view of succinate. (B) Isolated inside-out channel currents recorded with 140 mM Cl^- as the anion in the patch-pipette (at the extracellular surface of the membrane) and 140 mM succinate in the bath (at the cytoplasmic surface of the membrane). (C) I/V plot of the channel current amplitudes showing the zero current potential to be −15 mV. Note that succinate is able to carry current when the patch is sufficiently hyperpolarized. Such currents demonstrate permeability of succinate through the channel.

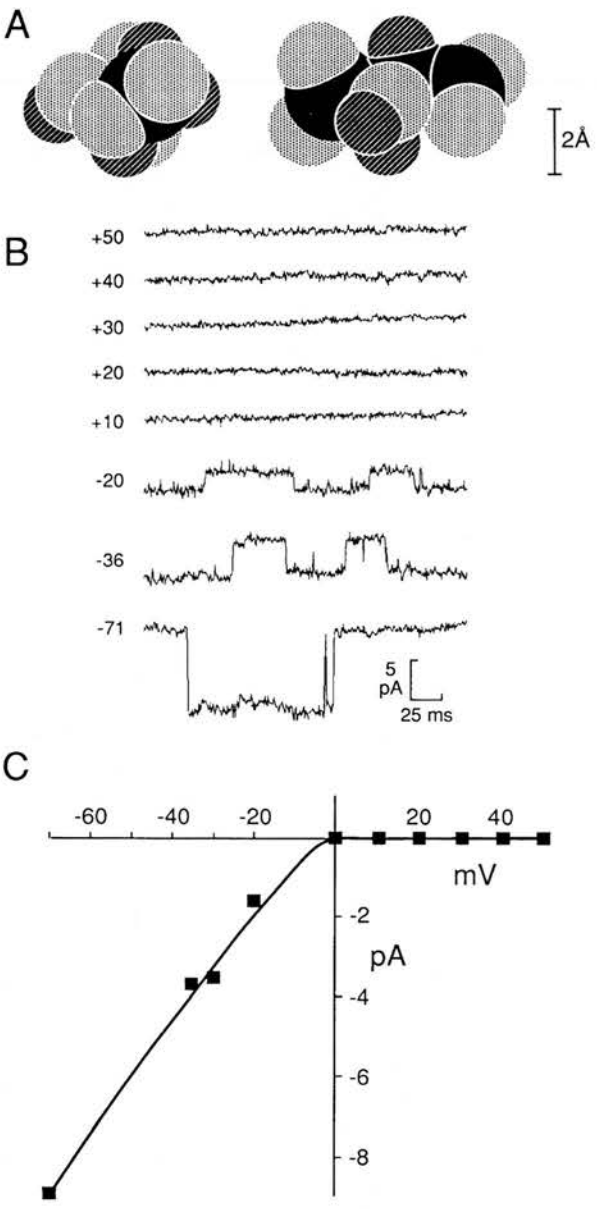

Fig. 5. (A) Space-filling model of the end view and side view of malate. (B) Isolated inside-out channel currents recorded with 140 mM malate as the anion in the patch-pipette (at the extracellular membrane surface) and 140 mM Cl^- in the bath (on the cytoplasmic surface of the membrane). (C) I/V plot of the channel current amplitudes. Note that malate is not able to carry current when the patch is depolarized. The lack of a malate currents at positive potentials demonstrates that malate does not permeate the channel.

et al. 1992). The density of these channels suggests that they are major contributors to the membrane potential. We have examined the permeability properties of this channel using single channel recording techniques (Valkanov, Martin & Dixon, 1994; Martin & Valkanov, 1995; Valkanov & Martin, 1995). The channel is a non-selective anion channel permeable to simple monocarboxylic anions (acetate to heptanoate, including α-methylbutyrate) with a pore diameter of around 6.5Å. We suggested as a result of these studies that the Ca^{2+}-dependent Cl^- channel could be involved in the excretion of carboxylic anions across the bag membrane and that the resting membrane potential, −30 mV, would facilitate the concentration of organic acids outside the cell membrane. The proposed mechanism for excretion of carboxylic acids does not require any specific carrier system for the organic anions. It would, however, require some active excretion of protons or a counter anion to prevent the loss of potential as the organic anion is excreted.

As a further test of this hypothesis, we have examined the permeability of the channel to the dicarboxylic anions: succinate, oxaloacetate and malate (Valkanov & Martin, 1995). Succinate is a major anion which is excreted from the muscle cell

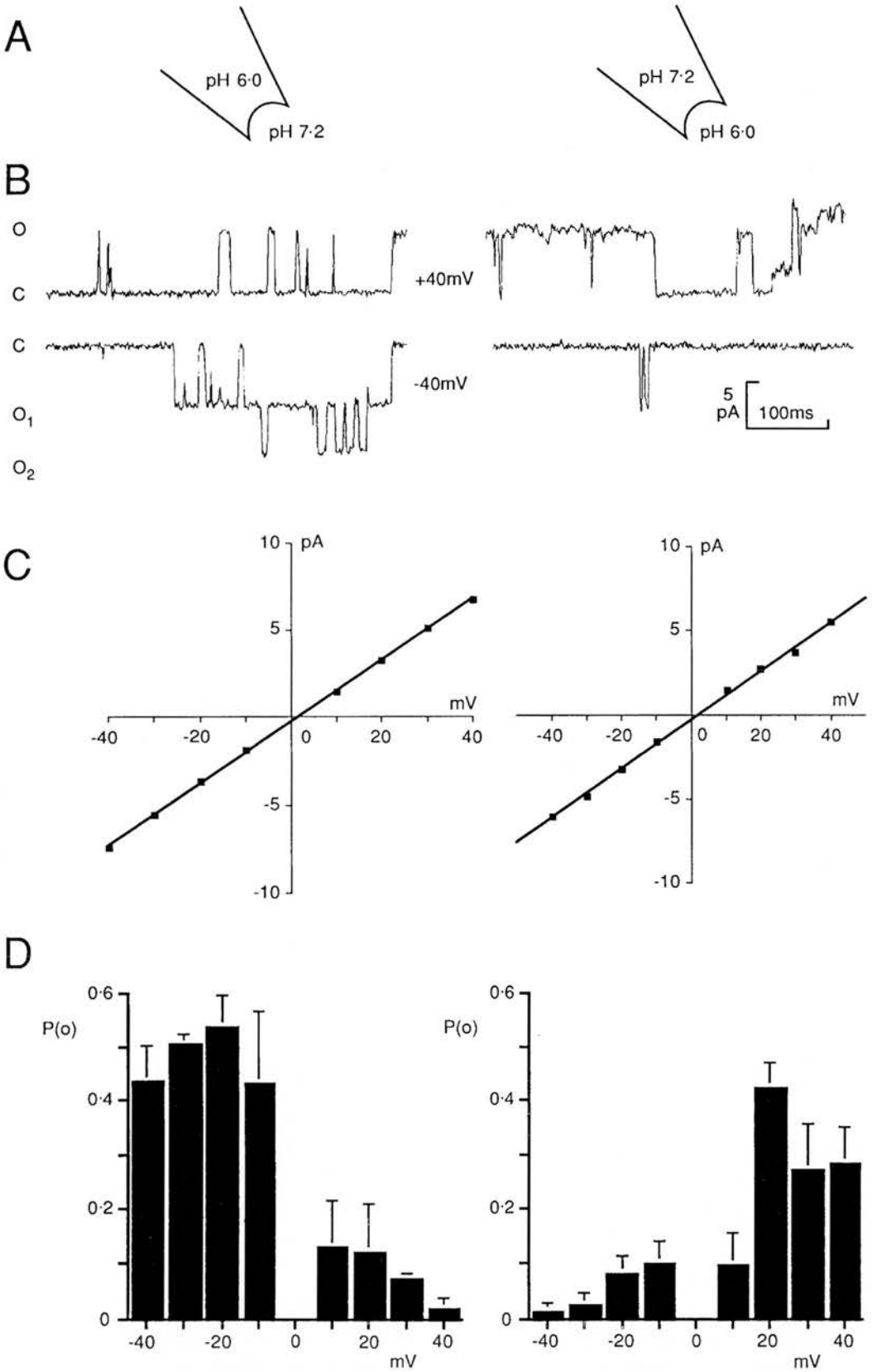

Fig. 6. Effect of reduced pH at the extracellular surface (right column of illustrations) and reduced pH at the cytoplasmic surface of the membrane (left column of illustrations). (A) Cartoon of the inside-out patch recording and the pH arrangement. (B) Representative traces of channel currents at +40 mV and −40 mV. (C) I/V plots of the channel currents. (D) Histogram of the probability of the channel being open at the different membrane potentials. Reduction of the extracellular pH had little effect on single channel conductance or on the effect of membrane potential on probability of opening and was similar to recordings made in symmetrical pH 7·2 (not shown). A

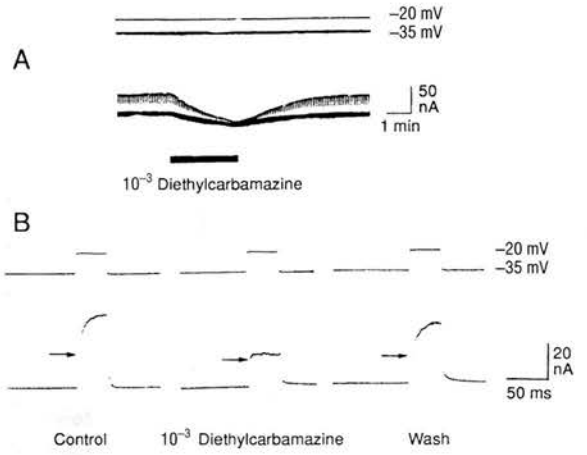

Fig. 7. Effect of diethylcarbamazine on the voltage-activated outward current of *Ascaris* muscle cells. (A) low time resolution recording; top, voltage steps to −20 mV from a holding potential of −35 mV; horizontal bar indicates the time of application of the diethylcarbamazine. (B) high-time resolution of the same events.

and it accumulates in the peri-enteric fluid. Malate and oxaloacetate are also produced in muscle cytoplasm during glucose fermentation but they are not excreted and do not accumulate in the peri-enteric fluid. If malate or oxaloacetate were to leak out of the cell then there would be a considerable energy drain on the cell. In addition, we have also examined the permeability of the monocarboxylic acids lactate and pyruvate.

Fig. 4 illustrates the currents that were recorded through the channel with succinate as the anion on the inside of the ion-channel and Cl^- on the outside of the channel; Fig. 5 illustrates the current recorded when malate was the anion on the outside of the membrane. From the reversal potentials, it is possible to determine the permeability of the test anion relative to Cl^- using the Goldman Constant field equation. It was found that all of the anions tested had a measurable permeability, but that only malate did not carry current through the channel. In *Ascaris*, the sarcoplasmic concentration of succinate and malate but not oxaloacetate, lactate or pyruvate may be significantly high (Tielens, 1994) because of activities of the intermediate enzymes. For example, activity of malate dehydrogenase is high so that oxaloacetate concentrations in the cytoplasm are low. The properties of the channel, conducting monovalent anions with a Stokes diameter less the 6.5Å and conducting succinate but not malate would permit excretion of acetate, propionate, succinate and α-methylbutyrate but not malate. Oxaloacetate, lactate, and pyruvate are not normally excreted in *Ascaris* and this may be explained by their low sarcoplasmic concentrations in *Ascaris*.

Because of the possible correlations between the activities of the Ca^{2+}-activated Cl^- channel and pH, we chose to investigate the effect of pH on the activity of the channel (Robertson & Martin, 1996). Fig. 6 shows the effect on channel opening of reducing the pH on the cytoplasmic surface of the channel. An increase in H^+ concentration inside the muscle cell has no effect on the conductance of the channel but the probability that the channel is open and the effect of membrane potential has reversed in polarity are seen. This means that at the normal resting membrane potential of the bag, −35 mV, the channel opens less often when the intracellular pH is more acid and opens more when the intracellular pH is alkaline. It means that if there is a proton pump excluding H^+ ions from the cell and increasing intracellular pH, the channel will open more frequently. Such a mechanism may be involved in the excretion of the carboxylic acid products of glucose metabolism.

Depolarizing potentials

The spontaneous depolarizing potentials that were first observed by Jarman (1959) were found to be myogenic in origin and appeared to arise from the syncytium (De Bell, Del Castillo & Sanchez, 1963; De Bell, 1965). Three types of depolarizing potential have been distinguished by Weisblat & Russel (1976): (1) spikes of varying amplitude but up to 30 mV and 5–50 ms duration; (2) slow waves up to 20 mV in amplitude and lasting 100–100 ms; (3) a long lasting modulation wave up to 5 mV in amplitude, lasting 3–20 sec and associated with contraction.

The electrical activity of the adjacent muscle cell is correlated and is explained by electrical coupling due to tight junctions between muscle cell (De Bell *et al.* 1963; Rosenbluth, 1965; Del Castillo *et al.* 1989). The coupling allows adjacent muscle cells to synchronize depolarization and contraction.

The ionic basis of the spike potentials and slow-waves has been investigated using ion-substitution experiments by Weisblat, Byerly & Russel, (1976). It was found that Ca^{2+} was required to support the spikes but that Na^+ or Ca^{2+} was required for the slow waves. The currents responsible for spike potentials have been recorded by us using a two microelectrode voltage-clamp technique (Martin *et al.* 1992). Depolarization of the bag membrane results in ac-

reduced intracellular pH had a dramatic effect on the membrane potential-probability of opening relationship and reversed the direction of its voltage sensitivity. The results were interpreted to indicate that the voltage-sensitive gate was pH sensitive and was accessible to protons from the cytoplasmic surface.

Table 1. Single-channel conductances, mean open-times, and probability of being open of the channels activated by nicotinic anthelmintics

Compound	Concentration (μM)	Conductance levels (pS)	Mean open-times (ms) at −75 mV	P open at −75 mV
Acetylcholine	1–10	25–35 & 40–50	1·96	0·03
Pyrantel	0·1–10	22 & 47	1·73	0·0057
Levamisole	1–10	19–46	1·47	0·0052
Oxantel	10	33·7	1·34	0·0014
Morantel	6	30 & 40	1·57	0·0076

tivation of an inward Ca^{2+} current and voltage-activated outward currents. Interestingly, part of the outward current may be blocked by 4-aminopyridine and by the anthelmintic diethylcarbamazine Fig. 7A and B (Martin, 1982).

ACETYLCHOLINE

Ascaris *muscle has acetylcholine receptors*

Baldwin & Moyle (1949) and then Norton & De Beer (1957) showed that bath application of acetylcholine produces contraction of *Ascaris* muscle strips, and they demonstrated the presence of acetylcholine receptors on muscle. Del Castillo, De Mello & Sanchez (1963) showed that the electrophysiological effect of acetylcholine was to produce depolarization and changes in spike frequency and amplitude. Originally it was reported by Del Castillo *et al.* (1963) that the acetylcholine receptors were only located at the syncytium region, but it was later shown, using focal application by ionophoresis, that there are also extrasynaptic nicotinic acetylcholine receptors located on the bag region of the muscle (Martin, 1982).

These extra-receptors on the bag region of the muscle were shown to be nicotinic since they were blocked by tubocurarine (Martin, 1982). Under voltage-clamp, ionophoresis of acetylcholine produces a current that has a reversal potential near 0 mV indicating that the acetylcholine nicotinic receptors are non-selective cation channels permeable to Na^+ and Ca^{2+} (Martin, 1982; Harrow & Gration, 1985).

The patch-clamp technique has allowed single-channel currents activated by acetylcholine to be recorded using a vesicle preparation of the bag membrane (Pennington & Martin, 1990). The channels have at least two conductance levels, the main conductance is 40–50 pS and a smaller conductance is 25–30 pS. The mean open-times are around 2 ms (Table 1).

Pharmacology of the Ascaris *nicotinic acetylcholine receptor*

Membrane potential or contraction responses of *Ascaris* muscle to acetylcholine are blocked by tubocurarine but not atropine, so the acetylcholine receptors have been classified as nicotinic (Natoff, 1969; Rozhova, Malyutina & Shishov, 1980; Colquhoun, Holden-Dye & Walker, 1991). Further sub-classification of the receptor, on the basis of agonists potencies, suggests that the *Ascaris* receptor is pharmacologically similar to vertebrate ganglionic nicotinic receptors, but this sub-classification does not hold up when potencies of other nicotinic antagonists are examined. Mecamylamine, a ganglionic nicotinic antagonist and benzoquinonium, a neuromuscular nicotinic receptor antagonist, are both potent antagonists; the ganglionic antagonist hexamethonium and the neuromuscular nicotinic receptor antagonists, decamethonium and pancuronium are all weak antagonists. The detailed pharmacology of the *Ascaris* nicotinic receptor therefore differs from that of vertebrate nicotinic receptors. The nematode nicotinic receptor is best thought of as having its own (nematode) subtype (e.g. $nACh_n$ receptors). The selective agonist levamisole can be exploited therapeutically: it acts potently and selectively on the nematode nicotinic acetylcholine receptors but does not have potent effects on the nicotinic receptors of the host.

The nicotinic anthelmintics

Fig. 8 shows the chemical structure of the nicotinic anthelmintics. These are the imidazothiazoles (levamisole and butamisole); the tetrahydropyrimidines (pyrantel, morantel and oxantel), the quaternary ammonium salts (bephenium and thenium), and the pyrimidines (methyridine). These compounds act as a agonists at nicotinic acetylcholine receptors of nematodes. Insoluble salts of pyrantel, morantel and oxantel are sold as oral preparations to prevent the active agent from leaving the gut and to minimize toxic effects on host receptors. They are therefore used against gastro-intestinal nematodes. Levamisole has less effect on host nicotinic receptors, and being partially unionized is well distributed in the host's body following oral administration or injection. Levamisole may be used to treat gastro-intestinal worms as well as lung worms. The electrophysiological effects of levamisole, pyrantel,

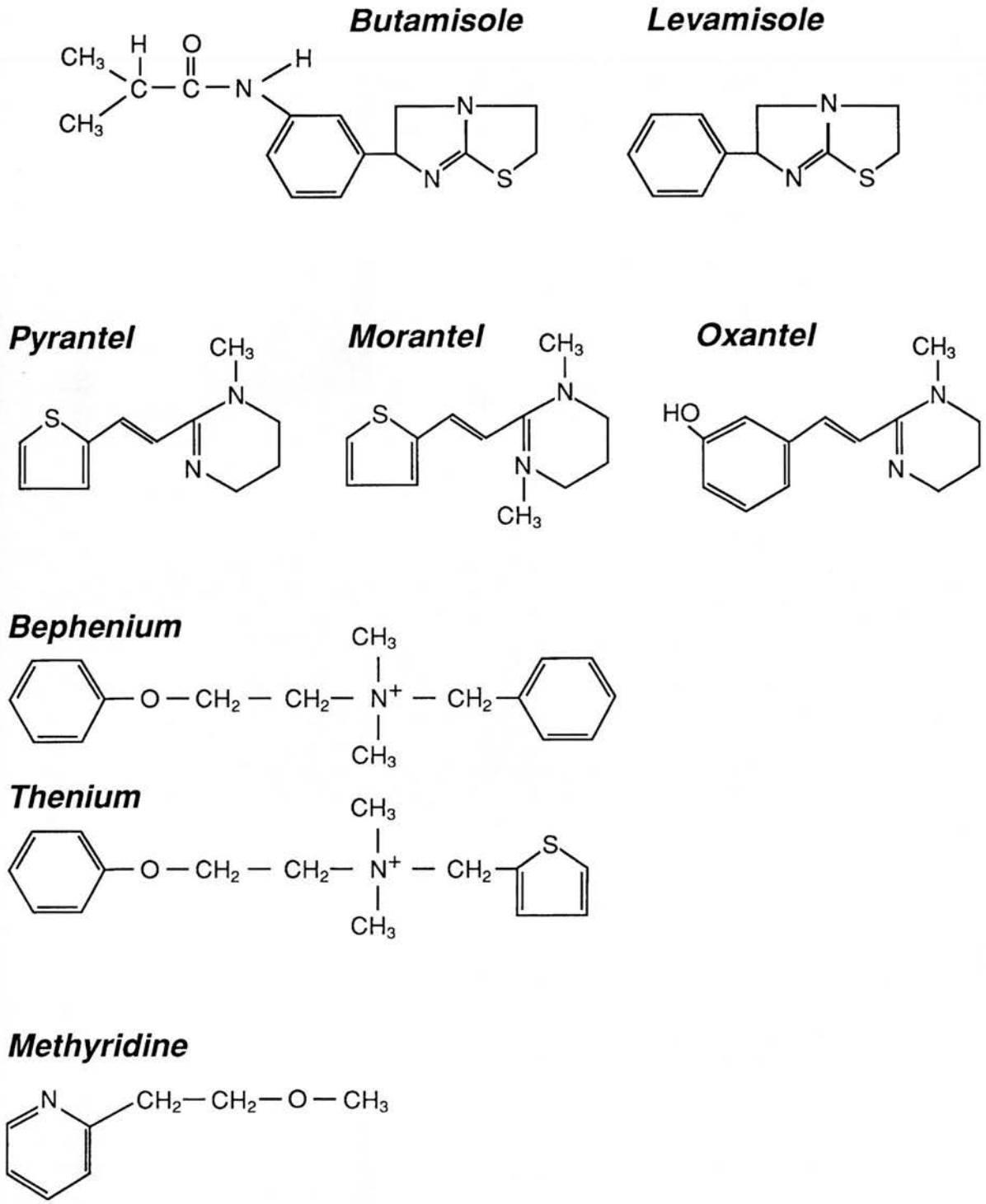

Fig. 8. The chemical structure of some nicotinic anthelmintics.

morantel, and oxantel have been studied in greatest detail.

Intracellular potential and conductance effects of nicotinic anthelmintics

Bath application of tetramisole, the D,L-racemic mixture of which levamisole is the laevo-isomer, produces depolarization, an increase in spike frequency and contraction when applied to body flap preparations of *Ascaris* (Aceves, Erliji & Martinez-Marnon, 1970). Pyrantel and its analogues also produce depolarization, increased spike activity and contraction when bath applied to *Ascaris* muscle (Aubry *et al.* 1970).

The two-microelectrode current-clamp and voltage-clamp technique has been used to examine the effects of acetylcholine, levamisole, pyrantel, morantel (Martin, 1982; Harrow & Gration, 1985). These

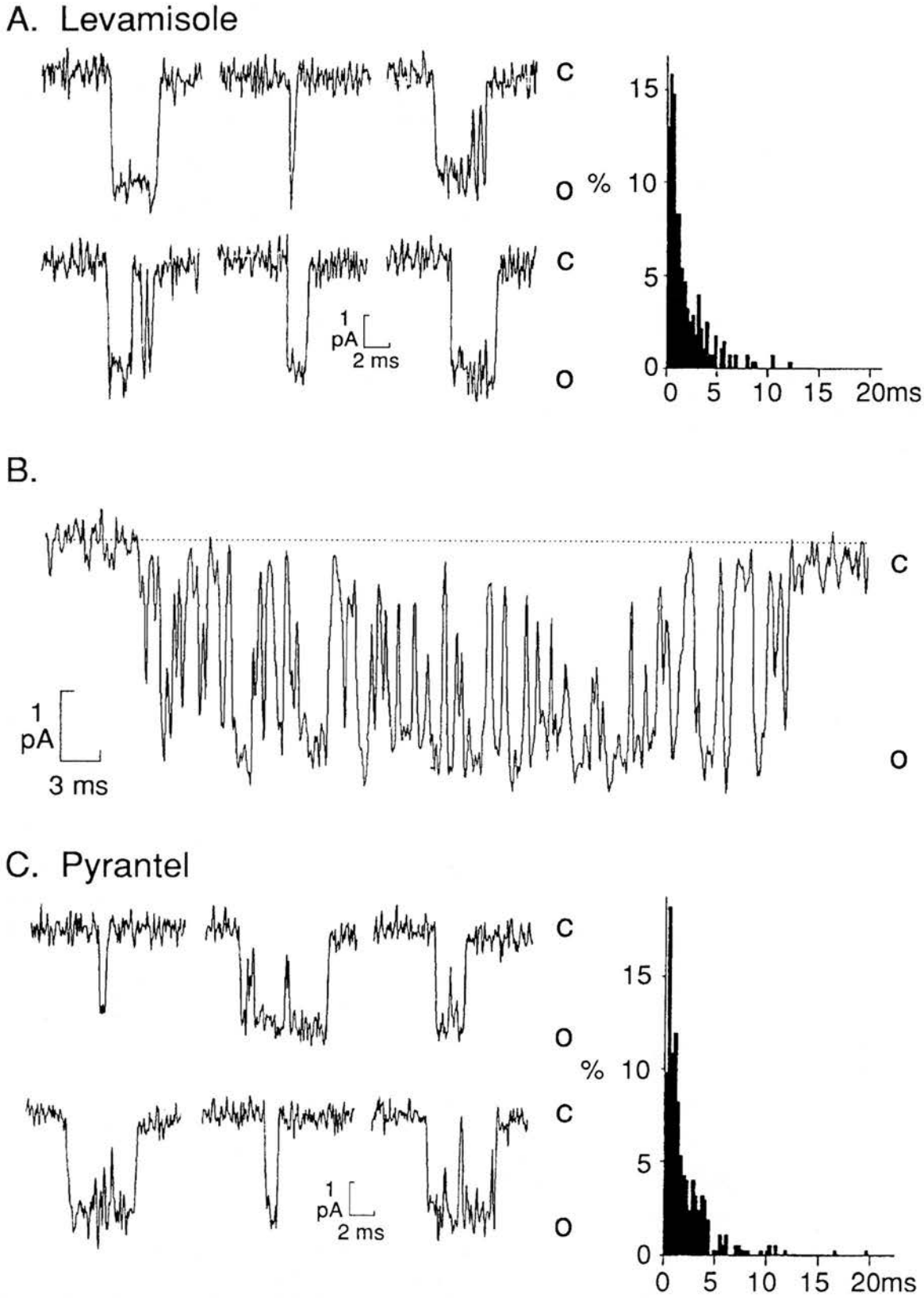

Fig. 9. Levamisole- and pyrantel-activated channel currents. (A) levamisole (10 μM) in the patch pipette activates the opening of fast non-selective cation channels in a cell-attached patch; c, closed state; o, open state. The distribution of the open times is shown in the histogram; the mean open time was 1·34 ms. (B) at higher levamisole concentrations (30 μM) levamisole produced a 'flickering open channel-block'. The dashed line indicate the level of the closed state. (C) pyrantel (0.1 μM) in the patch pipette activates the opening of fast non-selective cation channels in a cell-attached patch; c, closed state; o, open state. The distribution of the open times is shown in the histogram; the mean open time was 1.09 ms.

Table 2. The blocking rate constants (k_{+B}), the unblocking rate constants (k_{-B}), and dissociation constants (K_B), for the nicotinic anthelmintics derived from an analysis of the channel currents using the simple open channel-block model at −50 mV & −75 mV

Constants	Levamisole	Pyrantel	Morantel	Oxantel
k_{+B} −50 mV	$2{\cdot}1 \times 10^7$ M^{-1} s^{-1}	$2{\cdot}2 \times 10^7$ M^{-1} s^{-1}	2×10^7 M^{-1} s^{-1}	$2{\cdot}4 \times 10^7$ M^{-1} s^{-1}
k_{+B} −75 mV	$3{\cdot}8 \times 10^7$ M^{-1} s^{-1}	$3{\cdot}1 \times 10^7$ M^{-1} s^{-1}	2×10^7 M^{-1} s^{-1}	$2{\cdot}4 \times 10^7$ M^{-1} s^{-1}
k_{-B} −50 mV	$2{\cdot}1 \times 10^3$ s^{-1}	$0{\cdot}8 \times 10^3$ s^{-1}	$0{\cdot}24 \times 10^3$ s^{-1}	$0{\cdot}44 \times 10^3$ s^{-1}
k_{-B} −75 mV	$1{\cdot}8 \times 10^3$ s^{-1}	$0{\cdot}6 \times 10^3$ s^{-1}	$0{\cdot}14 \times 10^3$ s^{-1}	$0{\cdot}16 \times 10^3$ s^{-1}
K_B −50 mV	123 μM	37 μM	12 μM	18·5 μM
K_B −75 mV	46 μM	20 μM	1 μM	7·5 μM

anthelmintics increase the input conductance and depolarize the membrane by opening non-selective cation channels which are permeable to Na^+ and K^+. Simultaneous application of acetylcholine and pyrantel showed that both agonists acted on the same nicotinic receptor (Harrow & Gration, 1985). The relative potency of the anthelmintics is: morantel = pyrantel > levamisole (Harrow & Gration, 1985).

In addition to the effects of the anthelmintics on the input conductance of the membrane, Harrow & Gration (1985) described the conductance dose-response curves for pyrantel and morantel as being bell-shaped. The concentration–effect relationship of pyrantel and morantel increases then decreases as the concentration of the anthelmintics is raised. One explanation for this phenomena is that of open channel-block (Colquhoun & Sakmann, 1985) by the anthelmintic. The nicotinic anthelmintics (including pyrantel and morantel) are large organic cations and could enter the nicotinic ion-channel from the outside; they try to pass through the channel pore like Na^+ or K^+ ions and produce block at narrow portion of the ion-channel. This block would be voltage-sensitive and increase with hyperpolarization of the membrane and concentration of the antagonists.

Single-channel currents activated by nicotinic anthelmintics

Initially, levamisole-activated single-channel currents, Fig. 9A were recorded from the muscle vesicle preparation (Robertson & Martin, 1993). The ion-channels were shown to be cation selective and to have similar kinetics to acetylcholine-activated channels at low levamisole concentrations (Table 1). The channels had mean open-times of 1.7 ms and had conductances in the range 19–46 pS. At higher concentrations of levamisole a flickering channel-block that increased on hyperpolarization was observed (Fig. 9B).

The channel-block produced by levamisole was described using a simple open channel-block model in which it is assumed that a single molecule of levamisole enters the open ion-channel and binds in a site within the channel pore, blocking it (Robertson & Martin, 1993):

$$C \underset{\alpha}{\overset{\beta'}{\rightleftharpoons}} O \underset{k_{-B}}{\overset{k_{+B} \cdot x_a}{\rightleftharpoons}} B,$$

where C is the closed-state and O is the open-state of the channel, B represents the blocked-state with the anthelmintic occupying a block site in the channel pore. $\beta'\alpha$, k_{+B}, k_{-B} are rate constants and xa represents the anthelmintic concentration. β' is the opening rate of the channel and β' increases with concentration of the anthelmintic, α is the closing rate of the channel, k_{+B} is the blocking rate constant, and k_{-B} is the unblocking rate constant. The dissociation constant (K_B) for the anthelmintic binding to the block site is determined from the ratio k_B/k_{+B}. The lower the dissociation constant, the more potent the anthelmintic is as a channel-blocker.

The dissociation constant (K_B) of levamisole for the channel-block was 123 μM at −50 mV. Table 2 summarizes the kinetic parameters, including the association and dissociation rate constants of channel-block, that were measured at −50 mV and −75 mV (Robertson & Martin, 1993).

Pyrantel-activated channels (Fig. 9C) were then recorded using the same preparation and analytical technique (Robertson *et al.* 1994). The pyrantel-activated channels showed at least two distinguishable conductance levels: the main conductance level that was near 40 pS and the smaller conductance level that was near 22 pS. The pyrantel-activated channels showed a marked channel-block occurring at hyperpolarized potentials. The channel-block occurred more readily with pyrantel than with levamisole, and when the kinetics of the channel-block were analysed in the same way as had been done for levamisole it was found that the dissociation constant, K_B, for pyrantel was lower than for levamisole (pyrantel K_B at −50 mV, 37 μM; levamisole K_B at −50 mV, 123 μM).

Table 1 summarizes properties of the channel currents activated by different nicotinic anthelmintics studied; it shows the conductances of the channels activated by acetylcholine and nicotinic anthelmintics, the mean open-times of the channels

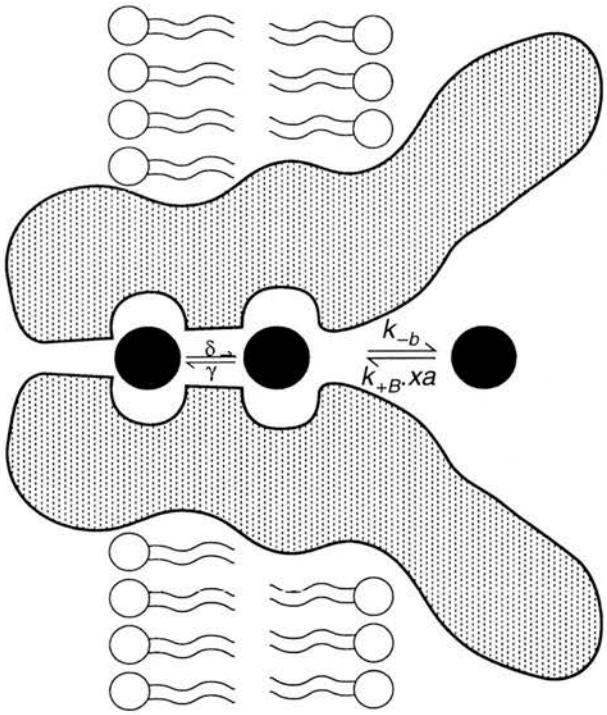

Fig. 10. Diagram of the two block site model used to describe the channel-block produced by morantel (Evans & Martin, 1996). It is assumed that a molecule of morantel at the extracellular entrance of the channel may enter and bind to a site near the entrance of the channel. The forward block rate is $k_{+B}.xa$, where xa is the molar concentration of morantel and k_{+B} is the rate constant M^{-1}. k_{-b} is the unblocking rate constant. The molecule of morantel, once bound may then proceed on to a second block site at a rate constant of γ and return from the second site to the first site at a rate of δ. Once a molecule of morantel has bound to the second block site, then the first block site may also be occupied by a second molecule of morantel. The nature of this block is that it shows a steep dose-response relationship with evidence of cooperativity. It is also possible to allow in the double block model to allow the rate at which the second molecule enters and leaves block site one to be different to when a single molecule of morantel enters an empty channel.

and the probability of the channel being open in the presence of the particular concentrations of anthelmintic. Table 2 shows values for the blocking rate (k_{+B}), unblocking rate (k_{-B}) and dissociation constant (K_B) derived using the same simple channel block model. The data were derived from Robertson & Martin (1993); Robertson *et al.* (1994); Dale & Martin (1995); Evans & Martin (1996).

Some general points may be made by examining the tables of the results. It can be seen that all the nicotinic anthelmintics produce channel-block, a form of self antagonism, and that levamisole is the least able to block its own channel. The channel-blocking ability of pyrantel is greater than levamisole: the greatest channel-block is produced by morantel (Evans & Martin, 1996).

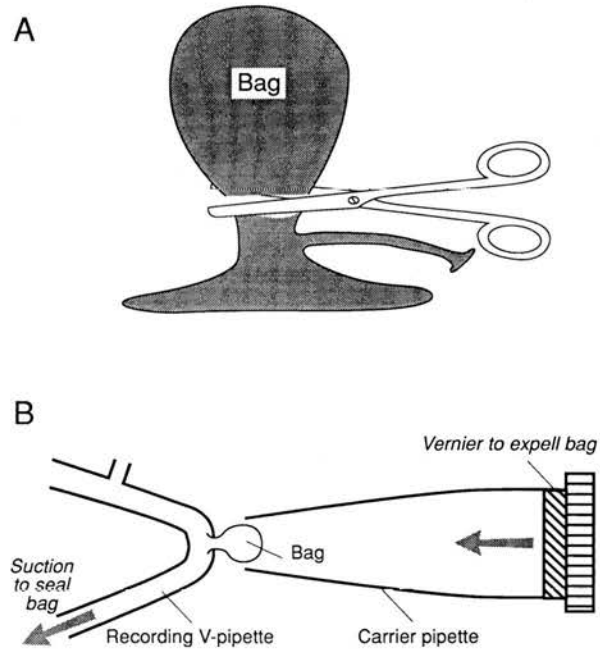

Fig. 11. (A) Diagram of the preparation and mounting of the isolated bag preparation for the Kostyuk voltage-clamp technique. After brief collagenase treatment, fine iris scissors were used to cut bags from the spindle region. (B) An isolated bag is then picked up in a manipulating pipette and placed with the neck in the mouth of the V-shaped pipette and sealed into the pipette by suction on the V-shaped micropipette.

It can also be seen that the least potent compound is oxantel which produced the lowest probability of opening even with high concentrations. The shortest mean open-times were observed with oxantel, 1·34 ms at −50 mV (Dale & Martin, 1995). Interestingly this compound is not effective therapeutically against ascariasis but is used instead to treat *Trichuris* infections. Presumably the efficacy of oxantel against *Trichuris* but not against *Ascaris* is due to differences in the nicotinic receptors of the two species of nematode. Oxantel may be effective and produce opening of the *Trichuris* nicotinic acetylcholine receptor but is not so effective on the *Ascaris* receptor.

There may be more than one block site in the pores of Ascaris *nicotinic channels*

It has been usual to analyse properties of channel-blocking molecules by assuming that only one blocking ion enters and binds to a single site in the ion-channel pore. We found however, that when the properties of the ion-channel-block produced by morantel were analysed in more detail (Evans & Martin, 1996) that the nature of the block could be better described by a multi-ion channel-block and that there is evidence of two block sites within the ion-channel. Fig. 10 illustrates a model we have proposed and used to describe the block produced by

morantel: it has the advantage of being able to explain more of the properties of the marked channel-block produced by morantel. Despite this, the simple channel-block model may be useful to allow a simple comparison of the degree of block produced by the different anthelmintics.

Non-nicotinic or 'muscarinic' cholinergic receptors in nematodes

In a number of vertebrate preparations, acetylcholine is able to alter the probability of voltage-dependent channel openings via G protein-coupled receptors. An action in nematodes, at receptors analogous to vertebrate muscarinic acetylcholine receptors modulating voltage-sensitive ion-channels, has yet to be fully reported.

There is biochemical evidence for the presence of 'muscarinic' receptors in *Ascaris suum* muscle: (i) Donahue, Yacoub & Harris (1982) have observed that effects of cholinergic stimulation includes increases in levels of cyclic-AMP; (ii) Arevalo & Saz (1992) have observed that acetylcholine increases levels of phosphorylcholine, 1,2 diacylglycerides and phosphatidic acid and demonstrated the presence of phospholipase C activity. Donahue *et al.* (1982) and Arevalo & Saz (1992) did not distinguish between 'muscarinic' or 'nicotinic' cholinergic receptors

Kostyuk technique for recording voltage-dependent currents from the bag region of the muscle and effects mediated by cholinergic receptors

One problem with a two microelectrode voltage-clamp technique (Martin, 1982) for recording voltage-activated currents from *Ascaris* muscle effects of neurotransmitters is that is difficult to be certain that all the voltage-activated current produced is from the bag region muscle cell under clamp: the space-clamp is not likely to be perfect and some parts of the cell will escape the voltage-clamp. In addition, if we wish to study the effects of intracellularly-applied substances such as putative second messengers then they would have to be membrane permeable and be applied from the outside of the cell. To ameliorate these problems we have developed and applied the Kostyuk voltage-clamp technique to the isolated bag region of the muscle.

Large cells may be voltage-clamped and perfused intracellularly using a technique developed in Kostyuk's laboratory (Kostyuk, Krishtal & Pidoplicho, 1984). The technique consists of using a V-shaped glass or polythene tube/micropipette with a small 20–30 μm hole at the tip. The isolated cell to be recorded from is drawn onto the tip by suction producing a seal so that it is then possible to record voltage-clamp currents. To apply this technique for recording from *Ascaris* 'bags', we have used collagenase briefly to separate the 'bags' and then the bags are cut with fine iris scissors, Fig. 11A. The bags are then drawn up into the V-shaped micropipette for recording of bag currents during voltage steps, Fig 11B.

We have found that acetylcholine, in the presence of 100 μM tubocurarine or 100 μM mecamylamine, will increase slow voltage-dependent currents recorded using the Kostyuk technique even in absence of external calcium, Fig. 12. These voltage-activated currents have a long inward 'tail current' and have a reversal near -20 mV. The currents can be explained by the activation of another type of non-selective cation channel that appears to have much slower kinetics than the nicotinic channel and that appears to be slightly more selective for potassium than the nicotinic channel which has a reversal potential near 0 mV. Interestingly, we have found that the FMRFamide peptide PF1 (Geary *et al.* 1992) has the opposite effect on the current to acetylcholine and reduces this current. The properties of the voltage-dependent cation channel seem to be consistent with the properties of currents required to generate slow waves (Weisblat *et al.* 1976) and the effects of acetylcholine can be explained by the presence of another type of acetylcholine receptor on the muscle bag. Low concentration (< 10 μM) of atropine are not effective as an antagonist of the effects of acetylcholine so that the receptor is best referred to as a non-nicotinic receptor rather than a muscarinic receptor.

Resistance to anthelmintics

Previous studies on nematodes have shown that resistance to nicotinic anthelmintics may take two forms: (1) The selection of genetically resistant mutants with modified nicotinic acetylcholine receptors on muscle (Lewis *et al.* 1980, 1992). (2) Accommodation and recovery of parasites following long periods of exposure to the anthelmintics (Coles, East & Jenkins, 1995) and which may be explained by nicotinic receptor desensitization.

These resistant or recovered nematodes no-longer respond to the nicotinic anthelmintics but interestingly may still respond to acetylcholine (Coles *et al.* 1975) One explanation for these results is that, in addition to the nicotinic receptor on nematode muscle, there are other non-nicotinic cholinergic receptors present on muscle and which are not stimulated by the anthelmintics. This receptor may facilitate contraction by being coupled via G proteins to voltage-activated channel currents.

Pharmacology of the Ascaris *GABA receptor*

In addition to the extrasynaptic acetylcholine receptors on the bag region of the muscle cells, there are also extrasynaptic GABA receptors (Martin, 1980). The pharmacology to the extrasynaptic GABA

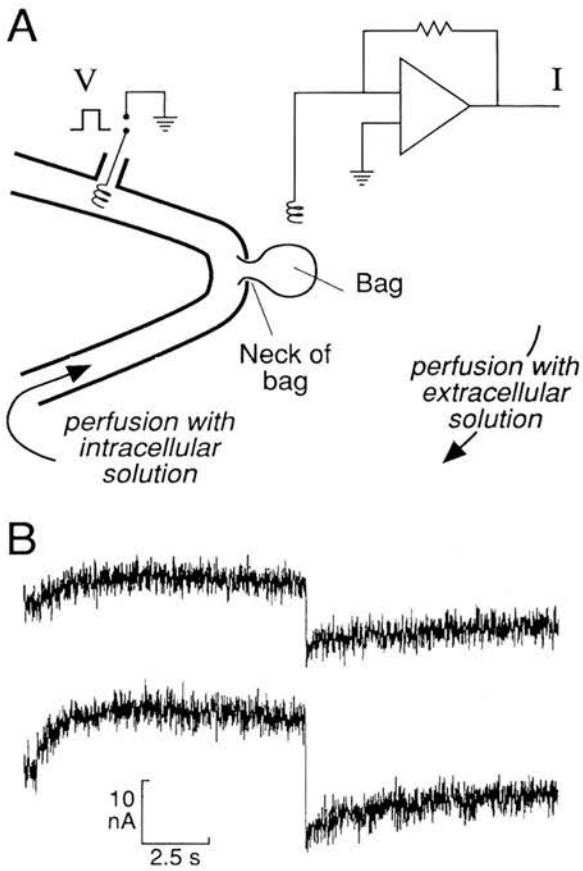

Fig. 12. (A) diagram of the Kostyuk voltage-clamp showing the V-shaped micropipette, the stimulation electrodes (*V*) and the recording of the current with the current voltage converter (*I*). Also illustrated is the ability to perfuse the isolated bag intracellularly or extracellularly. (B) Leak-corrected currents activated by step potential to +27 mV from a holding potential −40 mV. Extracellular. solution (mM): Cs acetate, 135; BaCl, 19; TEA, 10; 4-AP, 5; HEPES, 5; pH 7·2 with CsOH. Intracellular. solution (mM): Cs acetate, 135; EGTA, 0·5, HEPES, 5; pH 7·2 with CsOH. Top: Control. Bottom: 50 μM ACh in 100 μM mecamylamine applied extracellularly.

receptor on *Ascaris* muscle has been examined with the two microelectrode current-clamp technique and the bath application of agonist and antagonists to examine the conductance-dose response relationship (Martin, 1980; Holden-Dye & Walker, 1988; Holden-Dye *et al.* 1988; 1989; Duittoz & Martin, 1989, 1990; Martin *et al.* 1995).

The relative potency of a range of GABA agonists have been determined by Holden-Dye *et al.* (1989) the conductance dose–response relationships for of GABA agonists described by the Hill equation and the EC_{50}s determined by Duittoz & Martin (Martin, 1993) These observations showed that the agonist profile of the *Ascaris* receptor was similar to, but not identical to a vertebrate $GABA_A$ receptor.

In contrast it was found that vertebrate $GABA_A$ antagonists: bicuculline, securinine, pitrazepine, RU5135, dieldrin, and TBPS were weak or inactive (Martin, 1980; Holden-Dye *et al.* 1988; 1989; Martin *et al.* 1991). The potency of a series of arylaminopyidazine-GABA derivatives that act as competitive antagonists at vertebrate $GABA_A$ receptors as well as a the *Ascaris* GABA receptor do not show the same rank order potency (Duittoz & Martin, 1991*a*, *b*). These differences further distinguish the *Ascaris* GABA receptor pharmacologically from vertebrate $GABA_A$ receptors and confirm the earlier suggestion (Martin, 1987) that there is different GABA receptor in nematodes, i.e. a $GABA_N$ receptor (not antagonized by pictrotoxin, N for nematodes).

The differences in the potencies of the arlyaminopyridazine-GABA derivatives at vertebrate $GABA_A$ receptors and *Ascaris* GABA receptors and the fact that these compounds are competitive antagonists at both types of receptor was interpreted to indicate that there are different accessory binding site on the *Ascaris* receptor (Duittoz & Martin, 1991*b*). The study also indicated the action of novel arylaminopyridazine derivatives should be investigated with a view to examining further the structure activity of this series of compounds to find a more potent antagonist.

The structure-activity relationships of 35 novel derivatives of 2-(carboxypropyl)-3-amino-4-methyl -6-phenyl pyridazine (SR 95103) were examined as GABA antagonists in the flap preparation of *Ascaris* using a two-microelectrode current-clamp technique (Martin *et al.* 1995). All but one of the potent antagonists displaced GABA dose-response curves to the right without reduction in the maximum response. The dissociation constants of the more potent competitive antagonists were described using a model which assumed that two molecules of GABA were required to open the ion-channel but that only one molecule of antagonist acted on each ion-channel. By exploring the structure activity relationship, the potency of the antagonist was increased from a K_B of 64 μM for SR 95103 to a K_B of 4·7 μM for NCS 281–93 [2-(3-carboxypropyl)-3-amino-4-phenylpropyl-6-phenyl pyridazine] (Table 3).

Possible therapeutic uses of GABA antagonists

Selective cholinergic agonist like levamisole, are used as anthelmintics and appear to work by acting as agonists on nematode muscle acetylcholine receptors (Harrow & Gration, 1985; Martin, 1993). Stimulation of the acetylcholine receptors produces depolarization and spastic paralysis of the nematode leading to its expulsion. Unfortunately resistance to therapy with these compounds is increasing, requiring higher concentrations of anthelmintic to be used (Sangster & Bjorn, 1995) or the change to a drug that has another mode of action. One way of increasing the effectiveness of a therapeutic regime

Table 3. Derivatives modified in position 4

Compound	R	10 mM % antagonism	0·1 mM % antagonism	1 mM % inhibition	K_B (μM)
SR 95103	CH_3	-	-	93 ± 3 (n = 5)	64 ± 13 (n =13)
SR 95132	C_6H_5	-	-	89 ± 3 (n = 5)	65 ± 20 (n = 9)
NCS 247-90	CH_3CH_2	-	-	95 ± 3 (n = 5)	55 ± 16 (n = 13)
NCS 251-90	$C_6H_5CH_2$	-	24, 48 (n = 2)	99 ± 1 (n = 3)	31 ± 14 (n = 3)
NCS 252-90	$(CH_3)_2CH$	-	-	81 ± 3 (n = 3)	-
NCS 253-90	p-HO-$C_6H_5CH_2$	-	30 (n = 1)	91 ± 5 (n = 3)	-
NCS 254-90	$C_6H_5CH_2CH_2$	-	56 ± 4 (n = 4)	97, 100 (n = 2)	11 ± 3 (n = 4)
NCS 258-91	p-CH_3-$C_6H_4CH_2$	5, 11 (n = 2)	52, 42 (n = 2)	93,. 86 (n = 2)	-
NCS 266-92	P-MeO-$C_6H_4(CH_2)_2$	0 (n = 1)	15, 38 (n = 2)	88, 97 (n = 2)	-
NCS 267-92	m-MeO-$C_6H_4(CH_2)_2$	0, 0 (n = 2)	18, 35 (n = 2)	73, 93 (n = 2)	-
NCS 268-92	4, 3-methylenedioxy	0, 0 (n = 2)	0, 0 (n = 2)	74, 58 (n = 2)	-
NCS 281-93	$C_6H_5CH_2CH_2CH_2$	24, 10 (n = 2)	57, 50 (n = 2)	94, 96 (n = 2)	4·7 ± 0·7 (n = 11)
NCS 282-93	$(C_6H_5)_2CHCH_2$	11, 27 (n = 2)	75, 42 (n = 2)	73, 100 (n = 2)	Non-competitive

would be to add a selective GABA receptor antagonist along with the selective cholinergic agonist so that the two compounds could act in concert producing depolarization, contraction and spastic paralysis.

Further study of the structure activity relationships of arylaminopyridazines may permit the development of therapeutic approaches that can control nematode parasite resistant to other anthelmintic.

Piperazine

Piperazine has a heterocylic ring structure, Fig. 13, and is unlike GABA. Nonetheless, these two compounds act on the same receptor which is a ligand-gated Cl^- channel. GABA- and piperazine-activated channels have been recorded using cell-attached and isolated outside-out patches (Martin, 1985). Although the channels may have more than one conductance level, the most frequently observed was 22 pS for both agonists. However the mean open-time of the channels for piperazine was shorter, 14 ms, than that produced by GABA which produced channels that had mean open-times of 32 ms. GABA is more than 10 to 100 times more potent than piperazine when conductance-dose responses are examined during bath application of the agonists (Martin, 1985). The difference in potency may be explained by the fact that higher concentrations of piperazine are required to produce the same opening rate as produced by GABA and that the average duration of the channel openings produced by piperazine is much shorter. The same probability of the channel being open can be achieved with lower concentrations of GABA than piperazine. Therapeutically however, GABA would be ineffective because it is not selective like piperazine and is in addition highly ionized and does not cross the cuticle and get access to the muscle receptors.

The avermectin receptor

The avermectins are a group of broad spectrum macrocyclic lactone antibiotic anthelmintics used to control nematode parasites in man and animals (Campbell & Benz, 1984). They are used to control onchocerciasis (river blindness) in humans and gastro-intestinal, cardiac and respiratory nematode parasites of domestic animals. The mode of action of the avermectins is to selectively paralyze the parasite by increasing muscle Cl^- permeability but the identity of the channel targeted by the avermectins has been controversial, see Arena (1994) for a recent review. Cloning of a GluCl-α and a GluCl-β subunit from the model soil nematode *Caenorrhabditis elegans* and co-expression of the subunits in *Xenopus* oocytes has led to the identification of an avermectin-sensitive glutamate-gated chloride ion-channel (Cully *et al.* 1994). The effects of avermectins, at low concentrations, are to potentiate the effect of glutamate, and at higher concentrations, the avermectins open the glutamate gated channel directly. The selective therapeutic effects of the avermectins might be explained by an action on a glutamate-gated Cl^- ion-channel that is present in parasitic nematodes but that it is not present in the host animal. One limitation of this hypothesis for the selective action of avermectins is that certain strains of collie dogs are sensitive to avermectins because they are thought to have a 'deficiency' in their blood brain barrier: this

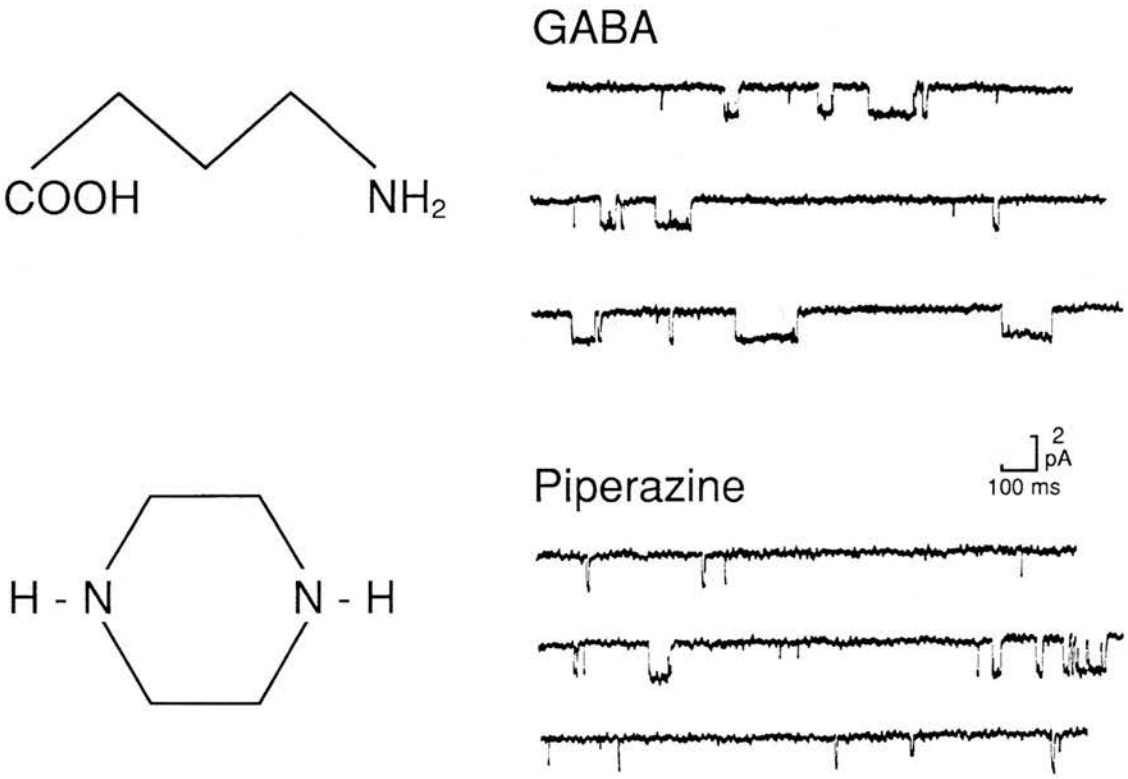

Fig. 13. Chemical structure of GABA and piperazine and their channel currents. Cell-attached patches. Transpatch potential −75 mV. Openings downwards. GABA: 3 μM GABA as the agonist in the patch pipette. Piperazine: 500 μM piperazine as the agonist. Effective mean open times: GABA 33 ms; piperazine 18 ms. Channel conductances 22 pS for both agonists.

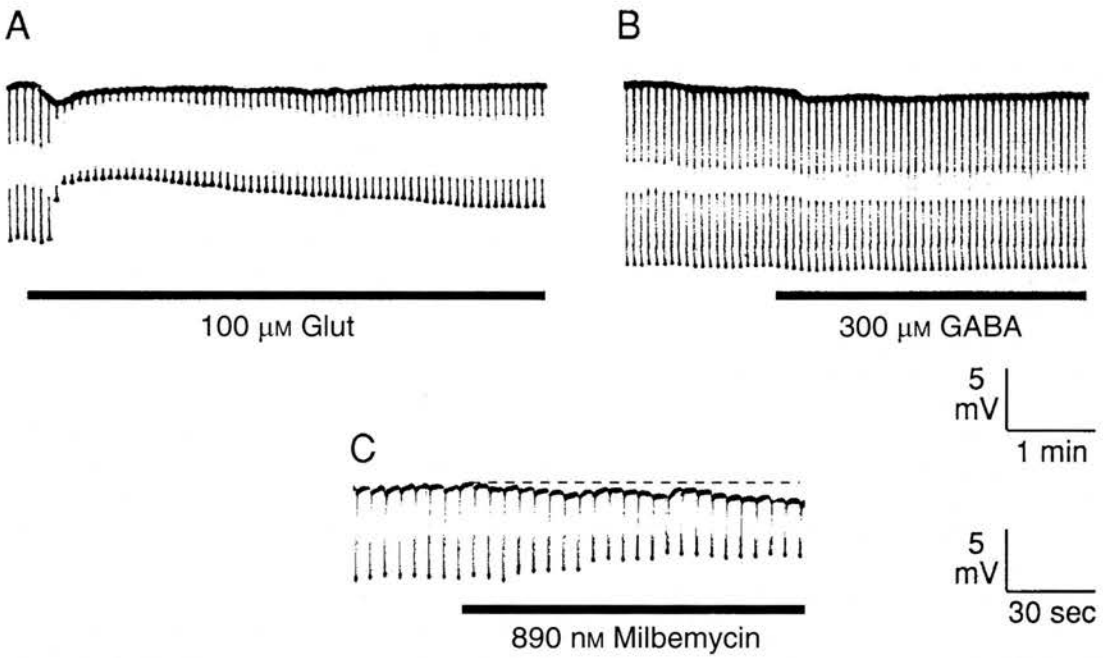

Fig. 14 (A) Effect of application of 100 μM L-glutamate on membrane potential and input conductance. Glutamate (applied during horizontal bar) produced a transient small hyperpolarization of 1 mV associated with an input conductance change from 157 μS to a peak of 429 μS (ΔG: 272 μS) desensitizing to 231 μS (ΔG: 74 μS) after 4 min. (B) After washing the preparation the input conductance of the pharynx returned towards control levels (142 μS) and the effect of 300 μM GABA was tested without effect (applied during the horizontal bar). The lack of effect of GABA was not due to desensitization because subsequent application of 100 μM L-glutamate increased the input conductance again (not shown). (C) Effect of 890 nM milbemycin D [different preparation to (A) and (B)] on the membrane potential and input conductance. Milbemycin slowly produced an increase in input conductance that was not reversed on washing (not shown).

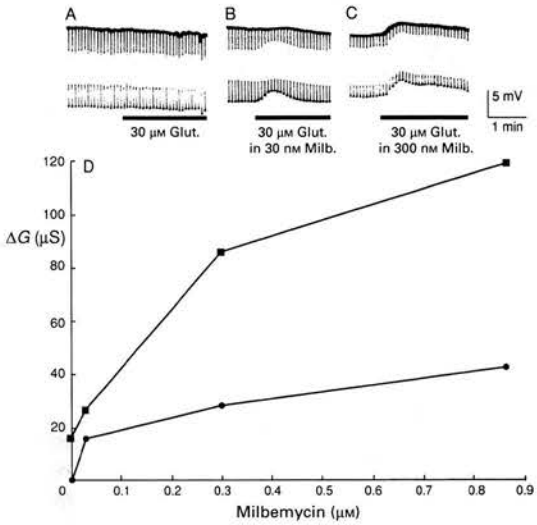

Fig. 15. Glutamate potentiation effects of milbemycin D. (A) Control 30 μM glutamate response, peak ΔG, is small, 16 μS. (B) In the presence of 30 nM milbemycin D the peak ΔG produced by 30 μM glutamate increased to 27 μS. (C) 300 nM milbemycin D increased the peak ΔG to 86 μS. In this particular preparation the glutamate response was a small depolarizing potential, indicating that the Cl-reversal potential was slightly depolarized relative to the membrane potential. (D) (■) plot of peak ΔG produced by 30 μM glutamate against milbemycin concentration; (●) plot of resting input conductance of the pharynx against milbemycin concentration. Results from the same experiment as (A), (B) & (C).

observation might suggest that there are avermectin sensitive Cl^- channels in the CNS of vertebrate hosts.

Molecular experiments using the *lacZ* marker suggest that the GluCl-β subunit of the glutamate channel is expressed in the pharynx of *C. elegans* pM4 muscle (Laughton, Wolstenholme & Lunt, 1995). The muscle is required for pharyngeal pumping/feeding and is known to receive an inhibitory motor neurone, M3, that is not likely to be GABAergic (Laughton *et al.* 1995) but glutamatergic (Avery, 1993). The location of the avermectin-sensitive glutamate-gated chloride channel, has been identified using a two microelectrode current-clamp technique (Martin, 1996) in *Ascaris* (Fig. 14). Experiments show that the pharyngeal muscle of this parasite possesses glutamate receptors that gate chloride channels and that are sensitive to the avermectin analogue milbemycin D.

Effect of glutamate

Fig. 15A shows effects of the application of 100 μM glutamate on *Ascaris* pharyngeal input conductance and membrane potential: glutamate produced a transient small hyperpolarization of 1 mV associated with an input conductance change from 157 μS to a peak of 429 μS (ΔG: 272 μS) desensitizing to 231 μS (ΔG: 74 μS) after 4 min. The effect of glutamate but not GABA (Fig. 14B) in all preparations was to produce a reversible increase in input conductance associated with a small change in membrane potential; the membrane potential change was usually hyperpolarizing but in some preparations a small depolarizing potentials was observed. The glutamate induced increase in conductance is dose-dependent, and was fitted by the modified Hill equation with an ED_{50} of 60 ± 11 μM (mean $\pm$ S.E., $n = 4$). Zero-Cl^- solutions reversibly abolished the glutamate conductance responses and were used to demonstrate that the glutamate effect was mediated by a Cl^- channel (Martin, 1996).

Effect of milbemycin D

The effect of the ivermectin-analogue anthelmintic, milbemycin D, on the *C. elegans* avermectin-sensitive glutamate receptor expressed in *Xenopus* oocytes is to produce a potentiation of glutamate effects and to produce a slow irreversible increase in conductance of the membrane (Cully *et al.* 1994). The effects of milbemycin D on the input conductance of the *Ascaris* pharyngeal preparation is shown in the Figs 14C and 15A–C. In Fig. 14C, 890 nM milbemycin D slowly increased the resting conductance of the membrane from 353 μS to 857 μS and gave rise to a 2 mV hyperpolarization. Although milbemycin D mimicked the effect of glutamate on membrane potential and conductance, its effect as with the expressed receptor was not reversed on repeated washing. A potentiating effect of milbemycin D on the effects of glutamate was also seen: Fig. 15A, B shows that 30 nM milbemycin D increased the peak ΔG produced by 30 μM glutamate from 16 μS to 27 μS and in Fig. 15C it is shown that 300 nM milbemycin D further increased the peak ΔG to 86 μS. In this particular preparation, the glutamate potential response was a small depolarizing potential. The effect of milbemycin D concentration was slightly depolarized relative to the membrane potential . The effect of milbemycin D concentration on the input conductance and the peak ΔG produced by 30 μM glutamate is plotted for this experiment in Fig. 15D: the Fig. emphasizes that the potentiation of glutamate as dose-dependent and that the potentiation increased as the effect of milbemycin on input conductance increased. The potentiation of the glutamate response by milbemycin D indicates that milbemycin and glutamate are interacting with the same channel and that the glutamate gated Cl^- channel described here is analogous to the *C. elegans* channel, expressed in *Xenopus* oocytes.

CONCLUSION

In this review we have outlined the electrophysiological properties of *Ascaris* muscle and described electrophysiological effects of anthelmintics whose

mode of action involves effects in membrane ion-channels. It is likely that some forms of resistance to anthelmintics will involve modification to of the properties of the target ligand-gated ion-channel.

ACKNOWLEDGMENT

We are pleased to acknowledge the financial support of the Wellcome Trust.

REFERENCES

ACEVES, J., ERLIJI, D. & MARTINEZ-MARNON, R. (1970). The mechanism of the paralyzing action of tetramisole on *Ascaris* somatic muscle. *British Journal of Pharmacology* **38**, 602–7.

ARENA, J. P. (1994). Expression of *Caenorhabditis elegans* messenger-RNA in *Xenopus* oocytes: a model system to study the mechanism of action of avermectins. *Parasitology Today* **10**, 35–7.

AREVALO, J. I. & SAZ, H. J. (1992). Effects of cholinergic agents on the metabolism of choline in muscle from *Ascaris suum*. *Journal of Parasitology* **78**, 387–92.

AUBRY, M. L., COWELL, P., DAVEY, M. J. & SHEVDE, S. (1970). Aspects of the pharmacology of new anthelmintics: pyrantel. *British Journal of Pharmacology* **38**, 332–44.

AVERY, L. (1993). Motor-neuron m3 controls pharyngeal muscle-relaxation timing in *Caenorhabditis elegans*. *Journal of Experimental Biology* **175**, 283–97.

BALDWIN, E. & MOYLE, V. (1949). A contribution to the physiology and pharmacology of *Ascaris lumbricoides* from the pig. *British Journal of Pharmacology* **4**, 145–52.

BRADING, A. F. & CALDWELL, P. C. (1971). The resting membrane potential of the somatic muscle cells of *Ascaris lumbricoides*. *Journal of Physiology* (*London*) **217**, 605–24.

CAMPBELL, W. C. & BENZ, G. W. (1984). Ivermectin: A review of efficacy and safety. *Journal of Veterinary Pharmacology and Therapeutics* **7**, 1–16.

CAPPE DE BAILLON, P. (1911). Étude sur les fibres musculaires d'*Ascaris*. I. Fibres parietales. *Cellule* **27**, 165–211.

COLES, G. C., EAST, J. M. & JENKINS, S. N. (1975). The mechanism of action of the anthelmintic levamisole. *General Pharmacology* **6**, 309–13.

COLQUHOUN, D. & SAKMANN, B. (1985). Fast events in single-channel currents activated by acetylcholine and its analogues at the frog muscle end-plate. *Journal of Physiology* (*London*) **369**, 501–57.

COLQUHOUN, L., HOLDEN-DYE, L. & WALKER, R. J. (1991). The pharmacology of cholinoceptors on the somatic muscle-cells of the parasitic nematode *Ascaris suum*. *Journal of Experimental Biology* **158**, 509–30.

COWDEN, C. & STRETTON, A. O. W. (1993). AF2, an *Ascaris* neuropeptide – isolation, sequence, and bioactivity. *Peptides* **14**, 423–30.

COWDEN, C., STRETTON, A. O. W. & DAVIS, R. E. (1989). AF1, a sequenced bioactive neuropeptide isolated from the nematode *Ascaris suum*. *Neuron* **2**, 1465–73.

CULLY, D. F., VASSILATIS, D. K., LIU, K. K., PARESS, P. S., VANDERPLOEG, L. H. T. & SCHAEFFER, J. M. (1994). Cloning of an avermectin-sensitive glutamate-gated chloride channel from *Caenorhabditis elegans*. *Nature* **371**, 707–11.

DALE, V. M. E. & MARTIN, R. J. (1995). Oxantel-activated single-channel currents in the muscle membrane of *Ascaris suum*. *Parasitology*. **110.** 437–48.

DE BELL, J. T. (1965). A long look at neuromuscular junctions in nematodes. *Quarterly Reviews of Biology* **40**, 233–51.

DE BELL, J. T., DEL CASTILLO, J. & SANCHEZ, V. (1963). Electrophysiology of the somatic muscle cells of *Ascaris lumbricoides*. *Journal of Cellular & Comparative Physiology* **62**, 159–77.

DEL CASTILLO, J., DE MELLO, W. C. & MORALES, T. (1963). The physiological role of acetylcholine in the neuromuscular system of *Ascaris lumbricoides*. *Archives International Physiologie Biochimie* **71**, 741–57.

DEL CASTILLO, J., DE MELLO, W. C. & MORALES, T. (1964). Influence of some ions on the membrane potential of *Ascaris* muscle. *Journal of General Physiology* **48**, 129–40.

DEL CASTILLO, J., RIVERA, A., SOLORZANO, S. & SERRATO, J. (1989). Some aspects of the neuromuscular system of *Ascaris*. *Quarterly Journal of Experimental Physiology and Cognate Medical Sciences* **74**, 1071–87.

DONAHUE, M. J., YACOUB, N. J. & HARRIS, B. G. (1982). Correlation of muscle-activity with glycogen-metabolism in muscle of *Ascaris suum*. *American Journal of Physiology* **242**, R514–R521.

DUITTOZ, A. H. & MARTIN, R. J. (1989). SR95103 acts as a GABA antagonist in *Ascaris suum* muscle. *British Journal of Pharmacology* **97**, 490P.

DUITTOZ, A. H. & MARTIN, R. J. (1990). Effects of the arylaminopyridazine-GABA derivatives, SR95103 and SR95531 on the *Ascaris* muscle GABA receptor: the relative potency of the antagonists in *Ascaris* is different to that at vertebrate GABAa receptors. *Comparative Biochemistry and Physiology C: Pharmacology Toxicology & Endocrinology* **98**, 417–22.

DUITTOZ, A. H. & MARTIN, R. J. (1991*a*). Effects of SR95103 on GABA-activated single-channel currents from *Ascaris suum* muscle. *Comparative Biochemistry And Physiology C–Pharmacology Toxicology & Endocrinology* **98**, 423–432.

DUITTOZ, A. H. & MARTIN, R. J. (1991*b*). Antagonist properties of arylaminopyridazine GABA derivatives at the *Ascaris* muscle GABA receptor. *Journal of Experimental Biology* **159**, 149–64.

EVANS, A. M. & MARTIN, R. J. (1996). Activation and cooperative multi-ion block of single nicotinic-acetylcholine channel currents of *Ascaris* muscle by the tetrahydropyrimidine anthelmintic, morantel. *British Journal of Pharmacology* **118**, 1127–40.

GEARY, T. G., PRICE, D. A., BOWMAN, J. W., WINTERROWD, C. A., MACKENZIE, C. D., GARRISON, R. D., WILLIAMS, J. F. & FRIEDMAN, A. R. (1992). 2 FMRFamide-like peptides from the free-living nematode *Panagrellus redivivus*. *Peptides* **13**, 209–14.

GOLDSCHMIDT, R. (1908). Das Nervensystem von *Ascaris lumbricoides* und *Megalocephala*. Ein Versuch, in den Aufbau eines einfachen Nervensystems einzudringan, Zweiter Teil. *Zeitschrift für wissenschaftliche Zoologie* **90**, 73–136.

GOLDSCHMIDT, R. (1909). Das Nervensystem von *Ascaris lumbricoides* und *Megalocephala*. Ein Versuch, in den Aufbau eines einfachen Nervensystems einzudringen, Zweiter Teil. *Zeitschrift für wissenschaftliche Zoologie* **92**, 357–396.

GUASTELLA, J., JOHNSON, C. D. & STRETTON, A. O. W. (1991). GABA-immunoreactive neurons in the nematode *Ascaris*. *Journal of Comparative Neurology* **307**, 584–97.

GUASTELLA, J. & STRETTON, A. O. W. (1991). Distribution of H^3 GABA uptake sites in the nematode *Ascaris*. *Journal of Comparative Neurology* **307**, 598–608.

HARROW, I. D. & GRATION, K. A. F. (1985). Mode of action of the anthelmintics morantel, pyrantel and levamisole in the muscle cell membrane of the nematode *Ascaris suum*. *Pesticide Science* **16**, 662–72.

HOBSON, A. D., STEPHENSON, W. & BEADLE, L. C. (1952*a*). Studies on the physiology of *Ascaris lumbricoides*. I. The relation of total osmotic pressure, conductivity and chloride content of the body fluid to that of the external environment. *Journal of Experimental Biology* **29**, 1–21.

HOBSON, A. D., STEPHENSON, W. & EDEN, A. (1952*b*). Studies on the physiology of *Ascaris lumbricoides*. II. The inorganic composition of the body fluid in relation to that of the environment. *Journal of Experimental Biology* **29**, 22–9.

HOLDEN-DYE, L., HEWITT, G. M., WANN, K. T., KROGSGAARD-LARSEN, P. & WALKER, R. J. (1988). Studies involving avermectin and the 4-aminobutyric acid (GABA) receptor of *Ascaris suum* muscle. *Pesticide Science* **24**, 231–245.

HOLDEN-DYE, L., KROGSGAARD-LARSEN, P., NEILSEN, L. & WALKER, R. J. (1989). GABA receptors on the somatic muscle cells of the parasitic nematode, *Ascaris suum*: stereoselectivity indicates similarity to a GABA-type agonist recognition site. *British Journal of Pharmacology* **98**, 841–50.

HOLDEN-DYE, L. & WALKER, R. J. (1988). ZAPA, (Z)-3-[(amino iminomethyl)thio]-2-propenoic acid hydrochloride, a potent agonist at GABA receptors on the *Ascaris* muscle cell. *British Journal of Pharmacology* **95**, 3–5.

JARMAN, M. (1959). Electrical activity in the muscle cells of *Ascaris lumbricoides*. *Nature* **184**, 1244.

JOHNSON, C. D. & STRETTON, A. O. W. (1985). Localization of choline acetyltransferase within identified motoneurones of the nematode *Ascaris*. *Journal of Neuroscience* **5**, 1984–92.

JOHNSON, C. D. & STRETTON, A. O. W. (1987). GABA-immunoreactivity in inhibitory motor neurons of the nematode *Ascaris*. *Journal of Neuroscience* **7**, 223–35.

KOSTYUK, P. K., KRISHTAL, O. A. & PIDOPLICHO, V. I. (1984). Perfusion of isolated neurons fixed in plastic film. In *Intracellular Perfusion of Excitable Cells* (eds. Kostyuk, P. K. & Krishtal, O. A.), pp. 35–51. Chichester, New York, Brisbane, Toronto, Singapore: John Wiley and Sons.

LAUGHTON, D. L., WOLSTENHOLME, A. J. & LUNT, G. (1995). The beta subunit of the *C. elegans* inhibitory glutamate receptor is expressed in the pm4 pharyngeal muscle cells. *Worm Breeders Gazette* **14**, 48.

LEWIS, J. A., WU, C.-H., LEVINE, J. H. & BERG, H. (1980). Levamisole-resistant mutants of the nematode *Caenorhabditis elegans* appear to lack pharmacological acetylcholine receptors. *Neuroscience* **5**, 967–89.

LEWIS, J. A., FLEMMING, J. T. & BIRD, D. (1992). Cloning nematode acetycholine receptor genes. In *Neurotox '91*, (ed. Duce, I. R.), pp. 155–164. London and New York: Elsevier Applied Science.

MARTIN, R. J. (1980). The effect of γ-aminobutyric acid on the input conductance and membrane potential of *Ascaris* muscle. *British Journal of Pharmacology* **71**, 99–106.

MARTIN, R. J. (1982). Electrophysiological effects of piperazine and diethylcarbamazine on *Ascaris suum* somatic muscle. *British Journal of Pharmacology* **77**, 255–65.

MARTIN, R. J. (1985). γ-Aminobutyric acid- and piperazine-activated single channel currents from *Ascaris suum* body muscle. *British Journal of Pharmacology* **84**, 445–61.

MARTIN, R. J. (1987). The γ-aminobutyric acid receptor of *Ascaris* as a target for anthelmintics. *Biochemical Society Transactions* **17**, 61–5.

MARTIN, R. J. (1993). Neuromuscular-transmission in nematode parasites and antinematodal drug-action. *Pharmacology & Therapeutics* **58**, 13–50.

MARTIN, R. J. (1996). An electrophysiological preparation of *Ascaris suum* pharyngeal muscle reveals a glutamate-gated chloride channel sensitive to the avermectin analogue milbemycin D. *Parasitology* **112**, 247–52.

MARTIN, R. J., PENNINGTON, A. J., DUITTOZ, A. H., ROBERTSON, S. & KUSEL, J. R. (1991). The physiology and pharmacology of neuromuscular-transmission in the nematode parasite, *Ascaris suum*. *Parasitology* **102**, S41–S58.

MARTIN, R. J., THORN, P., GRATION, K. A. F. & HARROW, I. D. (1992). Voltage-activated currents in somatic muscle of the nematode parasite *Ascaris suum*. *Journal of Experimental Biology* **173**, 75–90.

MARTIN, R. J., SITAMZE, J. M., DUITTOZ, A. H. & WERMUTH, C. G. (1995). Novel arylaminopyridazine-GABA receptor antagonists examined electrophysiologically in *Ascaris suum*. *European Journal of Pharmacology* **276**, 9–19.

MARTIN, R. J. & VALKANOV, M. A. (1995). A chloride channel in isolated muscle vesicles from *Ascaris suum* conducts products of anaerobic metabolism, suggesting a role in excretion of organic-anions. *Journal of Physiology* **482P**, 8.

NATOFF, I. L. (1969). The pharmacology of the cholinoceptor in muscle preparations of *Ascaris lumbricoides* cat. *suum*. *British Journal of Pharmacology* **37**, 251–7.

NORTON, S. & DE BEER, E. J. (1957). Investigations on the action of piperazine on *Ascaris lumbricoides*. *American Journal of Tropical Medicine* **6**, 889–905.

PENNINGTON, A. J. & MARTIN, R. J. (1990). A patch-clamp study of acetylcholine-activated ion channels in *Ascaris suum* muscle. *Journal of Experimental Biology* **154**, 210–21.

ROBERTSON, S. J., PENNINGTON, A. J., EVANS, A. M. & MARTIN, R. J. (1994). The action of pyrantel as an agonist and an open-channel-blocker at acetylcholine-receptors in isolated *Ascaris suum* muscle vesicles. *European Journal of Pharmacology* **271**, 273–82.

ROBERTSON, S. J. & MARTIN, R. J. (1993). Levamisole-activated single-channel currents from muscle of the nematode parasite *Ascaris suum*. *British Journal of Pharmacology* **108**, 170–8.

ROBERTSON, A. P. & MARTIN, R. J. (1996). Effects of pH on the Ca-dependent chloride channel: a patch-clamp study in *Ascaris suum*. *Parasitology* **113,** 191–8.

ROSENBLUTH, J. (1965). Ultrastructure of somatic muscle cells in *Ascaris lumbricoides*. II. Intermuscluar junctions, neuromuscular junctions, and glycogen stores. *Journal of Cell Biology* **26**, 579–91.

ROZHOVA, E. K., MALYUTINA, T. A. & SHISHOV, B. A. (1980). Pharmacological characteristics if cholinoreception in somatic muscle of the nematode *Ascaris suum*. *General Pharmacology* **11**, 141–46.

SANGSTER, N. C. & BJORN, H. (1995). Levamisole resistance in *Haemonchus contortus* selected at different stages of infection. *International Journal for Parasitology* **25**, 343–8.

SAZ, N. J. & WEIL, A. (1962). A pathway of formation of alpha-methyl valerate by *Ascaris lumbricoides*. *Journal of Biological Chemistry* **237**, 2053–6.

SCHNEIDER, A. (1895). *Monographie der Nematoden*. Berlin.

STRETTON, A. O. W., COWDEN, C., SITHIGORNGUL, P. & DAVIS, R. E. (1991). Neuropeptides in the nematode *Ascaris suum*. *Parasitology* **102**, S107-S116.

STRETTON, A. O. W., FISHPOOL, R. M., SOUTHGATE, E., DONMOYER, J. E., WALROND, J. P., MOSES, J. E. R. & KASS, I. S. (1978). Structure and physiological activity of the motoneurons of the nematode *Ascaris*. *Proceedings of the National Academy of Sciences, USA* **75**, 3493–7.

TIELENS, A. G. M. (1994). Energy generation in parasitic helminths. *Parasitology Today* **10**, 346–52.

TSANG, V. C. & SAZ, H. J. (1973). Demonstration and function of 2-methyl-butyrate racemase in *Ascaris lumbricoides*. *Comparative Biochemistry and Physiology B* **45B**, 617–23.

VALKANOV, M. A. & MARTIN, R. J. (1995). A Cl channel selectively conducts dicarboxylic products from anaerobic glucose metabolism and indicates a role in transmembrane transport of waste organic anions. *Journal of Membrane Biology* **147**, 41–9.

VALKANOV, M. A., MARTIN, R. J. & DIXON, D. M. (1994). The Ca-activated chloride channel of *Ascaris suum* conducts volatile fatty-acids produced by anaerobic respiration – a patch-clamp study. *Journal of Membrane Biology* **138**, 133–41.

WEISBLAT, D. A., BYERLY, L. & RUSSEL, R. L. (1976). Ionic mechanisms of electrical activity in the somatic muscle cell of the nematode *Ascaris lumbricoides*. *Journal of Comparative Neurology* **111**, 93–113.

WEISBLAT, D. A. & RUSSEL, R. L. (1976). Propagation of electrical activity in the nerve cord and muscle syncytium of the nematode *Ascaris lumbricoides*. *Journal of Comparative Neurology* **107**, 293–307.

WHITE, J. G., SOUTHGATE, E., THOMPSON, J. N. & BRENNER, S. (1976). The structure of the ventral cord of *Caenorhabditis elegans*. *Philosophical Transactions of the Royal Society London, Series B* **275**, 298–327.

WHITE, J. D., SOUTHGATE, E., THOMPSON, J. N. & BRENNER, S. (1986). The structure of the nervous system of *Caenorhabditis elegans*. *Philosophical Transactions of the Royal Society of London, Series B* **314**, 1–340.

Target sites of anthelmintics

R. J. MARTIN[1], A. P. ROBERTSON[1] *and* H. BJORN[2]

[1] *Department of Preclinical Veterinary Sciences, R.(D.)S.V.S., University of Edinburgh, Summerhall, Edinburgh EH9 1QH*
[2] *Department of Pharmacology and Pathobiology, Danish Centre for Experimental Parasitology, Royal Veterinary and Agricultural School, Bülowsvej 13, DK-1850 Frederiksberg C, Denmark*

SUMMARY

This paper reviews sites of action of anthelmintic drugs including: (1) levamisole and pyrantel, which act as agonists at nicotinic acetylcholine receptors of nematodes; (2) the avermectins, which potentiate or gate the opening of glutamate-gated chloride channels found only in invertebrates; (3) piperazine, which acts as an agonist at GABA gated chloride channels on nematode muscle; (4) praziquantel, which increases the permeability of trematode tegument to calcium and results in contraction of the parasite muscle; (5) the benzimidazoles, like thiabendazole, which bind selectively to parasite β-tubulin and prevents microtubule formation; (6) the proton ionophores, like closantel, which uncouple oxidative phosphorylation; (7) diamphenethide and clorsulon, which selectively inhibit glucose metabolism of *Fasciola* and; (8) diethylcarbamazine, which appears to interfere with arachidonic acid metabolism of filarial parasites and host. The review concludes with brief comments on the development of anthelmintics in the future.

Key words: acetylcholine receptor, levamisole, pyrantel, piperazine, ivermectin, praziquantel, benzimidazoles, closantel, diamphenethide, clorsulon, diethylcarbamazine.

INTRODUCTION

Anthelmintic drugs are used to control, prevent and treat nematode and trematode parasite infestations in both humans and domestic animals. They will continue to be used until effective vaccines are produced and/or hygiene standards have been improved. As anthelmintic drugs have been used continuously for parasite control, resistance has gradually developed and is now found in a number of parasite species against most of the anthelmintics (Prichard, 1994). This resistance occurs more frequently when the same anthelmintic agent has been used intensively and without good hygiene standards to assist control. If resistance to a particular anthelmintic occurs, it is likely that an anthelmintic that has the same mode of action will also be ineffective (cross-resistance). One reason for developing an understanding of the mode of action of anthelmintics is to enable selection of other anthelmintics that will be effective for therapeutic purposes. Another reason for pursuing the mode of action of anthelmintics is that we may be able to understand how parasites develop resistance to the anthelmintics.

There are two major modes of action of anthelmintics. There are the drugs that act on parasite membrane ion-channels and which usually have a more rapid therapeutic effect; the other group acts more slowly on a range of 'biochemical' target sites found in parasites. Table 1 summarizes the target site of anthelmintics that act on membrane ion-channels. The target ion-channels include: the excitatory nicotinic acetylcholine receptor on muscle of nematodes; the inhibitory γ-aminobutyric acid (GABA) receptor channel also present on nematode muscle; and the glutamate-gated Cl^- channel. Table 2 summarizes the modes of action of anthelmintics that act at more 'biochemical' target sites.

The target site (enzyme or ion-channel) of the anthelmintic may be present in the host animal as well as the parasite; it is usually pharmacologically distinct in the parasite in order to permit selective drug action. For example, the benzimidazole anthelmintics bind selectively to nematode β-tubulin to effect their action. β-tubulin is present in the host animal as well but is sufficiently different in its three dimensional protein structure in the mammalian host so that benzimidazole anthelmintics only bind to the nematode β-tubulin molecule. Other anthelmintics act on targets only present in parasites. The avermectins bind to a glutamate-gated Cl^- ion-channel that has only been found in certain invertebrates including nematodes. This permits the very selective toxic action of avermectins against nematode parasites without harming the host animal. Anthelmintics acting on a target protein only present in parasites are often favoured because of advantages of greater safety and selectivity.

This introductory review covers sites of actions of anthelmintic agents including the nicotinic acetylcholine channel of nematodes, the GABA channel, the glutamate-gated Cl^- channel and biochemical sites of action including β-tubulin and glycolytic enzymes. The review concludes with a brief comment on the future development of anthelmintics.

Table 1. Ion-channel target sites of anthelmintic drugs

Target site (and parasite group)	Generic drug name
Nicotinic acetylcholine receptor (in nematodes) (Martin, 1993; Robertson & Martin, 1993; Evans & Martin, 1996)	Levamisole, butamisole, pyrantel, morantel, bephenium, thenium, methyridine
GABA receptors (in large intestinal nematodes) (Martin, 1985)	Piperazine
GluCl receptor (in nematodes and insect parasites) (Cully *et al.* 1996; Martin, 1996)	Ivermectin, abamectin, doramectin, moxidectin
Membrane calcium permeability (in cestodes and trematodes) (Redman *et al.* 1996)	Praziquantel

Table 2. Anthelmintic target sites other than ion-channels

Target site (and parasite group)	Generic drug name
β-tubulin (in nematodes)	Thiabendazole, cambendazole, oxibendazole, albendazole, albendazole sulphoxide
β-tubulin (in nematodes, cestodes and trematodes) (Roos *et al.* 1995)	Fenbendazole, oxfendazole, mebendazole, flubendazole, febantel, netobimin, thiophanate, triclabendazole
Proton ionophores (concentrated and effective against blood feeders: flukes, *Haemonchus contortus*, *Oestrus ovis*) (McKellar & Kinabo, 1991)	Closantel, rafoxanide, oxyclozanide, brotianide, nitroxynil, niclopholan, hexachlorophene, dibromosalan, niclosamide
Malate metabolism (in immature *Fasciola*) (Edwards *et al.* 1981*a*, *b*)	Diamphenethide
Phosphoglycerate kinase and mutase (in *Fasciola*) (Schulman *et al.* 1982*a*)	Clorsulon
Arachidonic acid metabolism and innate immunity of host (effective against filaria) (Maizels & Denham, 1992)	Diethylcarbamazine

Readers interested in details of the dosages and administration, uses (spectrum of action) and host toxicity, in humans are referred to the recent comprehensive text of Martindale (1996) and for equivalent data for animals are referred to the Compendium of Data Sheets for Veterinary Products (NOAH, 1997).

NICOTINIC ACETYLCHOLINE RECEPTORS

Somatic muscle cells of nematodes possess both synaptic and extrasynaptic nicotinic acetylcholine receptors. This has been shown, for example, by the experiments of Martin (1982) and Harrow & Gration (1985). These electrophysiological experiments involved the use of micropipettes placed intracellularly in muscle cells of the large nematode parasite of the pig, *Ascaris suum*. They showed that application of acetylcholine and the anthelmintics, levamisole, pyrantel and morantel (Fig. 1) resulted in the depolarization and increase in input conductance of the muscle membrane to sodium and potassium. The affects of acetylcholine were antagonized by the nicotinic antagonist tubocurarine. Subsequently patch-clamp studies, (Robertson & Martin, 1993; Robertson *et al.* 1994; Dale & Martin, 1995; Evans & Martin, 1996) have shown that the nicotinic anthelmintics open non-selective cation channels. Each channel is characterized by a particular conductance but the conductance varies between channels recorded from different patches in the range 19–60 pS. The mean open-time of the channels varies with the anthelmintic but is in the range of 0·5 ms to 2·5 ms. Thus with these electrophysiological experiments it has been possible to establish that the nicotinic anthelmintics have an action on a receptor with properties similar to but not identical with the nicotinic receptors in mammalian and vertebrate species. There must be pharmacological differences between the nicotinic receptors of nematodes and those of their host since levamisole is a selective agent producing depolarization and spastic paralysis of the nematode without a significant action on the host

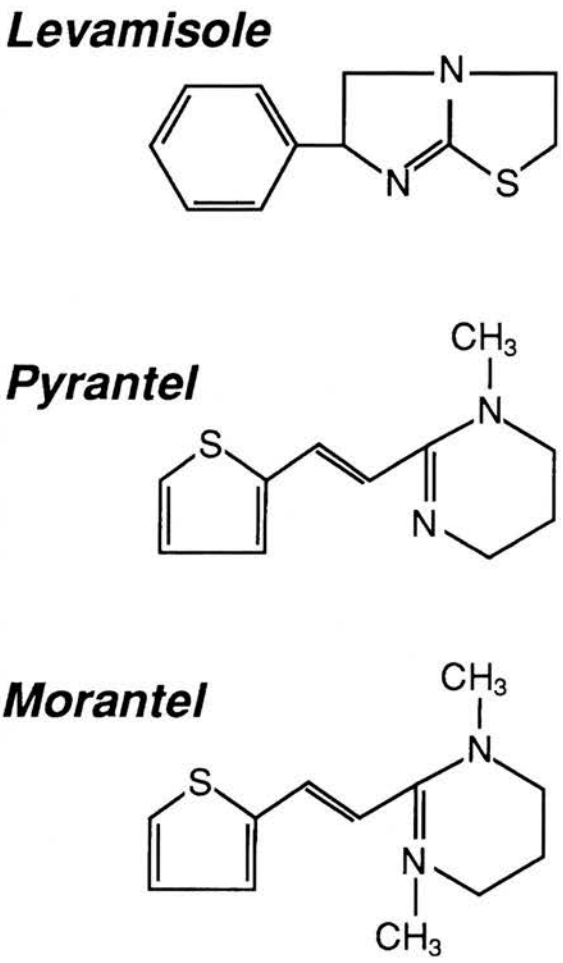

Fig. 1. The chemical structure of some nicotinic anthelmintics.

muscle. Thus the detailed pharmacology of the nematode nicotinic receptor must differ significantly from that of the host nicotinic receptors.

Structure of the nicotinic acetylcholine receptor ion-channel (nAChR)

The torpedo electric organ nicotinic receptor has been studied most extensively (Changeau, Devillers-Thiery & Chemouilli, 1996) because of its high concentration on the electric organ. It is a useful model for the nicotinic receptors of nematodes as well as higher species. The receptor-operated trans-membrane ion-channel is made up of 5 subunits arranged around a central ion-channel like the staves of a barrel. Each subunit is made up of between 437–501 amino acids (Fig. 2). The five subunits of *Torpedo* are: 2α, 1β, 1γ and 1δ, (Fig. 3). The α-subunits of all nicotinic receptors, including nematodes, are believed to contain the ligand binding site and are characterized by the presence of two adjacent cysteines at positions 192 and 193 coupled by -SS-bonds (Fig. 2). Fig. 3A shows that each subunit of the channel is formed from an extracellular loop at the *N*-terminal, four lipophilic α-helical units, M1, M2, M3 and M4 and a short *C*-terminal section. There is also an intracellular loop between M3 and M4. The pore of the ion channel is lined by the M2 sections. The pore of the ion channel formed by the M2 regions forms three negatively charged rings (Fig. 4). There is an extracellular ring lined by glutamate and aspartate which are negatively charged amino acids. There is a middle ring which is narrower and believed to form the selectivity filter of the ion-channel. It too is lined by negatively charge amino acids. This time just glutamate is involved. On the more intracellular region of the pore, another ring is formed, known as the cytoplasmic ring. It also contains negatively charged amino acids. The middle negatively-charged ring forms a narrow selectivity filter, passing only positively charged cations through the ion pore. The nicotinic acetylcholine receptor thus is able to conduct sodium, potassium and to a lesser extent, calcium through the pore. Large cationic structures like local anaesthetics, or indeed the anthelmintics like levamisole, pyrantel and morantel are too large to pass through the channel. They may pass through the extracellular ring but become blocked at the middle ring. Once they reach this site they are capable of producing channel block. Voltage-sensitive channel block by the anthelmintics, levamisole (Robertson & Martin, 1993), pyrantel (Robertson *et al.* 1994), oxantel (Dale & Martin, 1995) and morantel (Evans & Martin, 1996), has been described for the nicotinic receptors of the nematode *Ascaris suum*. These anthelmintics are agonists and antagonists of the nematode *nAChR*.

Vertebrate neuronal nicotinic receptors may be composed of a pentameric structure like that of the *Torpedo* nicotinic receptor but it is believed that only α and β-subunits combine to produce the ion channel (McGehee & Role, 1995). However, there are currently 7 different types of neuronal α-subunit and 3 different β-subunits, each of which may combine in a variety of ways to produce a large number of subtypes of *nAChR*s (McGehee & Role, 1995). It is known that injection of cRNA encoding α- and β-subunits into *Xenopus* oocytes will produce functional nicotinic channels of the neuronal type. These channels have been studied with the patch-clamp technique and it has been shown that they are characterized by heterogeneity (Papke & Heineman, 1996; Papke *et al.* 1996). The channels recorded from in each patch may be separated into subtypes which have different conductances and mean open-times. The subtype may be produced by: variations of the stoichiometry of the subunits of the channel ($\alpha\beta\alpha\beta\beta$ *vs.* $\alpha\beta\alpha\beta\alpha$); variations in the subunit composition ($\alpha\beta_2\alpha\beta_2\beta_2$ *vs.* $\alpha\beta_3\alpha\beta_3\beta_3$ – the subscript here refers to the different β subunit structure not the stoichiometry); or variations in the arrangement of the pentameric channel (i.e. $\alpha\alpha\beta\beta\beta$ *vs.* $\alpha\beta\alpha\beta\beta$).

Studies on the soil nematode, *Caenorhabditis elegans*, have shown that three genes: *lev-1*, *unc-38*

ACH1

```
                1                  11                  21            *     31                  41
MSVCTLLISC  AILAAPTLGS  LQERRLYEDL  MRNYNNLERP  VANHSEPVTV  HLKVALQQII
           51                  61                  71            *     81                  91                 101
DVDEKNQVVY  VNAWLDYTWN  DYNLVWDKAE  YGNITDVRFP  AGKIWKPDVL  LYNSVDTNFD
          111                 121                 S---          ----------  S  151                 161
STYQTNMIVY  STGLVHWVPP  GIFKISCKID  IQWFPFDEQK  CFFKFGSWTY  DGYKLDLQPA
          171                 181                 191           SS    201                 211
TGGFDISEYI  SNGEWALPLT  TVERNEKFYD  CCPEPYPDVH  FYLHMRRRTL  YYGFNLIMPC
-------M1-  --        241       ----------  -M2-----261       272       ------
ILTTLMTLLG  FTLPPDAGEK  ITLQITVLLS  ICFFLSIVSE  MSPPTSEAVP  LLGIFFTCCM
-----M3---  ----      301         311         321         331         341
IVVTASTVFT  VYVLNLHYRT  PETHDMGPWT  RNLLLYWIPW  ILRMKRPGHN  LTYASLPSLF
          351                 361                 371         381         391                 401
STKPNRHSES  LIRNIKDNEH  SLSRANSFDA  DCRLNQYIMT  QSVSNGLTSL  GSIPSTMISS
          411                 421                 431         441         451       --------
NGTTTDVSQQ  ATLLILHRIY  HELKIVTKRM  IEGDKEEQAC  NNWKFAAMVV  DRLCLYVFTI
----M4----  ---       481
FIIVSTIGIF  WSAPYLVA
```

UNC-38

```
                                    191         201
.....NSRV  AKRRAKNYPS  CCPQSAYIDV  TYYLQL...
```

Fig. 2. Amino-acid sequence of two α-subunits from *C. elegans*. Top: Amino acid sequence of an nAChR α-subunit (ACH1_CAEEL) from *C. elegans* determined from the gene sequence (Ballivet *et al.* 1996). During the synthesis of the receptor the signal sequence (*italics*) is cut off. The four putative membrane-spanning helical units M1, M2, M3 and M4 are indicated. The asterisk indicates an asparagine residue that is one site of high glycosylation. The region YDCC (tyrosine, aspartate, cysteine, cysteine) is the putative agonist binding site. The M2 region forms the putative pore region of the ion-channel. Bottom: Partial sequence of *unc-38* (Fleming *et al.* 1993 EMBL Accession Number: X98600) the α-subunit of *C. elegans* adult muscle receptor. Note that an extra amino acid proline separates the tyrosine (189) and the two cysteine (192, 193) amino acids. Deletion of the extra amino acid of *unc-38* (one from between tyrosine and the double cysteines) may remove the selective binding of levamisole and make the receptor like a mammalian receptor.

and *unc-29* of the 10–11 genes involved in levamisole resistance of this nematode (Table 3) encode the subunits of nicotinic ion-channels (Lewis *et al.* 1980; Fleming *et al.* 1997). Evidence for this is based on the homology of the *lev-1*, *unc-38* and *unc-29* amino acid sequences and the fact that when co-expressed in *Xenopus* oocytes they will produce functional channels gated by levamisole. Pairwise intranuclear injection of cDNA for *unc-38* along with *lev-1* is capable of producing functional channels (Fleming *et al.* 1997). Similarly, pairwise injection of *unc-38* with *unc-29* will also produce functional channels. This implies that the nicotinic receptor of *C. elegans* and perhaps that of nematodes could be comprised of varying combinations of subunits. An illustration of this varying structure which may make up the nicotinic channel is shown in Fig. 5: even in this illustration the number of possible arrangements is limited by maintaining the *unc-38* subunits, required for agonist binding, fixed in number and position. It is pointed out that other α subunits are also recognized in *C. elegans* including the subunit *ACh1* (also referred to as CE21, Ballivet *et al.* 1996) and have been cloned and expressed. Interestingly *ACh1* will express as a homo-oligomer in *Xenopus* oocytes and produce channels sensitive to nicotine but not levamisole. One explanation for the difference in the levamisole-sensitivity of channels produced with *unc-38* subunits in contrast to channels with *ACh1* subunits may relate to the addition of and extra amino acid at the putative agonist binding site between tyrosine (189) and cysteine (192) in *unc-38* which is not present in the levamisole insensitive *ACh1* subunit (Fig. 2).

It is believed that *unc-38* is required for the ligand-binding site. Evidence for this is based on the homology of *unc-38* with the α-subunit of torpedo and the fact that exclusion of *unc-38* from the pairwise cRNA injections into *Xenopus* oocytes results in the failure of expression.

It is known that the precise pharmacological profile of neuronal nicotinic receptors of vertebrates can vary with the molecular structure of the ion channel (Covernton *et al.* 1996). It varies with the molecular structure of the α-subunit and is also influenced by the β-subunit structure. It has been suggested that the agonist binding sites on nicotinic acetylcholine receptors may actually be on the interface between the α and β subunits (Karlin & Akabas, 1995). Thus in nematodes with the *unc-38*,

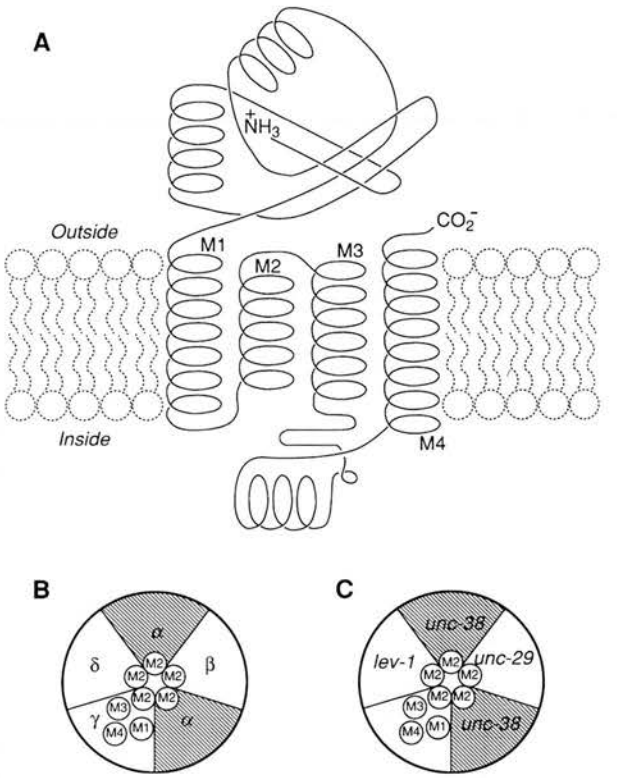

Fig. 3. The structure of the nicotinic channel. A: Diagram of the putative arrangement of the amino acid sequence in the membrane with the 4 α-helices M1, M2, M3 and M4 form transmembrane segments. There is a cytoplasmic loop between M3 and M4. B: The subunit arrangement of the *Torpedo* electric organ nicotinic receptor. Note that the M2 region forms the lining of the channel pore. C: A possible arrangement of the subunits *unc-38*, *unc-29*, *lev-1* that may make up the levamisole receptor. (Derived from Noda *et al.* 1983).

unc-29 and *lev-1* subunits, one could produce a variety of combinations of *unc-38* with *unc-29* and *lev-1* to produce the *nAChR* subtypes. Each of these particular combinations of ion channel will have slightly different pharmacological profiles and biophysical kinetics. It may be possible to separate out the properties of some of the individual combinations biophysically since they may have different conductance levels and mean open times.

We have examined the nicotinic receptor on *A. suum* muscle at the single channel level, using acetylcholine, levamisole, pyrantel and morantel as the agonists (Pennington & Martin, 1990; Robertson & Martin, 1993; Robertson *et al.* 1994; Evans & Martin, 1996). In all of these single channel studies, we have found that there is considerable variation in the conductance level of the channel observed between patch recordings. The conductance levels of the single channel currents have ranged between 15 pS at the lowest extreme up to 60 pS at the highest extreme. In some individual patch experiments it has been clear that more than one conductance level is present. The origin of this variability may be explained if we have different subunit combinations, some producing small conductance levels and others producing higher conductance levels. There are many other causes of variability. Our source of *Ascaris* varies dramatically and could easily influence the particular observations because factors like diet may alter the biophysical properties of the lipid membrane in which the ion channels site. To reduce this possibility, we have now conducted experiments on a smaller nematode, *Oesophagostomum dentatum* that may be infected from laboratory-maintained strains and produced in pigs under more controlled conditions. Our experiments on the nicotinic receptors of *O. dentatum* activated by levamisole also showed great variability. Fig. 6 shows an example of a channel recording at −75 mV where there are at least two amplitude current levels present. This implies that in this patch there are at least two different sub-types of nicotinic receptor, each may have a slightly different pharmacology, one channel type may be more resistant to opening by levamisole than the other. We have seen evidence suggesting that there are up to 4 nicotinic receptor subtypes present in *O. dentatum* (Martin *et al.* 1997). This heterogeneity may facilitate the development of anthelmintic resistance to nicotinic anthelmintics and perhaps other anthelmintics that act on membrane ion channels.

GABA AGONIST: PIPERAZINE

Piperazine is a heterocyclic ring without a carboxyl group. Despite this, it acts as a simple GABA agonist and gates open GABA receptors on the somatic muscle of nematodes (Del Castillo, De Mello & Morales, 1964; Corbett & Goose, 1971; Martin, 1985). It increases the Cl^- conductance of the muscle membrane leading to an increase in the membrane potential (a hyperpolarization) and a reduction in excitability. This leads to a relaxation of the body muscle and flaccid paralysis. Piperazine is effective against large intestinal nematodes and is potentiated by the presence of a high pCO_2. The CO_2 may interact with the heterocylic ring of piperazine and substitute for the carboxyl group of GABA.

AVERMECTINS

The avermectin anthelmintics (see Fig. 7) include ivermectin, abamectin, doramectin, and moxidectin, Their mode of action is to increase the Cl^- permeability of nerve and muscle membrane of invertebrates but the identity of the target ion-channel has been controversial (see Arena, 1994, for a review). The mode of action does not appear to be via GABA-gated Cl^- channels. Expression cloning experiments using *Xenopus* oocytes have suggested an action of avermectins on a glutamate-gated Cl^- (GluCl) channel (Cully *et al.* 1994). The channel is presumably a pentomer like that of the nicotinic

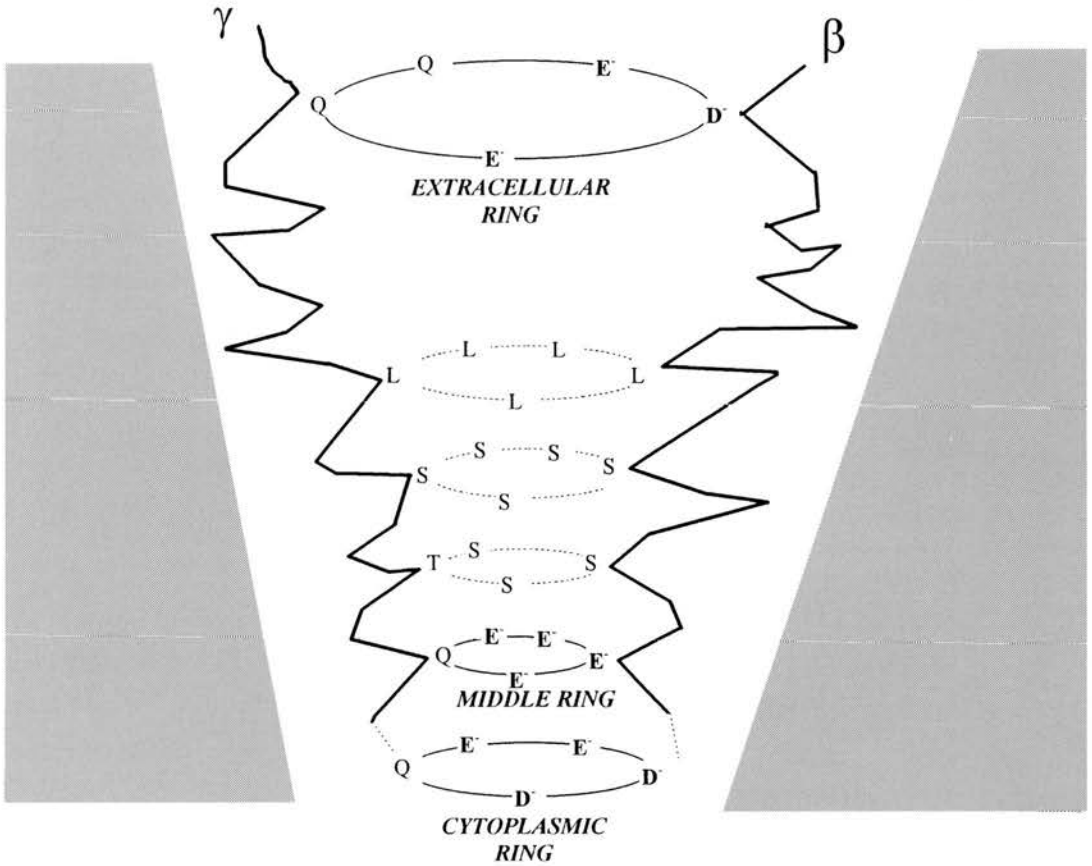

Fig. 4. The structure of the *Torpedo* nicotinic (derived from Revah *et al.* 1990). The organization of the pore of the nicotinic ion-channel showing: the presence of the outer extracellular ring lined with glutamate and aspartate amino acids; the middle ring which appears to act as a selectivity filter and is lined with glutamate amino acids forming a charged negative ring; the inner cytoplasmic ring lined with aspartate and glutamate amino acids.

Table 3. Genes responsible for levamisole resistance in *C. elegans* (Fleming *et al.* 1996)

Gene	Chromosome	Product
unc-38	I	α-subunit
unc-29	I	Non α-subunit
lev-1	IV	Non α-subunit
unc-74	I	Receptor expression
unc-50	III	Receptor expression
lev-8	X	Receptor expression
lev-9	X	Receptor expression
lev-10	I	Receptor expression
lev-11	I	Muscle specific Contraction defect
unc-22	IV	Muscle specific Contraction defect

Other *nAChR* subunit genes have been identified in the *C. elegans* genome. These subunits have not yet been demonstrated to be involved in levamisole resistance. They include: *ach1*, *ach2*, *ach3*, *deg-3*, *t09a5.3* and *ZC504*, *FO3F8.2*.

receptor but the equivalent of the M2 region which forms the ion channel pore of the *nAChR* channels is lined with positively charged sites so that the channel is selectively permeable to anions (Cl^-). The pentomer may be comprised of GluCl-α subunits which contain the glutamate binding site and the GluCl-β subunit that contains the ivermectin binding site.

The locations of the glutamate-gated chloride channel in nematodes were not determined by the expression studies of Culley *et al.* (1994). Molecular experiments using the *lac-Z* marker showed that the GluCl β-subunit of the glutamate channel was expressed in the pharyngeal muscle of *C. elegans* (Laughton, Wolstenholme & Lunt, 1995). The location of the GluCl-α subunit was not determined. As a result of these experiments, Martin (1996) used a two micro-electrode current clamp technique on the pharyngeal muscle of *A. suum*. These experiments demonstrated that the parasite possesses glutamate receptors that gate chloride channels and that this channel is potentiated by ivermectin analogues.

Fig. 8 shows the effect of application of glutamate on the pharyngeal muscle of *Ascaris* which is to produce a brief hyperpolarization and a reversible increase in conductance of the muscle. It also shows the effect of the application of milbemycin, an avermectin. Recent molecular experiments with *C. elegans* on an ivermectin resistance strain (*avr-15*)

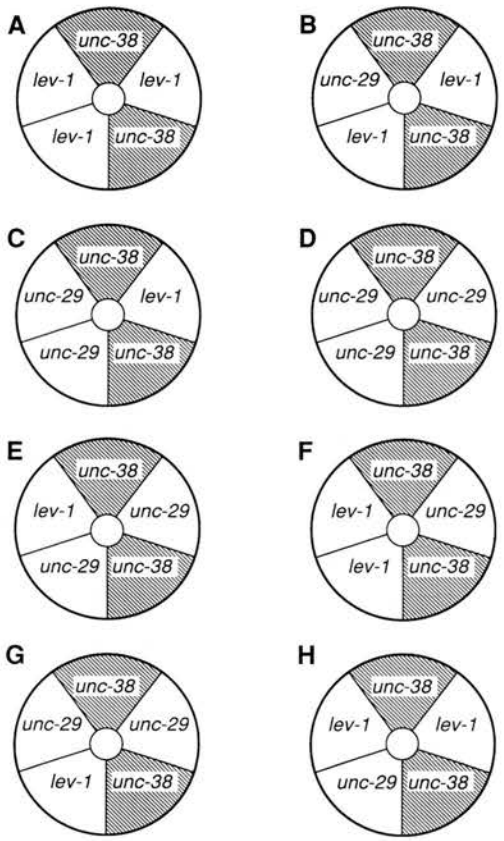

Fig. 5. Diagram of some possible subunit arrangments of *unc-38*, *unc-29* and *lev-1* subunits forming the nematode nAChR channel sensitive to levamisole. The *unc-38* is equivalent to the α subunit of vertebrate nicotinic channels. The *unc-29* and *lev-1* subunits are equivalent to vertebrate β subunits. The diagram shows that there are up to 8 different combinations possible if two *unc-38* subunits have to be maintained in the same relative position. If the conductance of the channel were altered only by the number of *unc-29* or *lev-1* subunits present in this scheme then 4 channel types would be distinguished on a basis of channel conductance. The diagram also illustrates that if the binding of the agonist molecule is at the interface of the *unc-38* subunit and an adjacent molecule then the binding of the agonist (including levamisole) will depend on subunit composition (derived from Martin *et al.* 1997).

suggests that it is a GluCl-α_2 subunit that is present in the pharyngeal muscle of *C. elegans*, not the GluCl-α_1 subunit (review, Cully *et al.* 1997). The location function and expression of the GluCl-α_1 remains to be determined. It does not appear to be present in the pharynx. The distribution of this subunit may help to determine other sites of action of the ivermectins.

CALCIUM PERMEABILITY: PRAZIQUANTEL

Praziquantel is used for the control of schistosomiasis and cestode infections. It has little action against nematode parasites. Its mode of action has been reviewed recently (Redman *et al.* 1996). Application of praziquantel to *Schistosoma mansoni* results in a slow depolarization of the tegument. Associated with the depolarization is an increase of influx of calcium (Fetterer, Pax & Bennett, 1980; Mehlhorn *et al.* 1981; Wolde-Mussie *et al.* 1982; Thompson, Pax & Bennett, 1984). The mode of entry of calcium is not known but Fig. 9 illustrates some possible routes. It is, however, known that its activity may be blocked by high concentrations of magnesium, lanthanum, nickel, and cobalt. The site of action of praziquantel appears to be the tegument of *Schistosoma* as application of praziquantel to isolated body muscle cells from *Schistosoma* has little effect. It is known that application of praziquantel to a muscle preparation from snails mimics the application of caffeine. In fact, prior application of caffeine to this snail muscle preparation pre-empts and abolishes the effect of praziquantel in low calcium extracellular solutions (Gardner & Brezden, 1984).

Thus it appears that the site of action of praziquantel may involve the same site as caffeine. Caffeine is known to act on a calcium-induced calcium release (CICR) channel in the sarcoplasmic reticulum of muscle. This channel releases a flood of calcium into the cytoplasm from the sarcoplasmic reticulum and is triggered by a smaller rise in cytoplasmic calcium produced through voltage-activated calcium channels in the cell (sarcolemma) membrane. The CICR channel of sarcoplasmic reticulum has a high conductance of several hundred pS and has some similarity to the large conductance channel in the tegument of *Schistosoma* (Day, Bennett & Pax, 1992).

It is also known that following the application of praziquantel through *S. mansoni* antigens are exposed that were not previously available to the host. As a result of this exposure, presumably by damage to the outer bilayer of the double bilayer of the tegument, host inflammatory cells move in to attack the schistosome. The exposure of the antigen may be a secondary effect of the elevated calcium since maintained calcium levels not only elevate the exposure of antigens but there is a blebbing of the schistosome membrane (Redman *et al.* 1996).

Most of the mode of action studies on praziquantel have involved *S. mansoni*. Less is known about the direct effect of praziquantel on cestode parasites. It is presumed the mode of action on both groups of parasite is the same.

BENZIMIDAZOLES: β-TUBULIN

The benzimidazole group of anthelmintics including thiabendazole, mebendazole and fenbendazole, are broad-spectrum anthelmintics which have an action against gastrointestinal nematodes and in some cases, at a higher concentration, actions against trematodes. Their mode of action is now known to involve binding to β-tubulin. β-tubulin along with

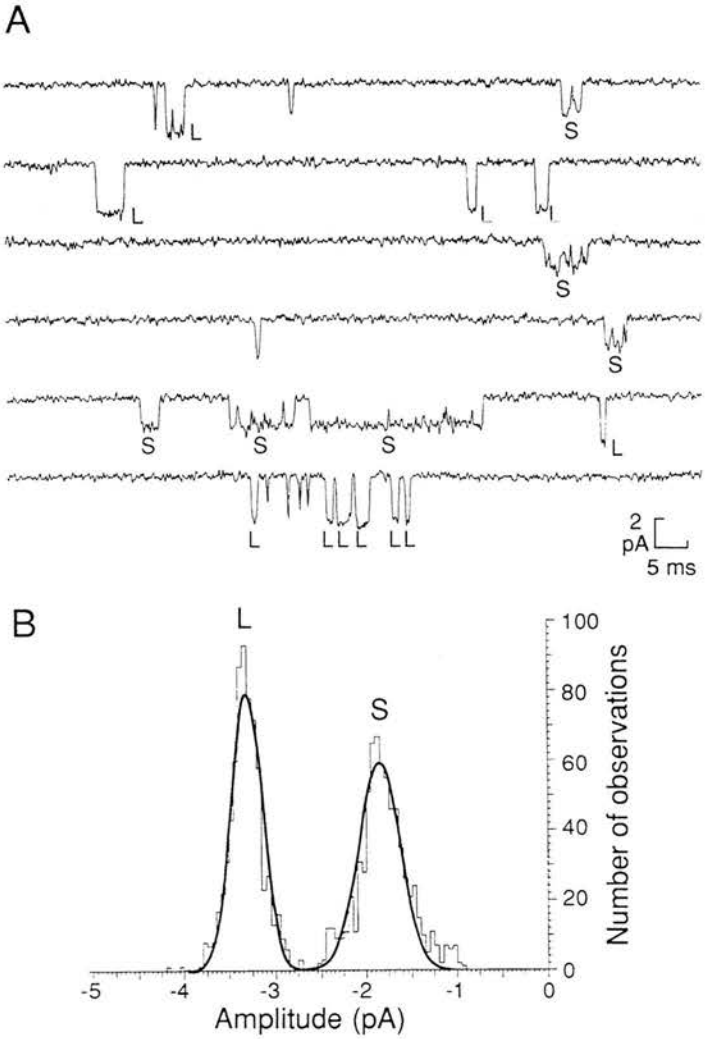

Fig. 6. A: Cell-attached patch recording at −75 mV showing a small (S) and larger (L) nAChR channel present. B: Amplitude histogram of open-channel amplitudes. Smaller conductance channel: mean current = −1·8 pA ± 0·2 (24·8 pS) labelled S in Fig. 5A. Larger conductance channel: mean current = −3·3 ± 0·2 pA (43·8 pS) labelled L in Fig. 5A). Histograms of the amplitudes of the open-channel currents were fitted with Gaussian distributions. 49 % of the events were to the smaller amplitude, 51 % were to the larger amplitude.

α-tubulin polymerizes to form microtubule structures inside the cells of nematodes and the host animal (Stryer, 1995).

The mode of action of the benzimidazoles started to be understood when it was realized that mebendazole given to *Ascaris* produced damage to the intestinal cells of the parasite. It was found that there was a loss of cytoplasmic tubules of both the intestinal cells and teguments of cestodes and nematodes (Van den Bossche & De Nollin, 1973; van den Bossche, Roshette & Horig, 1982). This was associated with a loss of transport of secretory vesicles and the failure of the intestinal cells to take up glucose. Thus following application of mebendazole, the parasite starved. It was found in *Ascaris* that mebendazole bound to cytoplasmic proteins that had a molecular weight of 50 kDa and 100 kDa which are monomers and dimers of tubulin. It was found that the benzimidazoles anthelmintics competed for the binding site on β-tubulin with colchicine, a substance known to block cell division in the metaphase (Sangster, Prichard & Lacey, 1985; Lacey & Gill, 1994). Microtubules serve a variety of intracellular functions including transport of cytoplasmic secretory vesicles (Stryer, 1995).

Structure and function of microtubules

Microtubules are formed in a dynamic process by the combination of two 450 amino acid proteins that are known as α-tubulin and β-tubulin (Stryer, 1995). The formation of the microtubules involves the polymerization of tubulin at one end, known as the positive pole, and the depolymerization at the other end, known as the negative pole. Microtubules that form are made up of thirteen tubulin molecule rings (6 α-tubulin plus 7 β-tubulin, alternating with 7 α-tubulin plus 6 β-tubulin rings). There are a number of factors which encourage polymerization and these factors include GTP, magnesium and an increase in

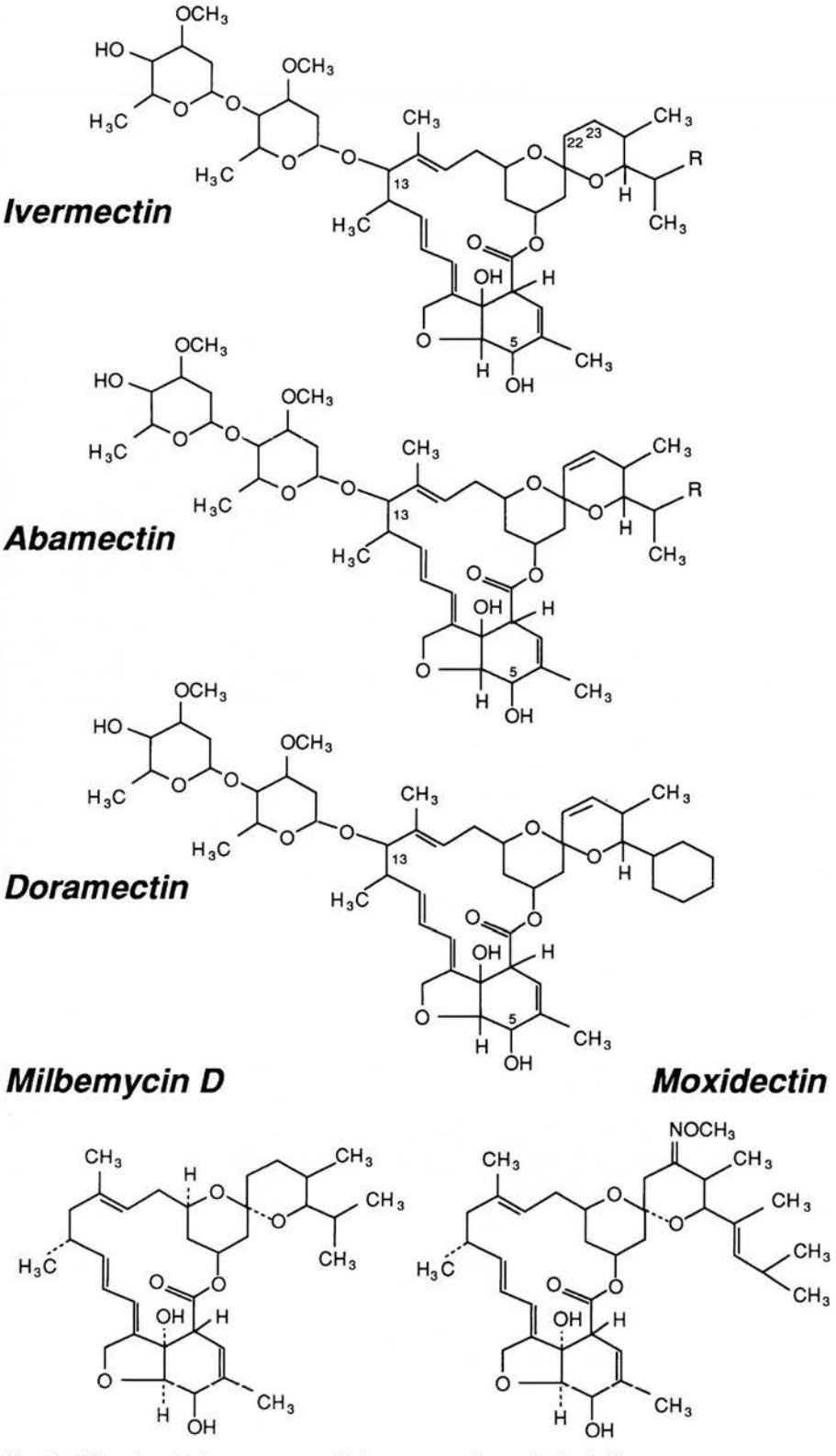

Fig. 7. The chemical structures of the avermectin anthelmintics.

temperature: a fall in temperature to 4 °C or the presence of calcium or calmodulin favours depolymerization. The formation of microtubules can be prevented or inhibited by substances that bind to the positive pole (the leading edge) of polymerization. This process is known as capping and it can be achieved by colchicine, vinblastine, vincristine, or the benzimidazoles, which do this by binding to β-tubulin molecules.

Thus we know that the mode of action of benzimidazole anthelmintics is to bind to nematode β-tubulin more selectively than the host microtubule β-tubulin. The onset of benzimidazole anthelmintic action is therefore slower than that of the anthel-

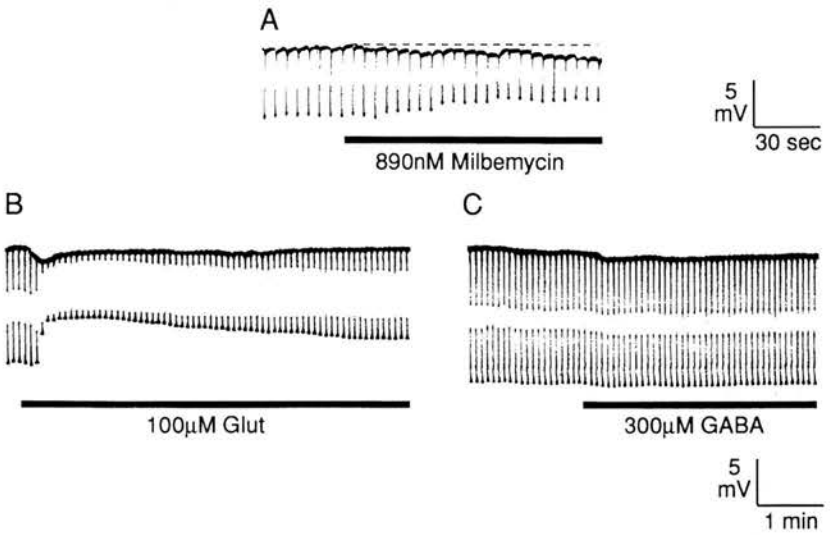

Fig. 8. A: Effect of 890 nM milbemycin D on the membrane potential and input conductance. Milbemycin slowly produced an increase in input conductance that was not reversed on washing (not shown). B: Effect of application of 100 μM L-glutamate on membrane potential and input conductance. Different preparation from B. Glutamate (applied during horizontal bar) produced a transient small hyperpolarization of 1 mV associated with an input conductance change from 157 μS to a peak of 429 μS (ΔG: 272 μS) desensitizing to 231 μS (ΔG: 74 μS) after 4 minutes. C: After washing the preparation the input conductance of the pharynx returned towards control levels (142 μS) and the effect of 300 μM GABA was tested without effect (applied during the horizontal bar). The lack of effect of GABA was not due to desensitization because subsequent application of 100 μM L-glutamate increased the input conductance again (not shown) (derived from Martin *et al.* 1995).

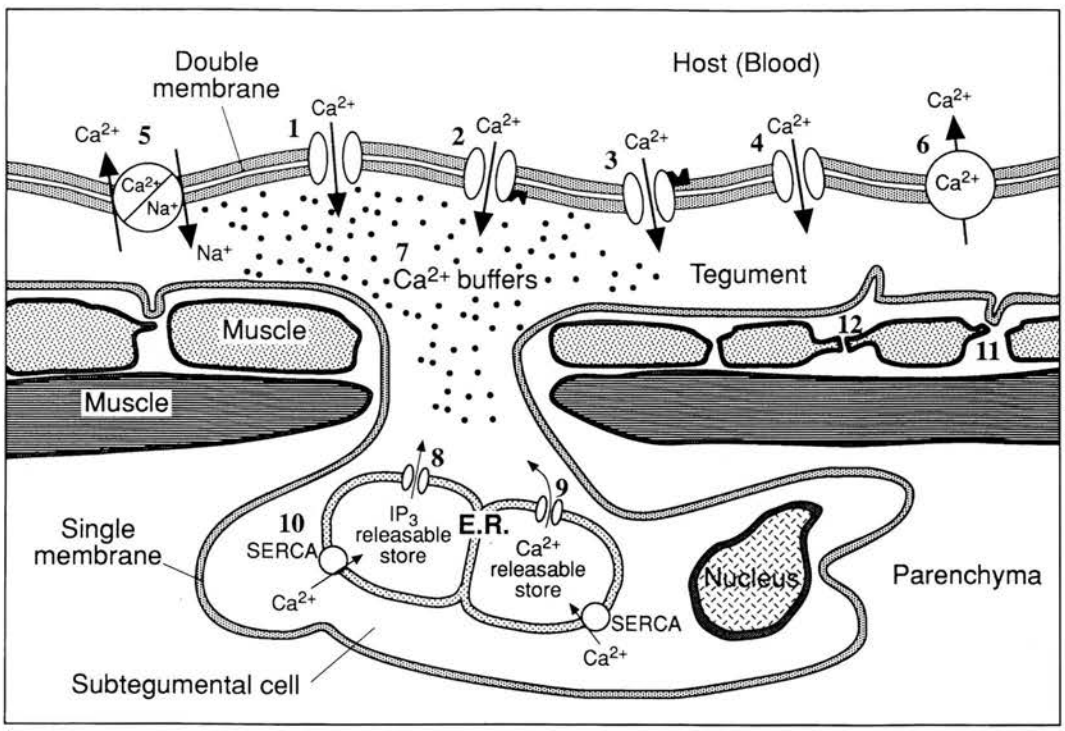

Fig. 9. Diagram of the structure of the body wall of *Schistosoma mansoni* showing the possible sites of action of praziquantel and mechanisms of Ca^{2+} transport into and out of the tegument. 1: voltage-activated Ca^{2+} channel. 2: Intracellular messenger activated Ca^{2+} channel. 3: Extracellular receptor operated Ca^{2+} channel. 4: Non-selective cation channel also allowing entry of Ca^{2+}. 5: Na^+/Ca^{2+} exchanger. 6: Ca^{2+} ATPase pumping out Ca^{2+}. 7: Intrategumental Ca^{2+} buffers. 8: IP_3 releasable store from the sarcoplasmic reticulum. 9: Ca^{2+}-induced Ca^{2+} release channel (CICR channel). 10: Ca^{2+} ATPase pump: sarcoplasmic endoplasmic reticulum Ca^{2+} (SERCA). 11: Electrical junction between muscle cell and tegument. 12: Electrical junctions between muscle cells. If praziquantel acts like caffeine it would act on site 9 (derived from Redman *et al.* 1996).

mintics that work directly on ion-channels. Benzimidazoles must produce starvation of the nematode by intestinal disruption and/or inhibition of egg production.

In *Haemonchus contortus*, two types of β-tubulin have been recognized: isotype 1 and isotype 2 (Roos, Kwa & Grant, 1995). These two isotypes have separate genes and have a number of alleles: there are up to six alleles for isotype 1 and up to 12 alleles for isotype 2. The function of the specific isotopes is not known in nematodes. Roos *et al.* (1995) has shown that there is a reduction in the number of isotype alleles for β-tubulin during the appearance of benzimidazole resistance. Observations made on the appearance of resistance of *H. contortus* showed that there was a progressive loss of alleles for isotype 1 and a total loss of alleles for isotype 2. Resistance may be explained by loss of susceptible phenotypes of the β-tubulin and the survival of resistance phenotypes. It is known that benzimidazole resistance in fungi is associated with the appearance of a different form of β-tubulin (Fujimura *et al.* 1992). It is characterized by the appearance of a tyrosine instead of phenylalanine in position 200 on the β-tubulin chain. Unfortunately, mammalian β-tubulins also have tyrosine at position 200 (Lewis, Lee & Cowen, 1985) so it is unlikely that benzimidazole resistance may be overcome by changes in the chemistry of the drug since the fungal benzimidazole has learned to mimic the host β-tubulin. If such a phenomenon occurs in nematode parasites, it would result in the inability of the benzimidazoles to exert a selective toxic effect.

PROTON IONOPHORES

The proton ionophores include the salicylanilides and substituted phenols (for a review see McKellar & Kinabo, 1991). They include closantel, rafoxanide, oxyclozanide and brotianide. They are a range of compounds that have anti-fluke action. Their mode of action is that of a proton ionophore which is usually called an oxidative phosphorylase uncoupler. Each of the salicylanilides or the substituted phenols contains a detachable proton group. The compounds are all very lipophilic so that they dissolve in the phospholipid membranes of cells and may shuttle across the membrane carrying protons. They do this particularly across the inner mitochondrial membrane and will reduce any proton gradient. Since a proton gradient is necessary for the production of ATP by mitochondria there is an inhibition of the energy production by the mitochondria following poisoning by the salicylanilide.

The selective mode of action of the series of compounds that act as oxidative phosphorylase uncouplers is believed to involve and to be associated with the very high plasma protein binding of these compounds which are effective therapeutically. The anthelmintics used in this way have a very long half-life of more than fourteen days. More than 95% of the salicylanilides are plasma protein bound. Thus the selective action of these anthelmintics may be explained by an action on blood-sucking parasites concentrating the anthelmintic in the parasite as it takes in high levels of plasma protein.

Pax & Bennett (1989) have examined the pH gradient across *S. mansoni* following treatment with salicylanilides. They were able to demonstrate an effect on the tegument of the parasite indicating that this may be a site of action for these anthelmintics. Thus mitochondria may not be the only site at which these compounds exert their effect.

MALATE METABOLISM

The compound diamphenethide is an agent that is effective against immature *Fasciola hepatica* in the liver but less effective against *Fasciola* in the bile ducts. Diamphenethide is deacetylated in the host liver to an active monoamine and diamine (Coles, 1976). The amine of diamphenethide has an action which produces an elevation of malate concentration in *Fasciola* (Edwards *et al.* 1981*b*). Malate is an intermediary break-down product of glucose in this parasite. It is known that dopamine, a putative neurotransmitter in *Fasciola*, has a protective effect against diamphenethide but the mode of action of a diamphenethide has yet to be defined in greaer detail (Edwards *et al.* 1981*a*).

PHOSPHOGLYCERATE KINASE AND MUTASE INHIBITION

Clorsulon is very similar in structure to 1,3-diphosphoglycerate and because of this it inhibits the enzymes phosphoglycerate kinase and phosphoglyceromutase of *Fasciola* (Schulman & Valentino, 1982; Schulman *et al.* 1982*a*). Thus it prevents the full breakdown of glucose by the Emden-Meyerhoff pathway and inhibits glucose utilization. The inhibition of the phosphoglycerate kinase was competitive with clorsulon inhibiting the binding of 3-phosphoglycerate and ATP to the kinase. Clorsulon thus has a dose-dependent inhibitory effect on immature and mature *Fasciola* (Schulman *et al.* 1982*b*).

ARACHIDONIC ACID METABOLISM AND INNATE IMMUNITY

Diethylcarbamazine is a piperazine derivative used in low doses as an anti-filarial drug. Although it has a good microfilaricidal action, it has limited macrofilaricidal action. Its action against some adult helminths requires nearly 10 times the prophylactic filarial dose and may involve another mode of action.

Although the structure of diethylcarbamazine might suggest it acts like piperazine, electro-

physiological studies following bath application to *A. suum* have shown that it does not mimic the actions of piperazine (Martin, 1982). It appears that there is little direct action on filariae when diethylcarbamazine is added to isolated parasites. It has quite marked *in vivo* effects in experiments in contrast to its *in vitro* effects. Following intravenous injection it produces an anti-filarial action within about 4 minutes (Hawking & Laurie, 1949). In mice that have had their immune system impaired genetically (nude, athymic mice) which are infected with *Brugia pahangi* there is a marked reduction in microfilariae following administration of diethylcarbamazine (Vickery, Nayar & Tamplin, 1986). These experiments show that T-cells and T-dependent responses (IgG and IgE) are not involved.

It is known that diethylcarbamazine has an antagonistic action on the metabolism of arachidonic acid which is produced from the breakdown of cell membranes under the influence of phospholipase A_2 (Maizels & Denham, 1992). It is often said that 5-lipoxygenase is the enzyme which is inhibited by diethylcarbamazine. But it has also been suggested that synthesis of LTA_4 by LTA_4-synthase from 5-HPETE is blocked by diethylcarbamazine in mast cells (Mathews & Murphy, 1982; Razin *et al.* 1984). Diethylcarbamazine is also believed to block production of PGI_2 (prostacyclin) by inhibition of endothelial cyclo-oxygenase (Kanesa-Thasan, Douglas & Kazura, 1991). It does not appear to have any effect on the production of thromboxane (TXA_2). Microfilariae also produce their own PGI_2 and PGE_2 and these too are inhibited by diethylcarbamazine during treatment (Kanesa-Thasan *et al.* 1991). It seems then that diethylcarbamazine inhibits production of PGI_2 and PGE_2 by both endothelial cells and microfilariae. These two eicosanoids are involved in the control of blood vessel tone and the inhibition of neutrophil aggregation and granulocyte aggregation.

Thus a reasonable explanation for the action of diethylcarbamazine at low doses to prevent microfilariae is that it alters the metabolism of arachidonic acids in the host endothelial cells and microfilariae. As a result of this, there is constriction of the blood vessels and aggregation of the host granulocytes and host platelets. Thus it appears that diethylcarbamazine activates an innate immune response rather than an adaptive response (Maizels & Denham, 1992). This mode of action could explain why diethylcarbamazine does not have an effect *in vitro* against the microfilariae and is not effective in non-immune animals.

FUTURE DEVELOPMENT OF ANTHELMINTICS

Continued economic losses in animal production and human disease due to parasites are still of concern to industrial chemists looking for new anthelmintic agents. The intensive use of drugs for the control of nematode parasites has and will continue to lead to the development of resistance. New anthelminitics are needed for the future but the huge costs associated with the development on new compounds and the small economic size of the market for anthelmintics will make future development slow. The limited market size and concerns over resistance and residues are reflected in the decrease in patent applications. With increased knowledge of parasite physiology, particularly the nicotinic acetylcholine receptors, the GABA receptors and the glutamate-Cl^- channel as examples, a directed rational search for new leads should be possible. Surveying natural substances (plant extracts and antibiotics) is also in an early stage with only a small fraction of the microbial ecosystem having been surveyed. Recently, the dioxapyrrolomycins as lead compounds for AC303630 (Hunt, 1994), the anthelmintic cyclodepsipeptide PF1022A (Martin *et al.* 1996) and paraherquamides (Schaeffer *et al.* 1990) have been reported. These show the continuing potential of such an approach. There remains a demand for new potent broad-spectrum anthelmintics which are effective against resistant parasites, harmless to the environment and can be cost-effective. Anthelmintics with different parasite target sites are to be expected in the future.

ACKNOWLEDGEMENTS

R. J. M. is pleased to acknowledge the financial support of The Wellcome Trust who have supported my electrophysiological work on the nicotinic anthelmintics and the glutamate receptors of *Ascaris*. H. B. is pleased to acknowledge the support of the Danish National Research Foundation.

REFERENCES

ARENA, J. P. (1994). Expression of *Caenorhabditis elegans* messenger RNA in *Xenopus*-oocytes: a model system to study the mechanism of action of avermectins. *Parasitology Today* **10**, 35–37.

BALLIVET, M., ALLIOD, C., BERTRAND, S. & BERTRAND, D. (1996). Nicotinic acetylcholine receptors in the nematode *Caenorhabditis elegans*. *Journal of Molecular Biology* **258**, 261–269.

CHANGEAU, J.-P., DEVILLERS-THIERY, A. & CHEMOUILLI, P. (1996). Acetylcholine receptor: An allosteric protein. *Science* **225**, 1335–1345.

COLES, G. C. (1976). The inactivity of diamphenethide against liver fluke in certain species of mammals. *Journal of Parasitology* **20**, 110–111.

CORBETT, J. R. & GOOSE, J. (1971). The biochemical mode of action of the fasciolicides, nitroxynil, hexachlorophene, and oxyclozanide. *Biochemical Journal* **121**, 41.

COVERNTON, P. J. O., KOJIMA, H., SIVILOTTI, L. G., GIBB, A. J. & COLQUHOUN, D. (1996). Comparison of neuronal nicotinic receptors in rat sympathetic neurones with

subunit pairs expressed in *Xenopus* oocytes. *Journal of Physiology (London)* **481**, 27–34.

CULLY, D. F., VASSILATIS, D. K., LIU, K. K., PARESS, P. S., VANDERPLOEG, L. H. T. & SCHAEFFER, J. M. (1994). Cloning of an avermectin-sensitive glutamate-gated chloride channel from *Caenorhabditis elegans*. *Nature* **371**, 707–711.

CULLY, D. F., WILKINSON, H., VASSILITIS, D. K., ETTER, A. & ARENA, J. P. (1996). Molecular biology and electrophysiology of glutamate-gated chloride channels of invertebrates. *Parasitology* **113**, S191–S200.

DALE, V. M. E. & MARTIN, R. J. (1995). Oxantel-activated single-channel currents in the muscle membrane of *Ascaris suum*. *Parasitology* **110**, 437–448.

DAY, T. S., BENNETT, J. L. & PAX, R. A. (1992). *Schistosoma mansoni*: patch-clamp study of a non-selective cation channel in the outer tegumental membrane of females. *Experimental Parasitology* **74**, 348–356.

DEL CASTILLO, J., DE MELLO, W. C. & MORALES, T. (1964). Mechanism of the paralysing action of piperazine on *Ascaris* muscle. *British Journal of Pharmacology* **22**, 463–477.

EDWARDS, S. R., CAMPBELL, A. J., SHEERS, M., MOORE, R. J. & MONTAGUE, P. E. (1981*a*). Protection of *Fasciola hepatica* against flukicidal action of the amine of diamphenethide *in vitro*. *Molecular and Biochemical Parasitology* **2**, 339–348.

EDWARDS, S. R., CAMPBELL, A. J., SHEERS, M., MOORE, R. J. & MONTAGUE, P. E. (1981*b*). Studies of the effect of diamphenethide and oxyclozanide on the metabolism of *Fasciola hepatica*. *Molecular and Biochemical Parasitology* **2**, 323–338.

EVANS, A. M. & MARTIN, R. J. (1996). Activation and cooperative multi-ion block of single nicotinic-acetylcholine channel currents of *Ascaris* muscle by the tetrahydropyrimidine anthelmintic, morantel. *British Journal of Pharmacology* **118**, 1127–1140.

FETTERER, R. H., PAX, R. A. & BENNETT, J. L. (1980). *Schistosoma mansoni*: characterization of the electrical potential from the tegument adult males. *Experimental Parasitology* **49**, 353–365.

FLEMING, J. T., BAYLIS, H. A., SATELLE, D. B. & LEWIS, J. A. (1996). Molecular cloning and *in vitro* expression of *C. elegans* and parasitic nematode ionotropic receptors. *Parasitology* **113**, S175–S190.

FUJIMURA, M., OEDA, K., INOUE, H. & KATO, T. (1992). A single amino acid substitution in the β-tubulin gene of *Neurospora* confers both carbendazim resistance and diethofencarb sensitivity. *Current Genetics* **21**, 399–404.

GARDNER, D. R. & BREZDEN, B. L. (1984). The sites of action of praziquantel in a smooth muscle of *Lymnaea stagnalis*. *Canadian Journal of Physiology and Pharmacology* **62**, 282–287.

HARROW, I. D. & GRATION, K. A. F. (1985). Mode of action of the anthelmintics morantel, pyrantel and levamisole on muscle-cell membrane of the nematode *Ascaris suum*. *Pesticide Science* **16**, 662–672.

HAWKING, F. & LAURIE, W. (1949). Action of hetrazan on filariasis and onchocerciasis. *Lancet* **2**, 146–147.

HUNT, D. A. (1994). 2-Arylpyrroles: novel uncouplers of ocidative phosphorylation. In: *Advances in the Chemistry of Insect Control III* (ed. G. G. Briggs), pp. 127–140. Cambridge, Royal Society of Chemistry.

KANESA-THASAN, N., DOUGLAS, J. G. & KAZURA, J. W. (1991). Diethylcarbamazine inhibits endothelial and microfilarial prostanoid metabolism *in vitro*. *Molecular and Biochemical Parasitology* **49**, 11–20.

KARLIN, A. & AKABAS, M. (1995). Towards a structural basis for the function of nicotinic acetylcholine-receptors and their cousins. *Neuron* **15**, 1231–1244.

LACEY, E. & GILL, J. H. (1994). Biochemistry of benzimidazole resistance. *Acta Tropica* **56**, 245–262.

LAUGHTON, D. L., WOLSTENHOLME, A. J. & LUNT, G. (1995). The beta subunit of the *C. elegans* inhibitory glutamate receptor is expressed in the pm4 pharyngeal muscle cells. *Worm Breeders Gazette* **14**, 48.

LEWIS, J. A., WU, C.-H., LEVINE, J. H. & BERG, H. (1980). Levamisole-resistant mutants of the nematode *Caenorhabditis elegans* appear to lack pharmacological acetylcholine receptors. *Neuroscience* **5**, 967–989.

LEWIS, S., LEE, M. G.-S. & COWEN, N. J. (1985). Five mouse tubulin isotypes and their regulated expression during development. *Journal of Cell Biology* **101**, 852–861.

MAIZELS, R. M. & DENHAM, D. A. (1992). Diethylcarbamazine (DEC): immunopharmacological interactions of an anti-filarial drug. *Parasitology* **105**, S49–S60.

MARTIN, R. J. (1982). Electrophysiological effects of piperazine and diethylcarbamazine on *Ascaris suum* somatic muscle. *British Journal of Pharmacology* **77**, 255–265.

MARTIN, R. J. (1985). γ-aminobutyric acid- and piperazine-activated single channel currents from *Ascaris suum* body muscle. *British Journal of Pharmacology* **84**, 445–461.

MARTIN, R. J. (1993). Neuromuscular transmission in nematodes and anthelmintic drug action. *Pharmacology and Therapeutics* **58**, 13–50.

MARTIN, R. J. (1995). An electrophysiological preparation of *Ascaris suum* pharyngeal muscle reveals a glutamate-gated chloride channel sensitive to the avermectin analogue milbemycin D. *Parasitology* **112**, 247–252.

MARTIN, R. J., HARCLER, A., LONDERSHAUSEN, M. & JESCHKE, P. (1996). Anthelmintic actions of the cyclic depsipeptide PF1022A and its electrophysiological effects on muscle cells of *Ascaris suum*. *Pesticide Science* **48**, 343–350.

MARTIN, R. J., ROBERTSON, A. P., BJORN, H. & SANGSTER, N. C. (1997). Heterogenous levamisole receptors: a single-channel study of nicotinic acetylcholine receptors from *Oesophagostomum dentatum*. *European Journal of Pharmacology* (in the Press).

MARTINDALE (1996). *The Extra Pharmacopoea*. 31st Edition. (ed. Reynold, J. E. F.), pp. 103–128. The Royal Pharmaceutical Society of Great Britain, London, England.

MATHEWS, W. R. & MURPHY, R. C. (1982). Inhibition of leukotriene biosynthesis in mastocytoma cells by diethylcarbamazine. *Biochemical Pharmacology* **31**, 2129–2132.

MCGEHEE, D. S. & ROLE, L. W. (1995). Physiological diversity of nicotinic acetylcholine receptors expressed by vertebrate neurons. *Annual Review of Physiology* **57**, 521–546.

McKELLAR, Q. A. & KINABO, L. D. B. (1991). The pharmacology of flukicidal drugs. *British Veterinary Journal* **147**, 306–319.

MEHLHORN, H., BECHER, B., ANDREWS, R., THOMAS, H. & FRENKEL, J. R. (1981). *In vivo* and *in vitro* experiments on the effect of praziquantel on *Schistosoma mansoni*: a light and electron microscope study. *Arzneimittel Forschung* **31**, 544–554.

NODA, M., TAKAHASHI, H., TANABE, T., TOYOSATA, M., KIKYOTANI, S., FUTUTANI, Y., HIROSE, T., TAKASHIMA, H., INAYAMA, S., MIYATATA, T. & NUMA, S. (1983). Structural homology of *Torpedo californica* acetylcholine receptor subunits. *Nature* (*London*) **302**, 528–532.

NOAH (1997). *Compendium of Data Sheets for Veterinary Products 1996–97*. Beccles, Suffolk. William Clowes Ltd.

PAPKE, R. L., BOULTER, J., PATRICK, J. & HEINMANN, S. (1996). Single channel currents of rat neuronal nicotinic acetylcholine receptors expressed in *Xenopus laevis* oocytes. *Neuron* **3**, 589–596.

PAPKE, R. L. & HEINEMAN, F. (1996). The role of the β_4-subunit in determining the kinetic properties of rat neuronal nicotinic acetylcholine α_4-receptors. *Journal of Physiology* (*London*) **440**, 95–112.

PAX, R. A. & BENNETT, J. L. (1989). Effect of closantel on intrategumental pH in *Schistosoma mansoni* and *Fasciola hepatica*. *Journal of Parasitology* **75**, 169–171.

PENNINGTON, A. J. & MARTIN, R. J. (1990). A patch-clamp study of acetylcholine-activated ion channels in *Ascaris suum* muscle. *Journal of Experimental Biology* **154**, 201–221.

PRICHARD, R. K. (1994). Anthelmintic resistance. *Veterinary Parasitology* **54**, 259–268.

RAZIN, E., ROMEO, L. C., KRILIS, S., LIU, F.-T. & LEWIS, R. A. (1984). An analysis of the generation and the secretion of preformed mediators from mouse bone marrow-derived mast cells. *Journal of Immunology* **133**, 938–945.

REDMAN, C. A., ROBERTSON, A. P., FALLON, P. G., MODHA, J., KUSEL, J. R., DOENHOFF, M. J. & MARTIN, R. J. (1996). Praziquantel: An urgent and exciting challenge. *Parasitology Today* **12**, 14–20.

REVAH, F., GALZI, J.-L., GIRAUDAT, J., HAUMONT, F., LEDERER, F. & CHANGEAUX, J.-P. (1990). The non-competitive blocker [H^3]chlorpromazine labels three amino acids of the acetylcholine receptor γ subunit: Implications for the α-helical organization of the regions MII and for the structure of the ion channel. *Proceedings of the National Academy of Sciences, USA* **87**, 4675–4679.

ROBERTSON, S. J., PENNINGTON, A. J., EVANS, A. M. & MARTIN, R. J. (1994). The action of pyrantel as an agonist and an open-channel blocker at acetylcholine-receptors in isolated *Ascaris suum* muscle vesicles. *European Journal of Pharmacology* **271**, 273–282.

ROBERTSON, S. J. & MARTIN, R. J. (1993). Levamisole-activated single-channel currents from muscle of the nematode parasite *Ascaris suum*. *British Journal of Pharmacology* **108**, 170–178.

ROOS, M. H., KWA, M. S. G. & GRANT, W. N. (1995). New genetic and practical implications of selection for anthelmintic resistance in parasitic nematodes. *Parasitology Today* **11**, 148–150.

SANGSTER, N. C., PRICHARD, R. K. & LACEY, E. (1985). Tubulin and benzimidazole-resistance in *Trichostrongylus colubriformis* (Nematoda). *Journal of Parasitology* **71**, 645–651.

SCHAEFFER, J. M., BLIZZARD, T. A., ONDEYKA, J. G., GOEGELMAN, R., SINCLAIR, P. J. & MROZIK, H. (1992). [^{3}H]Paraherquamide binding to *Caenorhabditis elegans*: studies on a potent new anthelmintic agent. *Biochemical Pharmacology* **43**, 679–684.

SCHULMAN, M. D., OSTLIND, D. A. & VALENTINO, D. (1982*a*). Mechanism of action of mk-401 against *Fasciola hepatica* – inhibition of phosphoglycerate kinase. *Molecular and Biochemical Parasitology* **5**, 133–145.

SCHULMAN, M. D., VALENTINO, D., CIFELLI, S. & OSTLIND, D. A. (1982*b*). Dose-dependent pharmacokinetics and efficacy of mk-401 against old, and young-mature infections of *Fasciola hepatica* in the rat. *Journal of Parasitology* **68**, 603–608.

SCHULMAN, M. D. & VALENTINO, D. (1982). Purification, characterization and inhibition by mk-401 of *Fasciola hepatica* phosphoglyceromutase. *Molecular and Biochemical Parasitology* **5**, 321–332.

STRYER, L. (1995). *Biochemistry*. New York. W. H. Freeman and Company.

THOMPSON, D. P., PAX, R. A. & BENNETT, J. L. (1984). Microelectrode studies on the tegument and sub-tegumental compartments of male *Schistosoma mansoni*: an analysis of compartments of electrophysiological properties. *Experimental Parasitology* **58**, 314–315.

VAN DEN BOSSCHE, H., ROSHETTE, F. & HORIG, C. (1982). Mebendazole and related anthelmintics. *Advances in Pharmacology and Chemotherapy* **19**, 67–128.

VAN DEN BOSSCHE, H. & DE NOLLIN, S. (1973). Biochemical effects of mebendazole on *Trichinella spiralis* larvae. *Journal of Parasitology* **59**, 970–976.

VICKERY, A. C., NAYAR, J. K. & TAMPLIN, M. L. (1986). Diethylcarbamazine on microfilariae of *Litomosoides carinii in vitro* and *in vivo*. *Zeitschrift für Parasitenkunde* **72**, 805–813.

WOLDE-MUSSIE, E., VANDE-WAA, J., PAX, R. A., FETTERER, R. H. & BENNETT, J. L. (1982). *Schistosoma mansoni*: calcium efflux and the effects of calcium-free media on the responses of the electrical potential from the tegument of adult males musculature to praziquantel and other agents inducing contraction. *Experimental Parasitology* **53**, 270–278.